MICELLAR STRATEGIES FOR TARGETING BONE DISEASES

by

Stewart Andrew Low

A dissertation submitted to the faculty of
The University of Utah
in partial fulfillment of the requirements for the degree of

Doctor of Philosophy

Department of Bioengineering

The University of Utah

December 2015

The University of Utah Graduate School

STATEMENT OF DISSERTATION APPROVAL

The dissertation of **Stewart Andrew Low**

has been approved by the following supervisory committee members:

Jindřich Kopeček	, Chair	**07/31/2015** Date Approved
Vladimir Hlady	, Member	**07/21/2015** Date Approved
Dong Wang	, Member	**07/14/2015** Date Approved
Scott Ruthardt Miller	, Member	**07/07/2015** Date Approved
David W. Grainger	, Member	**07/15/2015** Date Approved

and by **Patrick A. Tresco**, Chair/Dean of

the Department/College/School of **Bioengineering**

and by David B. Kieda, Dean of The Graduate School.

ABSTRACT

Bone diseases range from degenerative osteoporosis to bone cancers and metastasized malignancies. They can be congenital or developed late in life and represent a major cause of decreased quality of life and increased mortality. Large molecule drug delivery systems have been in development and are aimed at delivering targeted drugs to bone. They do this by increasing accumulation with targeting ligands to attach to bone, with large size increasing accumulation in inflamed and malignant tissue and extending circulation half-life due to their reduced clearance by the kidneys. Unfortunately, they often have large dispersities, making consistency among batches more complicated. Small molecules, on the other hand, can be replicated predictably for each batch but lack in extended circulation time and good accumulation due to their size. Micelles have the capability of bridging this gap. By conjugating a high-affinity bone-targeting ligand, aspartic acid octapeptide, to a hydrophobic drug by a degradable linker, a monodisperse unimer is formed that can self-assemble into a large molecule micelle.

This dissertation describes the development of a bone-targeted micelle and the incorporation of two different drugs, doxorubicin and 6-bromoindirubin-3'-oxime (6BIO), for the application of treating osteosarcoma and bone fractures, respectively.

Four doxorubicin-containing micelles were designed and synthesized. These micelles demonstrated micellar aggregation at low concentrations, increasing the overall size of the delivery system. The micelles also were able to retain their binding to

hydroxyapatite and release unmodified drug for treatment of osteosarcoma.

From osteosarcoma, efforts were made to examine the versatility of the micellar drug delivery system by applying it to bone fractures. We adapted the delivery system by conjugating it to the GSK3β inhibitor, 6BIO. The modified micelle retained its micelle-assembling capabilities and was able to release drug over several days. Animal studies demonstrated the micelles' high affinity to bone fractures and ability to increase the bone density of fractured femurs.

We have developed a drug delivery system that can be adapted for multiple applications. The micelle has demonstrated its capabilities both *in vitro* and *in vivo.*

To my family.

TABLE OF CONTENTS

ABSTRACT iii

LIST OF TABLES viii

LIST OF FIGURES ix

ACKNOWLEDGEMENTS xii

Chapters

1. INTRODUCTION 1

    1.1 Introduction 1
    1.2 Targeting 3
    1.3 Polymer carriers 10
    1.4 Therapeutics 24
    1.5 Conclusions 32
    1.6 Statement of objectives 35
    1.7 References 37

2. BONE-TARGETED ACID-SENSITIVE DOXORUBICIN CONJUGATE MICELLES AS POTENTIAL OSTEOSARCOMA THERAPEUTICS 64

    2.1 Introduction 64
    2.2 Experimental procedures 66
    2.3 Results and discussion 72
    2.4 Conclusions 79
    2.5 References 80

3. BIODISTRIBUTION OF FRACTURE-TARGETED GSK3β INHIBITOR LOADED MICELLES FOR IMPROVED FRACTURE HEALING 91

    3.1 Introduction 91
    3.2 Experimental procedures 95
    3.3 Results and discussion 103
    3.4 Conclusions 111
    3.5 References 112

4. HEALING EFFICACY OF FRACTURE-TARGETED GSK3β-LOADED MICELLES FOR IMPROVED FRACTURE HEALING....122

4.1 Introduction....122
4.2 Experimental procedures....124
4.3 Results and discussion....127
4.4 Conclusions....132
4.5 References....133

5. SUMMARY AND FUTURE PROSPECTS....141

5.1 Summary....141
5.2 Future directions....144
5.3 Conclusions....152
5.4 References....152

Appendices

A. CHAPTER 2 SUPPORTING INFORMATION....164

B. CHAPTER 3 SUPPORTING INFORMATION....175

C. CHAPTER 4 SUPPORTING INFORMATION....193

LIST OF TABLES

1.1 Maximal binding rate and dissociation constant of acidic oligopeptides 59

4.1 The comparison of bone morphometric analysis. 138

C.1 Bone morphometric analysis using the plate model.....194

LIST OF FIGURES

1.1 General osteoclast structure and function demonstrating unique environments ...56

1.2 General structure of bone-targeted polymeric nanomedicines 57

1.3 Structures of several bone-targeting molecules 57

1.4 MDP-Tc99 scan demonstrates the targeting specificity of biophosphonates 58

1.5 Atomic force microscopy histograms demonstrating rupture forces 59

1.6 Initial uptake and localization of FITC-labeled HPMA copolymer-Asp8 60

1.7 Biodistribution in BALB/c mice of 125I-labeled HPMA copolymer-Asp8.....61

1.8 Scheme of release of unmodified prostaglandin E1 61

1.9 General pathways affecting bone anabolism and cross-talk 62

1.10 Treatment of mCherry-labeled MG-63-Ras osteosarcoma tumor-bearing mice ...63

2.1 Illustration of micelle formation from amphiphilic unimer 84

2.2 Synthesis of amphiphilic unimers with linear and branched architecture 84

2.3 Determination of the critical micellar concentration of DOX-containing unimers85

2.4 Size distribution of micelles as determined by dynamic light scattering 86

2.5 TEM image of micelles in 0.01M HEPES at room temperature 87

2.6 In vitro adsorption of DOX-containing micelles 88

2.7 In vitro release profiles of DOX from DOX-containing micelles 89

2.8 Cytotoxicity of free DOX and micelles with variable structure 90

3.1 Fracture-targeting micelles from amphiphilic unimer 116

3.2 Synthesis of a clickable 6BIO and conjugation of 6BIO and linker to micelle ...117

3.3 Dynamic light scattering of the linear micelle BIO-A2-D8 118

3.4 Time dependent 6BIO release from the linear micelle 118

3.5 Synthesis of radio-iodinated micelles and 6BIO 119

3.6 Organ biodistribution of free 6BIO, the linear micelle BIO-A2-D8 120

3.7 SPECT/CT of mice at 1 h, 4 h, and 24 h 121

4.1 Structures of 6BIO, linear BIO-A-2-D8, and branched BIO-A2-K-D4 137

4.2 Densities of fracture callus 138

4.3 Average composite of fifty 6um slices 139

4.4 Histology sections of BIO-A2-D8, BIO-A2-K-D4, 6BIO, and PBS control 140

5.1 Basic construct, self-assembly, and release of designed micelles 162

5.2 The differentiation and activation of osteoblasts 162

5.3 Black Hole quenching dyes are capable of reducing fluorescence of NIR dyes .163

A.1 1H-NMR spectrum of Fmoc-hydrazine 164

A.2 HPLC elution profile of Fmoc-hydrazine 165

A.3 MALDI-ToF mass spectrum of Fmoc-aminoundecanoic acid 166

A.4 HPLC profile of Fmoc-aminoundecanoic acid 167

A.5 1H-NMR spectrum of Fmoc-aminoundcanoic acid 168

A.6 Structure and HPLC profile of A1-D8 169

A.7 Structure and HPLC profile of A2-D8 169

A.8 Structure and HPLC profile of A2-K-D4 170

A.9 Structure and HPLC profile of A4-K-D4 170

A.10 Structure and MALDI-ToF spectrum of A1-D8 171

A.11 Structure and MALDI-ToF spectrum of A2-D8 171

A.12 Structure and MALDI-ToF spectrum of A2-K-D4 172

A.13 Structure and MALDI-ToF spectrum of A4-K-D4 172

A.14 Chemical structure and HPLC profile of DOX-A1-D8 173

A.15 Chemical structure and HPLC profile of DOX-A2-D8 173

A.16 Chemical structure and HPLC profile of DOX-A2-K-D4 174

A.17 Chemical structure and HPLC profile of DOX-A4-K-D4 174

B.1 HPLC and mass spectrometry of purified 6BIO 175

B.2 NMR of 6BIO in DMSO 176

B.3 HPLC and mass spectrometry of the purified product of 6BIO 177

B.4 NMR of the purified product of 6BIO 178

B.5 HPLC and mass spectrometry of the unconjugated linear unimerA2-D8 179

B.6 HPLC and mass spectrometry of the branched unimer A2-K-D4 180

B.7 HPLC and mass spectra of linear unimer BIO-A2-D8 181

B.8 HPLC and mass spectra of linear unimer BIO-A2-K-D4 182

B.9 HPLC graphs from the release kinetic study of BIO-A2-D8 183

B.10 HPLC spectra of release kinetics for BIO-A2-K-D4 185

B.11 Four hour release of BIO conjugated to 4-pentynoic acid at room temperature ..187

B.13 HPLC and mass spectrum of stannylated 6BIO 188

B.14 Spectrum of o-alkylated stannylated 6BIO 189

B.15 Iodination of 6BIO product 190

B.16 Iodination of BIO-A2-D8 191

B.17 Iodination of BIO-A2-K-D4 192

ACKNOWLEDGEMENTS

First and foremost, I would like to thank Dr. Jindřich Kopeček, for the opportunity to work in his lab, the freedom to explore projects, and the effort to instill the love of science in those around him. I would also like to thank my thesis committee members, Drs. Dong Wang, Scott Miller, David Grainger, and Vladimir Hlady for the interest they take in helping grow young scientists, such as myself. My time at the university would not have been the same without Dr. Pavla Kopečková, to whom I am grateful for introducing me to polymer synthesis and taking time to teach me the concepts behind several laboratory techniques. I would also like to thank Dr. Jiyuan Yang for her help with experiments and matchless enthusiasm that keeps those around her going. I would like to thank Dr. Philip S. Low for the opportunity to work at Purdue University and for his contributions to the development of this project. I would also like to thank Dr. Chris Galliford for his insightful advice on synthesis and his detailed explanation of how chemistry works. I would like to thank Dr. Kazunori Kataoka for the opportunity to study micelles at the University of Tokyo. I would like to thank my lab mates, past and present, for helping me out and making the lab a fun place to work: Kuangshi, Larissa, Pan, Rui, Pavla, Moni, Joseph, Zoe, Te-Wei, Jon, Chris, Dalynn, and my colleagues at Purdue, Patti, Mingding, Maha, Jyoti, Isaac, Ananda, Srinavasa, Ian, Candice, Bingbing, Boning, Suilan, Danielle, Qingshou, Greg, Hanan, Estela, Samaresh, Alyssa, Kristina, and Pengcheng. Much of this work was supported by NIH grant GM69847.

I derive a great deal of motivation from my family. I am truly thankful for Andrew and Grey for giving me a break from work and for reminding me why I am working in the first place. I haven't words for my gratitude towards my wife, Lizzie, who has been so supporting and patient with me. I am grateful to her for not only editing my papers but making our family run.

CHAPTER 1

INTRODUCTION

Bone is a complex organ responsible for structure and calcium storage as well as being a structure for hematopoiesis to occur. Adult bone is 50-70% mineral, 20-40% organic matrix, 5-10% water, and 1-5% lipids. Hydroxyapatite (HAp) ($Ca_{10}(PO_4)_6(OH)_2$) is the main mineral component of bone. The crystallinity of HAp increases with time, however, in healthy bone the needle-like crystals never grow much more than 300 Å in length [1–3]. These crystals are continuously being broken down and replaced during bone turnover. Initially, monocytes receive several signals directing them to differentiate into osteoclasts. Critical to this process, osteoblasts present receptor activator of nuclear factor κB ligand (RANKL) to the receptor activator of nuclear factor κB (RANK) surface receptor triggering the TNF receptor associated factor 6 (TRAF6) cascade in monocytes, ensuring osteoclast development [4,5]. Mature osteoclasts then perform the catabolic process on bone. The osteoclast creates a sealing zone (Figure 1.1) over resorption sites (lacunae) and proceeds to release cathepsin K (Cat K) to degrade the organic matrix and HCl to dissolve the HAp. These mechanisms in combination with reactive oxygen species (ROS) produced by tartrate-resistant acid phosphatase (TRAP) degrade the bone

NOTE: This chapter is adapted with permission from the following publication: Low, S. A. and Kopeček, J. Targeting polymer therapeutics to bone. Advanced Drug Delivery Reviews 64 (2012) 1189-1204

preparatory for osteoblasts to lay down organic matrix called osteoid. The osteoid, primarily composed of type I collagen, is then calcified and becomes new bone [6,7].

When catabolism or anabolism in bone turnover is altered, the bone may become diseased. Osteoporosis, where catabolism effectively outweighs anabolism, predominately affects men and women over 50. Approximately 44 million people in the US suffer from low bone mass, and 10 million people already have osteoporosis. An estimated 61 million will have the disease by 2020 [8]. Complications of this disease include debilitating vertebral and hip fractures, costing between in $13.7 billion and $20.3 billion in 2005 [9]. Other imbalances in bone turnover include osteosarcoma and bone metastasis. Osteolytic and tumor-creating cancers of the bone both result in significant pain and morbidity or patients. Osteoarthritis, osteomyelitis, infections, and fractures all increase the economic toll on health systems worldwide as well as decrease quality of life for millions of people each year.

Nanomedicine plays an important role in recent advancements in bone therapeutics. Diseases that affect the bone may carry a range of receptor-specific targeting opportunities or they may carry none at all. However, by exploiting the mineral portion of the bone, bone diseases can be targeted using molecules such as bisphosphonate and acidic oligopeptides. Nanomedicines can be easily conjugated to several ionic targeting ligands, increasing binding avidity to bone. HAp crystal structures or HAp exposure are disease specific, and as such, modification of the targeting ligand itself or the density of the ligand may provide specific targeting opportunities. In addition to targeting, nanomedicines create an opportunity to image and synergistically combine multiple drugs to treat the diseased portion of the bone (Figure 1.2).

Aspects of this field have been reviewed previously [10-15]. In this chapter we discuss the selection of proper targeting agents, polymers, and drugs for application to specific bone disease states. The analysis also includes methods of increasing local drug accumulation by modification of the molecular weight and drug-polymer release mechanisms. We will also elaborate on how various bone anabolic agents interact, as well as how synergism of chemotherapeutics can be achieved by nanomedicine.

1.2. Targeting

Each bone disease state has similarities in that each causes local inflammation and/or results in the exposure of HAp to blood. These two characteristics can be utilized in order to deliver high drug loads specifically to diseased tissue. Inflamed tissue fills with exudate as various cytokines dilate vasculature. Macromolecular therapeutics then are able to travel into the tissue due to vascular fenestration and be retained in the tissue due to poor lymphatic clearance and any targeting ligands associated with the macromolecule. This enhanced permeability and retention (EPR) has been well documented in several publications and is extensively discussed in several reviews [16-19]. Delivery of therapeutics to bone also depends on the extravasation through vessels in or near the bone [20]. Larger molecules, for example albumin and polyvinylpyrrolidone (Mw 35 kDa), can extravasate and have been found in bone after i.v. administration [21]. In fact, it has been long known that the vasculature in bone is fenestrated with pore sizes up to 80 nm [22], which exceeds the hydrodynamic size of most circulating nanomedicines. Exposure of HAp to blood carries its own targeting possibilities. Various tetracyclines, bisphosphonates, acidic oligopeptides, chelating compounds, and salivary proteins have all been employed to target bone diseases. These

compounds bind to the inorganic HAp part of bone and have specificity for a certain size of HAp crystal. Therefore, as the crystallinity of newly deposited bone in a tumor is different from the crystallinity of HAp exposed during a bone fracture, so targeting molecules can be selected for specific disease states.

1.2.1 Tetracycline

Tetracycline was introduced as an antibiotic in 1947 [23]. The antibiotic is derived from *Streptomyces rimosus* and inhibits aminoacyl-tRNA from entering into bacterial ribosomes, inhibiting protein elongation [24]. Tetracycline affects general bacterial metabolism and is prescribed for a wide range of gram-positive and gram-negative bacteria. Soon after its incorporation into medicine, however, tetracycline was found to bind strongly to bone. Its usage was discontinued in pediatric medicine as the high affinity to HAp caused children's teeth to stain yellow [25]. Furthermore, other early studies found that tetracycline may inhibit skeletal growth in children [26,27]. Its use as an antibiotic in adults and a targeting ligand in bone disease, though, has not persisted.

Early studies indicate that tetracycline must be in the correct orientation in order to bind HAp. Oxygens bound to C2, C10, and C12 are among the primary HAp binding atoms [28]. As such, modifications around the 5, 6, and 7 carbons can be made with minimal effects on binding and biological activity (Figure 1.3). Other studies have shown that bone binding and antimicrobial activity may be retained even with a simplified tetracycline molecule. Neale et al. tried to reduce potential side effects caused by tetracycline's biological activity by minimalizing tetracycline structure so that it retains no biological activity yet is still able to bind to HAp. They found that 3-amino-

2,6-dihydroxybenzamide retains 50% of the ability to bind to HAp when compared to native tetracycline (Figure 1.3). To achieve bone anabolism, the new targeting ligand was bound to estradiol via a succinate linker. Following conjugation, the compound had a binding affinity of 105% over tetracycline alone. As estradiol alone did not bind to HAp, the increased affinity may be attributed to the addition of a succinate linker [29].

1.2.2 Bisphosphonates

Bisphosphonates (BPs) also bind strongly to HAp and retain much of the binding affinity after conjugation to other molecules or carriers. The first biological activity associated with BPs was noticed in 1968 [30]. Later, their effects on bone metabolism were discovered and they were prescribed to treat osteoporosis. BPs are derived from pyrophosphate and contain a carbon substitution for pyrophosphate's central oxygen. From the central carbon most BPs have been functionalized with a hydroxyl group and an R group by which they are classified (R groups containing nitrogen and those that do not) (Figure 1.3). Non-nitrogen-containing BPs incorporate into AMP, creating a modified ATP, which cannot be hydrolyzed. Buildup of this ATP analog inside osteoclasts leads to apoptosis and reduced bone turnover. Nitrogen-containing BPs (nBP) are much more potent. They inhibit farnesyl pyrophosphate synthase activity, and by so doing, disrupt the mevalonic acid pathway. Without the mevalonic acid pathway, protein prenylation is inhibited and osteoclasts lose their functionality or apoptose [31]. This inhibition may not completely arrest bone turnover, as mevalonic acid pathway inhibitors increase bone morphogenic protein production as well [32-34]. Clinically, the activity of BPs has a profound effect on osteoporosis. Clinical data demonstrate that BPs yield a 47%

reduction in vertebral fractures as well as wrist fractures, 50% in hip fractures, and a 19% overall drop in all nonvertebral fractures [35].

BP affinity to raw HAp is also clinically relevant in bone scintigraphy. Tc99 labeled methylene diphosphate (MDP) or hydroxy methylene diphosphate (HMDP) are used clinically for imaging bone abnormalities ranging from osteomyelitis to stress fractures. In many bone diseases bone is deposited (as in a tumor) or degraded (as in osteoporosis and osteoarthritis). Consequently, HAp crystals are exposed and can be targeted using bisphosphonates such as MDP (Figure 1.4).

The use of BPs as polymer/nanoparticle-targeting moieties has several advantages. nBPs contain a primary amine and can therefore readily be conjugated to carboxylic acids. Secondly, as with tetracycline, if they are conjugated to nanomedicines via a degradable linker such as a pH sensitive hydrazone bond, they are pharmacologically active and may produce synergistic effects when coupled with appropriate drugs. Finally, the patent protection of many BPs will expire soon, which makes them an economic option for a targeting moiety.

BPs are some of the most studied bone targeting molecules and much research has been done determining their binding properties to HAp [37-39]. Hrubý et al. determined that the number of targeting moieties on a polymer did not dramatically affect the rate of adsorption. Rather, the amount of adsorbed polymer was affected by the number of targeting moieties, as more ligands yielded higher binding avidity. The authors also concluded that there is a need for multiple targeting moieties to ensure that at least one is exposed [40]. Logically then, multiple targeting ligands become more critical as the nanomedicine size increases [41].

BP adsorption to HAp is a thermodynamic process primarily driven by entropy. Mukherjee et al. measured the thermodynamics of adsorption for several clinically used BPs as well as modified BPs in order to determine what aspects of the molecules are important for HAp binding. For instance, strongly basic side chain substituents, such as the nitrogen in alendronate, contribute dramatically to the binding in the free form. Furthermore, when measuring the difference between one Pi bond forming with HAp versus two Pi bonds forming (one phosphate versus both phosphates binding) they found that the hydroxyl group originating from the central carbon atom is necessary for both phosphates to bind [42]. By reducing a nanomedicine's thermodynamic strength of adsorption, either by manipulating the number of ligands or by modification of the ligand itself, one can target only the thermodynamically favored diseased area over the kinetically favored skeleton.

Numerous BP conjugates with natural or synthetic macromolecules demonstrate bone targeting *in vivo* [43-45]. Targeted osteoprotegerin (OPG) is one example. OPG is naturally produced by osteoblast's Wnt-β-catenin signaling pathway and is a potent RANKL inhibitor preventing osteoclastogenesis. With the intent to treat osteoarthritis, OPG was modified with a thiol-BP and administered intravenously (i.v.) to rats. Overall bone deposition of BP-targeted OPG was twice that of free OPG. In an osteoarthritis rat model, targeted OPG accumulated in the tibia 4x and femur 6x that of free OPG, demonstrating BP-targeting abilities [46].

BPs exhibit antiangiogenic properties by causing apoptosis, inhibiting migration, and reducing angiogenic sprouts of endothelial tissue, making it a good antineoplastic agent but reducing capabilities to heal bones [47]. Moreover, the half-life of BPs such as

alendronate in the bone is more than 10 years [48]. The inhibition of osteoclasts for extended periods of time can have serious detrimental effects on bone turnover, as osteoclasts secrete insulin-like growth factors and BMPs to promote the maturation of osteons to osteoblasts. Jawbones have a high blood supply and high turnover, resulting in BP accumulation. The combination of low bone turnover and lower blood flow causes osteonecrosis of the jaw (ONJ). ONJ is primarily associated, but not limited, to potent BPs used for chemotherapy, which completely inhibit osteoclast function [48,49]. Other toxicities include nephrotoxicity, hypocalcemia, and ocular dysfunction [50]. Therefore, BPs should not be used without considering some of the side effects.

1.2.3 Acidic oligopeptides (AO)

Bone sialoprotein is one of several naturally occurring proteins that exhibit strong affinity for HAp. Sialoprotein has several strings of acidic amino acids. Modeled after sialoprotein, glutamic acid, and aspartic acid oligopeptides 4-10, amino acids (AA) long provide a more biocompatible option when adequate blood flow and bone turnover are needed [51]. Biocompatibility can be further increased as D peptides, which are not easily recognized by the body's immune system, can replace L peptides. Similarly to BPs, the HAp binding capabilities of these oligopeptides are retained after conjugation to a nanomedicine carrier via the peptide's alpha amino group [52].

AO's chain length can be modified to fit an application. Sekido et al. compared binding rates of Asp_{2-10} and Glu_{2-10} to HAp (Table 1.1). Increase in AA chain length resulted in enhanced binding rate (B_{max}) up to hexapeptides; then the rate of binding plateaued and further increase in chain length was without effect. The dissociation

constant (K_d) decreased with increasing numbers of AA throughout the experiment and no differences were found between D and L AA. This indicates that an AO over 6 AA long is ideal for optimal binding efficiencies [53]. Nanomedicines, however, are not limited to a single targeting moiety; rather, multiple ligands may also decrease K_d. Ouyang et al. demonstrated the effect of multiple sets of AOs on binding rates. Dendrimers were synthesized with 1, 2 and 3 chains of Asp_{4-6} and a HAp binding assay was performed. The results indicated that two chains had nearly three times the binding of one alone but that the addition of a third chain resulted in poorer binding than two chains alone [52]. In the case of dendrimers, this means that steric hindrance may prevent binding of multiple AO chains. The extra chains then decrease the binding by increasing the size of the dendrimer itself or by reducing the ionic attraction of other dendrimers to the HAp by increasing the negative charge on the surface.

1.2.4 Estradiol analogs

Estrogen replacement therapy is being used for the treatment of osteoporosis related to low estrogen levels. Crooks and coworkers developed estradiol analogs that would localize in bone tissue but are lacking estrogenic properties. They designed bone-targeting compounds by attaching calcium chelators to an estradiol moiety through succinoyl [54] or carboxyethyl [55] linkers. To further improve the targeting potential they prepared a series of phosphate esters of the carboxyethyl linker-containing compound that possessed similar bone-targeting properties as tetracycline [56].

1.2.5 Specific applications

Reflecting their molecular structures, tetracycline, BPs, and AO do have some unique binding capabilities, which may affect the disease states for which they are most appropriate. The rate of binding of AOs to HAp is faster than that of BP [57]. One may hypothesize this to be a result of the larger binding area of AOs. Meanwhile, BPs have a greater binding strength, most likely due to greater specificity of BPs for HAp [57]. Wang et al. found that BP binds to all bone, while Asp_8 binds preferentially to higher crystalline HAp and thus to resorption surfaces [58]. In a follow-up study, AFM cantilever tips were modified with either Asp_8 or alendronate (ALN). Interactions with HAp such as binding, adhesion events, and rupture forces were measured (Figure 1.5). ALN binding at zero distance was 190 pN, as opposed to 105 pN with Asp_8. Furthermore, ALN had higher rupture forces [3]. There were two sets of rupture forces for ALN, which lends itself to the bonding mechanism described by Mukherjee et al. [42]. Using two HA surfaces with differing crystallinity, Wang et al. confirmed that ALN is less affected by crystallinity and that Asp prefers higher crystalline HAp [3]. Bringing targeting via ionic interactions full circle, Miller et al. demonstrated using fluorescence microscopy that tetracycline deposits preferentially onto growing surfaces, or those with low crystallinity (Figure 1.6) [59]. Application of these principles means that targeting osteoclasts should be done with AOs, which prefer absorbing surfaces, while targeting osteoblast should be done with tetracycline, which prefers growing surfaces of bone.

1.3 Polymer carriers

The conjugation of multiple targeting ligands to a polymeric backbone is an obvious advantage that polymeric drug delivery systems have over small molecule

systems. In addition to targeting ligands, modification of polymer size has a profound effect on blood circulation time as well as on whole body biodistribution. Once in target tissue, polymeric drug delivery systems have several modes of drug release, which range from passive diffusion from a degrading nanosphere to enzymatic cleavage of drug-polymer linkers. These drug release mechanisms, in combination with biodistribution, play a critical role in ensuring the drug is delivered to the right area for the right duration of time.

1.3.1 High molecular weight vs. low molecular weight carriers

The molecular weight and ultimately the hydrodynamic radius of polymeric carriers have a profound effect on the efficacy of drug delivery. Higher molecular weight polymers have longer circulating half-lives and ultimately higher deposition in diseased sites. However, as the molecular weight increases, so does uptake in the mononuclear phagocyte system (MPS). Therefore, careful selection of molecular weights with appropriate targeting ligand concentration (number per macromolecule) is essential to ensure biocompatibility and high deposition of drug in the affected area. Wang et al. compared 24 kDa, 46 kDa, and 96 kDa Asp_8 containing HPMA copolymers in a biodistribution study. Each polymer contained 4.4, 5.6, and 9.6 Asp_8 chains per macromolecule, respectively. Also included in the study was Tyr-D-Asp_8 as a control. As hypothesized, the study demonstrated enhanced blood circulation time for high molecular weight conjugates, with the highest bone accumulation being 96 kDa HPMA copolymer by several fold. However, the highest bone to MPS accumulation ratio was the Asp_8 targeting ligand by itself, followed by 24 kDa HPMA copolymer conjugates

[58]. The same group performed a similar biodistribution study on ALN containing HPMA copolymers of two molecular weights – 20 kDa and 90 kDa. In addition to molecular weight, the concentration of ALN (0%, 1.5%, and 8.5%) was also varied (Figure 1.7). All conjugates showed an initially high uptake in the heart, lungs, and kidneys, which reduced over time. Similarly to [58], the low molecular weight, 20 kDa conjugate cleared the body first as expected and each targeted molecule increased bone accumulation over time. The high molecular weight (90 kDa) conjugate yielded a higher MPS uptake. Similarly, higher ALN content also yielded higher MPS uptake. This indicates that the identification of ideal targeting ligand concentrations needs to take into account the polymer's overall charge (and therefore MPS uptake), number of targeting ligands per macromolecule (related to charge), and molecular weight. In the case above, the drug with the highest bone to MPS ratio was the 20 kDa, 1.5% ALN polymer [60]. In conditions where metabolism of a drug by the MPS is a concern, moderate molecular weights with a low percentage of targeting moieties are beneficial. However, uptake by the MPS generally means phagocytosis by mononuclear phagocytes. Phagosomes eventually fuse with lysosomes, creating an acidic environment with several proteolytic enzymes. Therefore, delivery of proteins and other molecules, which will be degraded by lysosomal enzymes, may not create biocompatibility issues following MPS uptake. In these situations, a high molecular weight and a high targeting moiety content may be the best option.

1.3.2 Degradable linkers

As critical as the biodistribution of a drug, the proper release rate and mechanism will determine the efficacy of a drug delivery system. Modification of the linker, which

connects polymer with the drug, can create release profiles that deliver high amounts of drug immediately upon arrival or deliver small amounts over time, extending the effective dose time of the drug. Furthermore, by utilizing bone-specific enzymes, disease-site-specific prodrugs can be created.

The bone itself has several enzymes, which can be used to release drugs. Among these enzymes are matrix metalloproteinases (MMP) 1, 2, 3, 4, 7, 8, 9, 12, 13, and 14 and Cat K. MMPs are expressed by osteoclasts and osteoblasts, and are overexpressed in many bone metastases [61-71]. Most MMPs function by cleaving peptide bonds holding collagen and other glycoproteins together. MMPs assist osteoclasts' function by degrading collagen within the bone at resorption lacunae while bone metastases use MMPs to degrade the basement membrane and spread throughout the body. Using MMP-sensitive linkers may provide site-specific delivery of drugs to bone; however, bone delivery using MMPs is limited by the fact that MMPs are inhibited by tetracycline and derivatives such as doxycycline [72]. Cat K, on the other hand, is expressed in resorption lacunae and is not sensitive to tetracycline derivatives (Fig 1.1). Due to secretion of Cat K into both the lacunae, Cat K-specific linkers are an excellent choice for signaling compounds such as prostaglandins and bone morphogenic protein-2 (BMP-2), whereas hydrazone bonds, disulfide bonds, and cathepsin B (Cat B)-sensitive linkers are better options for drugs such as chemotherapeutics, which rely on internalization by the cells prior to release.

Many classic degradable drug-polymer linkers rely on receptor-mediated endocytosis of cells or phagocytosis by osteoclasts. Following endocytosis, the endosomal compartment acidifies and ultimately fuses with lysosomes into an acidic

organelle (pH ~5). Acid-sensitive linkers are also effective in the low pH present in the interstitial space of tumors (pH 5-6) and the resorption lacuna of osteoclasts (pH 4-4.5) [73]. Hydrazone bonds are acid-sensitive linkers and are able to rapidly release an unaltered drug at pH 5.5, but remain intact at physiological pH 7.4. Hrubý et al. conjugated doxorubicin to an HPMA copolymer using a hydrazone linker and measured release kinetics of the HAp adsorbed polymer as well as the polymer in solution at pH 5 and 7.4. Release kinetics at pH 5 was logarithmic, with over 95% of the copolymer conjugate in solution releasing the DOX within 10 h. Release kinetics of the HAp bound polymer was slower, as after 10 h approximately 55% of the DOX was released and the remaining DOX was nearly all released over the first 50 h. Meanwhile, at pH 7.4 the drug linker was relatively stable, only releasing 20% of the drug after 50 h [40].

There are other release systems that rely on the endosomal environment. As the lysosome and endosome fuse, polymers within the endosome are exposed to proteases such as Cat B. Hrubý et al. also studied the release kinetics of a Cat B-sensitive tetrapeptide GFLG (glycine-phenylalanine-leucine-glycine) [74]. Release kinetics was nearly linear and much slower than the hydrazone bond discussed earlier. When the polymer was in solution, after 50 h less than 45% of the drug was released. Steric hindrance, preventing Cat B from accessing the tetrapeptide linker, reduced the DOX cleavage rate in HAp bound polymer to half the rate in solution, as only 22% was released after 50 h incubation [40].

Elongated spacers, which separate the enzymatically cleaved bond from the drug by a self-eliminating group, were designed by several groups [75-79]. The predominant example of an electronic cascade spacer is the 1,6-elimination spacer [77]. It contains,

e.g., a bifunctional p-aminobenzyl alcohol group that is linked to an enzymatically cleavable group through an amine moiety. After enzymatic cleavage, the strong electron-donating amine group of the 1,6-elimination spacer is unmasked and immediately initiates an electronic cascade that leads to cleavage of the benzyl-carbamate bond and release of carbamic acid. The unstable carbamic acid rapidly releases carbon dioxide and yields the unmodified drug [78,79]. Use of such spacers was shown in bone-targeted delivery of PGE_1 [59] and anticancer drugs to bone [80-82].

Once a polymer exits the endosome, it enters the cytosol. The cytosol has a reducing environment that is able to reduce disulfide linkers. Evidence also suggests that this reductive environment may start as early as the endosome during receptor-mediated endocytosis [83]. Kurtoglu et al. used disulfide linkers for dendrimer drug delivery and described the release at pH 5 and pH 7.4. Using either cysteine or glutathione at pH 7.4, release occurred within 20 min, while at pH 5, complete drug release occurred over 6 h or more. Furthermore, the amount of drug released was dramatically affected by glutathione and cysteine concentrations, as one cysteine can release only one drug [84].

1.3.2.1 Example of cathepsin K sensitive spacer design

The design of an oligopeptide sequence susceptible to cleavage by Cat K is demonstrated here. The aim was to design a conjugate that would deliver prostaglandin E_1 (PGE_1) to bone with subsequent PGE_1 release by osteoclast-secreted Cat K in the resorption lacuna (for macromolecular entry into osteoclasts see [85-87]).

The Cat K-sensitive spacer was designed based on known interactions of peptide substrates with the active site of the enzyme [88]. The specificities of S1–S4 subsites

(subsite nomenclature from Schechter and Berger [89]) of the Cat K active site have been screened with positional scanning libraries [90]. Their most striking result was the unique preference for proline in P2 position; therefore, it was selected. The favored amino acid residues in the P1 position were lysine and arginine. However, to ensure that the spacer is stable in the circulation [91], basic amino acid residues have been avoided and norleucine, the most active neutral amino acid residue, was chosen for position P1. It was shown that Gly-Pro in positions P3 and P2 were favorable for cleavage [90]. Consequently, glycine was seleceted for position P3. It had been observed previously that expanding the length of the oligopeptide spacer in side-chains of HPMA copolymers from three to four amino acid residues resulted in decreased steric hindrance upon the formation of the enzyme-substrate complex for chymotrypsin [92] and Cat B [74]. Thus, glycine was introduced into the position P4.

Chemically, the C end of Gly-Gly-Pro-Nle spacer cannot be directly connected to PGE_1 because the latter lacks a NH_2 group. To overcome this problem, a 1,6-elimination spacer based on 4-aminobenzyl alcohol (AB-OH) was inserted. The latter was used to link the peptide to the C-1 COOH group of PGE_1. Upon enzymatic cleavage of the peptide spacer, the strong electronic-donating amine group of the 1,6-elimination spacer is unmasked [75,76] and initiates an electronic cascade that leads to the cleavage of the ester bond and immediate release of unmodified PGE_1 (Figure 1.8). Finally, a methacryloyl group was attached at the N-terminus of the construct; the resulting macromonomer, MA-Gly-Gly-Pro-Nle-AB-PGE_1, may be copolymerized with HPMA to produce new PGE_1-containing macromolecular therapeutics. The release of PGE_1 from HPMA + MA-Gly-Gly-Pro-Nle-AB-PGE_1 copolymer indicated that a high rate of

cleavage occurred in osteoclast cultures followed by osteoblast cultures. Polymer incubation with nonskeletal and precursor cells resulted in minimal release of PGE_1, demonstrating the specificity of this linker [93]. The specificity of the linker was also validated *in vivo* [59,80,81].

1.3.3 Different polymers studied

Each polymer exhibits unique characteristics based on chemical and structural properties. We have classified polymers by their structural properties according to whether they form linear hydrophilic polymers or spherical micelle and nanoparticle structures.

1.3.3.1 Linear polymers

1.3.3.1.1 Cationic polymers

Polyethyleneimine (PEI) and poly(L-lysine) (PLL) are frequently-used cationic polymers in drug and gene delivery systems. Uludağ and coworkers incorporated a BP, 2-(3-mercaptopropylsulfanyl)-ethyl-1,1-bisphosphonic acid, to both polymers using heterobifunctional reagents. *In vitro* (HAp) and *in vivo* (unprocessed bone matrix from femurs/tibiae) mineral affinity of BP containing polymers was evaluated and compared with unmodified polymers. Interestingly, they found that *in vitro* binding to HAp was similar or lower after conjugation to BP and that both PEI and PLL were able to bind nearly 100% to HAp in many conditions on their own. This is not surprising, as positively charged molecules should adsorb to HAp. *In vivo* results on a rat model also showed no significant difference in bone affinity of modified and unmodified polymers

[94]. In addition, PEI and other cationic polymers are associated with toxicity *in vivo* [95,96].

Recently, modified PEI was used for the development of bone-seeking radiopharmaceuticals. To this end, PEI was functionalized with methylene phosphonate groups, thereby incorporating targeting and metal chelating ability in the polymer itself. *In vitro* tests demonstrated that fractionated *N,N',N'*-trimethylenephosphonate-poly(ethyleneimine) (PEI-MP) was able to carry radioactive tin ions to an HAp surface and then release them upon contact. By doing so, PEI-MP may work well as an imaging agent and as a possible radiotherapy delivery agent for metastatic bone cancer [97,98]. As such, prevention of any biocompatibility issues may be avoided by integrating PEI-MP into a block-copolymer of a more biocompatible polymer.

1.3.3.1.2 Poly[*N*-(2-hydroxypropyl)methacrylamide]

HPMA is one of the more studied polymer therapeutics to bone. PolyHPMA's biodistribution and bone-targeting abilities have been well documented and are discussed throughout this paper [58-60,80,81]. Other advantages of HPMA copolymers include a low toxicity profile and the ability to control the molecular weight and therefore biodistribution by RAFT polymerization [99-101]. This process also permits the incorporation of methacryloylated drug derivatives into the polymer by copolymerization [99,100], eliminating the chance of having unreacted (residual) groups remaining on the polymer backbone after postpolymerization modification. HPMA copolymers have also been used in the design of micelles [102,103] and dendrimers [104].

1.3.3.1.3 Other polymer carriers

Korzhikov et al. synthesized aldehyde-containing copolymers based on 2-deoxy-2-methacrylamido-D-glucose (MAG). Two methods were used for the introduction of aldehyde groups into the polysaccharide chains: i) copolymerization of MAG with *N*-vinylpyrrolidone and a comonomer that can be easily converted to an aldehyde, such as diethylacetal acrolein; and ii) the periodate oxidation of the saccharide units. The water-soluble polymers adsorbed on HAp. The ultimate aim is to use these polymers for construction of composite scaffolds for tissue regeneration [105].

Wang and coworkers synthesized a polyrotaxane delivery system targeted by ALN. They conjugated ALN to α-cyclodextrin and threaded it onto PEG (2000 mol. wt.) producing a pseudopolyrotaxane. Then, employing copper(I)-catalyzed Huisgen 1,3-dipolar cycloaddition, the pseudopolyrotaxane was copolymerized with bulky monomers containing imaging and/or therapeutic agents. The osteotropicity of the constructs was confirmed *in vivo* [106].

1.3.3.2 Vesicular polymer carriers

1.3.3.2.1 Micelles and liposomes

Micelles and liposomes are able to hold a great deal of drug when compared to linear polymers due to their three-dimensional shape. Although *in vivo* stability may be an issue for many polymeric spherical micelles and liposomes, these delivery systems are able to release their contents over long periods of time [107,108]. Finally, as alluded to before, this class of drug carriers may be able to protect drugs they carry from proteasomal degradation as well as protect the body from nontargeted effects of the

drugs.

Critical to their success, bone-targeted liposomes are able to retain their targeting ability. Hengst et al. designed a 1,2-diacyl-*Sn*-glycero-3-phosphocholine (EPC) liposome containing a BP targeting agent anchored by cholesterol. Each of the four conjugates tested had a low polydispersity of ≤0.1. Mole percents of the targeting ligand, cholesteryl-trisoxyethylene-bisphosphonic acid (CHOL-TOE-BP), were 0%, 3%, 14%, and 25% with zeta potentials of -18 ± 2, -28± 1, -34± 2, and -40± 2, respectively. The determination of the binding of each liposome revealed that 50% HAp binding was achieved using the 3 mol% CHOL-TOE-BP and binding progressed nearly linearly until 100% binding was achieved using the 25 mol% CHOL-TOE-BP liposome. This data suggests the bone targeting potential of this liposome [109].

Uludağ and coworkers incorporated BP-derivatized liposomes into collagen/hydroxyapatite scaffolds and decreased the rate of model drug release from the constructs. This provides a sustained drug release approach for bone regeneration [107].

The liposomal drug formulations for the treatment of rheumatoid arthritis vary from the scope of this chapter but have been recently reviewed [110].

1.3.3.2.2 Poly(lactic-co-glycolic acid)(PLGA) nanospheres

Poly(lactic-co-glycolic acid)(PLGA) nanospheres are a well-studied drug delivery modality that has been applied to bone targeting. Choi et al. designed PEG-PLGA block copolymers intermixed with ALN-functionalized PLGA to create surface-modified nanoparticles. The monomethoxy PEG formed a hydrophilic layer on the surface of nanoparticles with the potential to decrease MPS accumulation, and ALN was used as the

targeting moiety. The study of the relationship between structure and adsorption on HAp revealed decreasing adsorption correlated with a decreasing concentration on ALN at the surface; the increase in PEG mol. wt. (550, 750, and 2000) resulted in decreased adsorption apparently due to shielding of the ALN moieties by longer PEG chains [41]. As PLGA degradation yields naturally occurring products, it also has a low toxicity profile. Cenni et al. were able to synthesize ALN-functionalized nanospheres with a polydispersity index of 0.348 ± 0.020 nm and test their toxicity. Each *in vitro* test (hemolysis, leukocyte proliferation, platelet number, coagulation, and complement consumption) showed acceptable blood compatibility and an absence of cytotoxicity [111]. In follow-up studies, the authors loaded ALN-functionalized PLGA nanoparticles with doxorubicin (DOX) and evaluated their properties in an orthotopic mouse model of breast cancer bone metastases. Both free DOX and DOX-loaded nanoparticles reduced the occurrence of metastases in mice. Loaded and drug-free nanoparticles decreased the number of osteoclasts at the tumor site; the authors hypothesized that this may be the result of ALN activity [112].

Other advantages of PLGA include well-studied drug release kinetics. By modification of lactic glycolic acid ratios, PLGA nanospheres can release their contents over a wide time scale [113-115]. More *in vivo* tests such as bone targeting and whole body biodistribution are needed, however, in order to truly determine the efficacy of these targeted polymeric delivery systems.

1.3.3.2.3 Other vesicular structures

Ozcan et al. used nanoprecipitation to produce poly(γ-benzyl-L-glutamate) (PLGB) nanoparticles (< 80 nm; low polydispersity), which were functionalized with PEG-ALN for bone targeting. ALN presence did increase bone targeting dramatically *in vivo*. By labeling the PBLG-PEG-ALN nanospheres with FITC, Ozcan et al. were able to demonstrate preferential accumulation of targeted drug in bone [116].

Wang et al. evaluated bovine serum albumin (BSA) nanoparticles surface-coated with PEI-PEG-thiolBP and used them for the delivery of bone morphogenetic protein-2 (BMP-2). They found that the nanoparticles were not effective in bone targeting after i.v. administration. However, they were useful in localized delivery of BMP-2 in bone repair and regeneration [117].

1.3.4 Dendrimers, dendrons, dendronized polymers

Dendrimers are symmetrical vesicular carriers, whereas dendrons are tree-like fragments of dendrimers that can be attached to water-soluble polymers [118]. Thus, the "dendron-like" systems possess complex structures characterized by high density of functional groups and/or targeting moieties. Ideally (without structural defects), dendrimers are monodisperse, spherical compounds. Their size depends on the generation, i.e., the number of successive synthetic steps used. Numerous attempts have been made to exploit dendrimers in drug delivery, including targeting to bone. Ouyang et al. synthesized naproxene containing polyamide and poly-ether-amide dendrimers and decorated them with 2 or 3 $Asp_{(4-6)}$ peptides and demonstrated affinity for HAp [52]. In the following study the same group synthesized the "next generation" of naproxene

containing dendritic compounds with four or eight $Asp_{(4-6)}$ fragments. They did not observe a difference in HAp binding of constructs containing low or high $Asp_{(4-6)}$ content, and the total HAp binding only ranged from 63% to 75% [119]. Clementi et al. synthesized PEG-based dendrimers from heterobifunctional PEG; they were decorated with H_2N-PEG-b-Glu-(b-Glu)$_2$-$(COOH)_4$, exposing four carboxylic groups for the attachment of ALN and/or paclitaxel. This construct was able to achieve nearly 100% HAp binding and nearly 80% HAp binding following conjugation to paclitaxel (PTX). These conjugates were designed for the treatment of bone neoplasms and used a pH-sensitive linker for rapid release of the drug. *In vitro* studies demonstrated that drug release was highly effective, resulting in conjugated PTX having a similar IC_{50} as PTX alone, apparently due to fast drug release at physiological pH [120].

1.3.5 Vesicular vs. linear polymer carriers

The decision to use a spherical or linear polymer depends on the application. Both types can be designed so that they release drugs rapidly. Longer periods of time (such as a day to a week) may be achieved using linear polymers conjugated to drugs via enzyme-degradable linkers. For periods over a week, spherical polymers may be designed to release drug as the polymer degrades. The question then arises as to which yields better targeting and how it affects the treatment of disease. This may be answered by looking at zeta potentials. Excess surface charge is associated with high MPS uptake [121]. This means that for a specific polymer at a specific hydrodynamic radius, the addition of surface charge, in this case as a targeting moiety, could increase MPS uptake. As such, linear polymers may have an advantage. Linear polymers are able to bend and conform

to a surface, thereby reducing the number of targeting moieties needed to achieve bone specificity. Spherical polymers, on the other hand, have a three-dimensional shape, which reduces the amount of surface that can bind to bone, thereby increasing the need for several targeting moieties and increasing the zeta potential. Though this theory needs to be tested, one may consider that if MPS uptake does not contribute to a decrease in biocompatibility (such as with drugs that can be degraded by MPS lysosomes), then a spherical polymer as well as a linear polymer would work. However, if MPS uptake results in toxicity, as with nondegradable chemotherapeutics, then one may consider the use of a linear polymer over a spherical one.

1.4 Therapeutics

Life expectancy in the developed world continues to increase at a constant rate [122]. As such, age-related health complications also increase and the need for therapeutics to treat bone degenerative diseases and cancers expands. Critical to solving problems associated with bone disease is the selection of proper therapeutics. Bone disease causes a wide range of problems: too little bone growth, cancer and overgrowth, inflammation, and infection. In this paper, focus will be on bone anabolic agents (for osteoporosis) as well as cytotoxic agents (for cancer). Other topics, such as inflammation [123] and siRNA delivery to bone [124], are discussed in other reviews within this volume.

1.4.1 Osteoporosis and other low bone mineral density (BMD) related diseases

Osteoporosis is among the most common of the degenerative diseases. It is estimated that 1 out of 5 women over the age of 50 have osteoporosis and that approximately half of the women over 50 will fracture their hip, wrist or vertebra [125]. BPs, although helpful for some people, have several side effects, as described previously (section 2.3). Furthermore, a need exists for alternatives to Cat K and RANKL inhibitors [126-130]. Ultimately, these drugs yield inadequate bone turnover and therefore poor bone quality. The 1-34 fragment of recombinant parathyroid hormone (PTH), FDA approved in late 2002, is an effective bone anabolic agent. When compared to oral 10 mg/day ALN, the administration of s.c. injections 40 μg/day PTH yielded greater bone density [131]. However, there is a concern that lifelong injections may cause osteosarcomas to develop, and consequently, the drug may only be prescribed for 2 years during one's lifetime [132]. Other bone anabolic agents have also been investigated for treatment of osteoporosis but ultimately have significant drawbacks preventing their use. Prostaglandins are in clinical use for several medical conditions. In bone, they exhibit strong anabolic effects; however, the short half-life and serious cardiovascular side effects of free prostaglandins have prevented their use in osteoporosis. BMPs have been clinically applied to fuse vertebrae. BMPs have low systemic side effects, which may be in part due to their short blood half-life, which prohibits effective systemic administration. Targeting bone anabolic agents and/or extending their circulation half-life may open the door for new PTH alternatives.

1.4.2 Anabolic agents

Several potential bone anabolic agents exist. We will discuss their interactions in the hopes of elucidating possible synergistic mechanisms, which may be employed to create superdrugs (Figure 1.9).

1.4.2.1 Prostaglandins

Prostaglandins (PGEs), especially the E series (such as PGE_1 and PGE_2), have been studied extensively for their bone anabolic properties. Their importance in bone turnover is demonstrated by the lack of bone repair when patients are administered NSAIDs [133-137]. Systemically administered prostaglandins, however, cause diarrhea, lethargy, and flushing and thus are too toxic for nonlocal or nontargeted dosing [138]. Locally administered to bone, PGE affects osteoblasts by binding to four receptor subtypes (EP_{1-4}) of PGEs. EP_2 and EP_4 are the primary receptors associated with bone turnover; EP2 is normally associated with bone anabolism and EP_4 generally affects catabolism by upregulating RANKL through the MAPK pathway [139-143]. Both EP_2 and EP_4 have traditionally been associated with a dramatic increase in cAMP levels; however, these two receptors also contribute to the p38 MAPK and ERK MAPK signaling pathways, respectively [144]. There is also evidence that prostaglandins upregulate BMP-2 production [32]; however, another study contends that it is not through EP2 or EP4 [144].

Several studies have attempted to treat osteoporosis by either modification of PGE_2, making it specific for EP_2 or EP_4 receptors, or by conjugation to targeting moieties [59,138,145,146]. Miller et al. have attached PGE_1 via a Cat K sensitive spacer, Gly-Gly-Pro-Nle, to an HPMA copolymer (Mw 37.2 kDa), P-Asp_8-FITC-PGE_1.

Ovariectomized female Sprague-Dawley rats were administered a single i.v. bolus of either 10 mg P-FITC, P-Asp_8-FITC or P-Asp_8-FITC-PGE_1 (0.61 mg of PGE_1 equivalent), followed by a tetracycline label administration at the end of the study on day 25. Measuring the distance between the FITC-labeled polymer and the tetracycline label on the bone surface, they were able to determine the surface-referent bone formation rates ($\mu m^2\ \mu m^{-1}\ day^{-1}$). Bone deposition rates attributed to P-FITC, P-Asp_8-FITC or P-Asp_8-FITC-PGE_1 were 0.0362 ± 0.0062, 0.0541 ± 0.0108, and 0.1142 ± 0.0077, respectively, demonstrating the potential anabolic effects of targeted PGE_1 against osteoporosis [59].

1.4.2.2 Statins/bisphosphonates

Statins and BPs affect bone turnover by interacting with the mevalonic acid pathway and down-regulating protein prenylation. It is believed that down-regulating protein prenylation down-regulates RhoA and by so doing upregulates eNOS. The presence of eNOS increases synthesis of BMP-2 and therefore increases bone anabolism [147,148]. Furthermore, statins and BPs may also directly upregulate the PGE pathway, as COX-2 inhibitors dramatically reduce statin-induced bone anabolism by up to 77% [149]. Statins also induce VEGF, which contributes to osteoblast differentiation [150,151]. Statins, having been administered systemically for lowering cholesterol, also affect bone growth. Clinical evaluation of systemic delivery has shown no decrease in fractures, minimal increase in BMD, and no increase in bone turnover markers in postmenopausal women [152,153]; however, local administration in animals has shown significant bone turnover [33,154-158]. Systemic delivery of bone-targeted statins may increase local bone concentrations enough for higher BMD and bone turnover.

1.4.2.3 TGFβ superfamily

BMP-2 is a member of the TGFβ superfamily. It is produced by osteoclasts and the signal differentiation of osteoblasts through the SMAD5/8 pathway. SMAD5/8 combines with SMAD1 and translocates to the nucleus where Cbfa1/Runx2 is upregulated. CBFA1/Runx2 is responsible for promotion of several osteoblast differentiation genes as well as the upregulation of COX2 [159]. Although overlap can be seen in the two pathways, BMP-2 operates seperately from PGE. Research suggests that BMP-2 has a synergistic effect with PGE [160]. BMP-2 is clinically applied locally for spinal, oro-maxillary, and trauma surgeries [161-169]. Also part of the TGFβ superfamily, TGF-β1 and IGF-I are produced by osteoclasts [15] and affect transcription via several SMAD proteins. TGF-β1 and IGF-I activate NFκB, leading to increased levels of COX-2 and PGE2 production [170,171]. TGF-β1 is generally considered to inhibit osteoclasts, however, as with many growth hormones, their action is dose-dependent [172-174].

1.4.2.4 Fragment 1-34 of parathyroid hormone (PTH)

PTH1-34 (PTH contains 84 AA) is prescribed for treatment of osteoporosis. Systemically, PTH1-34 affects calcium resorption in the kidneys and intestine [175]. Within bone, PTH 1-34 affects osteoblasts and leads to increased cAMP/PKC production and differentiation even when COX-2 is inhibited [176]. Increased cAMP levels also open up calcium channels, leading to increased calcium levels in the cell. Consequently, the calcineurin pathway is triggered, which activates NFAT and yields increases in COX-2 expression [177]. Elevated levels of PTH1-34 reduce apoptosis by increasing PKC levels there by upregulating FOXO3a DNA repair mechanisms [178]. Overexpression of

cAMP/PKC leads to deleterious proteasomal (smurf1) degradation of CBFA1/Runx2, and therefore, regulation of BMP-2 effects [179-181]. Furthermore, proteosomal degradation will negate the anti-apoptotic effects of FOXO3a [182]. Therefore, intermittent administration of PTH1-34 leads to anabolism, while chronic administration leads to catabolism [183].

1.4.3 Delivery of proteins

Numerous attempts have been made to modify protein-based therapeutics with bone-seeking moieties to enhance their localization at skeletal sites [11,12,184]. Bansal et al. synthesized clustered BP-based targeting moieties composed of four bisphosphonic acid moieties linked through a benzene ring and conjugated them to bovine serum albumin (BSA) as a model protein. *In vitro* binding in both saline and 60% serum solutions resulted in less than 60% bound protein. However, *in vivo* results indicated a 4.7-fold increased accumulation in rat tibiae over controls (BSA and BSA targeted with a thiol-BP moiety). Thus the clustered BP possessed a considerably increased bone-seeking capacity *in vivo* when compared to HS-BP [185]. Interestingly, the accumulation of thiolBP modified osteoprotegerin in osteoarthritic rats undergoing active bone remodeling increased more than 4x over that of control unmodified OPG 24 h after i.v. administration [186].

Proteins such as BMP-2 have a circulation half-life of only about 1 min [187]. For successful systemic administration they may have to be modified by semitelechelic (ST) water-soluble polymers. It is well known that covalent attachment of PEG [188] or ST polyHPMA [189] may extend the intravascular half-life of proteins and/or vesicular drug

carriers.

1.4.4 Bone metastases

Paget's 1889 "seed and soil" theory of bone metastases remains the generally accepted theory regarding metastasis locating to bone. This theory simply reasons that as metastatic cells (the seeds) enter into the bloodstream they will be carried everywhere, but they will only attach and grow where the conditions are right (the soil) [190]. Examples of this include bone marrow expression of CXCL12 [191,192], whose complementary CXCR4 is found on several prostate and breast cancers [193-195]. Once in the bone, bone anabolism and catabolism causes patients severe bone pain and increased mortality [196]. Treatment of these metastases often involves small molecule therapeutics, which target various osteoclast mechanisms. Several small molecule osteoclast-targeted therapeutics have been studied: vacuolar H+-ATPase inhibitors, Reveromycin A, Methyl Gerfelin, C-Src Inhibitors, a_Vb_3 integrin inhibitors, Cat K inhibitors) [197] and BPs [50]. Although these do reduce bone pain and some degree of metastatic growth, their effects may be increased as other synergistic drugs are added to reduce growth and tumor progression.

As bone metastases progress, HAp is exposed, providing a target for BP attachment [198]. The Satchi-Fainaro group conducted several experiments combining the anti-angiogenic properties of ALN with other chemotherapies. Paclitaxel (PTX) has anti-angiogenic properties in low doses. They used ALN-targeted PTX containing HPMA copolymers to reduce migration and proliferation of human umbilical vein endothelial cells (HUVEC). Cat B is a protease expressed by both proliferating endothelial and

prostate cancer cells. Thus they incorporated a Cat B sensitive linker (GFLG) for both PTX and ALN. *In vitro* data suggest that the HPMA copolymer inhibited migration and proliferation of both human prostate adenocarcinoma (PC3) and HUVEC cells [199].

In a follow-up study, Miller et al. demonstrated the *in vivo* tumor inhibition and safety profiles on Balb/c mice. The PTX, ALN, HPMA copolymer showed no significant WBC toxicity, while free PTX significantly reduced WBC counts. Intratibial injections of mCherry-labeled 4T1 cells were used to mimic breast cancer metastasis to the bone. Following i.v. administration of either PTX, ALN HPMA copolymer or free PTX+ ALN in combination, the polymer conjugate inhibited tumor growth by 60%, while free PTX + ALN only inhibited 37% as compared to controls [200].

Segal et al. conducted a similar set of experiments using TNP-470 bound to an HPMA copolymer conjugate targeted with ALN. TNP-470 demonstrated high efficacy in clinical trials, but too many side effects prevented clinical applications [201]. Segal et al. sought to reduce TNP-470 side effects by conjugation and targeting. Both ALN and TNP-470 were conjugated to HPMA copolymer using Cat K sensitive linkers (Gly-Gly-Pro-Nle). *In vivo* studies demonstrated (Figure 1.10) that not only do ALN and TNP-470 have synergism, but revealed that the HPMA copolymer decreased osteosarcoma growth by 96% compared to the control, as opposed to 45% with free ALN in combo with TNP-470 [80]. Similar to the PTX, ALN, HPMA copolymer, TNP-470, ALN HPMA copolymer's toxicity is low, as opposed to ALN + TNP-470, which caused *in vivo* weight loss, neurological dysfunction, and low WBC counts [81].

1.4.5 Radiation therapy

Targeted delivery of radioisotopes provides opportunities to open up the field of theranostics. Several groups have effectively reduced tumor size and alleviated bone pain by radiolabeling BPs [202,203]. PEI-MP bound tin is one of the few studies which uses polymer attributes in radiation therapy to bone. Jansen et al. demonstrated effective HAp binding of Sn^{2+} and Sn^{4+} chelated PEI-MP. In order to demonstrate the EPR effect in combination with HAp adsorption, however, an *in vivo* study is still necessary [97,98]. Although more tests are needed in order to determine the efficacy of delivering radiolabeled polymers to bone metastases, one must still be curious about the possibilities. Although radioactive polymers may need to be kept small as to reduce circulation time, one may still see greater tumor accumulation due to the EPR effect. Furthermore, the dose can be increased with polymer therapeutics, as several chelating moieties can be attached to one molecule. Finally, a single polymer may be able to destroy cancer stem cells by radiosensitizing a tumor using a compound such as perifosin and then killing the stem cells using radiation [204].

1.5 Conclusions

Targeted polymer therapeutics continue to find niches in the medical world. Much of this research has focused on the EPR effect and delivery of chemotherapeutics and siRNA to solid tumors. Although this is excellent research, the characteristics of bone supply a fertile ground for future clinically relevant targeted polymer drug research. Many applications favor macromolecular drug delivery over small molecule drugs. For example, one must consider that achieving the highest binding constant possible may not

suit one's needs. Having an extremely low dissociation constant means that the polymer will most likely bind kinetically to the first bone that it comes in contact with. Modification of mole percent targeting ligands, or the ligand itself may reduce the K_d, thereby favoring thermodynamic adsorption over kinetic adsorption. By doing so, one may reduce promiscuity of the targeting ligand by limiting adsorption to the diseased area, such as a tumor. This method of targeting lends itself to targeted polymer therapeutics rather than their small molecule counterparts. Furthermore, many bone diseases are chronic conditions. Osteoporosis and osteoarthritis sufferers would benefit from extended controlled drug release mechanisms, which suit macromolecular drug delivery systems. As an underutilized application for targeted polymer drug delivery, bone-targeted polymer therapeutics have yet to reach their full potential.

1.5.1 Gaps in current research

Many novel bone-drug applications have yet to be explored, but first it is important to better develop disease-specific targeting and discover specific biochemical pathways involved in disease states. More accurate targeting to specific diseases involves finding out what bone conditions are present in each disease and then tailoring targeting mechanisms to those conditions. In this chapter we discussed several mechanisms by which modification of targeting mechanisms will lead to drug accumulation on varied HAp crystalline states. Currently, most papers stop prior to *in vivo* data, and pre-*in vivo* binding studies use a standard HAp. Appropriate pre-*in vivo* testing should include binding assays using HAp crystals sized for specific disease conditions. Information also lacking with regards to many bone diseases is a deep understanding of the pathology and

biochemistry that govern each disease. For example, this paper discussed some of the basic principles of bone anabolism affecting diseases such as osteoporosis. Some crosstalk between signaling pathways such as BMP-2 and PGEs were discussed, but great gaps in our knowledge remain. Studies such as Lee et al., where basic research on bone anabolic pathways are elucidated, can be performed side-by-side with applied research on discovering novel delivery approaches and are critical for progression of the field [115]. The realization of synergistic drugs delivered to bone depends on this basic research.

1.5.2 Future of the field

With attention to proper targeting techniques, bone-targeted therapeutics has several functions it can fulfill. Relatively few novel developments of bone-targeted antineoplastic agents delivered by polymers have been explored. Bone metastases are manifestations of severe cancers, representing a largely unsolved problem in oncology. As such, small improvements may go a long way in the clinic. As previously discussed, locally applied radiation therapy delivered with a sensitization drug, or two chemotherapeutics acting on different pathways are a good place to begin in solving this problem.

Combination therapies can also be applied to osteoporosis. It is clear that combining drugs such as BMP-2 and PGE2 is worth exploring, but dosing regimens may also yield some dogma-changing discoveries. Development of bone anabolic agents for the treatment of osteoporosis has always been a tricky balancing act. As seen with PTH1-34, overstimulation of an anabolic biological pathway over time can result in osteosarcoma. Reducing the chance of osteosarcoma may be accomplished by the

development of several targeted bone anabolic agents that affect different pathways and by applying them over different lengths of time, never exacerbating one particular pathway.

Lessons learned from targeting osteoporosis may then be applied to developing anabolic agents to aid healing following orthopedic surgeries and reduce long-term bone resorption around prosthetic stems. Furthermore, treatment of deep bone infections may be reduced by a pre- and postsurgery targeted antibiotic rather than antibiotic-loaded bone cements, which some argue have toxicity issues.

Bone diseases continue to increase in prevalence with aging populations. Successful advancements in bone-targeted polymer therapeutics will yield clinically relevant drugs that will reduce pain and increase quality of life for millions of people.

1.6 Statement of objectives

The primary objectives of the project are to develop a bone-targeted micellar drug delivery platform. This basic construct focuses on multifunctionality of each component to ensure simplicity of the final product. The targeting ligand aspartic acid octapeptide functions as both a targeting moiety as well as the corona of the micelle. In addition, the drug payload is covalently bound to the micelle by a hydrolyzable linker, and both functions as a therapeutic and stabilizes the micelle core. The micelle then features a flexible hydrophilic linker between the targeting ligand and a hydrophobic tail for increased stability. Our goal is to demonstrate this micelle construct's efficacy in osteosarcoma and bone fractures.

This project tested two main hypotheses:

1. The conjugation of a hydrophilic targeting ligand and a hydrophobic drug will self-assemble into a micelle.
2. Aspartic acid octapeptide has sufficient bone affinity to accumulate in a bone fracture callus.

In order to test these hypotheses the following specific aims were proposed:

1) Synthesize and characterize doxorubicin-containing micelles.
    a) Synthesize four micelles with varying unimer hydrophobicity and head group branching.
    b) Determine if the micelles provide sufficient size, shape, and stability for extended blood circulation.
    c) Measure the micelle's potential to bind to hydroxyapatite and release unmodified doxorubicin under desired stimuli.
2) Synthesize and characterize fracture-targeted micelles.
    a) Select two micelles from aim 1 and modify them with a bone anabolic agent.
    b) Confirm that the structure retains the ability to form micelles and release unmodified drug.
3) *In vivo* biodistribution and treatment.
    a) Radio-iodinate the drug on the micelles.
    b) Measure the micelles' biodistribution compared to free drug at 1 h, 4 h, and 24 h.
    c) Measure the micelles' ability to heal fractures against free drug and PBS control.

The Kopeček research group has extensive experience in macromolecular drug delivery,

including delivery to bone. The group's advances in treating osteoporosis has inspired interest in developing drug delivery systems aimed at other bone diseases. The theories tested in this dissertation were built on several of the concepts developed while studying osteoporosis, namely that aspartic acid octapeptide can target exposed hydroxyapatite, and that some bone anabolic agents elicit better responses when targeted by this method. In the following chapters we have demonstrated that in testing our main hypotheses by completing the designed aims that a micellar drug delivery system can be modified to accommodate treatment of multiple diseases. Furthermore, with very little development in targeting anabolic agents to bone fractures, these milestones are sufficient to command more development of the field.

1.7 References

[1] J.E. Shea, S.C. Miller, Skeletal function and structure: Implications for tissue-targeted therapeutics, Adv. Drug Delivery Rev. 57 (2005) 945-957.

[2] A.S. Posner, F. Betts, Synthetic amorphous calcium phosphate and its relation to bone mineral structure, Acc. Chem. Res. 8 (1975) 273-281.

[3] D. Wang, S.C. Miller, L.S. Shlyakhtenko, A.M. Portillo, X.-M. Liu, K. Papangkorn, P. Kopečková, Y. Lyubchenko, W.I. Higuchi, J. Kopeček, Osteotropic peptide that differentiates functional domains of the skeleton, Bioconjugate Chem. 18 (2007) 1375-1378.

[4] D. Lacey, E. Timms, H.L. Tan, M. Kelley, C. Dunstan, T. Burgess, R. Elliott, A. Colombero, G. Elliott, S. Scully, Osteoprotegerin ligand is a cytokine that regulates osteoclast differentiation and activation, Cell 93 (1998) 165–176.

[5] H. Yasuda, N. Shima, N. Nakagawa, K. Yamaguchi, M. Kinosaki, S. Mochizuki, A. Tomoyasu, K. Yano, M. Goto, A. Murakami, Osteoclast differentiation factor is a ligand for osteoprotegerin/osteoclastogenesis-inhibitory factor and is identical to TRANCE/RANKL, Proc. Natl. Acad. Sci. USA 95 (1998) 3597-3602.

[6] H. Väänänen, H. Zhao, M. Mulari, J.M. Halleen, The cell biology of osteoclast function, J. Cell Sci. 113 (2000) 377-381.

[7] S. Harada, Control of osteoblast function and regulation of bone mass, Nature 423 (2003) 349-355.

[8] R. Bartl, B. Frisch, C. Bartl, Osteoporosis: Diagnosis, Prevention, Therapy, Springer, 2009.

[9] D.W. Dempster, Osteoporosis and the burden of osteoporosis-related fractures, Am. J. Manag. Care 17 (2011) S164–S169.

[10] D. Wang, S.C. Miller, P. Kopečková, J. Kopeček, Bone-targeting macromolecular therapeutics, Adv. Drug Delivery Rev. 57 (2005) 1049-1076.

[11] S.A. Gittens, G. Bansal, R.F. Zernicke, H. Uludağ, Designing proteins for bone targeting, Adv. Drug Delivery Rev. 57 (2005) 1011-1036.

[12] H. Uludağ, J. Yang, Targeting systemically administered proteins to bone by bisphosphonate conjugation, Biotechnol. Prog. 18 (2002) 604-611.

[13] E. Segal, R. Satchi-Fainaro, Design and development of polymer conjugates as antiangiogenic agents, Adv. Drug Delivery Rev. 61 (2009) 1159-1176.

[14] K.A. Blackwell, L.G. Raisz, C.C. Pilbeam, Prostaglandins in bone: Bad cop, good cop?, Trends Endocrinol. Metab. 21 (2010) 294-301.

[15] K. Matsuo, N. Irie, Osteoclast-osteoblast communication, Arch. Biochem. Biophys. 473 (2008) 201-209.

[16] H. Maeda, G.Y. Bharate, J. Daruwalla, Polymeric drugs for efficient tumor-targeted drug delivery based on EPR-effect, Eur. J. Pharm. Biopharm. 71 (2009) 409-419.

[17] J. Fang, H. Nakamura, H. Maeda, The EPR effect: Unique features of tumor blood vessels for drug delivery, factors involved, and limitations and augmentation of the effect, Adv. Drug Delivery Rev. 63 (2010) 136-151.

[18] H. Maeda, Tumor-selective delivery of macromolecular drugs via the EPR effect: Background and future prospects, Bioconjugate Chem. 21 (2010) 797-802.

[19] V. Torchilin, Tumor delivery of macromolecular drugs based on the EPR effect, Adv. Drug Delivery Rev. 63 (2010) 131-135.

[20] D.U. Silverthorn, W.C. Ober, C.W. Garrison, A.C. Silverthorn, B.R. Johnson, Human Physiology: An Integrated Approach, Pearson/Benjamin Cummings, San Francisco, CA, 2004.

[21] M. Owen, C.R. Howlett, J.T. Triffitt, Movement of ^{125}I albumin and ^{125}I polyvinylpyrrolidone through bone tissue fluid. Calcif. Tissue Res. 23 (1977) 103-

112.

[22] C.R. Howlett, M. Dickson, A.K. Sheridan, The fine structure of the proximal growth plate of the avian tibia: vascular supply, J. Anat. 139 (Pt 1) (1984) 115-132.

[23] M.O. Griffin, G. Ceballos, F.J. Villarreal, Tetracycline compounds with non-antimicrobial organ protective properties: Possible mechanisms of action, Pharmacol. Res. 63 (2011) 102-107.

[24] Yu.P. Semenkov, E.M. Makarov, V.I. Makhno, S.V. Kirillov, Kinetic aspects of tetracycline action on the acceptor (A) site of Escherichia coli ribosomes, FEBS Lett. 144 (1982) 125-129.

[25] J.F. Madison, Tetracycline pigmentation of teeth, Arch. Dermatol. 88 (1963) 58-59.

[26] G. Lojodice, R. Vento, N.A. Cinque, G. Gilli, Effect on dental and skeletal development of administration of tetracycline in the infant, Minerva Pediatr. 17 (1965) 1358-1365.

[27] G. Bevelander, H. Nakahara, G.K. Rolle, Inhibition of skeletal formation in the chick embryo following administration of tetracycline, Nature 184(Suppl. 10) (1959) 728-729.

[28] D.D. Perrin, Binding of tetracyclines to bone, Nature 208 (1965) 787-788.

[29] J.R. Neale, N.B. Richter, K.E. Merten, K. Grant Taylor, S. Singh, L.C. Waite, N.K. Emery, N.B. Smith, J. Cai, W.M. Pierce Jr., Bone selective effect of an estradiol conjugate with a novel tetracycline-derived bone-targeting agent, Bioorg. Med. Chem. Lett. 19 (2009) 680–683.

[30] H. Fleisch, R.G. Russell, S. Bisaz, P.A. Casey, R.C. Mühlbauer, The influence of pyrophosphate analogues (diphosphonates) on the precipitation and dissolution, Calcif. Tissue Res. Suppl. (1968) 10-10a.

[31] K.L. Kavanagh, K. Guo, J.E. Dunford, X. Wu, S. Knapp, F.H. Ebetino, M.J. Rogers, R.G.G. Russel, U. Oppermann, The molecular mechanism of nitrogen-containing bisphosphonates as antiosteoporosis drugs, Proc. Natl. Acad. Sci. USA 103 (2006) 7829-34.

[32] J. Bradley, D. Cleverly, A. Burns, N. Helm, M. Schmid, D. Marx, D.M. Cullen, R.A. Reinhardt, Cyclooxygenase-2 inhibitor reduces simvastatin-induced bone morphogenetic protein-2 and bone formation in vivo, J. Periodontal Res. 42 (2007) 267–273.

[33] Y. Ayukawa, E. Yasukawa, Y. Moriyama, Y. Ogino, H. Wada, I. Atsuta, K.

Koyano, Local application of statin promotes bone repair through the suppression of osteoclasts and the enhancement of osteoblasts at bone-healing sites in rats, Oral Surgery, Oral Medicine, Oral Pathology, Oral Radiology, Endodontology 107 (2009) 336–342.

[34] K. Ohnaka, S. Shimoda, H. Nawata, H. Shimokawa, K. Kaibuchi, Y. Iwamoto, R. Takayanagi, Pitavastatin enhanced BMP-2 and osteocalcin expression by inhibition of Rho-associated kinase in human osteoblasts, Biochem. Biophys. Res. Commun. 287 (2001) 337–342.

[35] D.M. Black, S.R. Cummings, Randomised trial of effect of alendronate on risk of fracture in women with existing vertebral fractures, Lancet 348 (1996) 1535-1541.

[36] A. Arkader, C.D. Morris, Lymphatic spread of pagetic osteogenic sarcoma detected by bone scan, Cancer Imaging 8 (2008) 131-134.

[37] M.A. Lawson, Z. Xia, B.L. Barnett, J.T. Triffitt, R.J. Phipps, J.E. Dunford, R.M. Locklin, F.H. Ebetino, R.G. Russell, Differences between bisphosphonates in binding affinities for hydroxyapatite, J. Biomed. Mater. Res. Part B: Appl. Biomat. 92B (2010) 149-155.

[38] W. Jahnke, C. Henry, An in vitro assay to measure targeted drug delivery to bone mineral, Chem. MedChem. 5 (2010) 770–776.

[39] D. Wen, L. Qing, G. Harrison, E. Golub, S. Akintoye, Anatomic site variability in rat skeletal uptake and desorption of fluorescently labeled bisphosphonate, Oral Diseases 4 (2010) 427-432.

[40] M. Hrubý, T. Etrych, J. Kučka, M. Forsterová, K. Ulbrich, Hydroxybisphosphonate-containing polymeric drug-delivery systems designed for targeting into bone tissue, J. Appl. Polymer Sci. 101 (2006) 3192–3201.

[41] S.-W. Choi, J.-H. Kim, Design of surface-modified poly(D,L-lactide-*co*-glycolide) nanoparticles for targeted drug delivery to bone, J. Control. Release 122 (2007) 24-30.

[42] S. Mukherjee, Thermodynamics of bisphosphonates binding to human bone: a two-site model, J. Am. Chem. Soc. 131 (2009) 8374-8375.

[43] R.D. Ross, R.K. Roeder, Binding affinity of surface functionalized gold nanoparticles to hydroxyapatite, J. Biomed. Mater. Res. Part A 99A (2011) 58-66.

[44] G. Franc, C.O. Turrin, E. Cavero, J.P. Costes, C. Duhayon, A.M. Caminade, J.P. Majoral, gem-Bisphosphonate-ended group dendrimers: Design and gadolinium complexing properties, Europ. J. Org. Chem. 2009? (2009) 4290–4299.

[45] X.H. Shao, J.Q. Xu, Y.P. Jiao, C.R. Zhou, Synthesis and characterization of an alendronate-chitosan conjugate, Appl. Mechanics Mater. 140 (2012) 53–57.

[46] M.R. Doschak, C.M. Kucharski, J.E. Wright, R.F. Zernicke, H. Uludağ, Improved bone delivery of osteoprotegerin by bisphosphonate conjugation in a rat model of osteoarthritis, Mol. Pharmaceutics 6 (2009) 634–640.

[47] T. Ziebart, A. Pabst, M.O. Klein, P. Kämmerer, L. Gauss, D. Brüllmann, B. Al-Nawas, C. Walter, Bisphosphonates: restrictions for vasculogenesis and angiogenesis: Inhibition of cell function of endothelial progenitor cells and mature endothelial cells in vitro, Clin. Oral Invest. 15 (2009) 105-111.

[48] R.E. Marx, Y. Sawatari, M. Fortin, V. Broumand, Bisphosphonate-induced exposed bone (osteonecrosis/osteopetrosis) of the jaws: Risk factors, recognition, prevention, and treatment, J. Oral Maxillofacial Surg. 63 (2005) 1567–1575.

[49] A. O Hoff, B.B. Toth, K. Altundag, M.M. Johnson, C.L. Warneke, M. Hu, A. Nooka, G. Sayegh, V. Desrouleaux, J. Cui, A. Adamus, R.F. Gagel, G.N. Hortobagyi, Frequency and risk factors associated with osteonecrosis of the jaw in cancer patients treated with intravenous bisphosphonates, J. Bone Miner. Res. 23 (2008) 826-836.

[50] E.E. Prommer, Toxicity of bisphosphonates, J. Palliative Med. 12 (2009) 1061–1065.

[51] J. Ishizaki, Selective drug delivery to bone using acidic oligopeptides, J. Bone Miner. Metabol. 27 (2009) 1-8.

[52] L. Ouyang, W. Huang, G. He, L. Guo, Bone targeting prodrugs based on peptide dendrimers, Synthesis and hydroxyapatite binding in vitro, Lett. Org. Chem. 6 (2009) 272-277.

[53] T. Sekido, N. Sakura, Y. Higashi, K. Miya, Y. Nitta, M. Nomura, H. Sawanishi, K. Morito, Y. Masamune, S. Kasugai, K. Yokogawa, K. Miyamoto, Novel drug delivery system to bone using acidic oligopeptide: pharmacokinetic characteristics and pharmacological potential, J. Drug Target. 9 (2001) 111-121.

[54] J.R. Neale, N.B. Richter, K.E. Merten, K.G. Taylor, S. Singh, L.C. Waite, N.K. Emery, B. Smith, J. Cai, W.M. Pierce, Jr., Bone selective effect of an estradiol conjugate wih a novel tetracycline-derived bone-targeting agent, Bioorg. Med. Chem. Lett. 19 (2009) 680-683.

[55] S. Nasim, A. Vartak, W.M. Pierce, Jr., K.G. Taylor, P.A. Crooks, Improved and scalable synthetic route to the synthon 17-(2-carboxyethyl)-1,3,5 (10)-estratriene: An important itermediate in the synthesis of bone-targeting estrogens, Synth. Commun. 40 (2010) 772-781.

[56] S. Nasim, A.P. Vartak, W.M. Pierce, Jr., K.G. Taylor, N. Smith, P.A. Crooks, 3-O-Phosphate ester conjugates of 17-b-O-{1-[2-carboxy-(2-hydroxy-4-methoxy-3-carboxamido) anilido]ethyl}1,3,5(10)-estratriene as novel bone-targeting agents, Bioorg. Med. Chem. Lett. 20 (2010) 7450-7453.

[57] M.B. Murphy, Synthesis and in vitro hydroxyapatite binding of peptides conjugated to calcium-binding moieties, Biomacromolecules 8 (2007) 2237-2243.

[58] D. Wang, M. Sima, R.L. Mosley, J.P. Davda, N. Tietze, S.C. Miller, P.R. Gwilt, P. Kopečková, J. Kopeček, Pharmacokinetic and biodistribution studies of a bone-targeting drug delivery system based on *N*-(2-hydroxypropyl)methacrylamide copolymers, Mol. Pharmaceutics 3 (2006) 717–725.

[59] S. Miller, H. Pan, D. Wang, B. Bowman, P. Kopečková, J. Kopeček, Feasibility of using a bone-targeted, macromolecular delivery system coupled with prostaglandin E_1 to promote bone formation in aged, estrogen-deficient rats, Pharmaceutical Res. 25 (2008) 2889-2895.

[60] H. Pan, M. Sima, P. Kopečková, K. Wu, S. Gao, J. Liu, D. Wang, S.C. Miller, J. Kopeček, Biodistribution and pharmacokinetic studies of bone-targeting *N*-(2-hydroxypropyl)methacrylamide copolymer-alendronate conjugates, Mol. Pharmaceutics 5 (2008) 548-558.

[61] E.M. Noh, J.S. Kim, H. Hur, B.H. Park, E.K. Song, M.K. Han, K.B Kwon, W.H. Yoo, I.K. Shim, S.J. Lee, Cordycepin inhibits IL-1β-induced MMP-1 and MMP-3 expression in rheumatoid arthritis synovial fibroblasts, Rheumatology 48 (2009) 45-48.

[62] F. Hu, C. Wang, S. Guo, W. Sun, D. Mi, Y. Gao, J. Zhang, T. Zhu, S. Yang, δEF1 promotes osteolytic metastasis of MDA-MB-231 breast cancer cells by regulating MMP-1 expression, Biochim. Biophys.Acta-Gene Reg. Mech. 1809 (2011) 200-210.

[63] J.S. Nyman, C.C. Lynch, D.S. Perrien, S. Thiolloy, E.C. O'Quinn, C.A. Patil, G.M. Pharr, A. Mahadevan-Jansen, G.R. Mundy, Differential effects between the loss of MMP-2 and MMP-9 on structural and tissue-level properties of bone, J. Bone Mineral Res. 26 (2011) 1252–1260.

[64] H. Takaishi, T. Kimura, S. Dalal, Y. Okada, J. D'Armiento, Joint diseases and matrix metalloproteinases: a role for MMP-13, Curr. Pharmaceutical Biotech. 9 (2008) 47–54.

[65] G.C.N. Franco, M. Kajiya, T. Nakanishi, K. Ohta, P.L. Rosalen, F.C. Groppo, C.W.O. Ernst, J.L. Boyesen, J.D. Bartlett, P. Strashenko, Inhibition of matrix metalloproteinase-9 activity by doxycycline ameliorates RANK ligand-induced

osteoclast differentiation in vitro and in vivo, Exp. Cell Res. 317 (2011) 1454-1464.

[66] R.A. Mosig, O. Dowling, A. DiFeo, M.C.M. Ramirez, I.C. Parker, E. Abe, J. Diouri, A.A. Aqeel, J.D. Wylie, S.A. Oblander, Loss of MMP-2 disrupts skeletal and craniofacial development and results in decreased bone mineralization, joint erosion and defects in osteoblast and osteoclast growth, Human Mol. Genetics 16 (2007) 1113-1123.

[67] C.C. Lynch, A. Hikosaka, H.B. Acuff, M.D. Martin, N. Kawai, R.K. Singh, T.C. Vargo-Gogola, J.L. Begtrup, B. Fingleton, MMP-7 promotes prostate cancer-induced osteolysis via the solubilization of RANKL, Cancer Cell 7 (2005) 485–496.

[68] S.H. Mun, H.S. Kim, J.W. Kim, N.Y. Ko, D.K. Kim, B.Y. Lee, B. Kim, H.S. Won, H.S. Shin, J.W. Han, Oral administration of curcumin suppresses production of matrix metalloproteinase (MMP)-1 and MMP-3 to ameliorate collagen-induced arthritis: Inhibition of the PKCδ/JNK/c-Jun Pathway, J. Pharmacol. Sci. 111 (2009) 13–21.

[69] X.H. Luo, L.J. Guo, P.F. Shan, H. Xie, X.P. Wu, H. Zhang, X.Z. Cao, L.Q. Yuan, E.Y. Liao, Relationship of circulating MMP–2, MMP–1, and TIMP–1 levels with bone biochemical markers and bone mineral density in postmenopausal Chinese women, Osteoporosis Int. 17 (2006) 521–526.

[70] C. Gwack, S.S. Kim, S.B. Park, W.S. Son, Y.D. Kim, E.S. Jun, M.H. Park, The expression of MMP-1,-8, and-13 mRNA in the periodontal ligament of rats during tooth movement with cortical punching, Korean J. Orthodontics 38 (2008) 187–201.

[71] C.C. Lynch, L.M. Matrisian, Matrix metalloproteinases as key regulators of tumor–bone interaction, Cancer Degradome (2008) 541–566.

[72] G.N. Smith, E.A. Mickler, K.A. Hasty, K.D. Brandt, Specificity of inhibition of matrix metalloproteinase activity by doxycycline: relationship to structure of the enzyme, Arthritis Rheum. 42 (1999) 1140-1146.

[73] S. Georges, C. Ruiz Velasco, V. Trichet, Y. Fortun, D. Heymann, M. Padrines, Proteases and bone remodeling, Cytokine Growth Factor Rev. 20 (2009) 29–41.

[74] P. Rejmanová, J. Pohl, M. Baudyš, V. Kostka, J. Kopeček, Polymers containing enzymatically degradable bonds. 8. Degradation of oligopeptide sequences in *N*-(2-hydroxypropyl)methacrylamide copolymers by bovine spleen cathepsin B, Makromol. Chem. 184 (1983) 2009-2020.

[75] S. Gao, Z.R. Lu, B. Petri, P. Kopečková, J. Kopeček, Colon-specific 9-

aminocamptothecin-HPMA copolymer conjugates containing a 1,6-elimination spacer, J. Control. Release 110 (2006) 323-331.

[76] R.B. Greenwald, A. Pendri, C.D. Conover, H. Zhao, Y.H. Choe, A. Martinez, K. Shum, S. Guan, Drug delivery systems employing 1,4- or 1,6-elimination: Poly(ethylene glycol) prodrugs of amine-containing compounds, J. Med. Chem. 42 (1999) 3657-3667.

[77] P.L. Carl, P.K. Chakravarty, J.A. Katzenellenbogen, A novel connector linkage applicable in prodrug design, J. Med. Chem. 24 (1981) 479-480.

[78] B.E. Toki, C.G. Cerveny, A.F. Wahl, P. D. Senter, Protease-mediated fragmentation of p-amidobenzyl ethers: A new strategy for the activation of anticancer prodrugs, J. Org. Chem. 67 (2002) 1866-1872.

[79] F.M. de Groot, W.J. Loos, R. Koekkoek, L.W. van Berkom, G.F. Busscher, A.E. Seelen, C. Albrecht, P. de Bruijn, H.W. Scheeren, Elongated multiple electronic cascade and cyclization spacer systems in activatible anticancer prodrugs for enhanced drug release, J. Org. Chem. 66 (2001) 8815-8830.

[80] E. Segal, H. Pan, P. Ofek, T. Udagawa, P. Kopečková, J. Kopeček, R. Satchi-Fainaro, Targeting angiogenesis-dependent calcified neoplasms using combined polymer therapeutics, PLoS One 4 (2009) e5233.

[81] E. Segal, H. Pan, L. Benayoun, P. Kopečková, Y. Shaked, J. Kopeček, R. Satchi-Fainaro, Enhanced anti-tumor activity and safety profile of targeted nano-scaled HPMA copolymer-alendronate-TNP-470 conjugate in the treatment of bone malignances, Biomaterials 32 (2011) 4450-4463.

[82] K. Miller, R. Erez, E. Segal, D. Shabat, R. Satchi-Fainaro, Targeting bone metastases with a bispecific anticancer and antiangiogenic polymer-alendronate-taxane conjugates, Ang. Chem. Int. Ed. 48 (2009) 2949-2954.

[83] J. Yang, H. Chen, I.R. Vlahov, J.-X. Cheng, P.S. Low, Evaluation of disulfide reduction during receptor-mediated endocytosis by using FRET imaging, Proc. Natl. Acad. Sci. USA 103 (2006) 13872-13877.

[84] Y.E. Kurtoglu, R.S. Navath, B. Wang, S. Kannan, R. Romero, R.M. Kannan, Poly(amidoamine) dendrimer-drug conjugates with disulfide linkages for intracellular drug delivery, Biomaterials 30 (2009) 2112-2121.

[85] S.A. Nesbitt, M.A. Horton, Trafficking of matrix collagens through bone-resorbing osteoclasts, Science 276 (1997) 266-273.

[86] H. Palokangas, M. Mulari, H.K. Väänänen, Endocytic pathway from basal plasma membrane to the ruffled border membrane in bone-resorbing osteoclasts, J. Cell

Sci. 110 (1997) 1767-1780.

[87] M.T.K. Mulari, H.B. Zhao, P.T. Lakkakorpi, H.K. Väänänen (2003) Osteoclast ruffled border has distinct subdomains for secretion and degraded matrix uptake, Traffic 4 (2003) 113-125.

[88] H. Pan, P. Kopečková, D. Wang, J. Yang, S. Miller, J. Kopeček, Water-soluble HPMA copolymer—prostaglandin E1 conjugates containing a cathepsin K sensitive spacer, J. Drug Target. 14 (2006) 425-435.

[89] I. Schechter, A. Berger, On the size of active site in proteases. I. Papain, Biochem. Biophys. Res. Commun. 27 (1967) 157-162.

[90] F. Lecaille, Y. Choe, W. Brandt, Z. Li, C.S. Craik, D. Brömme, Selective inhibition of the collagenolytic activity of human cathepsin K by altering its S2 subsite specificity, Biochemistry 41 (2002) 8447-8454.

[91] P. Rejmanová, J. Kopeček, R. Duncan, J.B. Lloyd, Stability in rat plasma and serum of lysosomally degradable oligopeptide sequences in *N*-(2-hydroxypropyl)methacrylamide copolymers, Biomaterials 6 (1985) 45-48.

[92] J. Kopeček, P. Rejmanová, V. Chytrý, Polymers containing enzymatically degradable bonds. I. Chymotrypsin catalyzed hydrolysis of p-nitroanilides of phenylalanine and tyrosine attached to side-chains of copolymers of *N*-(2-hydroxypropyl)methacrylamide, Makromol. Chem. 182 (1981) 799-809.

[93] H. Pan, J. Liu, Y. Dong, M. Sima, P. Kopečková, M.L. Brandi, J. Kopeček, Release of prostaglandin E1 from *N*-(2-hydroxypropyl)methacrylamide copolymer conjugates by bone cells, Macromol. Biosci. 8 (2008) 599–605.

[94] S. Zhang, J.E.I. Wright, N. Ozber, H. Uludağ, The interaction of cationic polymers and their bisphosphonate derivatives with hydroxyapatite, Macromol. Biosci. 7 (2007) 656-670.

[95] Y. Wen, S. Pan, X. Luo, X. Zhang, W. Zhang, M. Feng, A biodegradable low molecular weight polyethylenimine derivative as low toxicity and efficient gene vector, Bioconjugate Chem. 20 (2009) 322–332.

[96] L. Aravindan, K.A. Bicknell, G. Brooks, V.V. Khutoryanskiy, A.C. Williams, Effect of acyl chain length on transfection efficiency and toxicity of polyethylenimine, Int. J. Pharmaceutics 378 (2009) 201–210.

[97] D.R. Jansen, J. Rijn Zeevaart, A. Denkova, Z.I. Kolar, G.C. Krijger, Hydroxyapatite chemisorption of *N,N′,N′*-trimethylenephosphonate−poly(ethyleneimine) (PEI−MP) combined with Sn2+ or Sn4+, Langmuir 25 (2009) 2790-2796.

[98] D.R. Jansen, G.C. Krijger, J. Wagener, R.M. Senwedi, K. Gabanamotse, M. Kgadiete, Z.I. Kolar, J.R. Zeevaart, Blood plasma model predictions for the proposed bone-seeking radiopharmaceutical [117mSn]Sn(IV)-*N,N',N'*-trimethylenephosphonate-poly(ethyleneimine), J. Inorganic Biochem. 103 (2009) 1265-1272.

[99] J. Yang, K. Luo, H. Pan, P. Kopečková, J. Kopeček, Synthesis of biodegradable multiblock copolymers by click coupling of RAFT-generated heterotelechelic polyHPMA conjugates, React. Funct. Polym. 71(2011) 294-302.

[100] H. Pan, J. Yang, P. Kopečková, J. Kopeček, Backbone degradable multiblock HPMA copolymer conjugates via RAFT polymerization and thiol-ene coupling reaction, Biomacromolecules 12 (2011) 247–252.

[101] K. Luo, J. Yang, P. Kopečková, J. Kopeček, Biodegradable multiblock *N*-(2-hydroxypropyl)methacrylamide copolymers via reversible addition-fragmentation chain transfer polymerization and click chemistry, Macromolecules 44 (2011) 2481-2488.

[102] M. Talelli, C.J.F. Rijcken, C.F. van Nostrum, G. Storm, W.E. Hennink, Micelles based on HPMA copolymers, Adv. Drug Delivery Rev. 62 (2010) 231-239.

[103] S. Krimmer, H. Pan, J. Liu, J. Yang, J. Kopeček, Synthesis and characterization of poly(e-caprolactone)-*block*-poly[*N*-(2-hydroxypropyl)methacrylamide] micelles for drug delivery, Macromol. Biosci. 11 (2011) 1041-1051.

[104] D. Wang, J.P. Kopečková, T. Minko, V. Nanayakkara, J. Kopeček, Synthesis of starlike *N*-(2-hydroxypropyl)methacrylamide copolymers: potential drug carriers, Biomacromolecules 1 (2000) 313-319.

[105] V.A. Korzhikov, S. Diederichs, O.V. Nazarova, E.G. Vlakh, C. Kasper, E.V. Panarin, T.B. Tennikova, Water-soluble aldehyde-bearing polymers of 2-deoxy-2-methacrylamido-D-glucose for bone tissue engineering, J. Appl. Polym. Sci. 108 (2008) 2386-2397.

[106] C.D. Hein, X.M. Liu, F. Chen, D.M. Cullen, D. Wang, The synthesis of a multiblock ostotropic polyrotaxane by copper(I)-catalyzed Huisgen 1,3-dipolar cycloaddition, Macromol. Biosci. 10 (2010) 1544-1556.

[107] G. Wang, M.E. Babadagli, H. Uludağ, Bisphosphonate-derivatized liposomes to control drug release from collagen/hydroxyapatite scaffolds, Mol. Pharmaceutics 8 (2011) 1025-1034.

[108] L.Y. Li, W.D. He, J. Li, B.Y. Zhang, T.T. Pan, X.L. Sun, Z.L. Ding, Shell-cross-linked micelles from PNIPAM-*b*-(PLL)2Y-shaped miktoarm star copolymer as drug carriers, Biomacromolecules 11 (2010) 1882-1890.

[109] V. Hengst, C. Oussoren, T. Kissel, G. Storm, Bone targeting potential of bisphosphonate-targeted liposomes: Preparation, characterization and hydroxyapatite binding in vitro, Int. J. Pharmaceutics 331 (2007) 224-227.

[110] J.M. van den Hoven, S. R. Van Tomme, J.M. Metselaar, B. Nuijen, J.H. Beijnen, G. Storm, Liposomal drug formulations in the treatment of rheumatoid arthritis, Mol. Pharmaceutics 8 (2011) 1002-1005.

[111] E. Cenni, D. Granchi, S. Avnet, C. Fotia, M. Salerno, D. Micieli, M.G. Sarpietro, R. Pignatello, F. Castelli, N. Baldini, Biocompatibility of poly(D,L-lactide-*co*-glycolide) nanoparticles conjugated with alendronate, Biomaterials 29 (2008) 1400-1411

.

[112] M. Salerno, E. Cenni, C. Fotia, S. Avnet, D. Granchi, F. Castelli, D. Micieli, R. Pignatello, M. Capulli, N. Rucci, A. Angelucci, A. Del Fattore, A. Teti, N. Zini, A. Giunti, N. Baldini, Bone-targeted doxorubicin-loaded nanoparticles as a tool for the treatment of skeletal metastases, Curr. Cancer Drug Targets 10 (2010) 649-659.

[113] C. Wischke, Y. Zhang, S. Mittal, S.P. Schwendeman, Development of PLGA-based injectable delivery systems for hydrophobic fenretinide, Pharmaceutical Res. 27 (2010) 2063-2074.

[114] N. Faisant, J. Siepmann, J.P. Benoit, PLGA-based microparticles: elucidation of mechanisms and a new, simple mathematical model quantifying drug release, Eur. J. Pharmaceutical Sci. 15 (2002) 355-366.

[115] R.C. Mundargi, V.R. Babu, V. Rangaswamy, P. Patel, T.M. Aminabhavi, Nano/micro technologies for delivering macromolecular therapeutics using poly(D,L-lactide-*co*-glycolide) and its derivatives, J. Control. Release 125 (2008) 193-209.

[116] I. Ozcan, K. Bouchemal, F. Segura-Sánchez, O. Ozer, T. Güneri, G. Ponchel, Synthesis and characterization of surface-modified PBLG nanoparticles for bone targeting: In vitro and in vivo evaluations, J. Pharmaceutical Sci. 100 (2011) 4877-87.

[117] G. Wang, C. Kucharski, X. Lin, H. Uludağ, Bisphosphonate-coated BSA nanoparticles lack bone targeting after systemic administration, J. Drug Target. 18 (2010) 611-626.

[118] S. Bai, C. Thomas, A. Rawat, F. Ahsan, Recent progress in dendrimer-based nanocarriers, Crit. Rev. Ther. Drug Carrier Syst. 23 (2006) 437-495.

[119] L. Ouyang, J. Pan, Y. Zhang, L. Guo, Synthesis of second-and third-generation Asp oligopeptide conjugated dendrimers for bone-targeting drug delivery, Synth.

Commun. 39 (2009) 4039–4052.

[120] C. Clementi, K. Miller, A. Mero, R. Satchi-Fainaro, G. Pasut, Dendritic poly(ethylene glycol) bearing paclitaxel and alendronate for targeting bone neoplasms, Mol. Pharmaceutics 8 (2011) 1063-1072.

[121] K. Xiao, Y. Li, J. Luo, J.S. Lee, W. Xiao, A.M. Gonik, R.G. Agarwai, K.S. Lam, The effect of surface charge on in vivo biodistribution of PEG-oligocholic acid based micellar nanoparticles, Biomaterials 32 (2011) 3435-3446.

[122] K. Christensen, G. Doblhammer, R. Rau, J.W. Vaupel, Ageing populations: the challenges ahead, Lancet 374 (2009) 1196-1208.

[123] F. Yuan, L.D. Quan, L. Cui, S. Goldring, D. Wang, Macromolecular prodrug delivery for arthritis, Adv. Drug Delivery Rev. 64 (2012) 1205-2019

[124] G. Grainger, RNA therapeutics targeting osteoclast-mediated excessive bone resorption, Adv. Drug Delivery Rev. 64 (2012) 1341-1357

[125] Osteoporosis information, available at, http://www.ncbi.nlm.nih.gov/pubmedhealth/PMH0001400, Accessed September 2011.

[126] S.K. Thompson, S.M. Halbert, M.J. Bossard, T.A. Tomaszek, M.A. Levy, B. Zhao, W.W. Smith, S.S. Abdel-Meguid, C.A. Janson, K.J. D'Alessio, M.S. McQueeney, B.Y. Amegadzie, C.R. Hanning, R.L. DesJarlais, J. Briand, S.K. Sarkar, M.J. Huddleston, C.F. Ijames, S.A. Carr, K.T. Garnes, A. Shu, R.J. Heys, J. Bradbeer, D. Zembryki, L. Lee-Rykaczeweski, I.E. James, M.W. Lark, F.H. Drake, M. Gowen, J.G. Cleason, D.F. Verber, Design of potent and selective human cathepsin K inhibitors that span the active site, Proc. Natl. Acad. Sci. USA 94 (1997) 14249 -14254.

[127] D. Wang, W. Li, M. Pechar, P. Kopečková, D. Brömme, J. Kopeček, Cathepsin K inhibitor–polymer conjugates: potential drugs for the treatment of osteoporosis and rheumatoid arthritis, Int. J. Pharmaceutics 277 (2004) 73-79.

[128] D. Wang, M. Pechar, W. Li, P. Kopečková, D. Brömme, J. Kopeček, Inhibition of cathepsin K with lysosomotropic macromolecular inhibitors, Biochem. 41 (2002) 8849–8859.

[129] S.K. Thompson, W.W. Smith, B. Zhao, S.M. Halbert, T.A. Tomaszek, D.G. Tew, M.A. Levy, C.A. Janson, K.J. DAlessio, M.S. McQueney, J. Kurdyla, C.S. Jones, R.L. DesJarlais, S.S. Abdel-Meguid, D.F. Veber, Structure-based design of cathepsin K inhibitors containing a benzyloxy-substituted benzoyl peptidomimetic, J. Med. Chem. 41 (1998) 3923-3927.

[130] S. Tanaka, Role of RANKL in physiological and pathological bone resorption and therapeutics targeting the RANKL–RANK signaling system, Immunol. Rev. 208 (2005) 30-49.

[131] J.J. Body, G.A. Gaich, W.H. Scheele, P.M. Kulkarni, P.D. Miller, A. Peretz, R.K. Dore, R. Correa-Rotter, A. Papaioannou, D.C. Cumming, A randomized double-blind trial to compare the efficacy of teriparatide [recombinant human parathyroid hormone (1–34)] with alendronate in postmenopausal women with osteoporosis, J. Clin. Endocrinol. Metabol. 87 (2002) 4528-4535.

[132] R. Okazaki, Osteosarcoma in rats receiving long-term PTH injection, Clin Calcium. 13 (2003) 42-44.

[133] D. Chikazu, Y. Fujikawa, H. Fujihara, H. Suenaga, H. Saijo, K. Ohkubo, T. Ohkubo, T. Ogasawara, Y. Mori, M. Iino, T. Takato, Cyclooxygenase-2 activity is important in craniofacial fracture repair, Int. J. Oral Maxillofac. Surg. 40 (2011) 322-326.

[134] L.C. Gerstenfeld, T.A. Einhorn, COX inhibitors and their effects on bone healing, Exp. Opin. Drug Safety 3 (2004) 131-136.

[135] K. Vuolteenaho, T. Moilanen, E. Moilanen, Non-steroidal anti-inflammatory drugs, cyclooxygenase-2 and the bone healing process, Basic Clin. Pharmacol. Toxicol. 102 (2008) 10-14.

[136] S.D. Glassman, S.M. Rose, J.R. Dimar, R.M. Puno, M.J. Campbell, J.R. Johnson, The effect of postoperative nonsteroidal anti-inflammatory drug administration on spinal fusion, Spine 23 (1998) 834-838.

[137] P. Giannoudis, D. MacDonald, S. Matthews, R. Smith, A. Furlong, P. De Boer, Nonunion of the femoral diaphysis: the influence of reaming and non-steroidal anti-inflammatory drugs, J. Bone Joint Surg. 82 (2000) 655-658.

[138] M. Li, H.Z. Ke, H. Qi, D.R. Healy, Y. Li, D.T. Crawford, V.M. Paralkar, T.A. Owen, K.O. Cameron, B.A. Lefker, A novel, non-prostanoid EP2 receptor-selective prostaglandin E2 agonist stimulates local bone formation and enhances fracture healing, J. Bone Mineral Res. 18 (2003) 2033–2042.

[139] M. Hirata, S. Harada, C. Matsumoto, M. Takita, C. Miyaura, M. Inada, Role of prostaglandin E in receptor activator of nuclear factor-κB ligand (RANKL) expression in osteoblasts induced by cell adhesion to bone marrow B-lymphocytes, J. Health Sci. 55 (2009) 832–837.

[140] R. Tsutsumi, C. Xie, X. Wei, M. Zhang, X. Zhang, L.M. Flick, E.M. Schwarz, R.J. O'Keefe, PGE2 signaling through the EP4 receptor on fibroblasts upregulates RANKL and stimulates osteolysis, J. Bone Mineral Res. 24 (2009) 1753–1762.

[141] J.Y. Park, M. Bae, H.G. Cheon, S.S. Kim, J.M. Hong, T.H. Kim, J.Y. Choi, S.H. Kim, J. Lim, C.H. Choi, A novel PPAR [gamma] agonist, KR62776, suppresses RANKL-induced osteoclast differentiation and activity by inhibiting MAP kinase pathways, Biochem. Biophys. Res. Commun. 378 (2009) 645–649.

[142] A. Idris, E. Mrak, I. Greig, F. Guidobono, S.H. Ralston, R. van't Hof, ABD56 causes osteoclast apoptosis by inhibiting the NFκB and ERK pathways, Biochem. Biophys. Res. Commun. 371 (2008) 94–98.

[143] H.Y. Tsai, H.Y. Lin, Y.C. Fong, J.B. Wu, Y.F. Chen, M. Tsuzuki, C.H. Tang, Paeonol inhibits RANKL-induced osteoclastogenesis by inhibiting ERK, p38 and NF-κB pathway, Eur. J. Pharmacol. 588 (2008) 124–133.

[144] T. Minamizaki, Y. Yoshiko, K. Kozai, J.E. Aubin, N. Maeda, EP2 and EP4 receptors differentially mediate MAPK pathways underlying anabolic actions of prostaglandin E2 on bone formation in rat calvaria cell cultures, Bone 44 (2009) 1177–1185.

[145] L. Gil, Y. Han, E.E. Opas, G.A. Rodan, R. Ruel, J.G. Seedor, P.C. Tyler, R.N. Young, Prostaglandin E2-bisphosphonate conjugates: Potential agents for treatment of osteoporosis, Bioorg. Med. Chem. 7 (1999) 901-919.

[146] P. Kamolratanakul, T. Hayata, Y. Ezura, A. Kawamata, C. Hayashi, Y. Yamamoto, H. Hemmi, M. Nagao, R. Hanyu, T. Natomi, T. Nakamoto, T. Amagasa, K. Akyoshi, M. Noda, Nanogel-based scaffold delivery of prostaglandin E2 receptor (EP4) specific agonist in combination with low dosage of growth factor heals critical size bone defect, Arthritis Rheumatism 10 (2010) 1-11.

[147] O. Fromigue, E. Hay, D. Modrowski, S. Bouvet, A. Jacquel, P. Auberger, P.J Marie, RhoA GTPase inactivation by statins induces osteosarcoma cell apoptosis by inhibiting p42/p44-MAPKs-Bcl-2 signaling independently of BMP-2 and cell differentiation, Cell Death Different. 13 (2006) 1845–1856.

[148] I. Kanazawa, T. Yamaguchi, S. Yano, M. Yamauchi, T. Sugimoto, Activation of AMP kinase and inhibition of Rho kinase induce the mineralization of osteoblastic MC3T3-E1 cells through endothelial NOS and BMP-2 expression, Am. J. Physiol. Endocrinol. Metabolism 296 (2009) E139 -E146.

[149] Y. Lee, X. Liu, A. Nawshad, D.B. Marx, D. Wang, R.A. Reinhardt, Role of prostaglandin pathway and alendronate-based carriers to enhance statin-induced bone, Mol. Pharmaceutics 8 (2011) 1035-1042.

[150] V. Midy, J. Plouët, Vasculotropin/vascular endothelial growth factor induces differentiation in cultured osteoblasts, Biochem. Biophys. Res. Commun. 199 (1994) 380-386.

[151] R.W.K. Wong, A.B.M. Rabie, Early healing pattern of statin-induced osteogenesis, Brit. J. Oral Maxillofacial Sur. 43 (2005) 46–50.

[152] B. Uzzan, R. Cohen, P. Nicolas, M. Cucherat, G.Y. Perret, Effects of statins on bone mineral density: A meta-analysis of clinical studies, Bone 40 (2007) 1581-1587.

[153] J. Yue, Statins and bone health in postmenopausal women: a systematic review of randomized controlled trials, Menopause 17 (2010) 1071-1079.

[154] Y. Moriyama, Y. Ayukawa, Y. Ogino, I. Atsuta, M. Todo, Y. Takao, K. Koyano, Local application of fluvastatin improves peri-implant bone quantity and mechanical properties: A rodent study, Acta Biomater. 6 (2010) 1610–1618.

[155] D. Stein, Y. Lee, M.J. Schmid, B. Killpack, M.A. Genrich, N. Narayana, D.B. Marx, D.M. Cullen, R.A. Reinhardt, Local simvastatin effects on mandibular bone growth and inflammation, J. Periodontology 76 (2005) 1861–1870.

[156] S. Pauly, F. Luttosch, M. Morawski, N. Haas, G. Schmidmaier, B. Wildemann, Simvastatin locally applied from a biodegradable coating of osteosynthetic implants improves fracture healing comparable to BMP-2 application, Bone 45 (2009) 505–511.

[157] T. Masuzaki, Y. Ayukawa, Y. Moriyama, Y. Jinno, I. Atsuta, Y. Ogino, K. Koyano, The effect of a single remote injection of statin-impregnated poly (lactic-co-glycolic acid) microspheres on osteogenesis around titanium implants in rat tibia, Biomaterials 31 (2010) 3327–3334.

[158] Y. Lee, M.J. Schmid, D.B. Marx, M.W. Beatty, D.M. Cullen, M.E. Collins, R.A. Reinhardt, The effect of local simvastatin delivery strategies on mandibular bone formation in vivo, Biomaterials 29 (2008) 1940–1949.

[159] D. Chikazu, X. Li, H. Kawaguchi, Y. Sakuma, O.S. Voznesensky, D.J. Adams, M. Xu, K. Hoshio, V. Katavic, H.R. Hershman, L.G. Raisz, C.C. Pilbeam, Bone morphogenetic protein 2 induces cyclo-oxygenase 2 in osteoblasts via a Cbfal binding site: role in effects of bone morphogenetic protein 2 in vitro and in vivo, J. Bone Mineral Res. 17 (2002) 1430-1440.

[160] K.A. Blackwell, P. Hortschansky, S. Sanovic, S. Choudhary, L.G. Raisz, C.C. Pilbeam, Bone morphogenetic protein 2 enhances PGE2 stimulated osteoclast formation in murine bone marrow cultures, Prostaglandins Other Lipid Mediat. 90 (2009) 76-80.

[161] P.V. Mummaneni, J. Pan, R.W. Haid, G.E. Rodts, Contribution of recombinant human bone morphogenetic protein-2 to the rapid creation of interbody fusion when used in transforaminal lumbar interbody fusion: a preliminary report, J.

Neurosurg. Spine 1 (2004) 19-23.

[162] J.D. Schwender, L.T. Holly, D.P. Rouben, K.T. Foley, Minimally invasive transforaminal lumbar interbody fusion (TLIF): technical feasibility and initial results, J Spinal Disord. Tech. 18 Suppl (2005) S1-6.

[163] D.S. Baskin, P. Ryan, V. Sonntag, R. Westmark, M.A. Widmayer, A prospective, randomized, controlled cervical fusion study using recombinant human bone morphogenetic protein-2 with the CORNERSTONE-SR allograft ring and the ATLANTIS anterior cervical plate, Spine 28 (2003) 1219-1224; discussion 1225.

[164] G.E. Riedel, A. Valentin-Opran, Clinical evaluation of rhBMP-2/ACS in orthopedic trauma: a progress report, Orthopedics 22 (1999) 663-665.

[165] S. Govender, C. Csimma, H.K. Genant, A. Valentin-Opran, Recombinant human bone morphogenetic protein-2 for treatment of open tibial fractures: a prospective, controlled, randomized study of four hundred and fifty patients, J. Bone Joint Surg. Am. 84-A (2002) 2123-2134.

[166] P.J. Boyne, R.E. Marx, M. Nevins, G. Triplett, E. Lazaro, L.C. Lilly, M. Alder, A feasibility study evaluating rhBMP-2/absorbable collagen sponge for maxillary sinus floor augmentation, Int. J. Periodontics Restorative Dent. 17 (1997) 11-25.

[167] R.W. Haid Jr, C.L. Branch Jr, J.T. Alexander, J.K. Burkus, Posterior lumbar interbody fusion using recombinant human bone morphogenetic protein type 2 with cylindrical interbody cages, Spine J. 4 (2004) 527-538; discussion 538-539.

[168] Y. Katayama, Y. Matsuyama, H. Yoshihara, Y. Sakai, H. Nakamura, S. Imagama, Z. Ito, N. Wakao, M. Kamiya, Y. Yukawa, Clinical and radiographic outcomes of posterolateral lumbar spine fusion in humans using recombinant human bone morphogenetic protein-2: An average five-year follow-up study, Int. Orthopaedics 33 (2009) 1061–1067.

[169] R.G. Triplett, M. Nevins, R.E. Marx, D.B. Spagnoli, T.W. Oates, P.K. Moy, P.J. Boyne, Pivotal, randomized, parallel evaluation of recombinant human bone morphogenetic protein-2/absorbable collagen sponge and autogenous bone graft for maxillary sinus floor augmentation, J. Oral Maxillofacial Surg. 67 (2009) 1947–1960.

[170] W. Shen, Interaction between macrophages, TGF-β1, and the COX-2 pathway during the inflammatory phase of skeletal muscle healing after injury, J. Cell Phys. 214 (2008) 405-412.

[171] Z. Niu, L. Wang, X. Hu, H. Wang, J. Ouyang, W. Huang, L. Yu, X, Qui, Promotion effect of nuclear factor kappa B p65 on early fracture healing of rat radius by elevating prostaglandins E2 production and regulating inhibitor of DNA

binding 2 protein expression, C. J. Repar. Recon. Surg. 25 (2011) 569-574.

[172] T. Yasui, Y. Kadono, M. Nakamura, Y. Oshima, T. Matsumoto, H. Masuda, J. Hirose, Y. Omata, H. Yasuda, T. Imamura, K. Nakamura, S. Tanaka, Regulation of RANKL-induced osteoclastogenesis by TGF-β through molecular interaction between Smad3 and Traf6, J. Bone Mineral Res. 26 (2011) 1447–1456.

[173] A. Gingery, E.W. Bradley, L. Pederson, M. Ruan, N.J. Horwood, M.J. Oursler, TGFβ coordinately activates TAK1/MEK/AKT/NFkB and SMAD pathways to promote osteoclast survival, Exp. Cell Res. 314 (2008) 2725–2738.

[174] N. Houde, E. Chamoux, M. Bisson, S. Roux, Transforming growth factor-beta1 (TGF-β1) induces human osteoclast apoptosis by up-regulating Bim, J. Biol. Chem. 284 (2009) 23397–23404.

[175] M.C. Peterson, M.M. Riggs, A physiologically based mathematical model of integrated calcium homeostasis and bone remodeling, Bone 46 (2010) 49–63.

[176] S. Choudhary, H. Huang, L. Raisz, C. Pilbeam, Anabolic effects of PTH in cyclooxygenase-2 knockout osteoblasts in vitro, Biochem. Biophys. Res. Commun. 372 (2008) 536-541.

[177] H. Huang, D. Chikazu, O.S. Voznesensky, H.R. Herschman, B.E. Kream, H. Drissi, C.C. Pilbeam, Parathyroid hormone induction of cyclooxygenase-2 in murine osteoblasts: role of the calcium-calcineurin-NFAT pathway, J. Bone Mineral Res. 25 (2010) 819-829.

[178] M. Schnoke, S.B. Midura, R.J. Midura, Parathyroid hormone suppresses osteoblast apoptosis by augmenting DNA repair, Bone 45 (2009) 590–602.

[179] Y. Tintut, F. Parhami, V. Le, G. Karsenty, L.L. Demer, Inhibition of osteoblast-specific transcription factor Cbfa1 by the cAMP pathway in osteoblastic cells, J. Biol. Chem. 274 (1999) 28875 -28879.

[180] M. Zhao, M. Qiao, B.O. Oyajobi, G.R. Mundy, D. Chen, E3 ubiquitin ligase Smurf1 mediates core-binding factor α1/Runx2 degradation and plays a specific role in osteoblast differentiation, J. Biol. Chem. 278 (2003) 27939 -27944.

[181] E.J.B. Murray, G.V. Bentley, M.S. Grisanti, S.S. Murray, The ubiquitin-proteasome system and cellular proliferation and regulation in osteoblastic cells, Exp. Cell Res. 242 (1998) 460–469.

[182] T. Bellido, A.A. Ali, L.I. Plotkin, Q. Fu, I. Gubrij, P.K. Roberson, R.S. Weinstein, C.A. O'Brien, S.C. Manolagas, R.L. Jilka, Proteasomal degradation of Runx2 shortens parathyroid hormone-induced anti-apoptotic signaling in osteoblasts, J. Biol. Chem. 278 (2003) 50259 -50272.

[183] R.L. Jilka, Molecular and cellular mechanisms of the anabolic effect of intermittent PTH, Bone 40 (2007) 1434-1446.

[184] S. Zhang, G. Gangal, H. Uludağ, "Magic bullets" for bone diseases: progress in rational design of bone-seeking medicinal agents, Chem. Soc. Rev. 36 (2007) 507-531.

[185] G. Bansal, J.E.. Wright, C. Kucharski, H. Uludağ, A dendritic tetra(bisphosphonic acid) for improved targeting of proteins to bone, Angew. Chem. Int. Ed. 44 (2005) 3710–3714.

[186] M.R. Doschak, C.M. Kucharski, J.E.I. Wright, R.F. Zernicke, H. Uludağ, Improved bone delivery of osteoprotegerin by bisphosphonate conjugation in a rat model of osteoarthritis, Mol. Pharmaceutics 6 (2009) 634-640.

[187] B. Vaibhav, P. Nilesh, S. Vikram, C. Anshul, Bone morphogenic protein and its application in trauma cases: a current concept update, Injury 38 (2007) 1227-1235.

[188] J.M. Harris, R.B. Chess, Effect of pegylation on pharmaceuticals, Nature Drug Disc. Rev. 2 (2003) 214-221.

[189] S. Kamei, J. Kopeček, Prolonged blood circulation in rats of nanospheres surface-modified with semitelechelic poly[*N*-(2-hydroxypropyl)methacrylamide], Pharmaceutical Res. 12 (1995) 663-668.

[190] G.A. Clines, T.A. Guise, Hypercalcaemia of malignancy and basic research on mechanisms responsible for osteolytic and osteoblastic metastasis to bone, Endocrine-Related Cancer 12 (2005) 549 -583.

[191] A. Schajnovitz, T. Itkin, G. D'Uva, A. Kalinkovich, K. Golan, A. Ludin, D. Cohen, Z. Shulman, A. Avigdor, A. Nagler, CXCL12 secretion by bone marrow stromal cells is dependent on cell contact and mediated by connexin-43 and connexin-45 gap junctions, Nature Immunol. 12 (2011) 391-398.

[192] T. Sugiyama, H. Kohara, M. Noda, T. Nagasawa, Maintenance of the hematopoietic stem cell pool by CXCL12-CXCR4 chemokine signaling in bone marrow stromal cell niches, Immunity 25 (2006) 977–988.

[193] T. Akashi, K. Koizumi, K. Tsuneyama, I. Saiki, Y. Takano, H. Fuse, Chemokine receptor CXCR4 expression and prognosis in patients with metastatic prostate cancer, Cancer Sci. 99 (2008) 539–542.

[194] S.R. Chinni, H. Yamamoto, Z. Dong, A. Sabbota, R.D. Bonfil, M.L. Cher, CXCL12/CXCR4 transactivates HER2 in lipid rafts of prostate cancer cells and promotes growth of metastatic deposits in bone, Mol. Cancer Res. 6 (2008) 446-457.

[195] Z. Liang, Y. Yoon, J. Votaw, M.M. Goodman, L. Williams, H. Shim, Silencing of CXCR4 blocks breast cancer metastasis, Cancer Res. 65 (2005) 967-971.

[196] M.J. Burdick, O. Sartor, Bone-targeted therapy in metastatic prostate cancer: osteoclast inhibitors and bone-seeking radiopharmaceuticals, Drug Disc. Today: Ther. Strat. 7 (2010) 23-29.

[197] M. Kawatani, Osteoclast-targeting small molecules for the treatment of neoplastic bone metastases, Cancer Sci. 100 (2009) 1999-2005.

[198] F. Saad, A. Lipton, SRC kinase inhibition: targeting bone metastases and tumor growth in prostate and breast cancer, Cancer Treat. Rev. 36 (2010) 177–184.

[199] K. Miller, R. Erez, E. Segal, D. Shabat, R. Satchi-Fainaro, Targeting bone metastases with a bispecific anticancer and antiangiogenic polymer-alendronate-taxane conjugate., Angew. Chem. Int. Ed. 48 (2009) 2949-2954.

[200] K. Miller, A. Eldar-Boock, D. Polyak, E. Segal, L. Benayoun, Y. Shaked, R. Satchi-Fainaro, Antiangiogenic antitumor activity of HPMA copolymer-paclitaxel-alendronate conjugate on breast cancer bone metastasis mouse model, Mol. Pharmaceutics 8 (2011) 1052-1062.

[201] P. Bhargava, J.L. Marshall, N. Rizvi, W. Dahut, J. Yoe, M. Figuera, K. Phipps, V.S. Ong, A. Kato, M.J. Hawkins, A Phase I and pharmacokinetic study of TNP-470 administered weekly to patients with advanced cancer, Clin. Cancer Res. 5 (1999) 1989-1995.

[202] R.H. Larsen, K.M. Murud, G. Akabani, P. Hoff, Ø.S. Bruland, M.R. Zalutsky, ^{211}At- and ^{131}I-Labeled bisphosphonates with high in vivo stability and bone accumulation, J. Nucl. Med. 40 (1999) 1197 -1203.

[203] K. Ogawa, H. Kawashima, K. Shiba, K. Washiyama, M. Yoshimoto, Y. Kiyono, M. Ueda, H. Mori, H. Saji, Development of [^{90}Y]DOTA-conjugated bisphosphonate for treatment of painful bone metastases, Nucl. Med. Biol. 36 (2009) 129-135.

[204] D. Hambardzumyan, O.J. Becher, M.K. Rosenblum, P.P. Pandolfi, K. Manova-Todorova, E.C. Holland, PI3K pathway regulates survival of cancer stem cells residing in the perivascular niche following radiation in medulloblastoma in vivo, Genes Devel. 22 (2008) 436-448.

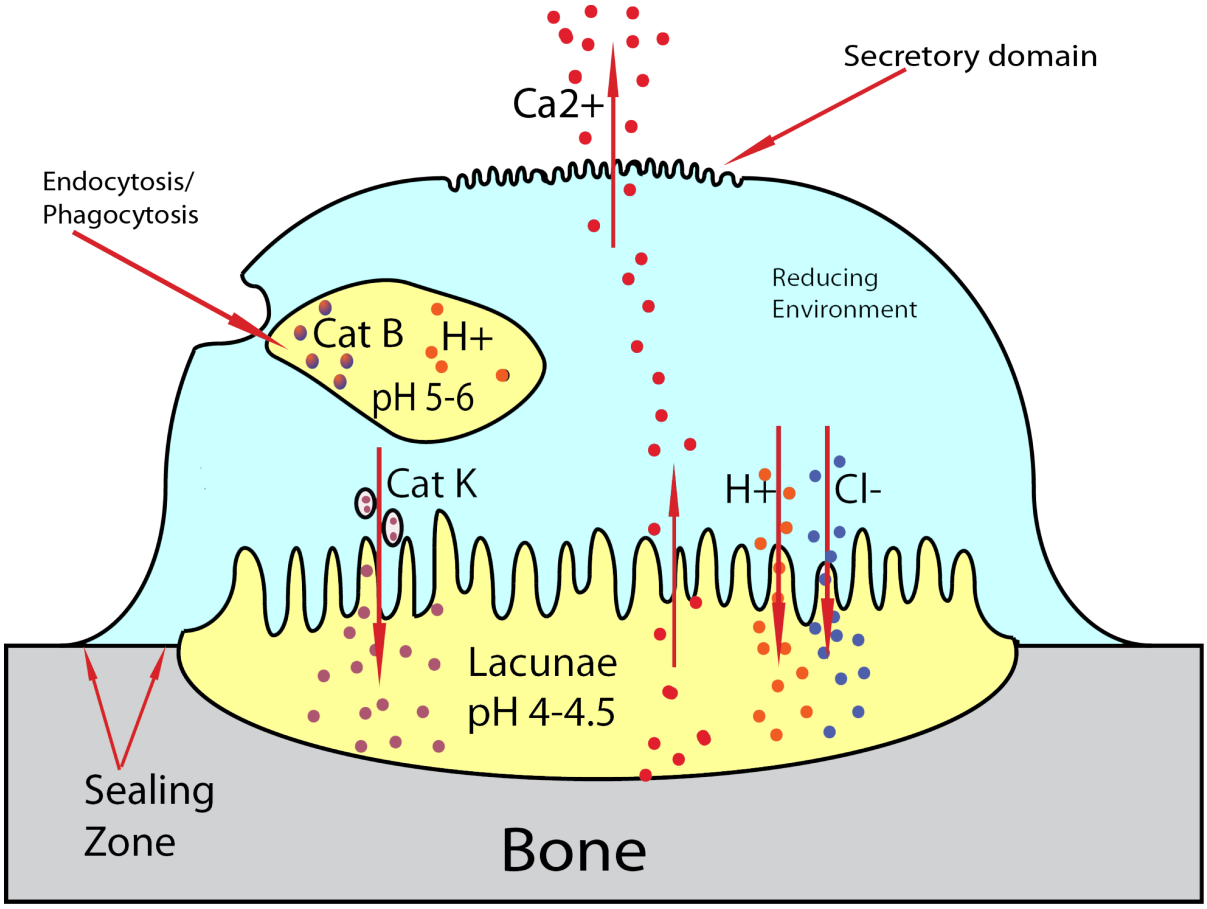

Figure 1.1. General osteoclast structure and function demonstrating unique environments, which can be utilized for site-specific release of drugs. Osteoclasts sequester portions of bone by sealing off areas called lacunae. The adjacent membrane to the bone ruffles and releases cathepsin K and HCl, reducing the pH to 4-4.5 and dissolving the bone. Calcium from the bone is then transported to the secretory domain and released into the interstitial space. Although not specific to osteoclasts endosomes/lysosomes reduce pH to 5-6 and contain cathepsin B, two environmentally specific attributes which can be used for the design of polymer-drug linkers.

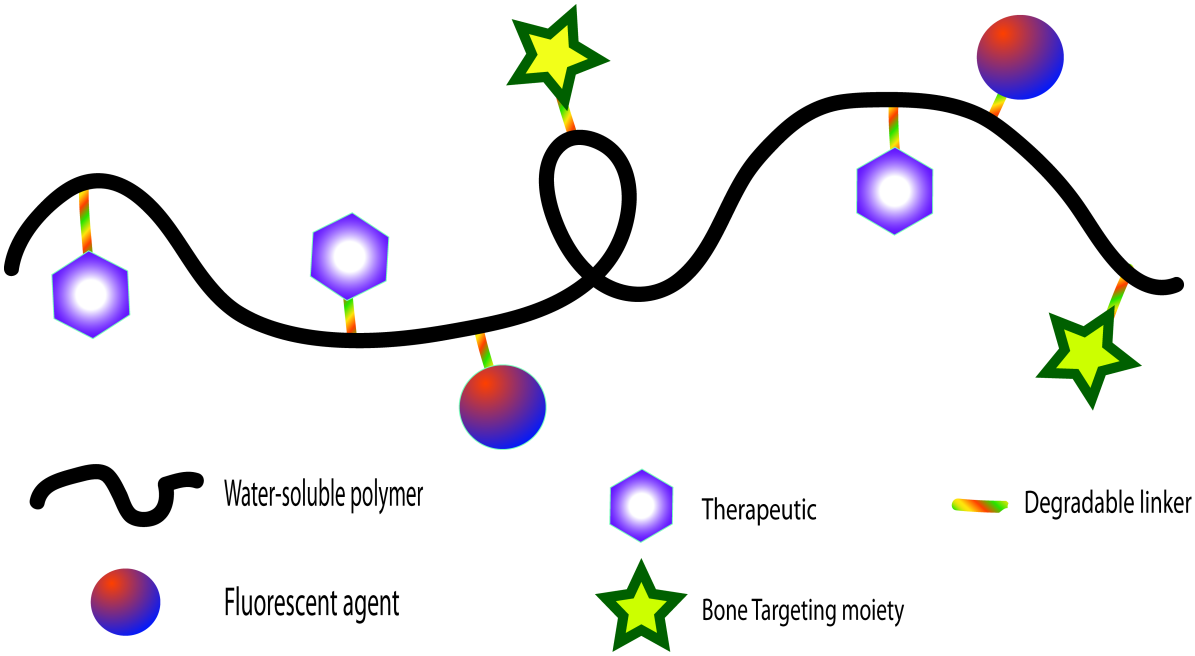

Figure 1.2. General structure of bone-targeted polymeric nanomedicines.

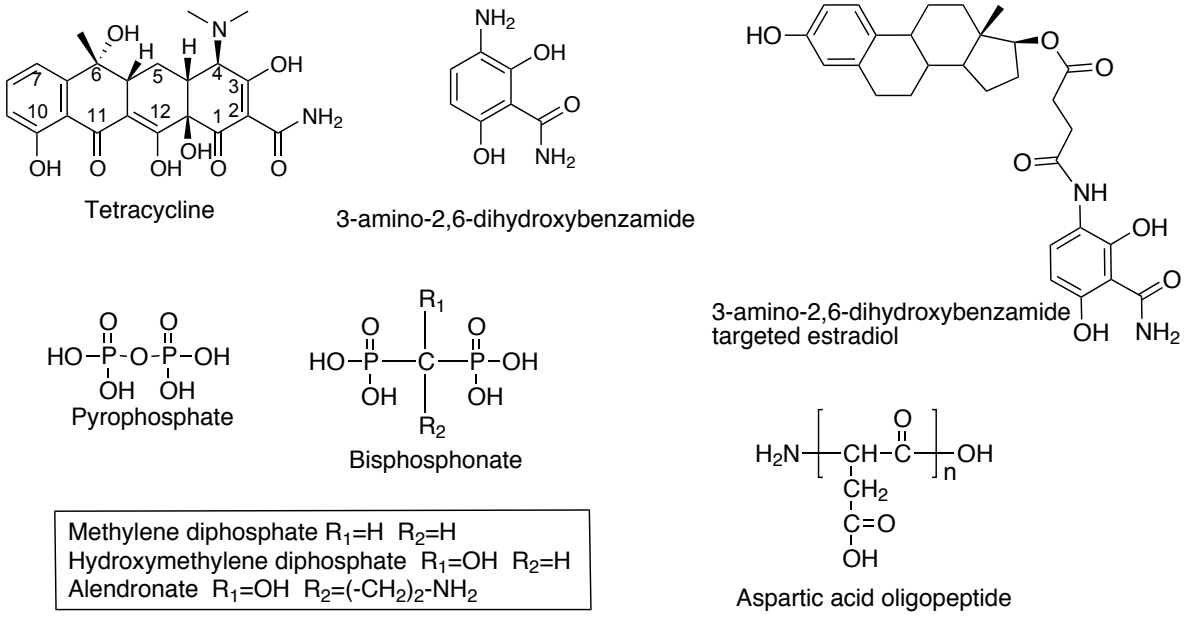

Figure 1.3. Structures of several bone-targeting molecules, including tetracycline as well as minimalized tetracycline (3-amino-2,6-dihydroxybenzamide) and its conjugate with estradiol [29]. Also shown are the structures of several bisphosphonates in comparison with pyrophosphate. Acidic oligopeptides such as aspartic acid (shown) or glutamic acid, 4-10 residues long are also excellent bone-targeting molecules.

Figure 1.4. MDP-Tc^{99} scan demonstrates the targeting specificity of bisphosphonates. Shown here is a primary osteogenic sarcoma from a 72-year-old man with Paget's disease. Dark arrows indicate a metastasis to inguinal lymph node. Reprinted with permission from reference [36].

Table 1.1 Maximal binding rate (B_{max}) and dissociation constant (K_d) of acidic oligopeptides with increasing number of amino acids.

Compound	K_d (μM)	B_{max} (nmol/h/100μg HAp)	B_{max}/K_d
Fmoc-(L-Asp)$_n$			
n=2	>100	n.d.	
4	12.1 ± 1.3*	0.34 ± 0.04	0.028
6	6.03 ± 0.84	1.57 ± 0.16	0.026
8	5.24 ± 0.55	1.61 ± 0.18	0.307
10	2.52 ± 0.23	1.66 ± 0.17	0.659
Fmoc-(L-Glu)$_n$			
n=2	>100	n.d.	
4	13.2 ± 1.1	0.42 ± 0.05	0.032
6	6.38 ± 0.71	1.59 ± 0.17	0.249
8	5.21 ± 0.61	1.61 ± 0.13	0.309
10	2.39 ± 0.25	1.66 ± 0.16	0.695

*Standard errors are shown. Adapted from reference [53].

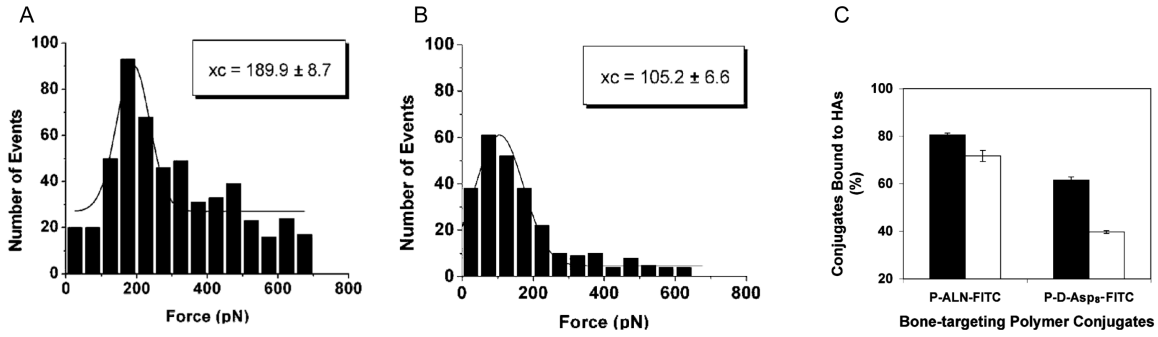

Figure 1.5. Atomic force microscopy histograms demonstrating rupture forces of (**A**) alendronate and (**B**) D-Asp$_8$ modified cantilever tips from a tooth enamel surface. (**C**) Binding ability of FITC-labeled HPMA copolymer-ALN conjugate (P-ALN-FITC) and HPMA copolymer-D-Asp$_8$ conjugate (P-D-Asp$_8$-FITC) to hydroxyapatites with different crystallinity; black bars are high crystallinity and white bars exhibit low crystallinity. Adapted from reference [3].

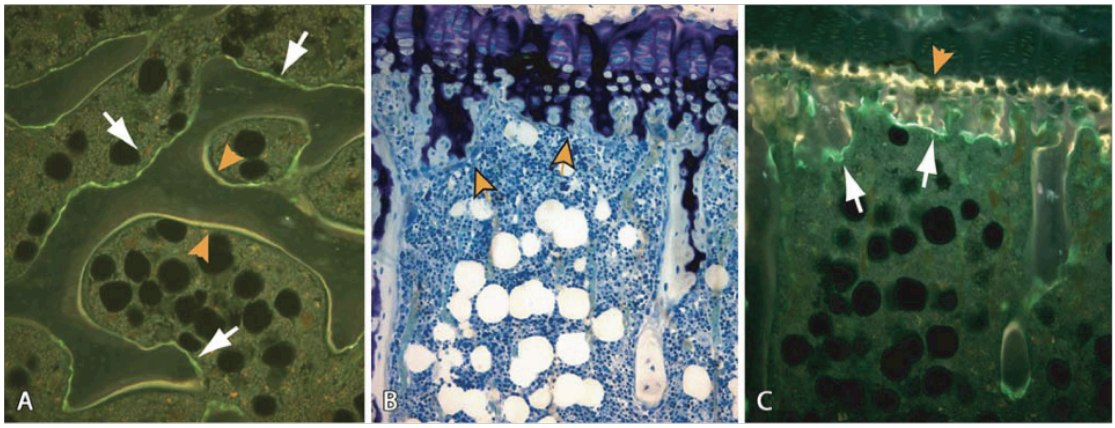

Figure 1.6. Initial uptake and localization of FITC- labeled HPMA copolymer-Asp_8 conjugate in bone compared with the uptake of tetracycline. (A) The conjugate preferentially incorporates in scalloped-appearing eroded surfaces in cancellous bone (white arrows); tetracycline (yellow label) is incorporated onto active bone mineralization surfaces. (B,C) Stained (B) and unstained (C) section of the same region of the proximal tibial growth plate and primary spongiosa. Tetracycline (yellow label) incorporated into the mineralizing zone of the growth plate (C, orange arrowhead) as expected, whereas HPMA copolymer-Asp_8 conjugate (green label) localized in the resorption areas of the primary spongiosa (C, white arrows). Magnifications: A=150x; B,C=125x. Reprinted with permission from reference [59].

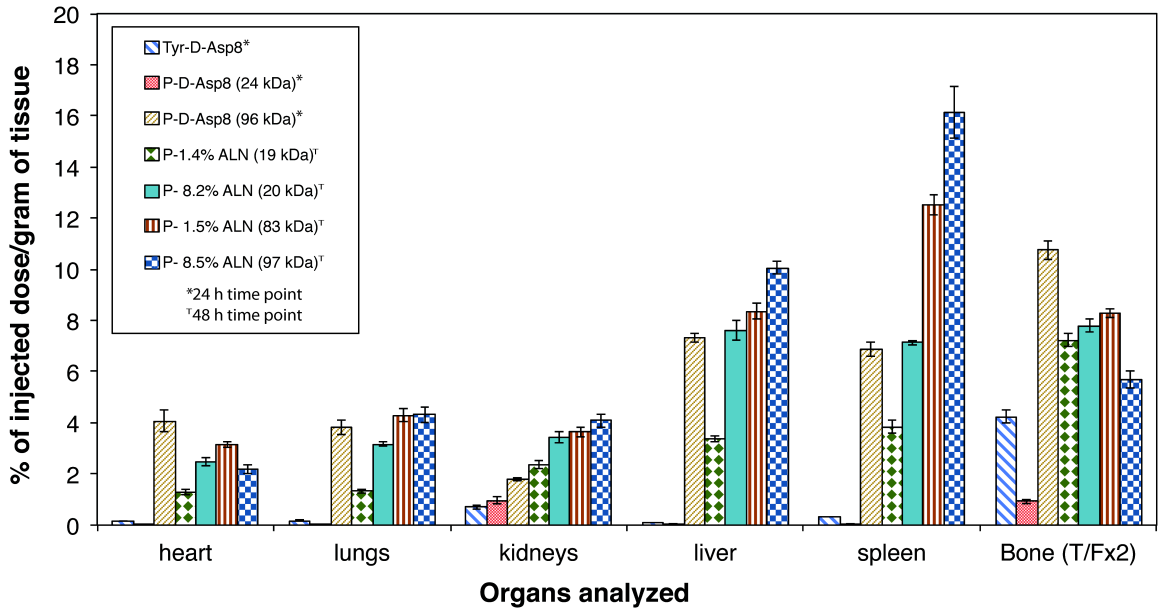

Figure 1.7. Biodistribution in BALB/c mice of ^{125}I-labeled HPMA copolymer-Asp$_8$ conjugates (P-Asp$_8$) 24 h and ^{125}I-labeled HPMA copolymer-ALN conjugates (P-ALN) 48 h after i.v. administration. The impact of molecular weight and ALN content was evaluated. Adapted from references [58,60].

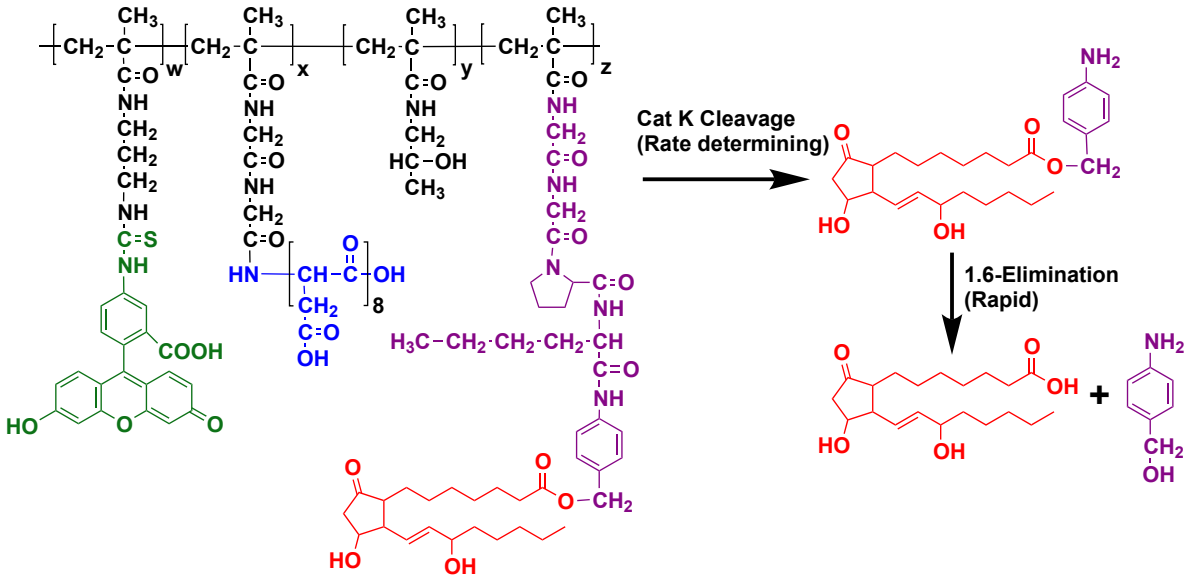

Figure 1.8. Scheme of release of unmodified prostaglandin E$_1$ (PGE$_1$) from HPMA copolymer-Asp$_8$-PGE$_1$ conjugate. Rate controlling cathepsin K cleavage is followed by fast 1,6 elimination.

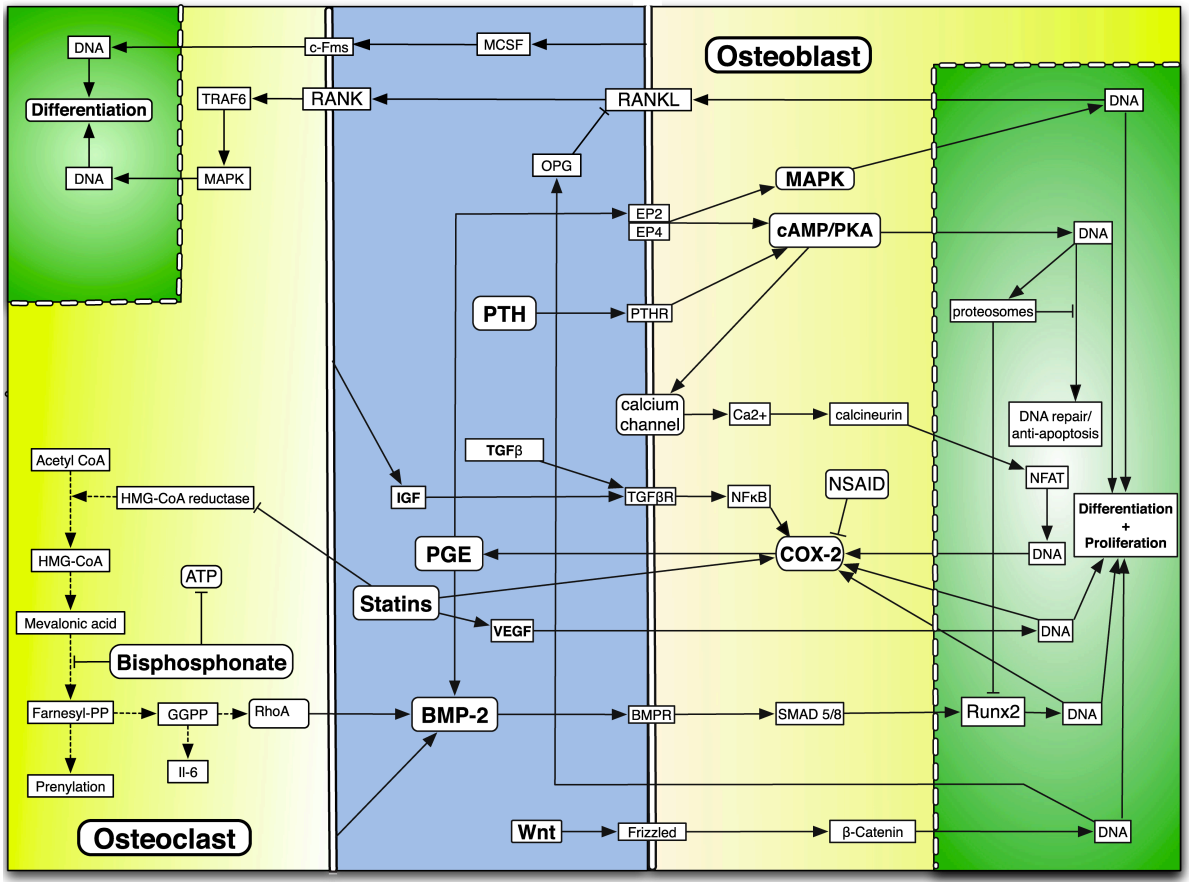

Figure 1.9. General pathways affecting bone anabolism and cross-talk between osteoclasts and osteoblasts. Most notably, PGE levels affect BMP-2 levels and vice versa, however, each contributes to bone anabolism by independent signaling pathways. Statins upregulate both BMP-2 and PGE through independent pathways. PGE and PTH1-34 upregulate cAMP however, stimulation of EP2 or EP4 by PGE will also trigger MAPK cascades. Not shown, PTH1-34 affects calcium levels in the body by regulating resorption in the kidneys and intestine. Wnt plays a critical role in bone turnover by production of osteoprotegerin and therefore inhibition of RANKL-RANK interactions. Also of note, COX-2 represents basic components PGE production rather than upregulation of COX-2 enzyme

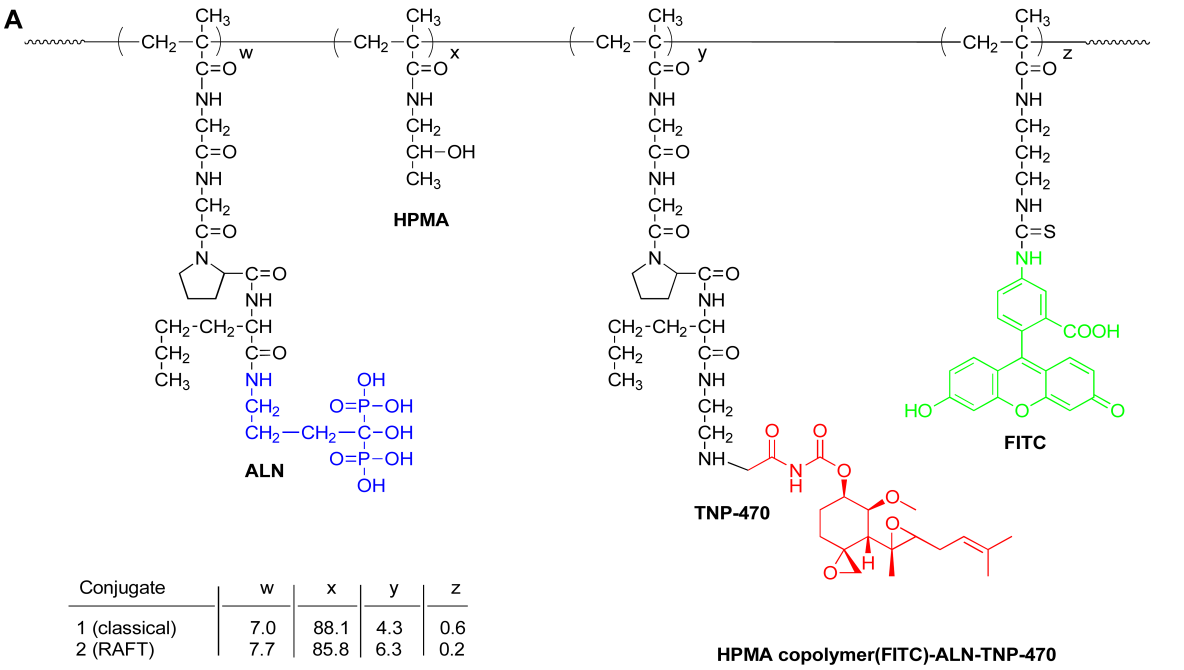

Conjugate	w	x	y	z
1 (classical)	7.0	88.1	4.3	0.6
2 (RAFT)	7.7	85.8	6.3	0.2

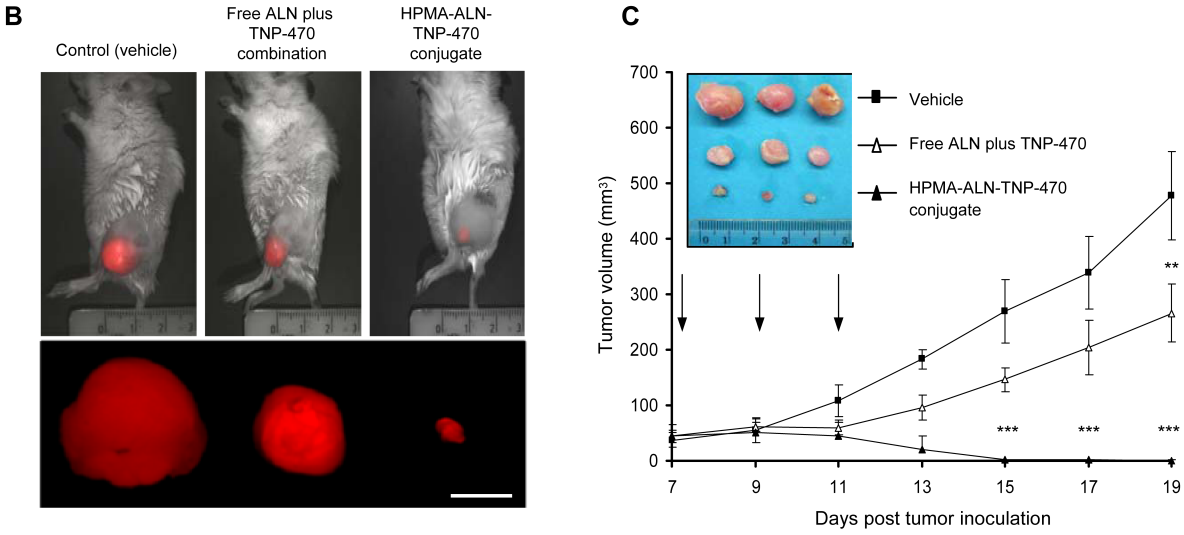

Figure 1.10. Treatment of mCherry-labeled MG-63-Ras osteosarcoma tumor-bearing mice with free ALN and TNP-470, HPMA copolymer-ALN-TNP-470 conjugate, or vehicle alone. (**A**) Structure of the HPMA copolymer-ALN-TNP-470 conjugate. (**B**) Intravital non-invasive fluorescence imaging of the tumor. (**C**) Tumor volume of mCherry-labeled MG-63-Ras tumor-bearing mice treated with free ALN and TNP-470 (open triangles), HPMA copolymer-ALN-TNP-470 conjugate (closed triangles), or vehicle alone (closed squares) [80].

CHAPTER 2

BONE-TARGETED ACID-SENSITIVE DOXORUBICIN CONJUGATE MICELLES AS POTENTIAL OSTEOSARCOMA THERAPEUTICS

2.1 Introduction

Osteosarcoma is a cancer of the bone that primarily affects adolescents. While improvements in treatment have increased the 5-year survival rate to 65%, it still lags behind overall cancer survival rates for that age group [1]. Furthermore, the metastatic or recurring disease 5-year survival rate is still at a meager 20% [2]. Current osteosarcoma therapies include surgical resection followed by chemotherapy regimens of doxorubicin (DOX), high-dose methotrexate with leucovorin rescue, cisplatin, and ifosfimide [3]. However, therapeutic indexes of these drugs are limited by severe toxicities; DOX, for instance, has well-documented cardiotoxicity [4].

Several groups have attempted to reduce this cardiotoxicity and enhance pharmacokinetics via large-molecule conjugation or nanoparticle entrapment. For example, Susa et al. increased intracellular drug accumulation by loading lipid-modified dextran nanoparticles with DOX, effectively overcoming multidrug resistance *in vitro* [5].

NOTE: This chapter is adapted with permission from the following publication: Low, S. A; Yang, J.; Kopeček, J. Bone-Targeted Acid-Sensitive Doxorubicin Conjugate Micelles as Potential Osteosarcoma Therapeutics. Bioconjugate Chemistry 25 (2014) 2012-2020

Other groups targeted drugs with molecules such as bisphosphonates and acidic oligopeptides, which have a strong affinity to bone [6]. Utilizing this targeting methodology, Salerno et al. demonstrated reduction in bone metastases in mouse metastatic breast cancer models [7]. Hrubý et al. have used bisphosphonate targeting ligands on linear HPMA copolymers containing DOX bound via pH-sensitive hydrazone bonds [8]. They demonstrated *in vitro* HAp binding as well as pH-dependent DOX release, due to the reduced pH associated with the interstitial space in some tumors.

In contrast to their small molecule counterparts, these delivery systems have enhanced antineoplastic properties by improving pharmacokinetics and reducing unwanted side effects. Improvements, however, can be made in these complex systems, as entrapped drugs may have a potential for premature release, and those with covalently bound drug yield drug-to-polymer weight percentages below 10%. Fundamentally, these are valid systems that exhibit the important elements of having a bone-targeting ligand, drug, degradable linker, and large molecules with favorable pharmacokinetics.

Conjugating a targeting ligand modeled after bone sialoprotein, such as an aspartic acid oligopeptide to DOX via a hydrazone bond, would yield a practical, simple drug that might improve drug accumulation in bone [6]. However, it would lack the pharmacokinetics that are associated with larger molecules [9,10]. A modest design modification can change this. DOX is a hydrophobic drug, but more importantly it has the tendency towards π-π stacking [11]. Furthermore, the aspartic acid oligopeptide-targeting moiety is very hydrophilic. By inserting aliphatic hydrocarbon chains and a flexible miniPEG spacer between DOX and the aspartic acid octapeptide, a novel micelle-forming unimer could be assembled (Figure 2.1). This design exhibits high drug

loading while retaining covalent bonds between the targeting ligand and the drug. The micellar self-assembly increases the size of the targeted delivery system, extending circulation and exposure to the tumor by reducing glomerular filtration. Additionally, the sequestration of DOX to the center of the micelle is designed to reduce metabolism by the myocardium and thus reduce cardiotoxicity.

In order to test the viability of the proposed micellar delivery system as well as the relationship between structure and properties, four novel DOX-containing unimers with varying hydrophobicity as well as architecture have been synthesized. Each unimer has been analyzed on its ability to form micelles, size, and adsorb to hydroxyapatite. In addition, drug release and *in vitro* osteosarcoma toxicity have been analyzed.

2.2 Experimental procedures

2.2.1 Materials

Solvents, dimethyl formamide (DMF), dichloromethane (DCM), methanol (MeOH), dimethyl sulfoxide (DMSO), ethyl acetate, ether, and acetonitrile (ACN) were purchased from VWR, Fisher Scientific or Sigma-Aldrich, and were reagent grade or better. Piperidine, diisopropyl ethylamine (DIPEA), trifluoroacetic acid (TFA), triisoproyl silane (TIS), 11-aminoundecanoic acid (AUA), hydrazine, sodium carbonate (Na_2CO_3), and Dulbecco's Modified Eagle Medium F-12 (DMEM) were purchased from Sigma-Aldrich. Magnesium sulfate and sodium sulfate were purchased from Fisher Scientific and Macron Chemicals, respectively. 1-(9-fluorenyl)methylchloroformate (Fmoc-Cl), Fmoc *N*-hydroxysuccinimide ester (Fmoc-OSu), and 2-[4-(2-hydroxyethyl)piperazin-1-yl]ethanesulfonic acid (HEPES) were purchased from AKsci. chloro-trityl resin, hydroxybenzotriazole (HOBt), 1-[Bis(dimethylamino)methylene]-1H-1,2,3-triazolo[4,5-

b]pyridinium 3-oxid hexafluorophosphate (HATU), and *N*-9-fuorenylmethoxycarbonyl-D-aspartic acid (Fmoc-D-Asp-OH) were purchased from P3Biosystems. Diisopropylcarbodiimide (DIC) was purchased from Research Chemicals. *N*-2-*N*-6-bis-(9-fluorenylmethyloxycarbonyl)-L-lysine (Fmoc-Lys(Fmoc)-OH) was purchased from Aapptec and 9-fluorenylmethoxycarbonyl-8-amino-3,6-dioxaoctanoic acid (Fmoc-miniPEG) was purchased from BioBlocks. CAPTAL S hydroxyapatite (HAp) was purchased from Plasma Biotal LTD. Holy carbon grids were purchased from Electron Microscopy Sciences. Sephadex LH20 beads were purchased from Amersham Pharmacia Biotech AM. Doxorubicin (DOX) was a generous gift from Meiji Seika Kaisha, Tokyo, Japan. Human osteosarcoma Saos-2 cells were purchased from ATTC. 2-(2-methoxy-4-nitrophenyl)-3-(4-nitrophenyl)-5-(2,4-disulfophenyl)-2H-tetrazolium monosodium salt (CCK-8) was purchased from Dojindo. Fetal bovine serum (FBS) was purchased from Hyclone.

2.2.2 Fmoc-Hydrazine

(9-fluorenylmethyl carbazate). Fmoc-hydrazine was synthesized as previously described [12] with modifications. Briefly, 1 g Fmoc-Cl was dissolved in 20 mL of precooled ether, and this solution was added dropwise to 5x excess hydrazine suspension in ether in 1 h, immediately producing a white precipitate. The reaction was stirred overnight and then added to 200 mL ethyl acetate under strong stirring. Water was slowly added and the organic solution was washed twice. The organic layer was transferred to a flask, and dried with anhydrous Na_2SO_4. Removal of ethyl acetate was performed by evaporation under vacuum to get white flurry product. Yield: 75%, mp

169.2-170.8 ^{o}C.

^{1}H-NMR (DMSO-d_6) δ 8.36 (s, 1H, CON**H**), 7.31-7.90 (m, 8H, Ar), 4.28 (m, 2H, CHC**H**$_2$), 4.23 (m, 1H, C**H**CH$_2$), 4.12 (br, s, 2H, N**H**$_2$)

2.2.3 Fmoc-11-aminoundecanoic acid

(11-(9-fluorenylmethoxycarbonylamino)undecanoic acid)) (Fmoc-AUA) was synthesized as previously described [13] with slight modification. 11-Aminoundecanoic acid (1 g, 5 mmol) was suspended in 50 mL of H_2O-dioxane (v/v 4:1). The pH of the suspension was adjusted to 9 using 10% Na_2CO_3. After the mixture became clear solution under reflux, Fmoc *N*-hydroxysuccinimide ester (Fmoc-OSu; 1.68 g, 5 mmol) in dioxane (50 mL) was added dropwise over 20 min. The reflux was kept overnight. Then the cloudy mixture was diluted with H_2O and acidified with 1 N HCl to pH 3. Dichloromethane (2 × 200 mL) was added to extract the product. The organic phase was washed with brine twice, dried with anhydrous magnesium sulfate, and then concentrated by rotary evaporation under reduced pressure. A white powder (1.83 g) was obtained with yield 86%; mp 127.8-128.5 °C.

^{1}H-NMR (DMSO-d_6) δ 7.30-7.90 (m, 8H, Ar), 7.25 (t, 1H, CON**H**), 4.28 (m, 2H, CHC**H**$_2$), 4.18 (m, 1H, C**H**CH$_2$), 2.95 (m, 2H, NHC**H**$_2$), 2.17 (m, 2H, C**H**$_2$CO), 1.47 (2H, NHCH$_2$C**H**$_2$). 1.38 (2H, C**H**$_2$CH$_2$CO), 1.24 (12H, (C**H**$_2$)$_6$)

2.2.4 Solid phase peptide synthesis

Synthesis of unimers was performed by standard Fmoc solid phase peptide synthesis. 2-chlorotrityl chloride resin (1.11 mmol/g) was loaded with 0.4 mmol/g Fmoc-

hydrazine in DCM (a small amount of DMF was added due to solubility) overnight. A 4-fold excess of DIPEA was added as a base. The resin was then capped with a mixture of DCM:MeOH:DIPEA 17:2:1 (20 mL x 4), followed by washing three times with DCM and DMF, consecutively. After removal of Fmoc-group with 20% (v/v) piperidine in DMF, a 2.5-fold excess of Fmoc-AUA was added using DIC/HOBt as coupling agents. The completion of each coupling step was verified by Kaiser test. To prepare branched unimers, Fmoc-Lys(Fmoc)-OH was added following AUA. The branched unimers have 4 aspartic acids on each branch with a total of eight instead of eight consecutive aspartic acids on the linear unimers (Figure 2.2). Upon completion the resin was washed with DMF, DCM, and MeOH and dried in a desiccator. Unimers were then cleaved using 95:2.5:2.5 TFA:TIS:H_2O and precipitated in diethyl ether. Precipitated product was dried and purified on a preparative HPLC column (Agilent Zorbax 300SB-C18) using water with 0.1% trifluoroacetic acid (TFA) as the aqueous phase and ACN with 0.1% TFA as the organic phase. Purified fractions had their volume reduced under low-pressure rotoevaporation followed by freeze-drying. Purity was confirmed using HPLC (see Supporting Information). Molecular weight for each unimer was confirmed using positive mode MALDI-ToF mass spectrometry (see Supporting Information). Linear unimers are abbreviated A1-D8 and A2-D8, indicating that they have eight consecutive aspartic acids (D8) and delineating whether they have one (A1) or two (A2) AUA moieties, respectively. The branched unimers are labeled A2-K-D4 and A4-K-D4 indicating their lysine branch (K) and the four consecutive aspartic acids (D4), as well as two (A2) or four (A4) AUAs, respectively. Both linear and branched unimers contain 8-amino-3,6-dioxaoctanoic acid (miniPEG) between the aspartic acids and the rest of the

sequence.

2.2.5 Conjugation to DOX

Purified unimers were conjugated to DOX via hydrazone bond using a 1:2 unimer to DOX molar ratio. Dry DMSO was added to the dry ingredients until the mixture fully dissolved and mixed freely (approximately 10 μL DMSO to 1 mg DOX/unimer). The solution was mixed in the dark at room temperature for three days and the progression of the reaction was tracked by HPLC (data not shown). Following the reaction, free DOX was removed using an LH20 column. The DMSO reaction solution was diluted five fold in methanol and added to an LH20 column. Methanol was used as an eluent and collected fractions were dried under nitrogen yielding DOX-A1-D8, DOX-A2-D8, DOX-A1-K-D4, and DOX-A4-K-D4. The final DOX content in micelles was determined using UV-vis spectrophotometry by measuring the methanol solution absorbance at 495 nm. Purity was confirmed using HPLC (see Supporting Information).

2.2.6 Dynamic light scattering (DLS)

Size, polydispersity, and critical micelle concentration (CMC) measurements were all taken using a Wyatt DynaPro™ Plate Reader II and analyzed using Dynamics 7 software. Each DOX-bound unimer was dissolved in 0.01 M HEPES, pH 7.4. For CMC measurement, dilutions were made in triplicates from 5 mg/mL down to 0.01 μg/mL on 96-well plates (NUNC optical bottom black polystyrene plates), final volumes per well being 200 μL. Plates were then sealed and refrigerated overnight prior to running DLS at 20°C. For size/ polydispersity measurements, samples with concentration of 1 mg/mL

were selected to coincide with cryoEM measurements (see below).

2.2.7 Cryo-electron microscopy (CryoEM)

CryoEM (FEI Tecnai 12) was used to confirm the size of the micelles as well as observe their shape. Samples were prepared at room temperature at 1 mg/mL DOX-bound unimers in 0.01 M HEPES. The samples were then manually added to holey-carbon coated copper grids. A FEI Vitrobot then blotted and plunged the samples into liquid ethane. The samples were transferred to liquid nitrogen until imaged.

2.2.8 Hydroxyapatite adsorption assay

Hydroxyapatite (HAp) adsorption was assessed for each DOX-bound unimer. HAp was added to microcentrifuge tubes (3 mg/50 μL HEPES vehicle) followed by 350 μL of 60 μM DOX-bound unimer solution. The centrifuge tube was then vortexed for the allotted time and centrifuged at 7000 RPM for 1 min. The supernatant was measured at 480 nm on a Cary 400Bio UV-Spectrophotometer. Data points measured in triplicates included times 0, 15 s, 30 s, 1 min, and 2 min.

2.2.9 DOX release kinetics

DOX release kinetics were measured using an Agilent 1100 HPLC with heated autosampler plate. Samples were prepared in triplicate at 0.1 mg/mL DOX-bound unimer in pH 5.5 and 7.4 in 1 M HEPES solutions. Samples were placed in the HPLC autosampler, which retained a temperature of 37°C over the course of the experiment. Samples were run at 0, 1, 2, 3, 5, 10, and 24 h. pH-dependent DOX release was

measured using HPLC UV absorption and calculated using the following equation:

$$\frac{Free\ DOX}{(Free\ DOX + micellar\ DOX)}\ x\ 100$$

2.2.10 Cytotoxicity

Cytotoxicity of DOX-bound unimers and free DOX toward human osteosarcoma Saos-2 cells was assessed using the CCK-8 bioassay. Saos-2 cells were maintained in DMEM/F12 medium supplemented with 10% fetal bovine serum. Plates (CELLSTAR TC 96-well) were seeded at a cell density of 4,000 cells/well and were administered dilutions of each unimer in triplicates. Concentrations administered reflected hydrazone-bound DOX content in each micelle and was confirmed using spectrophotometer measurements in MeOH. Following a 72 h treatment with drug, cytotoxicity was measured using CCK-8 per manufacturers' instructions. Each assay was repeated 3 times, IC50 values were expressed as the mean ± S.E.M. of three experiments. The data were analyzed using one-way analysis of variance to compare more than two groups, with p-values <0.05 considered to be significant.

2.3 Results and discussion

Drug carriers are often employed to increase solubility of hydrophobic drugs as well as boost their pharmacokinetics. In designing a new carrier effective against osteosarcoma, it is important to produce a molecule that has a defined structure, produces micelles with reproducible polydispersity, and is stable. Rather than focusing on increasing solubility, we decided to utilize the hydrophobic nature of chemotherapeutics to stabilize a micellar delivery system. The targeting moiety, D-aspartic acid octapeptide

(D-Asp8), was selected for its optimized targeting potential,[14] its stability toward protease degradation associated with D-peptides, as well as its hydrophilic nature [15,16]. The addition of 11-aminoundecanoic acid (AUA) resulted in increased hydrophobicity. 8-Amino-3,6-dioxaoctanoic acid (miniPEG) was placed between the AUA and the D-Asp8 for additional flexibility of the backbone. An acid-sensitive hydrazone bond was incorporated at the unimer's C terminus to bind DOX, a model drug selected for its hydrophobic nature as well as an ability to π-π stack with itself [17,18]. As such the prototype unimer DOX-A1-D8 was formed (Figure 2.2).

Thermodynamic stability of micelles increases as the hydrophilic/lipophilic balance (HLB) is lowered, e.g., by increasing the weight percent of the hydrophobic moiety.[17] In order to verify this theory regarding stability in our micelles, an additional AUA moiety was added to DOX-A1-D8 to form DOX-A2-D8. Continually adding hydrophobic AUA to the micelle has its potential drawbacks; if the hydrophobic portions far exceed the hydrophilic portions in a linear unimer, the conical shape of a single unimer may be lost, and the risk of an inverse micelle or other undesirable structures increases.[18] To counteract this effect, yet retain the ability to increase stability by adding hydrophobic moieties, a modification was needed. Branched head groups will, in theory, increase the lateral area of the head group, thereby retaining the conical structure of the micelle. DOX-A2-K-D4 demonstrates a simple addition of this branched head group (when compared to DOX-A2-D8), while DOX-A4-K-D4 doubles the number of hydrophobic AUAs (Figure 2.2).

2.3.1 Assessment of micelle formation and hydrodynamic diameter via dynamic light scattering

Verification of unimer self-assembly was determined by DLS. Scattered light count rates exponentially increase as nucleation and assembly of micelles occur. Therefore, plotting the normalized light-scattering count rate (counts per second) vs. concentration (LOG-LOG) graph (Figure 2.3) made the point of nucleation of the micelles readily apparent. Micelle thermodynamic stability increased as expected when the number of AUA moieties was increased from two to four: DOX-A2-K-D4 0.0027 mg/mL to DOX-A4-K-D4 0.00036 mg/mL. By contrast, very little difference in thermodynamic stability was observed between branched and nonbranched micelles DOX-A2-D8, 0.0035 mg/mL vs. DOX-A2-K-D4, 0.0027 mg/mL. Of note, by comparing documented blood volume (<100 mL/kg of mouse) with standard *in vivo* DOX dosages (3 mg/kg/dose), even the least stable micelle DOX-A1-D8 at 0.0053 mg/mL is expected to remain above its critical micelle concentration after dilution during dosing [19–21]. Likewise, the average patient receives 60-75 mg/m^2 dose of DOX and would also be above the CMC of the micelles upon dosing.[22–26]

The architecture, branched vs. linear, had a profound effect on the size of the micelles. The higher degree of conicality created as head groups are branched should reduce the diameter of the micelle [27]. Indeed, the diameters of both branched unimers, DOX-A2-K-D4 and DOX-A4-K-D4 were 28.4 nm and 28.0 nm, respectively, smaller than their linear counterparts, DOX-A1-D8, DOX-A2-D8, which were 53.3 nm and 50.4 nm. All four micelles had polydispersities below 0.1 as determined by DLS (Figure 2.4).

2.3.2 Cryo-electron microscopy (CryoEM)

In addition to DLS, the size of the micelles was confirmed via CryoEM. The shape was regular and spherical (Figure 2.5). One anomaly that was observed in both DLS and CryoEM, however, was the surprisingly large size of the micelles. Each unimer length is far shorter than the radius of an individual micelle. Due to the discrepancy in expected size vs. what was experimentally observed, the self-assembly into a liposomal structure rather than a micelle was hypothesized. Further analysis of the cryoEM images did not reveal an evident bilayer; thus we believe that the structures are still micelles. Also of note, the overall size of the micelles is above the renal threshold, but the size of the unimers is under the renal threshold. Although blood vessel shear forces and protein-micelle interactions drastically complicate predictions, it is feasible that under ideal conditions micelles could circulate above their critical micelle concentration; their size, above the renal threshold, could extend circulation time [28,29]. Over time, the micelles could extravasate from the blood stream as they bind to the bone at the tumor site, and eventually the blood concentration would dip below the critical micelle concentration; micelles then destabilize into unimers, which are readily cleared, as is the covalently bound DOX.

2.3.3 HAp binding

Bone is a complex weave of organic fibers and inorganic mineral, giving it both rigidity as well as some elasticity. The inorganic portion, hydroxyapatite HAp, composed of $Ca_{10}(PO_4)_6(OH)_2$, increases in crystallinity over time. It is this higher crystalline state that aspartic acid oligopeptides (AO) preferentially bind to [30,31]. In

osteosarcoma patients, highly active osteoclasts produce extensive resorption surfaces by exposing highly crystalline HAp surfaces to which AO is able to target [32,33]. This specificity of AO for highly crystalline HAp additionally may reduce nonspecific binding to the majority of the noncancerous bone.

In an attempt to simulate bone binding, a HAp binding assay was carried out. A low ratio of HAp to unimers was selected where saturation of the HAp occurred and an excess of all four unimers was present in measurable amounts, demonstrating the difference in binding between the four micelles. Slight increases in HAp concentration yielded complete binding nearly immediately, reducing the discrepancy between each of the micelles (data not shown). Still, each micelle reached their respective binding maximum (Bmax) nearly immediately, as previously noted [8,28]. Differences were observed in the amount of unimer needed to saturate the given HAp, although the rate of binding was nearly identical. A general trend of lower saturation levels was observed for larger molecules. The largest unimer, DOX-A4-K-D4, reached Bmax at 55±3.0%, whereas the lowest MW unimer, DOX-A1-D8, reached Bmax at 91±3.1% (Figure 2.6). This phenomenon may be due to steric hindrance [34]. An alternative explanation is that, due to the high surface energy of HAp, more hydrophobic molecules have reduced binding [35]. This hypothesis is unlikely as it would predict that slight variations in HAp concentration would have little affect on Bmax. There was very little difference between branched and linear unimers of close molecular weights, DOX-A2-D8 and DOX-A2-K-D4, reaching Bmax at 78±4.6% and 83±6.4%, respectively.

2.3.4 Release kinetics

Osteosarcoma provides a unique microenvironment, which can be exploited by a pH-sensitive hydrazone bond. The hydrazone bond is stable at pH 7.4 but labile at acidic pHs. Therefore it would be cleaved in endosomal compartments (assuming cell internalization) [9]. Supposing strong adsorption of micelles with HAp occurs, an osteoclast-assisted release mechanism in the interstitial space is hypothesized. Osteoclasts, as stated previously, are highly active in osteosarcoma. The micelles that preferentially bind to resorption surfaces will be covered by osteoclasts. The osteoclasts then produce a sealing zone or strong bond to the bone. A resorption lacuna will be formed underneath the osteoclasts as these osteoclasts release cathepsin K, degrading the collagen fiber network, as well as protons, reducing the pH and degrading the HAp [36]. The reduced pH could cleave hydrazone bond and release the DOX from the unimers. Incidentally, other bone metastases also recruit osteoclasts. In turn, the osteoclasts, during resorption, release essential growth factors trapped in bone [37]. These micelles utilize osteoclast-assisted release, and therefore might have the potential to treat bone metastases.

Though lacunae have a pH of around 4-4.5, other groups measure hydrazone release kinetics at pH of 5.5, mimicking conditions in an endosome [38,39]. By using a pH of 5.5 for our studies we are able to compare to what others have observed while gaining insight to what we might expect with lacunae release. Trends in release seem to mirror the micellar thermodynamic stability established in the CMC experiments. As stability of micelles increases, the rate of DOX release decreases (Figure 2.7).

We see a sigmoidal curve that may indicate a certain degree of destabilization is

necessary in order to achieve rapid release. Ultimately, pH 5.5 release kinetics falls in the normal range of what is observed in literature [8,9,40,41]. However, at pH 7.4 we observed no detectable release, which appears to be slightly lower than what others have reported [8,9,40,41].

A lower-than-expected release of DOX from DOX-A4-K-D4 micelles was observed. This is most probably connected to increased thermodynamic stability of the micelles. We hypothesize that more thermodynamically stable secondary packing is responsible for the low release rate of DOX from DOX-A4-K-D4 micelles. Before self-assembly into micelles, the unimers were eluted at higher elution time (12.5 min), indicating hydrophobic character. However, after extended Incubation (48 h, 37°C) the peak moved to 3.6 min, indicating a very hydrophilic molecule, such as an intact micelle. Release kinetics of the DOX-A4-K-D4 following incubation at 37°C was consistent with the HPLC observations.

2.3.5 Cytotoxicity

IC50 values of DOX-containing micelles were determined and correlated with the drug release data. Free DOX had a lower IC50 value 0.077± 0.009 μM than the micelles ($p<0.01$) (Figure 2.8). Three of the micelles (DOX-A1-D8 0.39± 0.012 μM, DOX-A2-D8 0.39± 0.021 μM, and DOX-A4-K-D4 0.45± 0.026 μM) did not differ significantly from each other ($p>0.05$). However DOX-A2-K-D4 consistently produced slightly higher mean IC50 values (0.61± 0.086 μM) than the linear micelles ($p<0.05$), it was not statistically different from DOX-A4-K-D4 ($p>0.05$), its most similar compound. Both DOX-A2-K-D4 and DOX-A4-K-D4 demonstrated slower release kinetics that may have

reduced the IC50 slightly for the test. Most importantly, each unimer delivered its payload and demonstrated that it is pharmacologically active and has potential for future *in vivo* studies. DOX-A4-K-D4 ended up being the most interesting because it forms the most stable micelle and yet retains nearly all the activity of the others. In addition, the cytotoxicity of A1-D8 (control; unimer without DOX) was minimal (94±5.2% cell viability at 1,000 μM).

2.4 Conclusions

The premise of this study was to design, characterize, and optimize unimers for the treatment of osteosarcoma. Each unimer component has one or more purposes for being included. Most importantly, the targeting ligand provided both hydrophilicity to the amphiphile as well as targeting to HAp. The drug, being covalently bound to the unimers via hydrazone bond, provided hydrophobic stability in addition to its therapeutic properties. DOX-A1-D8 is the simplest unimer containing drug, degradable hydrazone bond, a single AUA, miniPEG, and a D-Asp8 targeting ligand. By adding an additional AUA to DOX-A1-D8 we increased hydrophobicity (DOX-A2-D8) as well as the thermodynamic stability of the micelles. Branched unimers incorporating longer hydrophobic chains were synthesized; DOX conjugates of branched unimers (DOX-A2-K-D4 and DOX-A4-K-D4) possessed higher stability and smaller size of the micelles when compared to linear architectures. Each unimer maintained its affinity to hydroxyapatite adsorption when in a micellar assembly. In addition, at reduced pH (5.5) the hydrazone bond hydrolyzed and released unaltered DOX. The rate of DOX release can be extended by increasing the stability of the micelles. Ultimately, each micelle was

able to release unmodified drug *in vitro*.

Future studies may benefit from several of the micelle's characteristics. The sizes of the assembled micelles are above the renal threshold and we expect to see increased circulation and improved pharmacokinetics as compared to a targeted small molecule. Other key aspects of this delivery system include its potential for diverse applications. For example, this construct might be used to target a variety of bone maladies with other hydrophobic drugs that contain ketone or aldehyde groups in their structures. Additional imaging moieties may be introduced and co-assembled into micelles, providing location and biodistribution information about the drug delivery system.

2.5 References

[1] Holland-Frei, Cancer Medicine, 6th ed., BC Decker, 2003.

[2] J. PosthumaDeBoer, B.J. van Royen, M.N. Helder, Mechanisms of therapy resistance in osteosarcoma: A review, Cancer Treat. Rev. 40 (2013) 523–532.

[3] A. Luetke, P.A. Meyers, I. Lewis, H. Juergens, Osteosarcoma treatment - where do we stand? A state of the art review, Cancer Treat. Rev. 40 (2014) 523–532.

[4] T. Horie, K. Ono, H. Nishi, K. Nagao, M. Kinoshita, S. Watanabe, Y. Kuwabara, Y. Nakashima, R. Takanabe-Mori, E. Nishi, Acute doxorubicin cardiotoxicity is associated with miR-146a-induced inhibition of the neuregulin-ErbB pathway, Cardiovasc. Res. 87 (2010) 656–664.

[5] M. Susa, A.K. Iyer, K. Ryu, F.J. Hornicek, H. Mankin, M.M. Amiji, Z. Duan, Doxorubicin loaded polymeric nanoparticulate delivery system to overcome drug resistance in osteosarcoma, BMC Cancer. 9 (2009) 399–411.

[6] S.A. Low, J. Kopeček, Targeting polymer therapeutics to bone, Adv. Drug Deliv. Rev. 64 (2012) 1189–1204.

[7] M. Salerno, E. Cenni, C. Fotia, S. Avnet, D. Granchi, F. Castelli, D. Micieli, R. Pignatello, M. Capulli, N. Rucci, A. Angelucci, A. Del Fattore, A. Teti, N. Zini, A. Giunti, N. Baldini, Bone-targeted doxorubicin-loaded nanoparticles as a tool for the treatment of skeletal metastases, Curr. Cancer Drug Targets. 10 (2010) 649–659.

[8] M. Hrubý, T. Etrych, J. Kučka, M. Forsterová, K. Ulbrich, Hydroxybisphosphonate‐containing polymeric drug‐delivery systems designed for targeting into bone tissue, J. Appl. Polym. Sci. 101 (2006) 3192–3201.

[9] M. Prabaharan, J.J. Grailer, S. Pilla, D.A. Steeber, S. Gong, Amphiphilic multi-arm-block copolymer conjugated with doxorubicin via pH-sensitive hydrazone bond for tumor-targeted drug delivery, Biomaterials. 30 (2009) 5757–5766.

[10] M. Hrubý, Č. Koňák, K. Ulbrich, Polymeric micellar pH-sensitive drug delivery system for doxorubicin, J. Controlled Release. 103 (2005) 137–148.

[11] S. Eksborg, Extraction of daunorubicin and doxorubicin and their hydroxyl metabolites: Self-association in aqueous solution, J. Pharm. Sci. 67 (1978) 782–785.

[12] L.A. Carpino, G.Y. Han, 9-Fluorenylmethoxycarbonyl amino-protecting group, J. Org. Chem. 37 (1972) 3404–3409.

[13] C. Galoppini, S. Meini, M. Tancredi, A. Di Fenza, A. Triolo, L. Quartara, C.A. Maggi, F. Formaggio, C. Toniolo, S. Mazzucco, A. Papini, P. Rovero, A new class of pseudopeptide antagonists of the kinin B1 receptor containing alkyl spacers, J. Med. Chem. 42 (1999) 409–414.

[14] T. Sekido, N. Sakura, Y. Higashi, K. Miya, Y. Nitta, M. Nomura, H. Sawanishi, K. Morito, Y. Masamune, S. Kasugai, K. Yokogawa, K. Miyamoto, Novel drug delivery system to bone using acidic oligopeptide: pharmacokinetic characteristics and pharmacological potential, J. Drug Target. 9 (2001) 111–121.

[15] N. Zhou, Z. Luo, J. Luo, X. Fan, M. Cayabyab, M. Hiraoka, D. Liu, X. Han, J. Pesavento, C.-Z. Dong, Y. Wang, J. An, H. Kaji, J.G. Sodroski, Z. Huang, Exploring the Stereochemistry of CXCR4-Peptide Recognition and Inhibiting HIV-1 Entry with d-Peptides Derived from Chemokines, J. Biol. Chem. 277 (2002) 17476–17485.

[16] A. Verdoliva, F. Pannone, M. Rossi, S. Catello, V. Manfredi, Affinity purification of polyclonal antibodies using a new all-D synthetic peptide ligand: comparison with protein A and protein G, J. Immunol. Methods. 271 (2002) 77–88.

[17] Y. Tian, L. Bromberg, S.N. Lin, T. Alan Hatton, K.C. Tam, Complexation and release of doxorubicin from its complexes with Pluronic P85-b-poly(acrylic acid) block copolymers, J. Controlled Release. 121 (2007) 137–145.

[18] K. Kataoka, T. Matsumoto, M. Yokoyama, T. Okano, Y. Sakurai, S. Fukushima, K. Okamoto, G.S. Kwon, Doxorubicin-loaded poly (ethylene glycol)–poly (β-benzyl-l-aspartate) copolymer micelles: Their pharmaceutical characteristics and biological significance, J. Controlled Release. 64 (2000) 143–153.

[19] A.C. Riches, J.G. Sharp, D.B. Thomas, S.V. Smith, Blood volume determination in the mouse, J. Physiol. 228 (1973) 279–284.

[20] M.L. Tan, A.M. Friedhuber, D.E. Dunstan, P.F.M. Choong, C.R. Dass, The performance of doxorubicin encapsulated in chitosan–dextran sulphate microparticles in an osteosarcoma model, Biomaterials. 31 (2010) 541–551.

[21] C.R. Dass, E.T. Ek, K.G. Contreras, P.F. Choong, A novel orthotopic murine model provides insights into cellular and molecular characteristics contributing to human osteosarcoma, Clin. Exp. Metastasis. 23 (2006) 367–380.

[22] Simplified Calculation of Body-Surface Area, N. Engl. J. Med. 317 (1987) 1098–1098.

[23] G. Bacci, P. Picci, S. Ferrari, R. Casadei, A. Brach Del Prever, A. Tienghi, A. Mancini, Influence of adriamycin dose in the outcome of patients with osteosarcoma treated with multidrug neoadjuvant chemotherapy: results of two sequential studies, J. Chemother. Florence Italy. 5 (1993) 237–246.

[24] S. Ferrari, E. Palmerini, E.L. Staals, M. Mercuri, B. Franco, P. Picci, G. Bacci, The treatment of nonmetastatic high grade osteosarcoma of the extremity: review of the Italian Rizzoli experience. Impact on the future, in: Pediatr. Adolesc. Osteosarcoma, Springer, 2010: pp. 275–287.

[25] S. Ferrari, M. Mercuri, P. Picci, F. Bertoni, A. Brach del Prever, A. Tienghi, A. Mancini, A. Longhi, S. Rimondini, D. Donati, M. Manfrini, P. Ruggieri, R. Biagini, G. Bacci, Nonmetastatic osteosarcoma of the extremity: results of a neoadjuvant chemotherapy protocol (IOR/OS-3) with high-dose methotrexate, intraarterial or intravenous cisplatin, doxorubicin, and salvage chemotherapy based on histologic tumor response, Tumori. 85 (1999) 458–464.

[26] S.B. Nadler, J.H. Hidalgo, T. Bloch, Prediction of blood volume in normal human adults, Surgery. 51 (1962) 224–232.

[27] J.N. Israelachvili, Intermolecular and surface forces, Academic press London, 1991.

[28] S.M. Moghimi, A.C. Hunter, J.C. Murray, Long-Circulating and Target-Specific Nanoparticles: Theory to Practice, Pharmacol. Rev. 53 (2001) 283–318.

[29] A.N. Lukyanov, V.P. Torchilin, Micelles from lipid derivatives of water-soluble polymers as delivery systems for poorly soluble drugs, Adv. Drug Deliv. Rev. 56 (2004) 1273–1289.

[30] S. Miller, H. Pan, D. Wang, B. Bowman, P. Kopečková, J. Kopeček, Feasibility of using a bone-targeted, macromolecular delivery system coupled with prostaglandin E1 to promote bone formation in aged, estrogen-deficient rats, Pharm. Res. 25

(2008) 2889–2895.

[31] D. Wang, S.C. Miller, L.S. Shlyakhtenko, A.M. Portillo, X.-M. Liu, K. Papangkorn, P. Kopečková, Y. Lyubchenko, W.I. Higuchi, J. Kopeček, Osteotropic peptide that differentiates functional domains of the skeleton, Bioconjug. Chem. 18 (2007) 1375–1378.

[32] F. Lamoureux, P. Richard, Y. Wittrant, S. Battaglia, P. Pilet, V. Trichet, F. Blanchard, F. Gouin, B. Pitard, D. Heymann, Therapeutic relevance of osteoprotegerin gene therapy in osteosarcoma: blockade of the vicious cycle between tumor cell proliferation and bone resorption, Cancer Res. 67 (2007) 7308–7318.

[33] S.B. Rodan, G.A. Rodan, H.A. Simmons, R.W. Walenga, M.B. Feinstein, L.G. Raisz, Bone resorptive factor produced by osteosarcoma cells with osteoblastic features is PGE2, Biochem. Biophys. Res. Commun. 102 (1981) 1358–1365.

[34] L. Ouyang, W. Huang, G. He, L. Guo, Bone targeting prodrugs based on peptide dendrimers, synthesis and hydroxyapatite binding in vitro., Lett. Org. Chem. 6 (2009) 272–277.

[35] D. Aronov, R. Rosen, E.Z. Ron, G. Rosenman, Tunable hydroxyapatite wettability: effect on adhesion of biological molecules, Process Biochem. 41 (2006) 2367–2372.

[36] S.L. Teitelbaum, Bone resorption by osteoclasts, Science. 289 (2000) 1504–1508.

[37] G.D. Roodman, Mechanisms of bone metastasis, N. Engl. J. Med. 350 (2004) 1655–1664.

[38] S. Georges, C. Ruiz Velasco, V. Trichet, Y. Fortun, D. Heymann, M. Padrines, Proteases and bone remodelling, Cytokine Growth Factor Rev. 20 (2009) 29–41.

[39] O. Seksek, J. Biwersi, A.S. Verkman, Evidence against defective trans-Golgi acidification in cystic fibrosis, J. Biol. Chem. 271 (1996) 15542–15548.

[40] J.A. MacKay, M. Chen, J.R. McDaniel, W. Liu, A.J. Simnick, A. Chilkoti, Self-assembling chimeric polypeptide–doxorubicin conjugate nanoparticles that abolish tumours after a single injection, Nat. Mater. 8 (2009) 993–999.

[41] H.S. Yoo, E.A. Lee, T.G. Park, Doxorubicin-conjugated biodegradable polymeric micelles having acid-cleavable linkages, J. Controlled Release. 82 (2002) 17–27.

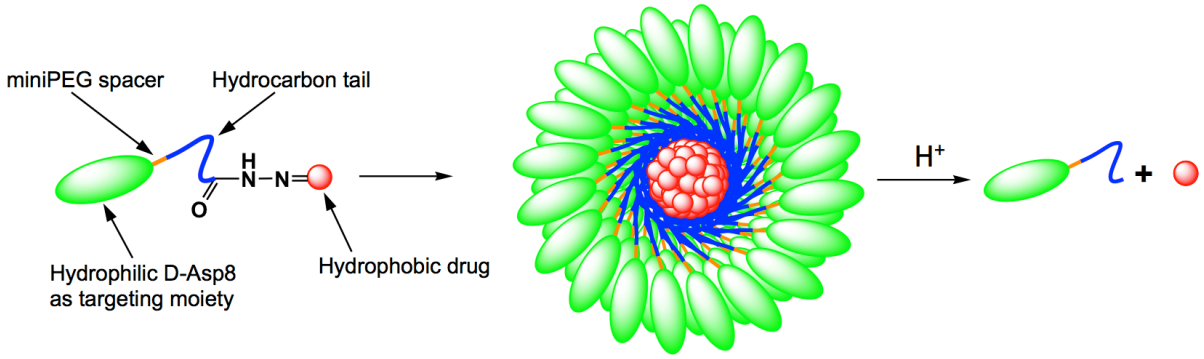

Figure 2.1. Illustration of micelle formation from amphiphilic unimer consisting of D-aspartic acid octapeptide (D-Asp8), miniPEG spacer, hydrophobic tail based on 11-aminoundecanoic acid and doxorubicin bound via an acid-sensitive hydrazone bond.

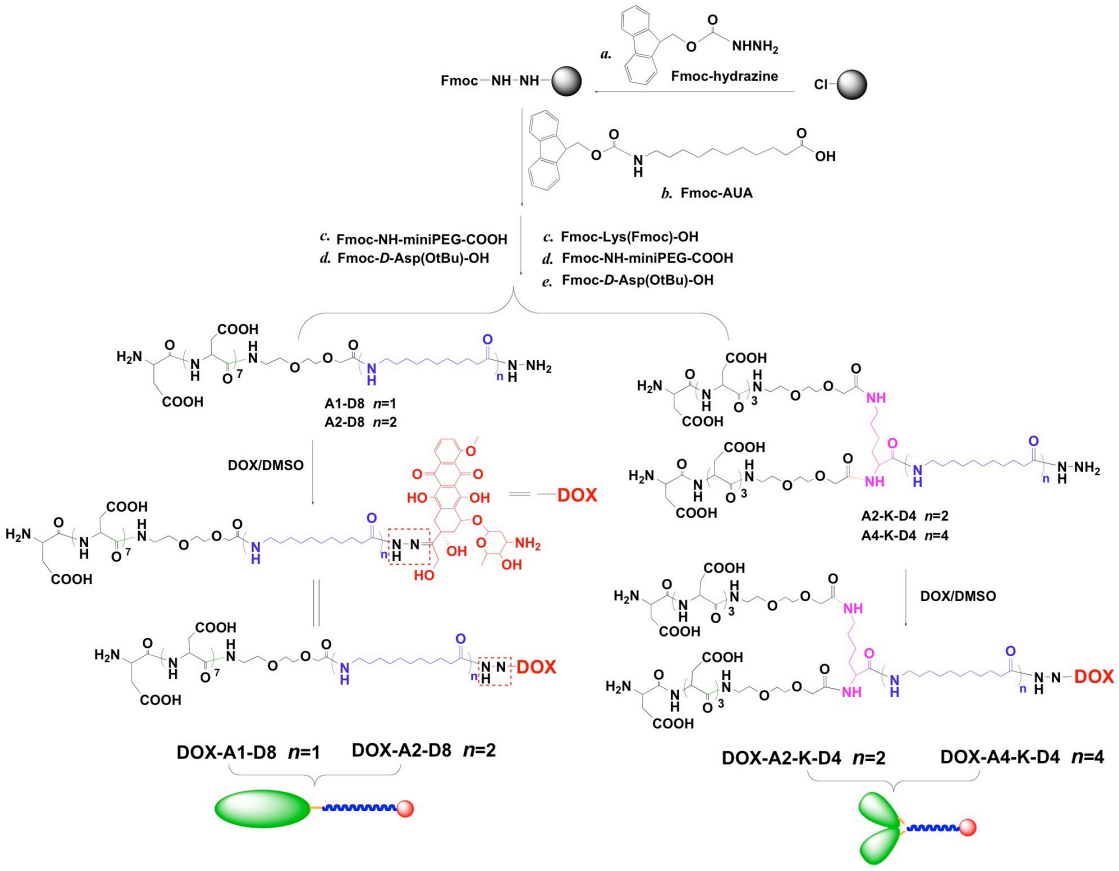

Figure 2.2. Synthesis of amphiphilic unimers with linear and branched architecture.

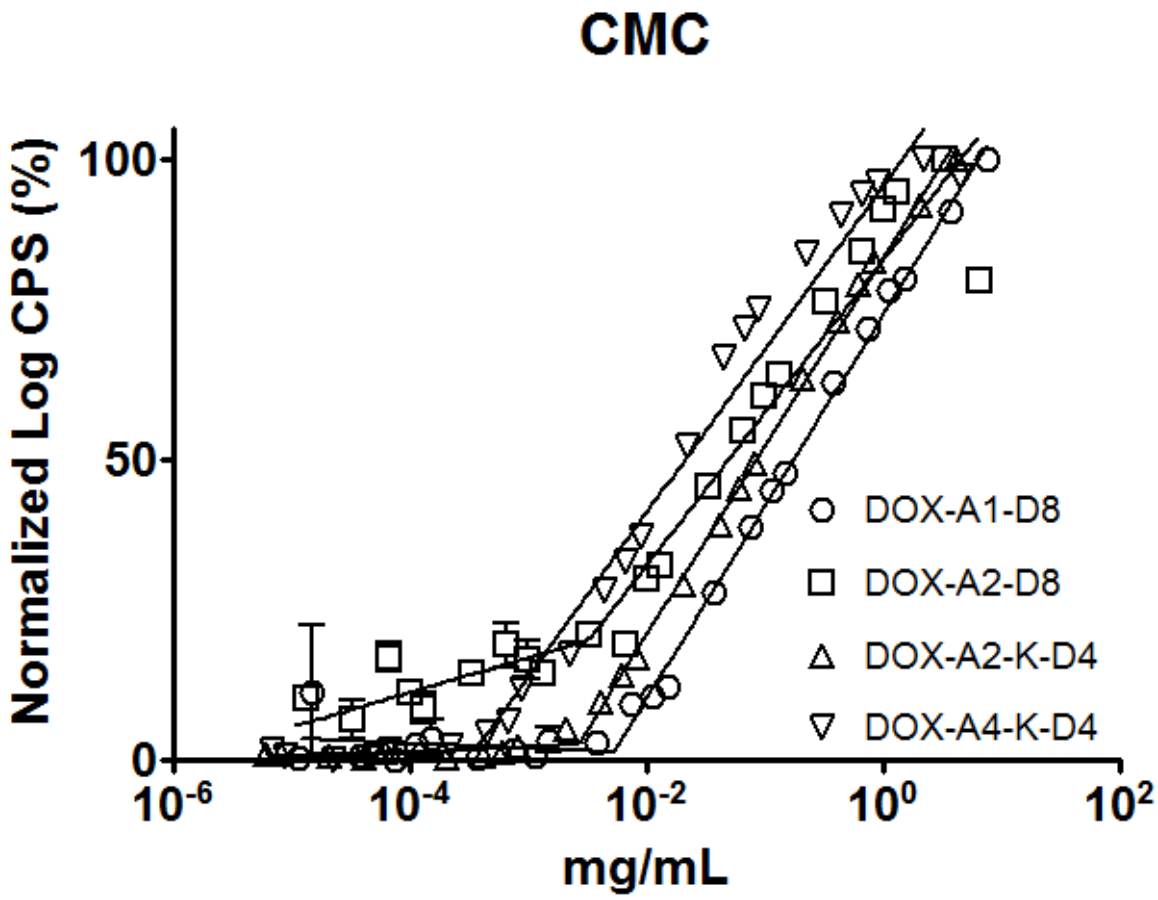

Figure 2.3. Determination of the critical micellar concentration (CMC) of DOX-containing unimers. A logarithmic plot of the intensity ratio in counts per second (CPS) vs. the logarithm of the unimer concentration. The figure demonstrates the increased thermodynamic stability of more hydrophobic micelles.

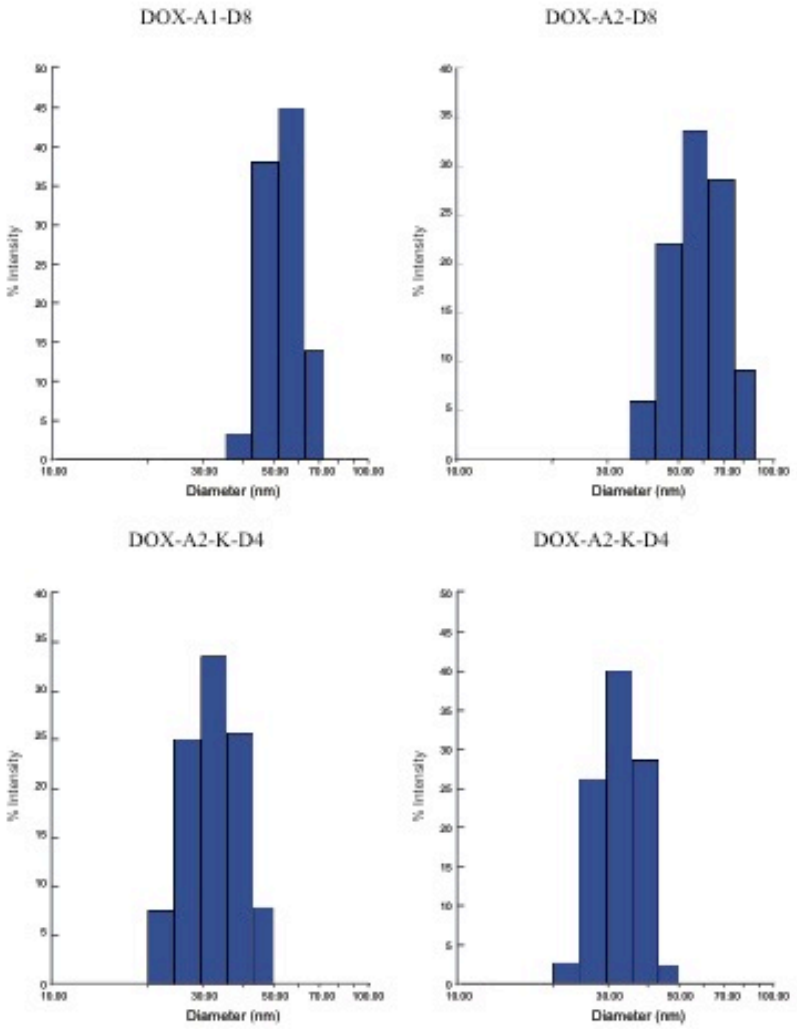

Figure 2.4. Size distribution of micelles as determined by dynamic light scattering in 0.01 M HEPES (pH 7.4; 1 mg·mL^{-1}). A clear division between linear and branched unimers was observed: linear unimers form larger micelles than do branched unimers.

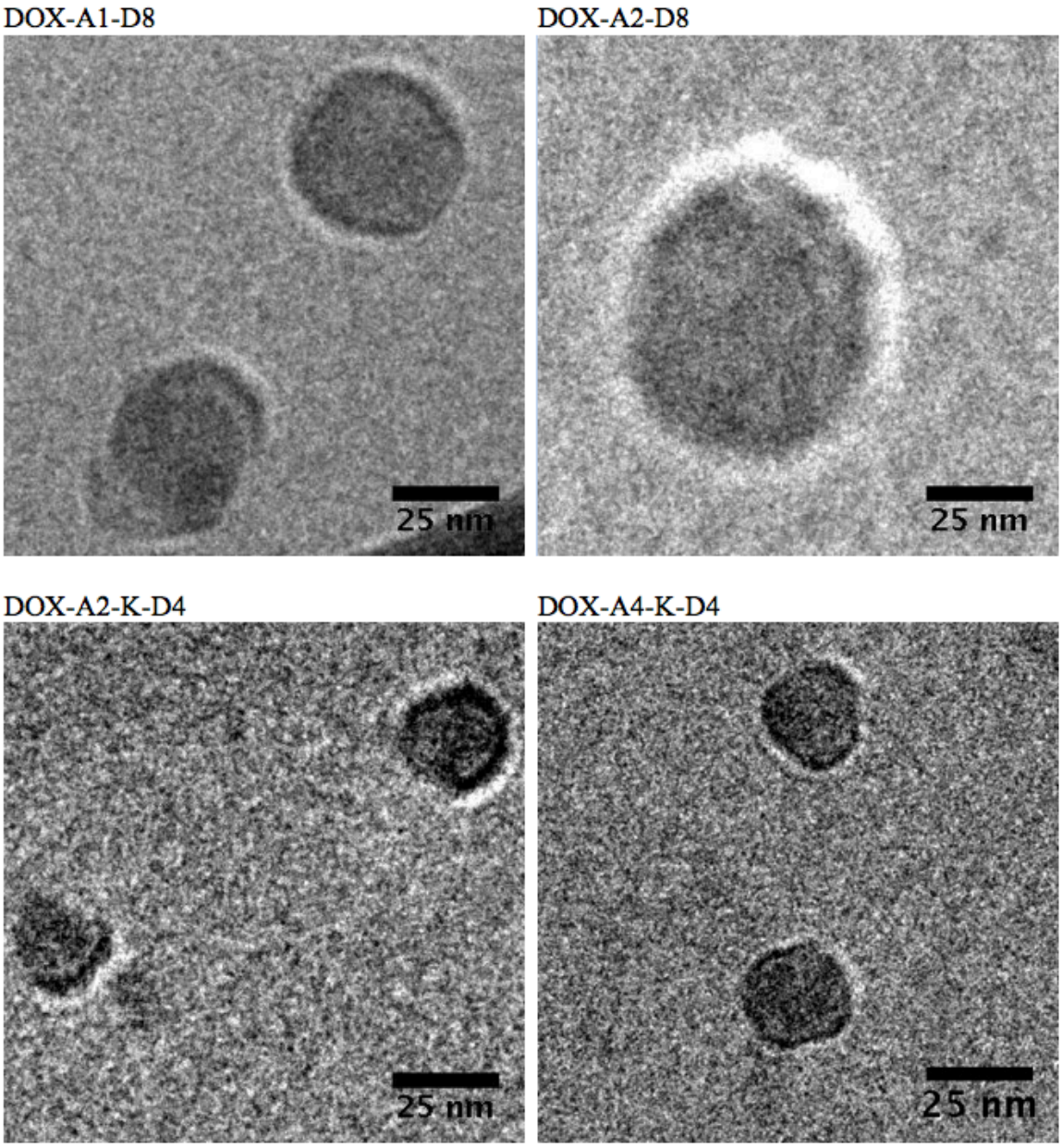

Figure 2.5. TEM image of micelles in 0.01M HEPES (1 mg·mL^{-1}) at room temperature. The images confirm the sizes observed in the DLS studies as well as demonstrate the spherical nature of the micelles.

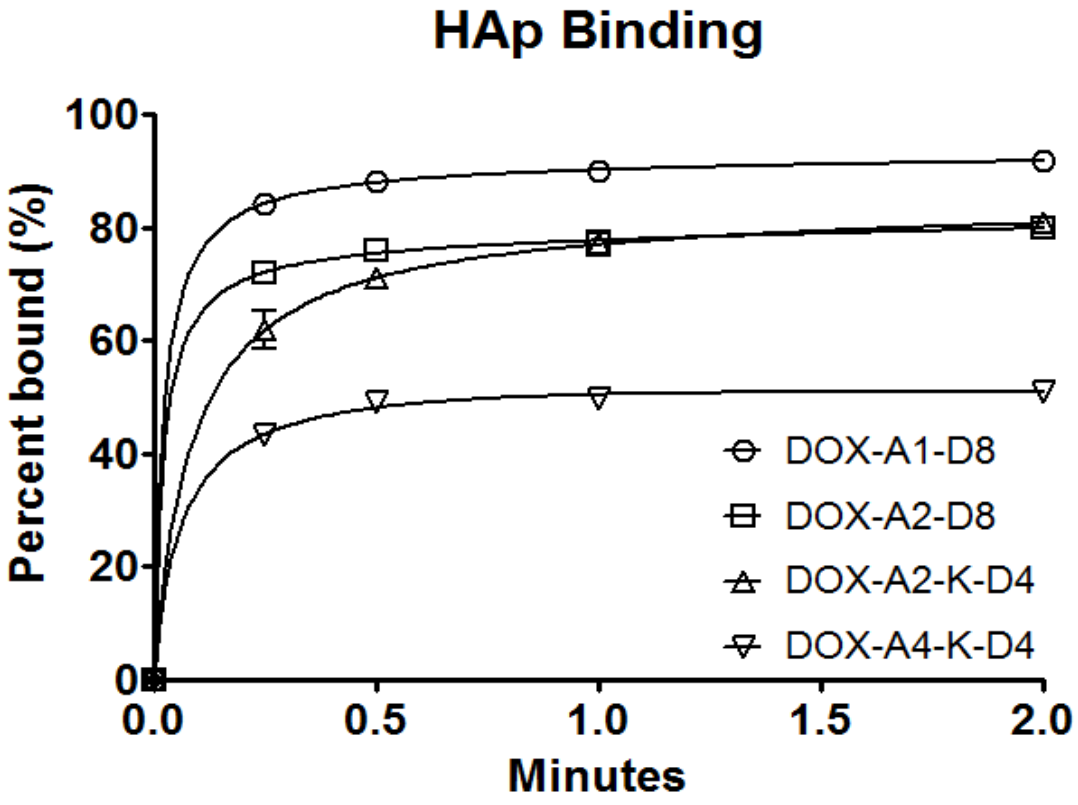

Figure 2.6. *In vitro* adsorption of DOX-containing micelles (52.5 μM) to HAp at subsaturation levels of HAp (7.5 $mg \cdot mL^{-1}$).

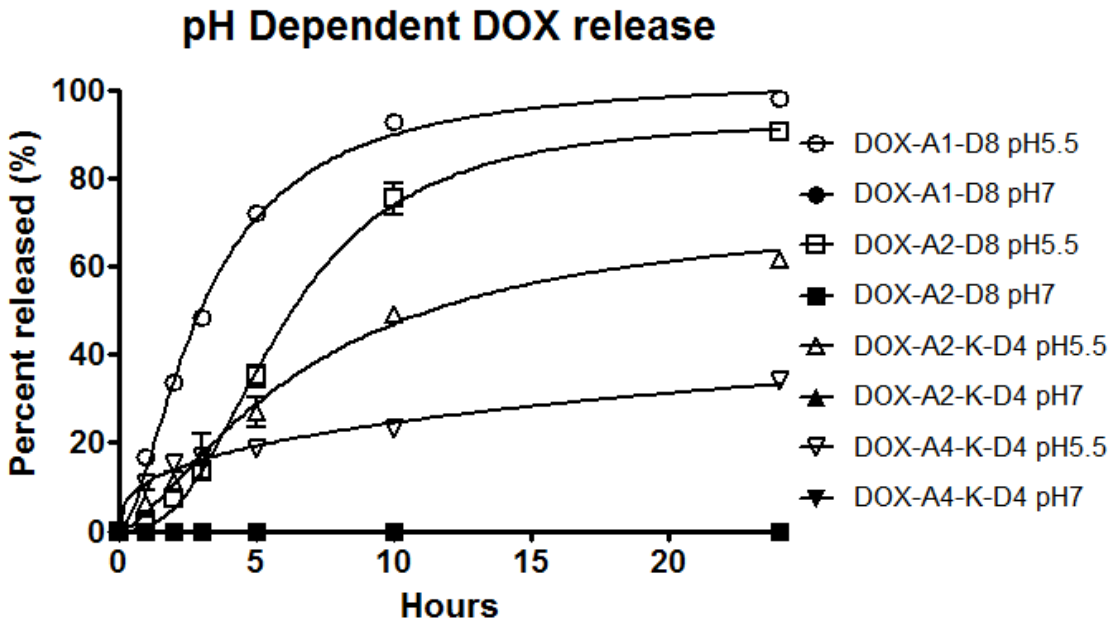

Figure 2.7. *In vitro* release profiles of DOX from DOX-containing micelles (at pH 5.5 and pH 7.4 at 37 ^{o}C) measured by HPLC. Of note, all of the pH 7.4 data are on the baseline due to lack of detectable DOX release.

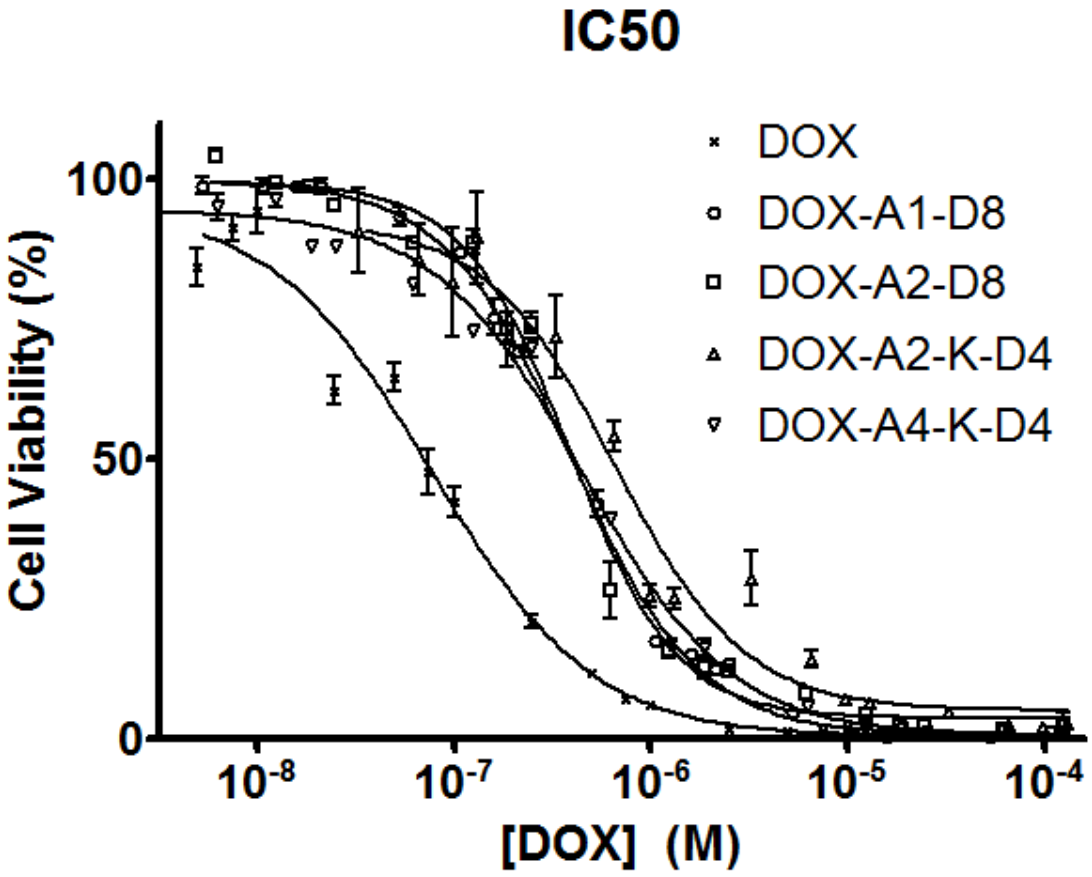

Figure 2.8. Cytotoxicity of free DOX and micelles with variable structure towards human osteosarcoma Saos-2 cells following 72 h incubation.

CHAPTER 3

BIODISTRIBUTION OF FRACTURE-TARGETED GSK3β-LOADED MICELLES FOR IMPROVED FRACTURE HEALING

3.1 Introduction

Healthy bone is a mix of 50-70% mineral, 20-40% organic matrix, 5-10% water, and 1-5% lipids and is constantly being recycled into new bone in order to maintain its rigidity and flexibility [1–3]. At the beginning of this recycling process, monocytes receive several signals, pushing them to differentiate into osteoclasts. Osteoblasts then express Receptor Activator of Nuclear Factor κ B Ligand (RANKL) to the Receptor Activator of Nuclear Factor κ B (RANK) surface receptor in monocytes, initiating the TRAF6 cascade, committing the monocytes to osteoclastogenesis.[4,5] Mature osteoclasts then initiate healthy catabolic bone resorption. Anabolic processes begin as mesenchymal stem cells (MSCs) are stimulated to become osteoblasts by the BMP-2/Runx2 and Wnt/β-catenin pathways. Matured osteoblasts then deposit osteoid, a component of the bone matrix primarily composed of type I collagen, which mineralizes

NOTE: This chapter is adapted from the following publication being submitted Biomacromolecules: Low, S. A; Galliford, C.V.; Yang, J.; Low, P.S.; Kopeček, J. Biodistribution of Fracture-Targeted GSK3β-Loaded Micelles for Improved Fracture Healing.

and becomes new bone [6,7].

A narrow balance of catabolism or anabolism is responsible for healthy bone. Alteration of this balance results in diseased bone. Osteoporosis occurs when catabolism surpasses anabolism wherein a two-standard deviation decrease in bone density from healthy bone is observed. In the US, approximately 44 million people have low bone density, and 10 million people suffer from osteoporosis. By 2020, an estimated 61 million are projected to have osteoporosis [8]. In general, osteoporosis can be treated with a regimen of bisphosphonates, which inhibits osteoclasts, thereby slowing catabolism and healthy bone turnover. This becomes problematic when bone fractures occur and proper bone turnover is retarded by bisphosphonates. These complications include crippling vertebral and hip fractures with estimated costs between in $13.7 billion and $20.3 billion in 2005 [9].

Clinical treatment of these fractures generally does not include site-specific anabolic drugs. In fact, the only drugs approved for clinical use on fractures are BMP-2 and BMP-7, which are applied locally for use in open long-bone fractures and spinal fusions [10]. However, the need for broader application of anabolic drugs to treat bone maladies such as osteoporotic fractures is evident when one considers that 85% of the use of anabolics are off-label [11]. Still, the FDA judiciously continues to limit approved use of locally administered drugs to fractures that are already open and at risk of infection. This limitation necessitates a clinically relevant approach to treating these fractures: a fracture treatment drug that is administered systemically yet targets the fracture site.

Efficacy in targeting fractures in humans has been demonstrated for quite some time, as radiolabeled methylene diphosphate and hydroxymethylene diphosphate are used

to diagnose hairline fractures. The use of bisphosphonates as fracture-targeting ligands inhibits both osteoclasts and angiogenesis, returning to the original problem of retarding bone turnover, which is critical for fracture healing [12–14]. Nature has a more biocompatible answer. Sialoprotein is one of several naturally occuring proteins that display a strong affinity for hydroxyapatite (HAp), a mineral found in bone. Several strings of acidic amino acids are responsible for sialoprotein's bone affinity. Modeled after sialoprotein, a biocompatible targeting ligand can be produced by combining a string of eight aspartic acids [15]. The aspartic acid octapeptide prefers the crystalline state of HAp, which is exposed at the time of a fracture [3,16]. Our previous studies involving aspartic acid octapeptide targeted doxorubicin containing micelles for the treatment of osteosarcoma demonstrated that after conjugation to a drug and self-assembly into a micelle, the aspartic acid retains its HAp binding abilities [17].

Having a bone-targeted peptide that targets fractures locally means that it is important to select a drug which acts locally to stimulate bone growth. Of particular interest in this area are GSK3β inhibitors. GSK3β is an enzyme that can degrade beta-catenin and thus impact the Wnt/catenin pathway. Inhibition of GSK3β, therefore, promotes a robust osteoblast population and aggressive bone anabolism, as several groups have shown [18]. Chen et al. demonstrated that levels of β-catenin in fractures far exceed those of healthy bone. By using a β-catenin knockout transgenic mouse model, fracture healing is essentially stopped with the removal of β-catenin. More importantly, they demonstrated that the addition of lithium chloride, a basic GSK3β inhibitor, to the mouse diet increased the bone density of the fracture callus [19]. Sisask et al. demonstrated that a much more potent GSK3β inhibitor administered orally increased

load failure of fractured femurs by 270% compared to the vehicle alone [20]. Toxicity profiles of GSK3β inhibitors in these studies are low enough for oral administration of the drug; however, the targets of GSK3β, Wnt and Hedgehog signaling, are pathways found in many cell types and tissues, and one must be cautious of both short-term and long-term side effects. The potential off-target effects of GSK3β inhibitors as well as their high potency and large therapeutic window make them excellent candidates for a targeted therapeutic. We have selected 6-bromoindirubin-3'-oxime (6Bio), a potent GSK3β inhibitor with an enzymatic IC50 of 5 nmol because of its proven track record growing bone [18,21].

Conjugating the targeting ligand aspartic acid oligopeptide to 6BIO via a hydrolyzable oxime ester bond would yield a simple drug that would likely improve drug accumulation in bone. However, with slight modifications it is possible to target the site of inflammation in addition to the bone [22,23]. 6BIO is a drug that is hydrophobic, while the aspartic acid oligopeptide-targeting moiety is very hydrophilic. Upon addition of aliphatic hydrocarbon chain between 6BIO and the aspartic acid chain a micelle unimer is formed (Figure 3.1). The micelle increases the overall size of the drug carrier, thereby increasing uptake in the inflamed tissue. Unlike traditional micelles, however, each unimer contains a targeting ligand as well as a drug, ensuring high drug loading. Additionally, should the micelle destabilize in the blood stream, the drug will remain targeted to the fracture.

3.2 Experimental procedures

3.2.1 Materials

Solvents, dimethylformamide (DMF), dichloromethane (DCM), methanol (MeOH), dimethyl sulfoxide (DMSO), ethyl acetate, ether, and acetonitrile (ACN) were purchased from VWR, Fisher Scientific, or Sigma-Aldrich and were reagent grade or better. Piperidine, diisopropyl ethylamine (DIPEA), trifluoroacetic acid (TFA), triisopropyl silane (TIS), lithium hydroxide, bis(benzonitrile)palladium(II) chloride, copper(I) bromide, ethylenebis(diphenylphosphine) (DPPE), Chloramine T trihydrate, lithium diisopropyl amide (LDA), propargyl chloride, and sodium carbonate (Na_2CO_3), were purchased from Sigma-Aldrich. Sodium sulfate was purchased from Macron Chemicals. Fmoc-11-aminoundecanoic acid (Fmoc-AUA), 1-[bis(dimethylamino)methylene]-1H-1,2,3-triazolo[4,5-b]-pyridinium 3-oxide hexafluorophosphate (HATU), chloro-trityl resin, and *N*-9-fuorenylmethoxycarbonyl-L-aspartic acid (Fmoc-L-Asp-OH) were purchased from AKsci. *N*-2-*N*-6-Bis(9-fluorenyl-methyloxycarbonyl)-L-lysine (Fmoc-Lys(Fmoc)-OH) was purchased from Aapptec and 9-fluorenylmethoxycarbonyl-8-amino-3,6-dioxaoctanoic acid (Fmoc-miniPEG) was purchased from BioBlocks. Sephadex LH20 beads were purchased from Amersham Pharmacia Biotech AM. Fmoc–Azidohomoalanine (Fmoc-Dab(N3)-OH), 3-acetoxylindole, and Bromostatin were purchased from Chem-Impex International.

3.2.2 Synthesis of 6’-bromoindirubin (I)

6’-Bromoindirubin was synthesized as previously described [24] with modifications. Briefly, 615 mL of anhydrous methanol was set stirring under nitrogen in

a 2 L round bottom flask. 6-Bromoisatin 3.37 g (15 mmol) and 3-acetoxylindole 2.63 g (15 mmol) were then added and the solution was bubbled with nitrogen for 45 min. Anhydrous sodium carbonate 3.98 g (37.5 mmol) was added and the reaction was stirred for 5 h in the dark. The resultant dark purple precipitate was isolated by centrifugation, the solid decanted with methanol and resuspended in ethyl acetate. The 6'-bromoindirubin was washed 3x with brine. The organic layer was dried with sodium sulfate and the solvent removed under reduced pressure to yield a dark purple solid. Yield: >90%, mass: 338.94, 340.93 (the two masses are due to the two common isotopes of bromine).

3.2.3 Synthesis of 6'-bromoindirubin-3'-oxime

(**II**, 6BIO). 6′-bromoindirubin-3′-oxime (6BIO) was synthesized as described in Polychronopoulos et al. [24]. 6-Bromoindirubin 3.06 g (9 mmol) and hydroxylamine hydrochloride 6.25g (90 mmol) were combined in a pressure reaction tube. Ninety mL of pyridine was added and purged under argon for 30 min. The reaction was sealed and stirred at 115-120° C for 2.5 h. The pyridine was removed under reduced pressure and the dark red product solid was washed with hexanes. The product was suspended in ethyl acetate and washed 2x with water followed by a wash with brine. The organic phase was dried with sodium sulfate and solvent removed under reduced pressure yielding a dark red solid (See Supporting Information). Yield >90% mass: 353.96, 355.96.

3.2.4 Synthesis of 2,2-dimethylpent-4-ynoic acid

Briefly, a round-bottom flask was dried and purged with nitrogen and cooled to -78°C. LDA 2M 6.1 mL (13 mmol) was added and a stream of nitrogen was used to bubble the reaction. Methyl isobutyrate 1.6 mL (14 mmol) was added dropwise as the reaction was stirred. Propargyl chloride 891 µL (10 mmol) was also added dropwise as the reaction was stirred vigorously. The solution was allowed to warm to room temperature and was stirred over night. The reaction was then quenched with concentrated NH_4Cl and extracted with ethyl acetate. The organic layer was dried with sodium sulfate and solvent removed under reduced pressure until a yellow oil remained.

Lithium hydroxide 480 mg (20 mmol) and MeOH were added to the product and stirred overnight, removing the methyl ester. Water was added to the reaction and acidified to pH 2 prior to extracting twice with ethyl acetate. The organic layer was dried with sodium sulfate and the solvent was removed under reduced pressure. Yield was 7% (2,2-dimethylpent-4-ynoic acid).

3.2.5 Synthesis of (2Z,3E)-6'-bromo-3-(((2,2-dimethylpent-4-ynoyl)oxy)imino)-[2,3'-biindolinylidene]-2'-one (III)

6BIO was conjugated to 2,2-dimethylpent-4-ynoic acid using standard DCC-assisted ester coupling. 6BIO 18 mg (0.05 mmol), 2,2-dimethylpent-4-ynoic acid (7.5 mg; 0.06 mmol), and DCC 12.4 mg (0.06 mmol) were added to 3 mL of DMF under nitrogen. DIPEA 26 µL (0.15 mmol) was then added and the reaction was stirred under nitrogen for 4 h. The product was filtered and dissolved in ethyl acetate. The solution was then washed 3 times with water and dried with sodium sulfate. The solvent was

removed under reduced pressure onto celite (diatomite) and purified using flash chromatography (hexanes / ethyl acetate) (see Supporting Information). Yield: 80%.

3.2.6 Synthesis of amphiphilic unimers flanked with C-terminal azide

Unimers were synthesized as previously described with slight modifications [17]. Briefly, in a small glass vial, 2-chlorotrityl resin (1.11 mmol/g) was loaded at 0.4 mmol/g with Fmoc-Dab(N3)-OH overnight in DCM and DIPEA. The resin was transferred to a SPPS vessel capable of bubbling nitrogen. The resin was then capped with four 5 mL washes of DCM:MeOH:DIPEA (17:2:1) followed by three washes of DMF. Following each amino acid addition, Fmoc-groups were removed during two 20-min incubations with 20% (v/v) piperidine in DMF. The resin was then washed three times with DMF prior to the next amino acid being added. Fmoc-AUA was added twice in a five-fold excess using HATU/DIPEA. Following addition of Fmoc-AUA, branched unimers (N3-A2-K-D4) were prepared by adding Fmoc-Lys(Fmoc)-OH followed by miniPEG and 4 aspartic acids. Linear unimers were created by adding miniPEG and 8 aspartic acids to the AUA. Both unimers were capped with acetic acid, HATU, and DIPEA. The final resin-bound products were washed with DMF, DCM, MeOH (3 x each) and dried under nitrogen. The products were cleaved from resin using TFA:TIS:H_2O (90:5:5) and precipitated in diethyl ether prior to HPLC purification.

3.2.7 Click conjugation of (2Z, 3E)-6'-bromo-3-(((2,2-dimethylpent-4-ynoyl)oxy)imino)-[2,3'-biindolinylidene]-2'-one to unimers

N3-A2-D8 and N3-A2-K-D4 (both 0.01 mmol) were dissolved in DMF and purged with nitrogen for 20 min. Additional DMF was purged with nitrogen and was used to dissolve a mixture of (2*Z*,3*E*)-6'-bromo-3-(((2,2-dimethylpent-4-ynoyl)oxy)imino)-[2,3'-biindolinylidene]-2'-one (0.03 mmol), copper(I)bromide (0.01 mmol), and TBTA (0.01 mmol). The two solutions were combined and stirred under nitrogen for 20 min. Ascorbic acid (0.01 mmol) and a drop of water were then added. The reaction proceeded for 40 min, after which it was diluted in MeOH and purified on LH20 column. The fractionated peaks were dried under reduced pressure. Yields for BIO-N3-A2-D8 and BIO-N3-A2-K-D8 were 65% and 48%, respectively (see Supporting Information).

3.2.8 Dynamic light scattering measurements of micelles

The hydrodynamic radius of the micelles were determined using Malvern Zetasizer Nano ZS. Measurements of both unimers were taken using 2.4 nmol/mL unimer at 25°C. Malvern software was used to determine hydrodynamic diameter.

3.2.9 Release kinetics of 6BIO from micelles

Release kinetics was measured for each of the micelles. Unimer (0.1 mg) was dissolved in 1 mL of PBS containing 30% MeOH. Samples for each time point (0, 1 h, 2 h, 4 h, 8 h, 12 h, and 24 h) were made in triplicate. Each sample was incubated in a water bath at 37°C for the allotted length of time. Each sample was then measured at λ=290 nm on an Agilent 1200 (0.01 M NH_4HCO_3, ACN). Area under the curve was measured

using MestReNova software and the percent of the drug peak released was calculated as follows:

$$\frac{\text{Free 6BIO}}{\text{Free 6BIO} + \text{Micellar 6BIO}} * 100$$

3.2.10 Stannylation of 6BIO

Stannylation of 6BIO was performed as previously described for other indols [25]. To a pressure tube, 6BIO (1 mmol) was dissolved in 20 mL dioxane and purged with argon for 30 min. $PdCl_2(PhCN)_2$ (0.05 mmol), DPPE (0.1 mmol), and tributyl tin (3 mmol) were then added. The tube was purged with argon for an additional 10 min and sealed. The reaction was stirred vigorously at 110°C for 12 h. The product was dried on celite and purified using flash chromatography (hexanes 1% TEA/ EtOAc). The solvent was removed under reduced pressure resulting in a brown red solid (2*Z*,3*E*)-3-(hydroxyimino)-6'-(tributylstannyl)-[2,3'-biindolinylidene]-2'-one (see Supporting Information).

3.2.11 O-Alkylation of stannylated BIO ((2Z,3E)-3-(hydroxyimino)-6'-(tributylstannyl)-[2,3'-biindolinylidene]-2'-one)

DMF was added to a mixture of (2*Z*,3*E*)-3-(hydroxyimino)-6'-(tributylstannyl)-[2,3'-biindolinylidene]-2'-one (56 mg; 0.1 mmol), propargyl chloride (7.2 μL; 0.1 mmol), and cesium carbonate 38 mg (0.1 mmol) and stirred vigorusly [26]. The reaction was monitored every half hour throughout the reaction by LC/MS. At 1.5 h a small amount of dialkylated side-product was formed, and the reaction was stopped by adding water. The product was then extracted into EtOAc and washed 3 times with water and dried on

sodium sulfate. Celite was added and the solvent was removed by reduced pressure. The product was purified by reverse phase chromatography (H_2O-1% DIPEA; ACN-1% DIPEA). The product, (2*Z*,3*E*)-3-((prop-2-yn-1-yloxy)imino)-6'-(tributylstannyl)-[2,3'-biindolinylidene]-2'-one, was brownish purple (see Supporting Information).

3.2.12 Conjugation of alkylated stannylated 6BIO to unimers

Each unimer (N3-A2-D8 or N3-A2-K-D4) (0.01 mmol) was dissolved in DMF and purged with nitrogen for 20 min. To a separate vial of DMF purged with nitrogen (2*Z*,3*E*)-3-((prop-2-yn-1-yloxy)imino)-6'-(tributylstannyl)-[2,3'-biindolinylidene]-2'-one (0.03 mmol), copper(I)bromide (0.01 mmol), DIPEA (0.1 mmol), and TBTA (0.01 mmol) were added. The two solutions were combined and stirred under nitrogen for 40 min. Upon completion the reaction was diluted in MeOH and purified on LH20 column (MeOH 1% DIPEA). The fractionated peaks were dried under reduced pressure, yielding a bluish purple solid.

3.2.13 Radio-iodination of micelles and 6BIO

The stannylated unimers and stannylated 6BIO (0.3–0.5 μmol) were dissolved in 100 μL DMF. The solutions were transferred to Wheaton V-vials containing a solution of [^{125}I]NaI (5.0 mCi) in 100 μL DMF phosphate-buffered saline (PBS) (pH 7.4). Chloramine-T was added, and the reaction mixture stirred for 15 min at ambient temperature. Purification of the iodinated micelles was performed using a LH20 column eluted with MeOH. Iodinated 6BIO was dissolved in EtOAc and was washed twice with water. The solvent of all three reactions was evaporated using a stream of nitrogen, and

the residue was dissolved with PBS (pH 7.4) to obtain solutions with an activity concentration of 370 kBq/100 μL. The overall radiochemical yield was ca. 10% (see Supporting Information).

3.2.14 Murine fracture induction

All animal studies were reviewed and approved by Purdue's animal care and use committee protocol and were performed as described in the literature. CD4 Swiss mice (30-35 g) acquired from Harlan laboratories were used for these experiments. A stabilized femoral fracture was performed under aseptic conditions with isoflurane anesthesia. Skin around the knee was shaved and cleaned with an alcohol pad first, then with Betadine solution. The skin incision was made medial parapetellar. The patella was then dislocated and an incision was made under the patella. A 25 gauge needle was used to ream the intramedullary canal. A 22-guage locking nail (where both ends are flattened to produce rotational stability), was then inserted. The wound was sutured and the bone was then fractured using a three point bending device that has a built-in stop to prevent excess injury. Subcutaneous Buprenorphine (0.05 – 0.1 mg/kg) was administered at the time of surgery, followed by a dose every 12 h for 3-7 days post operation.

3.2.15 Injection and dissection techniques/counting for 24 h biodistribution

From the iodinated products described previously 1 uCi/mL solutions were made in sterile PBS. The study was performed on 3 groups of mice with 5 mice per group. Two weeks following fracture induction, each mouse received a 0.1 μCi (0.1 mL) dose of the radio-iodinated linear micelles, branched micelle, or free drug. Animals were then placed

back in their cages for 24 h. At 24 h they were euthanized using CO_2 excess. Blood was drawn from a cardiopuncture and all other organs measured were removed (lungs, liver, spleen, kidneys, fractured femur, healthy femur). The activity was counted using Packard Cobra Auto-Gamma and was normalized by dividing the count rate by the weights of each organ.

3.2.16 Injection and techniques for imaging

From the iodinated products described previously, 1 mCi/mL solutions were made in sterile PBS. The study was performed on 3 groups of mice with 5 mice per group. Two weeks following fracture induction each mouse received 0.1 mCi (0.1 mL) of dose. Animals were then returned to their cages until euthanasia by CO_2 overdose at the desired time point (1 h, 4 h, 24 h). Animals were imaged using MiLabs U-SPECT-II/CT. 3D reconstructions were performed using Image J software.

3.3 Results and discussion

3.3.1 Design and characterization of micelles

We set out to develop a fracture-targeted anabolic-loaded micelle by utilizing the unique microenvironment available in bone fractures. That is, freshly exposed HAp due to a fracture, additional HAp exposed by osteoclasts during resorption, newly exposed calcified bone, and the local inflammatory response.

HAp can be targeted using any one of several bone adsorbing ligands, including bisphosphonates, tetracycline, and acidic oligopeptides. Both bisphosphonates and tetracycline have biocompatibility issues with osteonecrosis of the jaw and the staining of

teeth yellow, respectively [27–29]. In order to maintain bone homeostasis, the more biocompatible option is acidic oligopeptides. Aspartic acid octapeptide, as evidence suggests, is near an ideal number of aspartic acids to ensure rapid binding [30]. Unlike bisphosphonates and tetracyclines, aspartic acid octapeptide has a low toxicity even in very high concentrations [17,31].

Targeting a drug to a fracture site via aspartic acid octapeptides by itself does not fully exploit the microenvironment of a fracture. In fractured bones, the extent of bone accumulation is expected to be far more dramatic when using large molecules. Yuan et al. proposed a mechanism by which inflamed tissue leads to leaky vasculature and subsequent inflammatory cell-mediated sequestration (ELVIS). This theory essentially states that large molecules will readily be extravasated from the leaky vasculature of the inflamed fracture callus. Then, inflammatory cells actively phagocytose and sequester any large molecules in the area [32,33]. Bone fracture calluses certainly fall under the category of inflamed tissue, and as such, higher drug accumulation could hypothetically be achieved by increasing the size of a drug delivery system.

The proposed micellar design is a simplified way of increasing the size of the drug delivery system to increase accumulation in inflamed tissue. By using the hydrophilic targeting peptide, aspartic acid octapeptide, covalently bound by a hydrolyzable linker to a hydrophobic drug, a micelle-forming unimer was created. The designed unimer was largely synthesized using solid-phase peptide synthesis (SPPS). Synthesis began with an azide-containing amino acid (azidohomoalanine) that provided a clickable point of attachment for a drug/linker. To the azide-containing amino acid, two 11-aminoundecanoic acids (AUAs) were attached to increase the hydrophobicity and

therefore the stability of the micelle. A miniPEG spacer (8-amino-2,6-dioxaoctanoic acid) was added for flexibility, followed by aspartic acid octapeptide for targeting. Finally, the unimer was capped with acetic acid, preventing the terminal primary amine from initiating premature hydrolysis of the amine-sensitive drug linker yielding the finalized linear unimer, BIO-A2-D8 (Figure 3.2). BIO-A2-D8 indicates that it is a 6BIO (BIO)-containing unimer with two aminoundecanoic acids (A2) and eight aspartic acids in a linear fashion (D8).

The stability of the micelle can be modified by increasing or decreasing the number of AUAs. However, increasing the number of AUAs in a linear micelle by too much can result in aggregates and nonmicellar structures. To increase the number of AUAs and avoid the formation of nonmicellar structures, we also studied a branched aspartic acid head group. Building from the original azide-aminoundacanoic acid base, lysine was added to the second aminoundecanoic acid. Both primary amines on the lysine were deprotected and miniPEG was added to both, followed by four aspartic acids each and capping with acetic acid. The 6BIO (BIO)-conjugated unimer containing two aminoundecanoic acids (A2) is branched at the lysine (K) and ends in two branches of four aspartic acids (D4), yielding BIO-A2-K-D4. This branched conformation increased the head group size and therefore the conicity of the unimer. By increasing the head group size, far greater hydrophobic portions could be incorporated before the conicity of the unimer was lost, and a bilayer, aggregate, or other conformation was formed [17].

The designed micelles, in addition to increasing the fracture accumulation by increasing the size, have several unique features. By building the unimers by SPPS, the unimers were monodisperse, which aided in characterization. Furthermore, each unimer

featured a targeting ligand and a drug. This means that in the event of the micelle rupturing in the blood stream, the drug still could accumulate in the fracture site by aspartic acid octapeptide-HAp interactions. In addition, whereas many micelles have inconsistent drug loading, the linear and branched micelles contained a consistent 17% or 15% drug loading by weight, respectively.

The drug being attached to the unimers was a GSK3β inhibitor, 6BIO. It has been used for increasing osteoblast activity and has an enzymatic IC50 of 5 nmol [18,21,34]. 6BIO by itself, however, is not soluble in water. By including 6BIO in the unimer design, the unimer solubilized the drug while the drug stabilized the micelle. The oxime of 6BIO was first conjugated to the carboxylic group of a 4-pentynoic acid derivative and then clicked to the azide-containing unimer by the alkyne on the 4-pentynoic acid derivative. Upon completion of the click reaction, the micelle was purified, dried, and formed micelles upon reconstitution in PBS.

3.3.2 Size determination by dynamic light scattering

Dynamic light scattering was used to determine the hydrodynamic diameter of the micelles. The micelles self-assembled at the concentrations theorized to be sufficient for injection for fracture healing. BIO-A2-D8 and BIO-A2-K-D4 were 28.8 nm and 11.2 nm, respectively (Figure 3.3). Sizes were slightly smaller than the micelles with similar structures in our previous work with doxorubicin-loaded micelles [17].

3.3.3 Micellar drug release

Drug-linker selection plays an important role in maintaining targeting ligand to drug integrity until the drug has reached the target tissue. This micelle features an oxime linkage which is base sensitive and hydrolytically cleavable at the pH ranges found in a bone fractures (6.9-7.6) [35]. Simple 4-pentynoic oxime esters degrade within hours (see Supporting Information) and would likely release 6BIO prior to fracture accumulation. To improve the hydrolytic stability of the conjugate, germinal dimethyl substituents were introduced into the structure (Figure 3.2). This increased steric hindrance to the 107° Bürgi-Dunitz angle required for a B_{ac2} reaction to release the drug and completely eliminate the possibility of an E_{1cb} reaction. The stabilized oxime ester linkage slowly reached 30% release over 24 h and continued to release over several days (Figure 3.4). Though the linker is not specific to the fracture microenvironment, the slow degradation would reduce the amount of drug released in the blood stream prior to fracture accumulation, and reduces the frequency of necessary dosing for treatment.

3.3.4 Biodistribution

3.3.4.1 Organ biodistribution at 24 h

BIO-A2-D8 and BIO-A2-K-D4 have hydrolyzable oxime ester linkages designed to release the 6BIO for treatment of bone fractures. Although a cleavable linker is necessary for therapy studies, it may pose a problem with biodistribution studies. At 24 h of an *in vivo* study, 30% of the drug may be released. In a biodistribution study, premature release would not give accurate information on how well the targeting ligand is able to remain in the fracture site. A nondegradable oxime ether linker replaced the

oxime-ester linker in the micelles for biodistribution. Radiolabeling BIO-A2-D8, BIO-A2-K-D4 and 6BIO was done by substituting the bromine on 6BIO with ^{125}I. These minor modifications allowed the majority of the molecule to remain unmodified while giving information on targeting and free drug clearance (Figure 3.5).

In bone, HAp increases in crystallinity over time. It is this higher crystalline state to which AOs preferentially bind [3,16]. In bone fracture patients, highly active osteoclasts produce extensive resorption surfaces by exposing highly crystalline HAp surfaces to which AOs are able to target [36]. This specificity to highly crystalline HAp may additionally reduce nonspecific binding to the majority of the nonfractured bone. An organ biodistribution was performed to elucidate this and other questions about the fate of the micelles *in vivo*.

Several interesting observations emerged from the biodistribution. 6BIO is a hydrophobic drug and its high accumulation in the lungs, liver, and spleen was likely due to the drug aggregating. By turning the drug into an amphiphile, the particle size was controlled, and the liver, spleen, and lung accumulation all decreased significantly ($p<0.001$) (Figure 3.6). However, kidney uptake dramatically increased with both micelles ($p<0.001$). The kidney accumulation may be due to the kidney's ability to recycle peptides such as the aspartic acid octapeptide back into the blood stream [37,38]. As long as the micelle is not internalized into renal cells, the 6BIO should eventually hydrolyze, be cleared, and not inhibit GSK3β expression.

The primary purposes of this study were to elucidate the bone- and fracture-targeting potential of targeted micelles over free drug, as well as the differences between branched and linear designs. Naturally, accumulation in healthy femurs was higher in

both the linear (1.0±0.27; $p<0.01$) and the branched (1.4±0.14; $p<0.001$) micelles than free 6BIO (0.5± 0.10). This is also the first evidence of the branched micelle having a higher accumulation than the linear micelle in bone ($p<0.05$). These trends were amplified when comparing the fractured femurs. The fractured femurs of the free 6BIO, linear, and branched micelles were each statistically different from each other ($p<0.001$), with values of 0.4±0.05, 1.9±0.32, and 6.0±0.51, respectively. Both unimers demonstrated an important increase of accumulation in the fractured femurs over the free drug control.

The micelles were able to show fracture-specific targeting compared to healthy bone. While there was no statistical difference in accumulation of the free drug between the healthy and the fractured femurs, both the linear and the branched micelles showed significantly ($p<0.001$) higher drug uptake in the fractured femur by a 1.8 and a 4.3 fold increase, respectively.

3.3.4.2 SPECT/CT biodistribution

In order to validate the organ biodistribution and study the clearance of the micelles, SPECT/CT imaging was performed at 1 h, 4 h, and 24 h (Figure 3.7). In general, fracture-specific uptake was more evident at later time points than earlier ones. At 1 h, a small amount of fracture accumulation was visible in both micelles; however, high signal intensities in both the lungs and kidneys made them difficult to discern. On the other hand, at 1 h, the free drug was primarily found in the stool. At 4 h, free drug was still primarily contained in the bowel; however, spleen accumulation began to be more evident. Again this bowel uptake was likely due to aggregation of free 6BIO and

the resultant uptake by macrophages in the lungs, liver, and spleen, resulting in clearance through the bile into the bowels. Meanwhile, the linear micelle had cleared somewhat from the lungs, was still strong in the kidneys, but much more visible in the fracture. The branched unimer showed superior targeting at 4 h, with the majority of accumulation in the femur and kidneys. At 24 h, free drug appears to be cleared; all signals were background. Both micelles had their highest fracture accumulation intensities at 24 h relative to other organs. Liver to kidney accumulation was lower in the branched unimer, which correlates with the 24-h organ biodistribution data (Figure 3.7-24 h compared to Figure 3.6). In both micelles throughout the experiment there was no apparent accumulation in the bowels, leading us to believe that most was excreted through urination. Most importantly, there was no noticeable uptake in the healthy bone while the fractured bone had high accumulation.

Between the SPECT data and the organ biodistribution data there were a few discrepancies. Primarily, the high ratio of renal accumulation to fracture accumulation in the organ biodistribution is not as pronounced in the SPECT data. There are several explanations for this. First, the kidneys contain proteins for the reabsorption of peptides from the urine [37,38]. It is plausible that peptide kidney transporters were saturated in the SPECT study due to a 100-fold increase in drug dose compared to the organ biodistribution. Bone fracture targeting is not limited by a finite number of receptors as in the kidney; rather, it is limited by the surface area of the bone and may not have been similarly saturated.

In addition, the organ biodistribution is measured in *injected dose/gram* and does not account for differences in tissue type or location of accumulation within an organ.

Bone is far more dense (1900 kg/m^3) than soft tissue organs such as kidneys or liver (1030-1060 kg/m^3) [39]. This difference in density dilutes the injected dose/gram measurements in bone compared to an organ such as a kidney. While no hotspots are found in the kidney due to the accumulation being distributed throughout the entire kidney, the signal in fractured femur is further muted by the entire bone being weighed for the measurement rather than the fracture alone. The combination of these factors better explains why in the SPECT study, accumulation per volume is much higher in the fracture compared to the kidney.

3.4 Conclusions

In this study we created two fracture-targeted micelles designed to increase the rate of healing in bone fractures. These micelles are built on the concept that the micellar corona can function as both a moiety that gives amphiphilicity, as well as being a low-toxicity targeting ligand. Likewise, the 6BIO drug both functions as a pharmaceutical and gives stability to the micelle core. The micelles also feature a hydrolyzable oxime ester bond to the drug that releases the drug unmodified over several days.

In vivo, both the branched and linear micelle designs demonstrated excellent uptake in fractured bone versus healthy bone. The branched unimer demonstrated both a higher ratio of fracture to kidney uptake and fracture to healthy bone accumulation over the linear unimer. Future treatment studies will elucidate fracture-healing capabilities of these micelles and include histology of the kidneys and liver to assess any acute toxicities associated with the treatment.

With an aging population and an increase in prescription bisphosphonates,

debilitating nonunion and delayed union bone fractures are inevitable. The development of a bone anabolic agent delivery system has not caught up with the demand of an aging population. The problem needs to be approached in a two-fold manner. First, more basic research into understanding biochemical pathways in the fracture that might be employed in developing anabolic agents and understanding the bone microenvironment in order to develop better release mechanisms. Second, applied research needs to be conducted controlling the deposition and release of anabolic agents. This research answers some of the questions. With additional studies, a nonsurgical treatment for delayed union and nonunion fractures may be possible.

3.5 References

[1] J.E. Shea, S.C. Miller, Skeletal function and structure: Implications for tissue-targeted therapeutics, Adv. Drug Deliv. Rev. 57 (2005) 945–957.

[2] A.S. Posner, F. Betts, Synthetic amorphous calcium phosphate and its relation to bone mineral structure, Acc. Chem. Res. 8 (1975) 273–281.

[3] D. Wang, S.C. Miller, L.S. Shlyakhtenko, A.M. Portillo, X.-M. Liu, K. Papangkorn, P. Kopečková, Y. Lyubchenko, W.I. Higuchi, J. Kopeček, Osteotropic peptide that differentiates functional domains of the skeleton, Bioconjug. Chem. 18 (2007) 1375–1378.

[4] D. Lacey, E. Timms, H.L. Tan, M. Kelley, C. Dunstan, T. Burgess, R. Elliott, A. Colombero, G. Elliott, S. Scully, et al., Osteoprotegerin ligand is a cytokine that regulates osteoclast differentiation and activation, Cell. 93 (1998) 165–176.

[5] H. Yasuda, N. Shima, N. Nakagawa, K. Yamaguchi, M. Kinosaki, S. Mochizuki, A. Tomoyasu, K. Yano, M. Goto, A. Murakami, E. Tsuda, T. Morinaga, K. Higashio, N. Udagawa, N. Takahashi, T. Suda, Osteoclast differentiation factor is a ligand for osteoprotegerin/osteoclastogenesis-inhibitory factor and is identical to TRANCE/RANKL, Proc. Natl. Acad. Sci. 95 (1998) 3597–3602.

[6] H. Väänänen, H. Zhao, M. Mulari, J.M. Halleen, The cell biology of osteoclast function, J. Cell Sci. 113 (2000) 377–381.

[7] S. Harada, Control of osteoblast function and regulation of bone mass, Nature. 423 (2003) 349–355.

[8] R. Bartl, B. Frisch, C. Bartl, Osteoporosis: Diagnosis, prevention, therapy, Springer, 2009.

[9] D.W. Dempster, Osteoporosis and the burden of osteoporosis-related fractures, Am J Manag Care. 17 (2011) S164–S169.

[10] G.B. Bishop, T.A. Einhorn, Current and future clinical applications of bone morphogenetic proteins in orthopaedic trauma surgery, Int. Orthop. 31 (2007) 721–727.

[11] K.L. Ong, M.L. Villarraga, E. Lau, L.Y. Carreon, S.M. Kurtz, S.D. Glassman, Off-label use of bone morphogenetic proteins in the United States using administrative data, Spine. 35 (2010) 1794–1800.

[12] P. Fournier, S. Boissier, S. Filleur, J. Guglielmi, F. Cabon, M. Colombel, P. Clézardin, Bisphosphonates inhibit angiogenesis in vitro and testosterone-stimulated vascular regrowth in the ventral prostate in castrated rats, Cancer Res. 62 (2002) 6538–6544.

[13] E. Giraudo, M. Inoue, D. Hanahan, An amino-bisphosphonate targets MMP-9–expressing macrophages and angiogenesis to impair cervical carcinogenesis, J. Clin. Invest. 114 (2004) 623–633.

[14] T. Ziebart, A. Pabst, M.O. Klein, P. Kämmerer, L. Gauss, D. Brüllmann, B. Al-Nawas, C. Walter, Bisphosphonates: restrictions for vasculogenesis and angiogenesis: inhibition of cell function of endothelial progenitor cells and mature endothelial cells in vitro, Clin. Oral Investig. 15 (2009) 105–111.

[15] J. Ishizaki, Selective drug delivery to bone using acidic oligopeptides, J. Bone Miner. Metab. 27 (2009) 1–8.

[16] S. Miller, H. Pan, D. Wang, B. Bowman, P. Kopečková, J. Kopeček, Feasibility of using a bone-targeted, macromolecular delivery system coupled with prostaglandin E1 to promote bone formation in aged, estrogen-deficient rats, Pharm. Res. 25 (2008) 2889–2895.

[17] S.A. Low, J. Yang, J. Kopeček, Bone-targeted acid-sensitive doxorubicin conjugate micelles as potential osteosarcoma therapeutics, Bioconjug. Chem. 25 (2014) 2012–2020.

[18] R. Baron, G. Rawadi, Targeting the Wnt/beta-catenin pathway to regulate bone formation in the adult skeleton, Endocrinology. 148 (2007) 2635–2643.

[19] Y. Chen, H.C. Whetstone, A.C. Lin, P. Nadesan, Q. Wei, R. Poon, B.A. Alman,

Beta-catenin signaling plays a disparate role in different phases of fracture repair: implications for therapy to improve bone healing, PLoS Med. 4 (2007) 1216–1229.

[20] G. Sisask, R. Marsell, A. Sundgren-Andersson, S. Larsson, O. Nilsson, Ö. Ljunggren, K.B. Jonsson, Rats treated with AZD2858, a GSK3 inhibitor, heal fractures rapidly without endochondral bone formation, Bone. 54 (2013) 126–132.

[21] E. Piters, E. Boudin, W. Van Hul, Wnt signaling: A win for bone, Arch. Biochem. Biophys. 473 (2008) 112–116.

[22] M. Prabaharan, J.J. Grailer, S. Pilla, D.A. Steeber, S. Gong, Amphiphilic multi-arm-block copolymer conjugated with doxorubicin via pH-sensitive hydrazone bond for tumor-targeted drug delivery, Biomaterials. 30 (2009) 5757–5766.

[23] M. Hrubý, Č. Koňák, K. Ulbrich, Polymeric micellar pH-sensitive drug delivery system for doxorubicin, J. Controlled Release. 103 (2005) 137–148.

[24] P. Polychronopoulos, P. Magiatis, A.-L. Skaltsounis, V. Myrianthopoulos, E. Mikros, A. Tarricone, A. Musacchio, S.M. Roe, L. Pearl, M. Leost, P. Greengard, L. Meijer, Structural basis for the synthesis of indirubins as potent and selective inhibitors of glycogen synthase kinase-3 and cyclin-dependent kinases, J. Med. Chem. 47 (2004) 935–946.

[25] E.B. Corcoran, A.B. Williams, R.N. Hanson, A synthetic method for palladium-catalyzed stannylation at the 5- and 6-benzo positions of indoles, Org. Lett. 14 (2012) 4630–4633.

[26] A.J. McCarroll, J.C. Walton, Photolytic and radical induced decompositions of O-alkyl aldoxime ethers, J. Chem. Soc. Perkin Trans. 2. (2000) 1868–1875.

[27] R.E. Marx, Y. Sawatari, M. Fortin, V. Broumand, Bisphosphonate-induced exposed bone (osteonecrosis/osteopetrosis) of the jaws: risk factors, recognition, prevention, and treatment, J. Oral Maxillofac. Surg. 63 (2005) 1567–1575.

[28] A. O Hoff, B.B. Toth, K. Altundag, M.M. Johnson, C.L. Warneke, M. Hu, A. Nooka, G. Sayegh, V. Guarneri, K. Desrouleaux, J. Cui, A. Adamus, R.F. Gagel, G.N. Hortobagyi, Frequency and risk factors associated with osteonecrosis of the jaw in cancer patients treated with intravenous bisphosphonates, J. Bone Miner. Res. 23 (2008) 826–836.

[29] J.F. Madison, Tetracycline pigmentation of teeth., Arch. Dermatol. 88 (1963) 58–59.

[30] S.A. Low, J. Kopeček, Targeting polymer therapeutics to bone, Adv. Drug Deliv. Rev. 64 (2012) 1189–1204.

[31] T. Sekido, N. Sakura, Y. Higashi, K. Miya, Y. Nitta, M. Nomura, H. Sawanishi, K. Morito, Y. Masamune, S. Kasugai, K. Yokogawa, K. Miyamoto, Novel drug delivery system to bone using acidic oligopeptide: pharmacokinetic characteristics and pharmacological potential, J. Drug Target. 9 (2001) 111–121.

[32] F. Yuan, L. Quan, L. Cui, S.R. Goldring, D. Wang, Development of macromolecular prodrug for rheumatoid arthritis, Adv. Drug Deliv. Rev. 64 (2012) 1205–1219.

[33] K. Ren, P.E. Purdue, L. Burton, L.-D. Quan, E.V. Fehringer, G.M. Thiele, S.R. Goldring, D. Wang, Early detection and treatment of wear particle-induced inflammation and bone loss in a mouse calvarial osteolysis model using HPMA copolymer conjugates, Mol. Pharm. 8 (2011) 1043–1051.

[34] U. Krause, S. Harris, A. Green, J. Ylostalo, S. Zeitouni, N. Lee, C.A. Gregory, Pharmaceutical modulation of canonical Wnt signaling in multipotent stromal cells for improved osteoinductive therapy, Proc. Natl. Acad. Sci. USA. 107 (2010) 4147–4152.

[35] O. Swenson, Biochemical changes in the fracture hematoma, J. Bone Joint Surg. Am. 28 (1946) 288–293.

[36] A. Schindeler, M.M. McDonald, P. Bokko, D.G. Little, Bone remodeling during fracture repair: The cellular picture, Semin. Cell Dev. Biol. 19 (2008) 459–466.

[37] Y. Kanai, M.A. Hediger, Primary structure and functional characterization of a high-affinity glutamate transporter, Nature. 360 (1992) 467–471.

[38] M.E. Ganapathy, W. Huang, H. Wang, V. Ganapathy, F.H. Leibach, Valacyclovir: a substrate for the intestinal and renal peptide transporters PEPT1 and PEPT2, Biochem. Biophys. Res. Commun. 246 (1998) 470–475.

[39] J. Newman, Physics of the life sciences, Springer Science & Business Media, 2008.

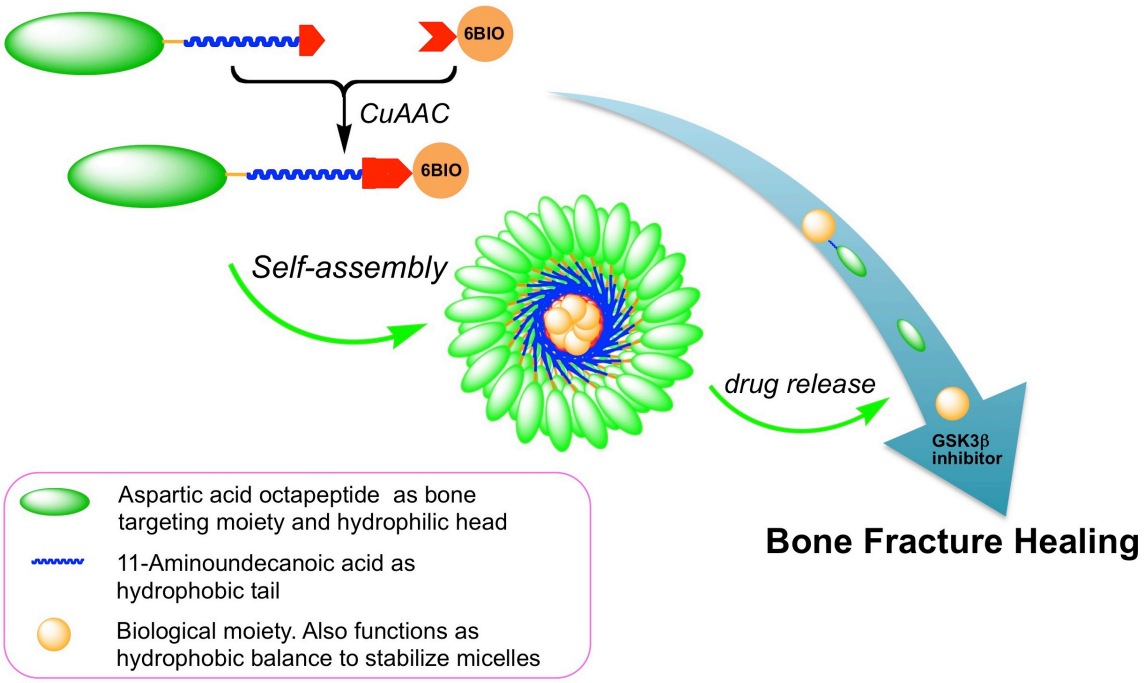

Figure 3.1. Fracture-targeting micelles from amphiphilic unimer consisting of aspartic acid octapeptide, miniPEG spacer, hydrophobic tail based on 11-aminoundecanoic acid and GSK3β inhibitor.

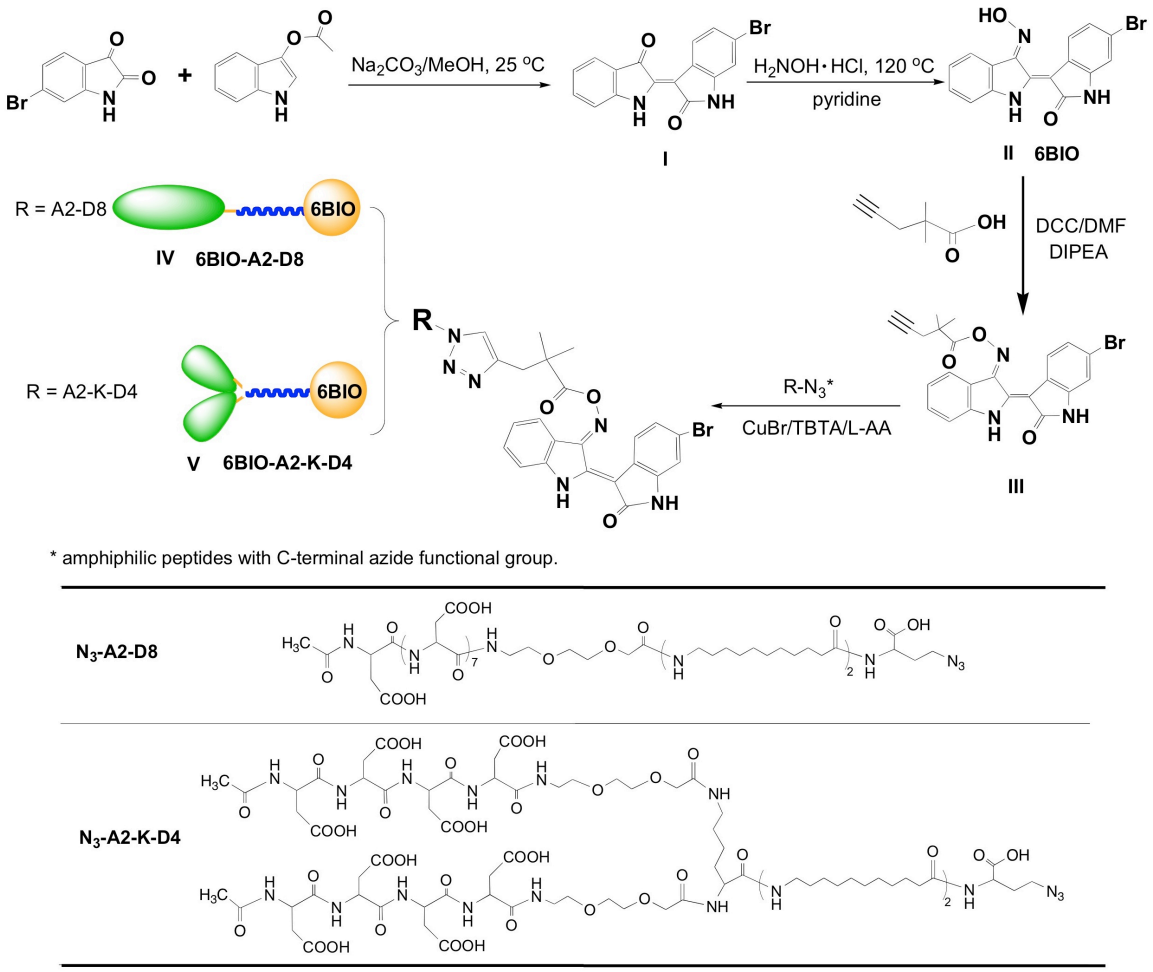

Figure 3.2. Synthesis of a clickable 6BIO and conjugation of 6BIO and linker to micelle unimers.

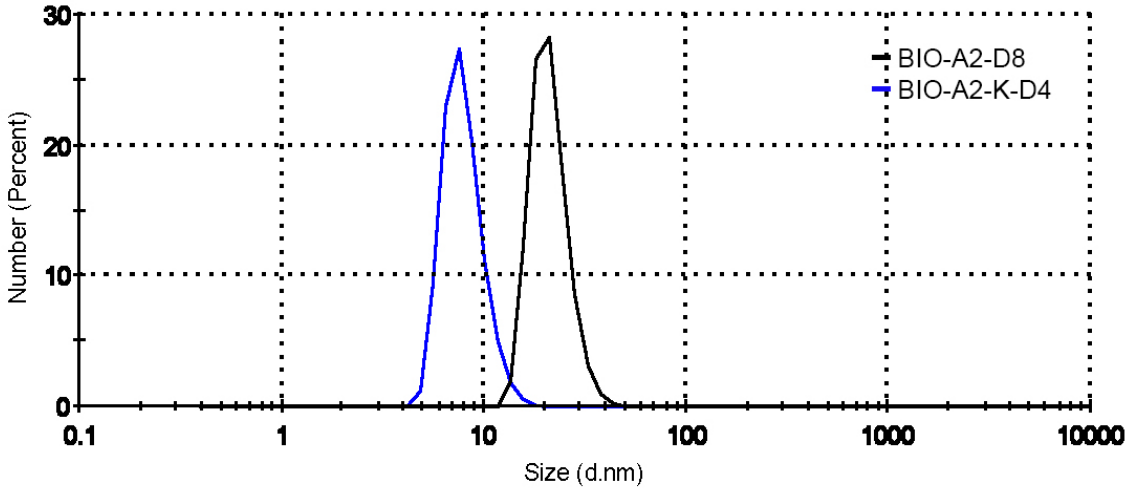

Figure 3.3: Dynamic light scattering of the linear micelle BIO-A2-D8 and the branched micelle BIO-A2-K-D4 in PBS at 25°C.

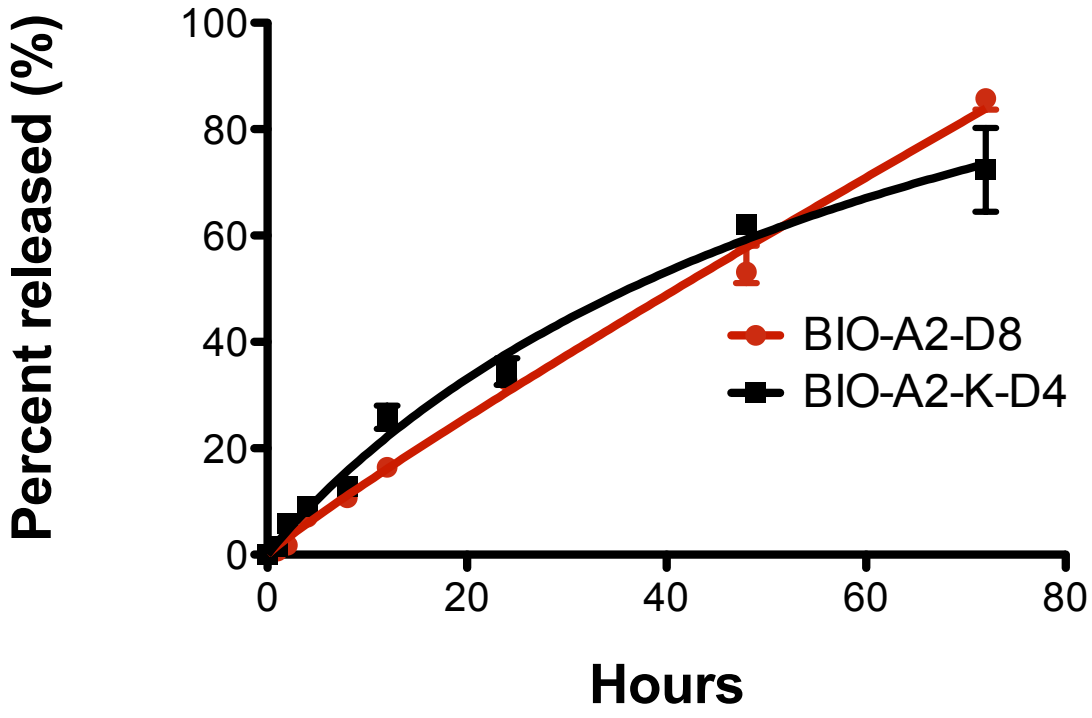

Figure 3.4. Time dependent 6BIO release from the linear micelle BIO-A2-D8 and from the branched micelle BIO-A2-K-D4 in PBS at 25°C

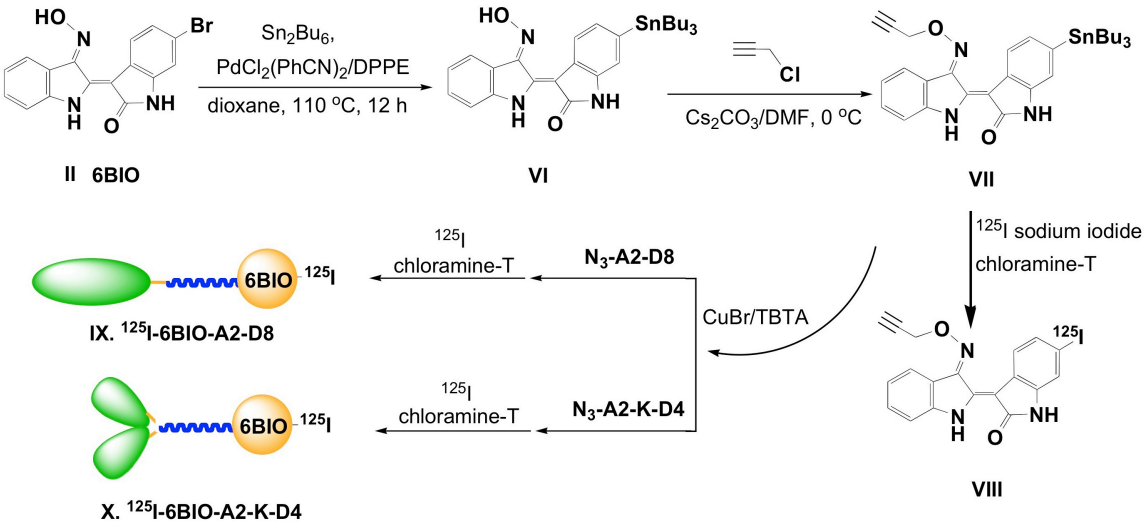

Figure 3.5. Synthesis of radio-iodinated micelles and 6BIO.

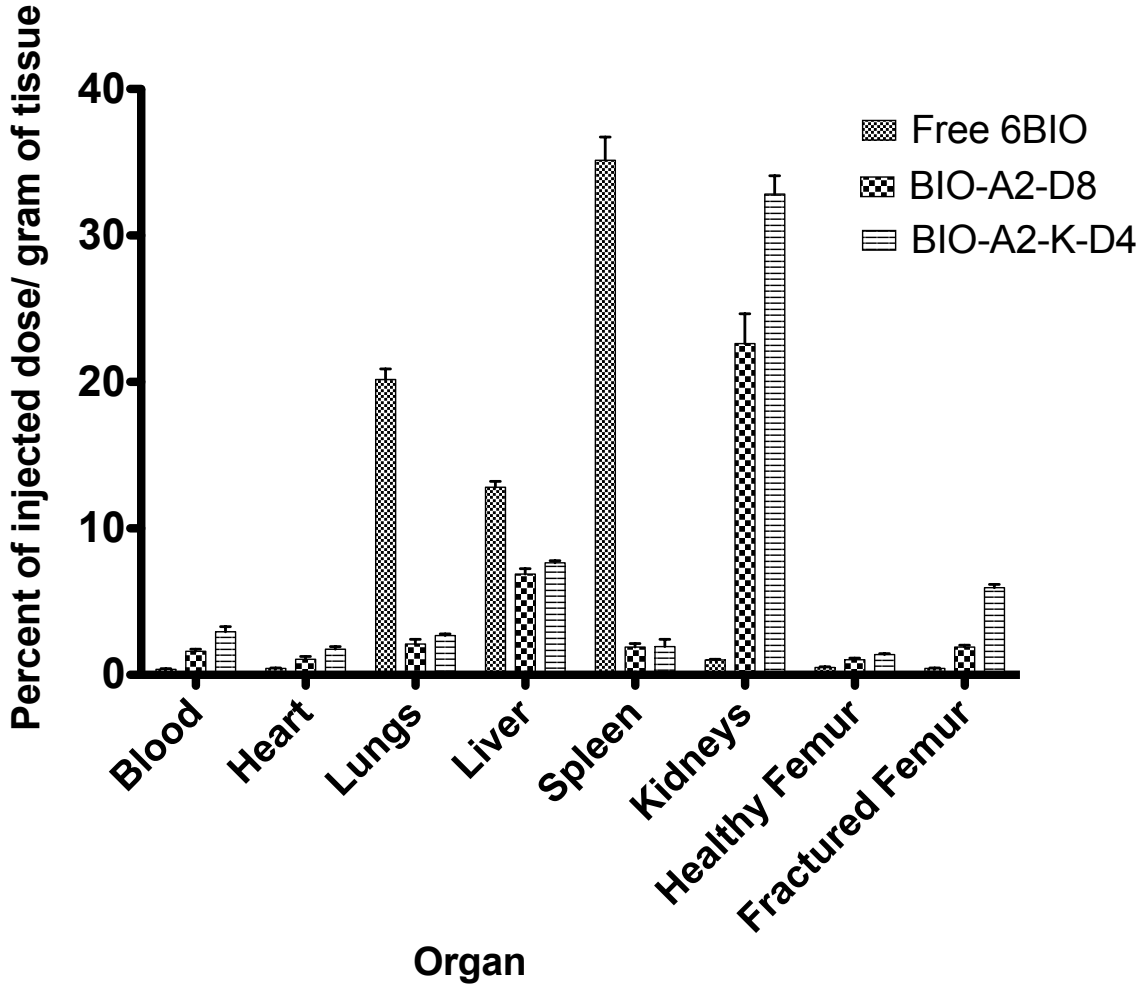

Figure 3.6. Organ biodistribution of free 6BIO, the linear micelle BIO-A2-D8, and the branched micelle BIO-A2-K-D4 measured in percent of injected dose/gram of tissue.

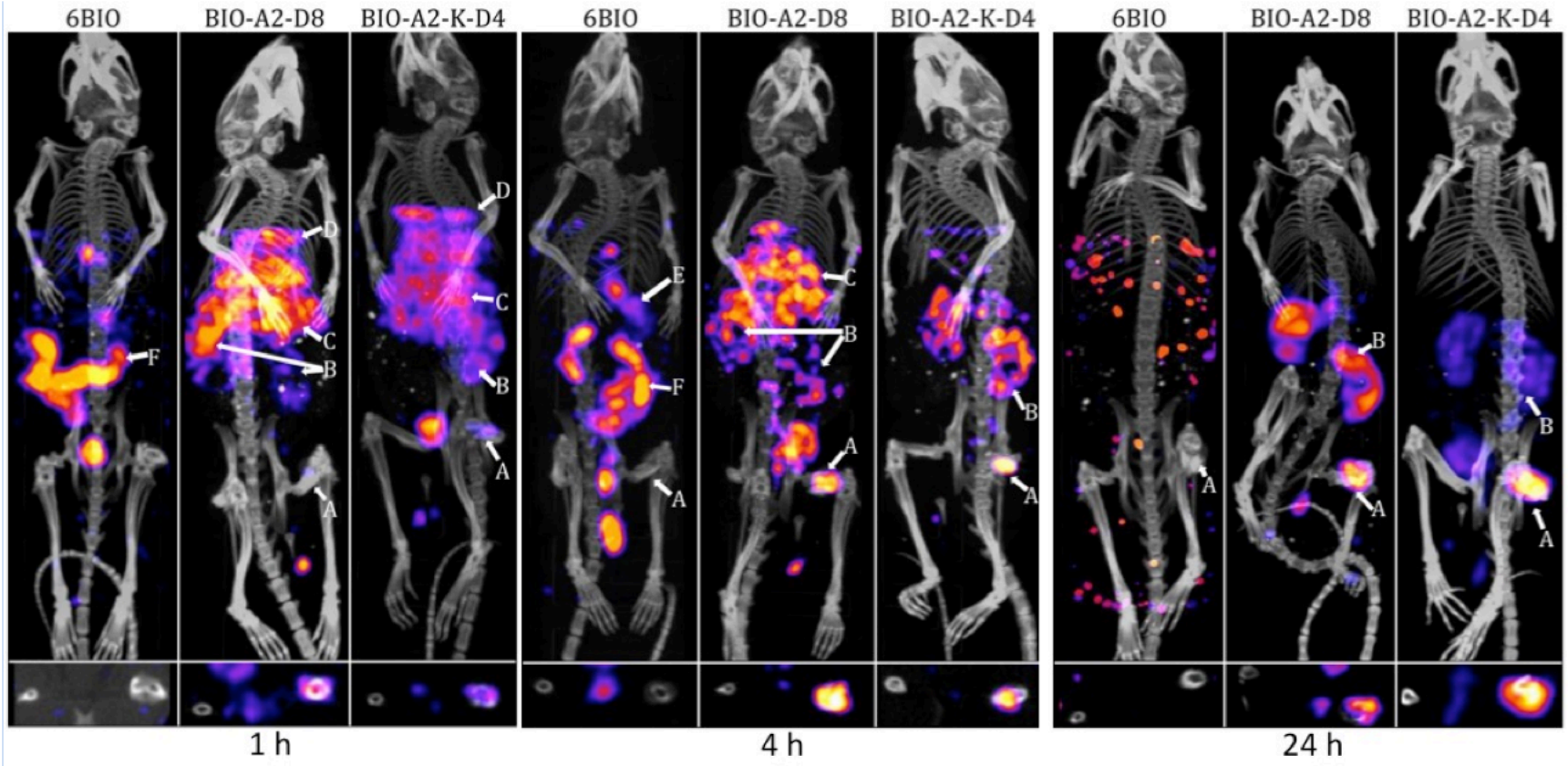

Figure 3.7 SPECT/CT of mice at 1 h, 4 h, and 24 h. The upper frames are a 3D reconstruction of the whole mouse. The lower frames are a cross section of femurs with the fractured femur on the right. Organs are labeled as follows: A: fracture, B: kidneys, C: Liver, D: Lungs, E: Spleen, F: Bowels.

CHAPTER 4

HEALING EFFICACY OF FRACTURE-TARGETED GSK3β-LOADED MICELLES FOR IMPROVED FRACTURE HEALING

4.1 Introduction

Delayed-union bone fractures are common repercussions of decreased bone mass associated with old age. In youth and young adults, common medical practice is able to heal most fractures. As people age, however, common fractures have difficulty healing and cause a significant decrease in quality of life and an increase in morbidity. Advances in treatment of these fractures have yet to catch up with aging populations. The only anabolic drugs that are used for treating bone fractures are bone morphogenic protein 2 (BMP-2) and teriparatide. BMP-2's route of administration is a local application during surgery, limiting the breadth of its application. Teriparatide (recombinant human parathyroid hormone [rPTH] fragment 1-34), on the other hand, is applied systemically but affects bone mass of the entire body rather than just the fracture site. The use of both of these anabolic agents for treating fractures is off label. This leaves a gap for other anabolic agents such as GSK3β inhibitors to fill a need and be used for fracture therapy.

The primary rationale for the use of a GSK3β inhibitor is that elevated Wnt leads to intramembranous bone formation and accelerated fracture healing [1–3]. Targeting or

deletion of various proteins in the Wnt pathway such as frizzled-related protein-1 [4], sclerostin (a Wnt antagonist), antisclerostin [5], and Lrp5 (a critical transmembrane protein in the Wnt signaling pathway) [6] significantly affects bone turnover and fracture healing. Furthermore, significant upregulation of B-catenin was found during fracture healing (12-week old mice) [7] and is partially responsible for the bone anabolic effects of both BMP-2 [8] and PTH signaling (teriparatide) [9].

There is a concern, however, with the promiscuity of the Wnt signaling pathway and its association with cancer [10–18]. Wnt is a signaling pathway in many types of cells and is associated with oncogenes, prompting the concern in upregulating the pathway through the inhibition of GSK3β inhibition. Targeting the drug to bone fractures can mitigate these theoretical side effects. By targeting the drug to bone, the GSK3β inhibition is primarily limited to the bone, kidneys, and liver. The issue is then reduced to: what involvement does Wnt have with liver, kidney, and bone cancers? Although it is evident that Wnt plays a critical role in many of these cancers, any association with GSK3β inhibitors administered over the short time to heal a fracture is weak [19–24]. The rationale for pursuing this pathway, however, is robust.

The high bone-affinity aspartic acid octapeptide provides a promising method for targeting a promiscuous yet potent drug such as the GSK3β inhibitor, 6-bromoindirubin-3'-oxime (6BIO), to bone fractures, accelerating healing with very few side effects. Previously, we developed an aspartic acid octapeptide containing a fracture-targeted micellar system that increases 6BIO accumulation preferentially in the bone fracture over healthy bone. This micelle featured aspartic acid octapeptide targeting ligands that provide both targeting abilities as well as the structural corona of the micelle [25,26].

The targeting ligand is linked by a flexible miniPEG linker to two aminoundecanoic acids for increased micellar stability and ends in a 'clickable' azide-containing synthetic amino acid (azidohomoalanine). The drug, 6BIO, is covalently bound to an alkyne-containing linker by a hydrolyzable oxime ester bond. The linker is then clicked to the rest of the unimer and assembles into a micelle when reconstituted in an aqueous medium. A second branched micelle was also developed that demonstrated superior fracture accumulation over the linear micelle. The second micelle is branched between the aminoundecanoic acid and the miniPEG by a lysine forming two branches, each with four aspartic acids on them. This study seeks to employ the targeting potential of the micelle and the anabolic action of 6BIO to treat bone fractures *in vivo*.

4.2 Experimental procedures

4.2.1 Synthesis of unimers

6BIO and all unimer synthesis was performed as described previously in Low et al. [26]. Briefly, micelle 6BIO was conjugated to 2,2-dimethylpent-4-ynoic acid using DCC/DIPEA coupling followed by purification with flash chromatography. Unimers were constructed on chlorotrityl resin using solid phase peptide synthesis starting with Fmoc-Dab(N3)-OH. Each amino acid was added through using HATU/DIPEA coupling and 20% piperidine in DMF for Fmoc deprotection. Unimers were purified using reverse phase HPLC and coupled to the 6BIO linker using copper catalyzed azide-alkyne Huisgen cycloaddition chemistry and were purified using LH20 column chromatography.

4.2.2 Mouse handling

All animal experiments were performed in accordance with Purdue University's IACUC approved protocols. Forty (10 per group) 31-35g male CD4 Swiss Webster mice were purchased from Harlan laboratories. Mice were able to move freely throughout the experiment. At 3 weeks following fracture induction, mice were euthanized using a CO_2 overdose. Both fractured and healthy femurs were excised and fixed in formalin solution along with the kidneys and liver. Mice were excluded from the study upon migration of the fracture stabilization pin or an insufficient fracture where the fracture did not pass through the bone.

4.2.3 Mouse bone fracture

A stabalized femoral fracture was performed under aseptic conditions with isoflurane anesthesia. Skin around the knee was shaved and cleaned with an alcohol pad first, then with Betadine solution. The skin incision was made over the knee. The patella was then dislocated and a small hole was made under the patella with a 25-guage needle. The needle was used to ream the intramedullary canal. A 22-guage locking nail produced by flattening both ends was then inserted. The incision site was sutured and the femur was then fractured using a three-point bending device. Buprenorphine (0.05 – 0.1 mg/kg) was administered subcutaneously at the time of fracture, and dosed every 12 h for 3-7 days postoperation.

4.2.4 Mouse dosing

Mice were dosed intravenously by tail vein injection every 3 days, starting on the day of fracture induction. Micelles were reconstituted in sterile PBS while 6BIO was reconstituted in 1% DMSO and PBS. Dosages were calculated assuming 1% fracture accumulation with a 20 nM concentration being necessary to elicit accelerated bone growth for the 5 nM enzymatic IC50 of 6BIO. Mice receiving drug dosages were administered 6.9 nmol/kg/dose in approximately 0.1 mL of PBS. PBS control mice received 0.1 mL of PBS.

4.2.5 μCT analysis

Scanco *μCT* 40 was used to collect CT images and data of bone. The bones were scanned while immersed in PBS to prevent dehydration. Scanco μCT software was used to analyze the images for bone density, total volume (TV), relative bone volume (BV/TV), trabecular thickness (Tb.Th), and trabecular spacing (Tb.Sp). Volumes of interest included the fracture callus, and both cortical and trabecular bone between the points on the cortical bone where the bone was fractured.

4.2.6 Images

Images collected from the μCT were studied using Image J software. Average pixels of a 3-dimensional reconstruction of a 50-slices stack were used and represent approximately 0.3 mm of tissue in depth. Minimum brightness threshold was adjusted to 4273 on all images to eliminate non-calcified tissue from view.

4.2.7 Statistical analysis

Statistical analyses were calculated using Prism GraphPad software. Data are presented in results as mean ± standard error of the mean (SEM). An unpaired student's t-test was used to determine statistical significance, with P values less than 0.05 being considered statistically significant.

4.2.8 Slide preparation

Tissues were fixed in PBS-buffered formalin solution for at least 24 h. Following fixation, tissues were embedded in paraffin, sectioned, and floated on slide. Slides were deparaffinized and rehydrated for staining.

4.3 Results and discussion

We have developed two micelles designed to improve fracture healing in long bone fractures. Previous studies of the micelles demonstrated their specificity to bone fractures. Here, we tested the healing efficacy and biocompatibility of the micelles. The first of the micelles is composed of a linear unimer design [25,26]. The drug, 6BIO, was conjugated to 2,2-dimethyl-3-butynoic acid by DCC/DIPEA coupling. The 6BIO plus linker was then conjugated by copper-catalyzed azide-alkyne Huisgen cycloaddition to a unimer built using solid phase peptide synthesis. The unimer was assembled starting with azidohomoalanine followed by two aminoundecanoic acids (A2), miniPEG (8-amino-3,6-dioxaoctanoic acid), eight aspartic acids (D8), and capped with acetic acid, yielding BIO-A2-D8 (Figure 4.1). BIO-A2-D8 features a targeting ligand that, upon micellar assembly, acts as the corona of the micelle. 6BIO is hydrophobic and acts both

as the drug and the core of the micelle, increasing the micelle's stability. Micelles gain their stability from hydrophobic interactions, so adding additional aminoundecanoic acids will make the micelle more stable [25]. Addition of too many aminoundecanoic acids, however, causes the unimers to aggregate in nonmicellar structures [25,26]. To circumvent this, a branched head group unimer was designed that increases conicity of the unimer [25]. The basic assembly was analogous to the linear unimer; however, following the two aminoundecanoic acids (A2), a lysine (K) was added that had both primary amines unprotected, providing two branches. From the lysine, miniPEG was added, followed by four aspartic acids per arm (D4), and was capped with acetic acid, yielding the branched unimer BIO-A2-K-D4. BIO-A2-K-D4 contains a total of eight aspartic acids, like the linear BIO-A2-D8, but is capable of being further stabilized with several additional aminoundecanoic acids while retaining a micellar structure.

6BIO provided a good candidate drug for a therapy study due to its hydrophobicity as well as its excellent suppression of GSK3β. Wnt works by inducing mesenchymal stem cells to differentiate into pre-osteoblasts. The continual activation of the pre-osteoblasts by Wnt leads to differentiated, active osteoblasts [27–30]. This means that as long as Wnt is active in the general fracture area, osteoblasts will continually be produced and active. This is evident in fracture healing, as Wnt expression peaks during days 3-5 and decreases between 14 and 21 days postfracture [2]. Previous studies on GSK3β-inhibitor treatment of fractures have been successful by extending and amplifying Wnt expression, starting treatment on the day of fracture and continuing dosing on a daily basis until the end of the experiment [3]. Similarly, in this experiment we elevate Wnt signaling over the entirety of the experiment. However, the oxime ester bond in our

micellar system delivered drug over 3 days, reducing administration by tail vein on every third day possible.

The study was designed to replicate aged fractures while minimizing variance. In order to best simulate an aged fracture, mature CD4 Swiss Webster mice (31-35g) were used. Potential variance was mitigated by using male mice. Estrogen levels play a significant role in bone growth with large changes in estrogen levels and bone densities occurring at pregnancy, lactation, and menopause [31–34]. Although these variations of estrogen levels are often associated with long-term changes in bone densities, there is evidence that estrogen levels can have dramatic effects with acute variations in estrogen [35], potentially correlating with estrous cycles.

4.3.1 μCT analysis

Upon completion of the study, femurs were harvested and underwent μCT testing. Information about the bone density, fracture volume, and callus structure was analyzed and used in determining the efficacy of the treatment regimen. Bone density is an important tool for assessing bone healing, giving information about cellular activity as well as changes in structural integrity. Bone density was calculated from the mass of the hydroxyapatite (HAp) mineralized part of the fracture callus per unit of the total volume of the fracture callus. The linear and branched micelles yielded 411.1±17.3 mg HAp/cm^3 and 409.7±13.8 mg HAp/cm^3, respectively, and were significantly higher than the free 6BIO and PBS control, which were 337.8±14.2 mg HAp/cm^3 and 348.6±22.7 mg HAp/cm^3, respectively (Figure 4.2). This overall increase of bone density in the treated micelles over the controls indicated both activity of the micelle-released 6BIO *in vivo* as

well as targeted accumulation in the bone. Although previous studies demonstrated a 2-fold increase in fracture accumulation of the branched micelle over the linear micelle, the resultant bone densities of the linear and branched micelle treatments were not significantly different from each other. Also of note, the PBS control and free drug did not differ significantly, indicating that the dose chosen for the study was lower than the amount needed for free 6BIO to initiate bone anabolism.

The relative bone volume (BV/TV) is the mineralized volume of the total volume and is a similar measurement to bone density. Completing the trend observed by the bone density, the micelles outperformed the controls significantly. The BV/TV of the linear micelle BIO-A2-D8 was 0.409±0.019 and branched micelle BIO-A2-K-D4 was 0.409±0.011, while the free 6BIO was 0.338±0.015 and PBS control was 0.332±0.021 (Table 4.1).

The differences in bone densities can be explained partly by measured differences in the bone architecture. Trabecular thickness (Tb.Th) is a measurement of the thickness of all of the mineralized trabeculae. Greater Tb.Th is indicative of a more robust osteoblast population [36,37]. The BIO-A2-D8 and BIO-A2-K-D4 values were 0.175±0.011 mm and 0.170±0.007 mm, respectively, and again significantly higher than the free 6BIO and PBS control, which were 0.134±0.007 mm and 0.139±0.014 mm, respectively.

The converse of Tb.Th, the trabecular spacing (Tb.Sp), is a deleterious attribute that measures the distances of noncalcified portions of bone between the calcified portions [36]. Little difference between the samples was observed. The only significant difference was the BIO-A2-D8 (0.208±0.003 mm) having an increase in spacing over the

PBS control (0.181±0.004 mm). By comparing Tb.Th to Tb.Sp, it is evident that the greatest contribution to bone density is produced by the thickness of the trabeculae.

In addition to the densities and microstructure of the callus, larger callus volumes are associated with improved mechanical properties [38]. The callus volume is calculated from the total volume (TV) occupied by both calcified bone and soft tissue. The BIO-A2-D8 and BIO-A2-K-D4 micelles had TVs of 60.8±3.4 mm^3 and 66.9±6.8 mm^3, respectively, while the free 6BIO and PBS control were 48.2±5.8 mm^3 and 44.1±8.8 mm^3, respectively. The combination of a significantly larger callus volume and increased bone density are clinically important signs that the targeted micelles are working.

During the fracture healing process the original cortical bone undergoes remodeling by degradation and replacement with new bone. Under extreme GSK3β inhibition, remodeling favors osteoblasts and osteopetrosis may occur. It is unclear whether GSK3β inhibition resulting in osteopetrosis is a result of systemic inhibition of osteoclasts and whether local GSK3β inhibition will inhibit local favorable catabolism [39]. Transverse μCT sections 0.3 μm thick revealed that in both the micelle groups, the original cortical bone has undergone a great deal of remodeling, indicating that dosages were either not high enough to suppress local osteoclast activity, or migration of osteoclasts into the fracture was sufficient to overcome local suppression (Figure 4.3). Evidence of remodeling appears to be greater in the targeted micelles over the controls as the lines differentiating between the original cortical bone and the fracture callus are difficult to discern in many places.

4.3.2 Histology of kidneys and liver

Biodistribution studies showed high uptake in the lungs, liver and kidneys compared to the fracture in both micelle groups at 1 h. By 4 h, both micelle groups demonstrated high uptake in the femurs. The linear micelle still had high uptake in the liver and kidneys while the branched micelle had only high kidney uptake. By 24 h both micelles demonstrated high signals in the femurs [26]. In this study, liver and kidneys were harvested. Liver sections showed no evident liver toxicity in morphology or cell concentrations (Figure 4.4b). Some potential kidney toxicity was visible in the drug groups where slight glomerular constriction and cell accumulation was evident but data was inconclusive as to whether damage would significantly hinder kidney function (Figure 4.4a).

4.4 Conclusions

We demonstrated accelerated fracture healing by targeting the GSK3β inhibitor, 6BIO, to the fracture site. Both fracture bone mineral density and volume were significantly higher in the micelle treatment groups over both the free 6BIO and PBS controls. Both micelles performed relatively well in the tissues analyzed for toxicity. Additional dose escalation studies are needed to determine whether the slight abnormalities in glomular health are caused by the micelle and whether fracture healing can be accelerated further. Although differences between the micelles were minimal, the branched micelle is likely the best candidate for further studies due to its greater ability to modify its hydrophobic moieties.

4.5 References

[1] M. Hadjiargyrou, F. Lombardo, S. Zhao, W. Ahrens, J. Joo, H. Ahn, M. Jurman, D.W. White, C.T. Rubin, Transcriptional profiling of bone regeneration. Insight into the molecular complexity of wound repair, J. Biol. Chem. 277 (2002) 30177–30182.

[2] N. Zhong, R.P. Gersch, M. Hadjiargyrou, Wnt signaling activation during bone regeneration and the role of Dishevelled in chondrocyte proliferation and differentiation, Bone 39 (2006) 5–16.

[3] G. Sisask, R. Marsell, A. Sundgren-Andersson, S. Larsson, O. Nilsson, Ö. Ljunggren, K.B. Jonsson, Rats treated with AZD2858, a GSK3 inhibitor, heal fractures rapidly without endochondral bone formation, Bone 54 (2013) 126–132.

[4] P.V.N. Bodine, B. Stauffer, H. Ponce-de-Leon, R.A. Bhat, A. Mangine, L.M. Seestaller-Wehr, R.A. Moran, J. Billiard, S. Fukayama, B.S. Komm, K. Pitts, G. Krishnamurthy, A. Gopalsamy, M. Shi, J.C. Kern, T.J. Commons, R.P. Woodworth, M.A. Wilson, G.S. Welmaker, E.J. Trybulski, W.J. Moore, A small molecule inhibitor of the Wnt antagonist secreted frizzled-related protein-1 stimulates bone formation, Bone 44 (2009) 1063–1068.

[5] M.S. Ominsky, C. Li, X. Li, H.L. Tan, E. Lee, M. Barrero, F.J. Asuncion, D. Dwyer, C.-Y. Han, F. Vlasseros, R. Samadfam, J. Jolette, S.Y. Smith, M. Stolina, D.L. Lacey, W.S. Simonet, C. Paszty, G. Li, H.Z. Ke, Inhibition of sclerostin by monoclonal antibody enhances bone healing and improves bone density and strength of nonfractured bones, J. Bone Miner. Res. 26 (2011) 1012–1021.

[6] D.E. Komatsu, M.N. Mary, R.J. Schroeder, A.G. Robling, C.H. Turner, S.J. Warden, Modulation of Wnt Signaling Influences Fracture Repair, J. Orthop. Res. 28 (2010) 928–936.

[7] Y. Chen, H.C. Whetstone, A.C. Lin, P. Nadesan, Q. Wei, R. Poon, B.A. Alman, Beta-catenin signaling plays a disparate role in different phases of fracture repair: implications for therapy to improve bone healing, PLoS Med. 4 (2007) 1216–1229.

[8] Y. Chen, H.C. Whetstone, A. Youn, P. Nadesan, E.C.Y. Chow, A.C. Lin, B.A. Alman, β-Catenin signaling pathway Is crucial for bone morphogenetic protein 2 to induce new bone formation, J. Biol. Chem. 282 (2007) 526–533.

[9] S. Kakar, T.A. Einhorn, S. Vora, L.J. Miara, G. Hon, N.A. Wigner, D. Toben, K.A. Jacobsen, M.O. Al-Sebaei, M. Song, P.C. Trackman, E.F. Morgan, L.C. Gerstenfeld, G.L. Barnes, Enhanced chondrogenesis and Wnt signaling in PTH-treated fractures, J. Bone Miner. Res. Off. J. Am. Soc. Bone Miner. Res. 22 (2007) 1903–1912.

[10] P. Polakis, Wnt signaling and cancer, Genes Dev. 14 (2000) 1837–1851.

[11] L. Meijer, M. Flajolet, P. Greengard, Pharmacological inhibitors of glycogen synthase kinase 3, Trends Pharmacol. Sci. 25 (2004) 471–480.

[12] J.Á.F. Vara, E. Casado, J. de Castro, P. Cejas, C. Belda-Iniesta, M. González-Barón, PI3K/Akt signalling pathway and cancer, Cancer Treat. Rev. 30 (2004) 193–204.

[13] T. Reya, H. Clevers, Wnt signalling in stem cells and cancer, Nature. 434 (2005) 843–850.

[14] M. Bienz, H. Clevers, Linking colorectal cancer to Wnt signaling, Cell 103 (2000) 311–320.

[15] R. Fodde, T. Brabletz, Wnt/β-catenin signaling in cancer stemness and malignant behavior, Curr. Opin. Cell Biol. 19 (2007) 150–158.

[16] R.H. Giles, J.H. van Es, H. Clevers, Caught up in a Wnt storm: Wnt signaling in cancer, Biochim. Biophys. Acta BBA-Rev. Cancer 1653 (2003) 1–24.

[17] A. Klaus, W. Birchmeier, Wnt signalling and its impact on development and cancer, Nat. Rev. Cancer 8 (2008) 387–398.

[18] M. Katoh, WNT/PCP signaling pathway and human cancer (review), Oncol. Rep. 14 (2005) 1583–1588.

[19] S. Cairo, C. Armengol, A. De Reyniès, Y. Wei, E. Thomas, C.-A. Renard, A. Goga, A. Balakrishnan, M. Semeraro, L. Gresh, Hepatic stem-like phenotype and interplay of Wnt/β-catenin and Myc signaling in aggressive childhood liver cancer, Cancer Cell 14 (2008) 471–484.

[20] D.F. Calvisi, E.A. Conner, S. Ladu, E.R. Lemmer, V.M. Factor, S.S. Thorgeirsson, Activation of the canonical Wnt/β-catenin pathway confers growth advantages in c-Myc/E2F1 transgenic mouse model of liver cancer, J. Hepatol. 42 (2005) 842–849.

[21] D.W. Chan, C.-Y. Chan, J.W. Yam, Y.-P. Ching, I.O. Ng, Prickle-1 negatively regulates Wnt/β-catenin pathway by promoting Dishevelled ubiquitination/degradation in liver cancer, Gastroenterology 131 (2006) 1218–1227.

[22] C.-A. Renard, C. Labalette, C. Armengol, D. Cougot, Y. Wei, S. Cairo, P. Pineau, C. Neuveut, A. de Reyniès, A. Dejean, Tbx3 is a downstream target of the Wnt/β-catenin pathway and a critical mediator of β-catenin survival functions in liver cancer, Cancer Res. 67 (2007) 901–910.

[23] Y. Takigawa, A. Brown, Wnt signaling in liver cancer, Curr. Drug Targets 9 (2008)

1013–1024.

[24] W. Yang, H.-X. Yan, L. Chen, Q. Liu, Y.-Q. He, L.-X. Yu, S.-H. Zhang, D.-D. Huang, L. Tang, X.-N. Kong, Wnt/β-catenin signaling contributes to activation of normal and tumorigenic liver progenitor cells, Cancer Res. 68 (2008) 4287–4295.

[25] S.A. Low, J. Yang, J. Kopeček, Bone-targeted acid-sensitive doxorubicin conjugate micelles as potential osteosarcoma therapeutics, Bioconjug. Chem. 25 (2014) 2012–2020.

[26] S.A. Low, C.V. Galliford, J. Yang, P.S. Low, J. Kopeček, Biodistribution of fracture-targeted GSK3β-loaded micelles for improved fracture healing, Prep. (n.d.).

[27] S.R. Goldring, M.B. Goldring, Eating bone or adding it: The Wnt pathway decides, Nat. Med. 13 (2007) 133–134.

[28] R. Baron, M. Kneissel, WNT signaling in bone homeostasis and disease: From human mutations to treatments, Nat. Med. 19 (2013) 179–192.

[29] D.A. Glass II, P. Bialek, J.D. Ahn, M. Starbuck, M.S. Patel, H. Clevers, M.M. Taketo, F. Long, A.P. McMahon, R.A. Lang, G. Karsenty, Canonical Wnt signaling in differentiated osteoblasts controls osteoclast differentiation, Dev. Cell 8 (2005) 751–764.

[30] C. Zhang, Transcriptional regulation of bone formation by the osteoblast-specific transcription factor Osx, J. Orthop. Surg. 5 (2010) 37.

[31] E.G. Vajda, B.M. Bowman, S.C. Miller, Cancellous and cortical bone mechanical properties and tissue dynamics during pregnancy, lactation, and postlactation in the rat, Biol. Reprod. 65 (2001) 689–695.

[32] S.C. Miller, B.M. Bowman, Comparison of bone loss during normal lactation with estrogen deficiency osteopenia and immobilization osteopenia in the rat, Anat. Rec. 251 (1998) 265–274.

[33] D.T. Felson, Y. Zhang, M.T. Hannan, D.P. Kiel, P. Wilson, J.J. Anderson, The effect of postmenopausal estrogen therapy on bone density in elderly women, N. Engl. J. Med. 329 (1993) 1141–1146.

[34] R.M. Neer, C.D. Arnaud, J.R. Zanchetta, R. Prince, G.A. Gaich, J.Y. Reginster, A.B. Hodsman, E.F. Eriksen, S. Ish-Shalom, H.K. Genant, others, Effect of parathyroid hormone (1-34) on fractures and bone mineral density in postmenopausal women with osteoporosis, N. Engl. J. Med. 344 (2001) 1434–1441.

[35] B.M. Bowman, S.C. Miller, The proliferation and differentiation of the bone-lining

cell in estrogen-induced osteogenesis, Bone 7 (1986) 351–357.

[36] T. Hildebrand, A. Laib, R. Müller, J. Dequeker, P. Rüegsegger, Direct three-dimensional morphometric analysis of human cancellous bone: microstructural data from spine, femur, iliac crest, and calcaneus, J. Bone Miner. Res. 14 (1999) 1167–1174.

[37] A M AM Parfitt, Age-related structural changes in trabecular and cortical bone: Cellular mechanisms and biomechanical consequences, Calcif. Tissue Int. 36 (1984) S123–S128.

[38] R.J. Pacheco, M.D. Bradbury, A.G. Kasis, M. Saleh, Review management of nonunion in trauma, Trauma 6 (2004) 225–247.

[39] H.D. Jang, J.H. Shin, D.R. Park, J.H. Hong, K. Yoon, R. Ko, C.-Y. Ko, H.-S. Kim, D. Jeong, N. Kim, S.Y. Lee, Inactivation of glycogen synthase kinase-3β is required for osteoclast differentiation, J. Biol. Chem. 286 (2011) 39043–39050.

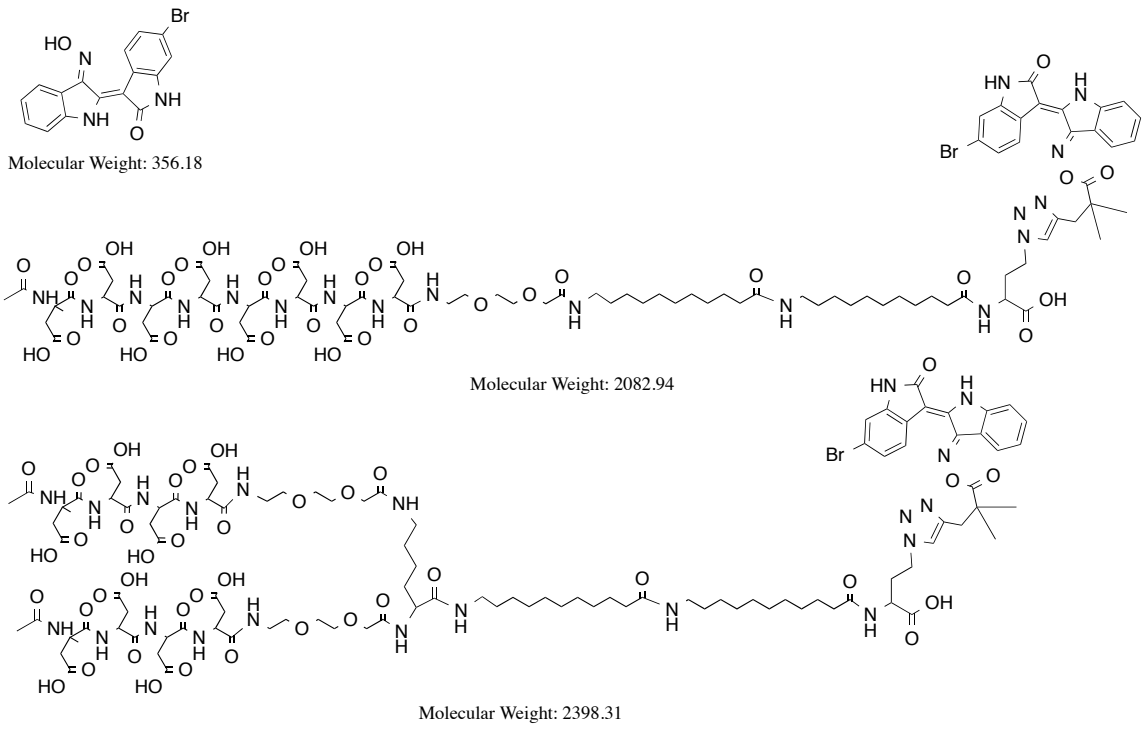

Figure 4.1. Structures of 6BIO (top), linear BIO-A2-D8 (middle), and branched BIO-A2-K-D4 (bottom).

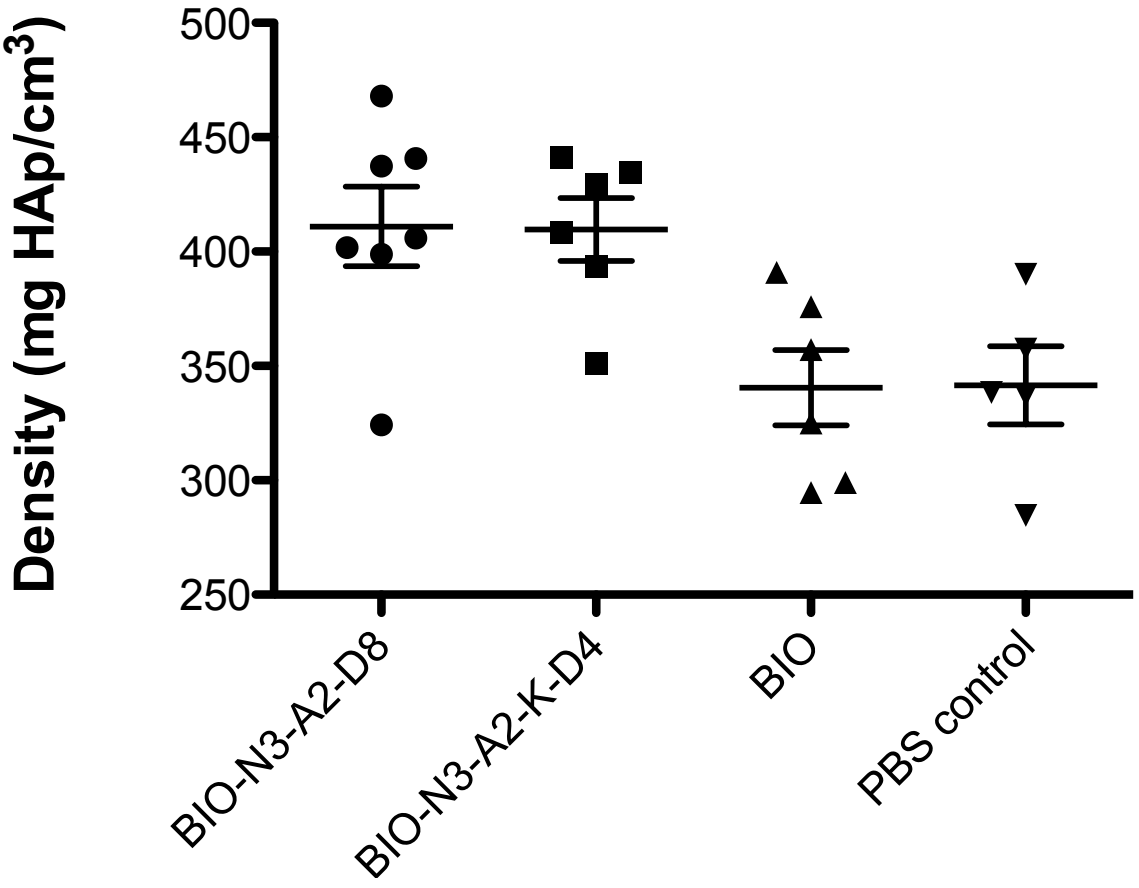

Figure 4.2. Densities of fracture callus [mg HAp/cm^3]. Both unimers are statistically different than the free 6BIO and PBS control

Table 4.1. The comparison of bone morphometric analysis (^{f} indicates that the unimer is statistically different than the free drug and ^{p} indicates that the unimer is statistically different than the PBS control).

Direct Model	Linear	Branched	Free 6BIO	PBS
TV [mm^3]	60.8±3.4^{f,p}	66.9±6.8 ^{f,p}	48.2±5.8	44.1±8.8
BV/TV	0.409±0.019 ^{f,p}	0.409±0.011 ^{f,p}	0.338±0.015	0.332±0.021
Tb.Th[mm]	0.175±0.011 ^{f,p}	0.170±0.007 ^{f,p}	0.134±0.007	0.139±0.014
Tb.Sp[mm]	0.208±0.003^p	0.190±0.004	0.191±0.009	0.181±0.004

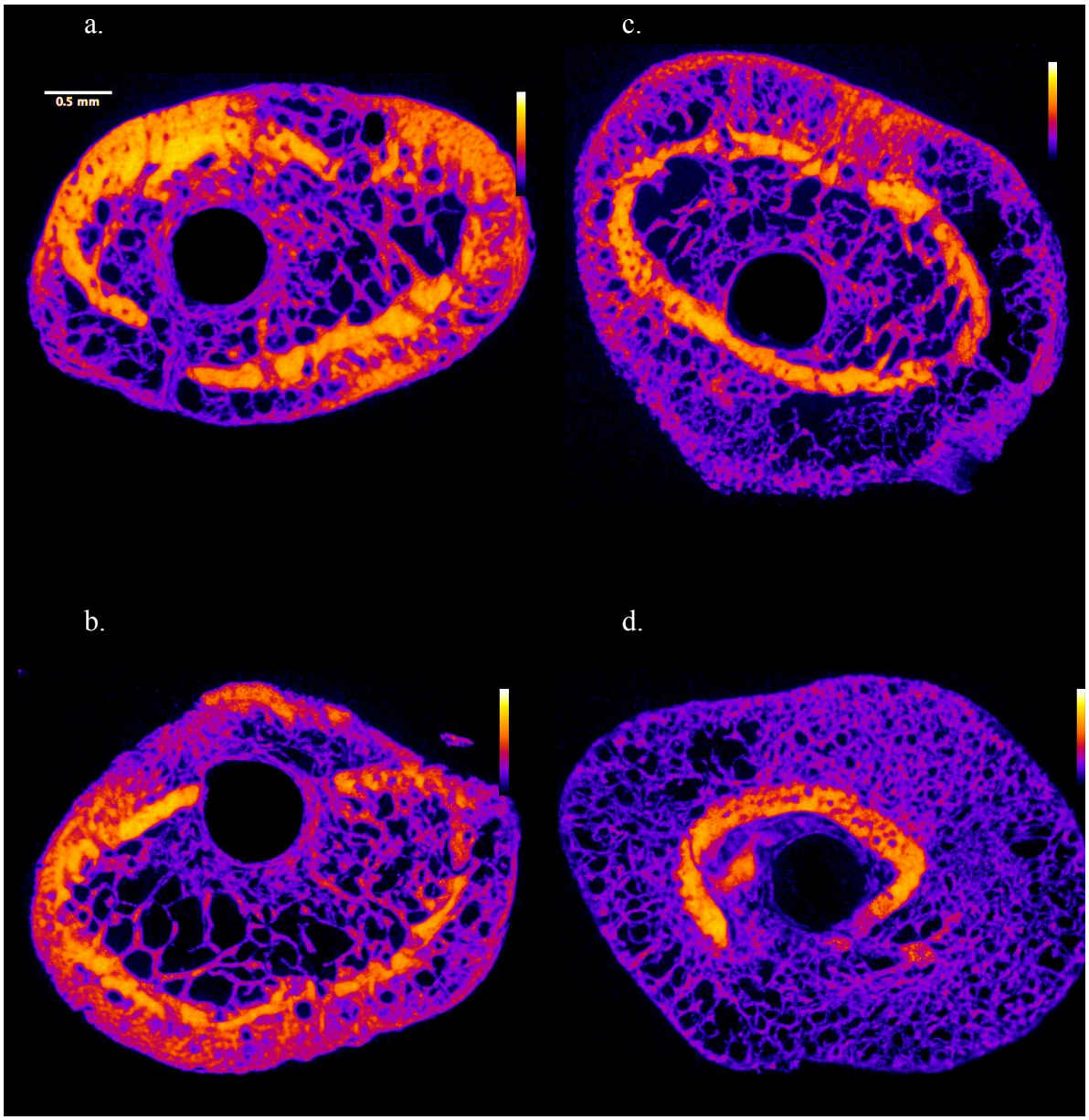

Figure 4.3. Average composite of fifty 6 µm (0.3 mm) slices a) linear, b) branched, c) free 6BIO, and d) PBS control. Whites and yellows indicate higher densities than blues and purples. The original bone from the femurs of the treatment groups are being resorbed and incorporated into the fracture callus.

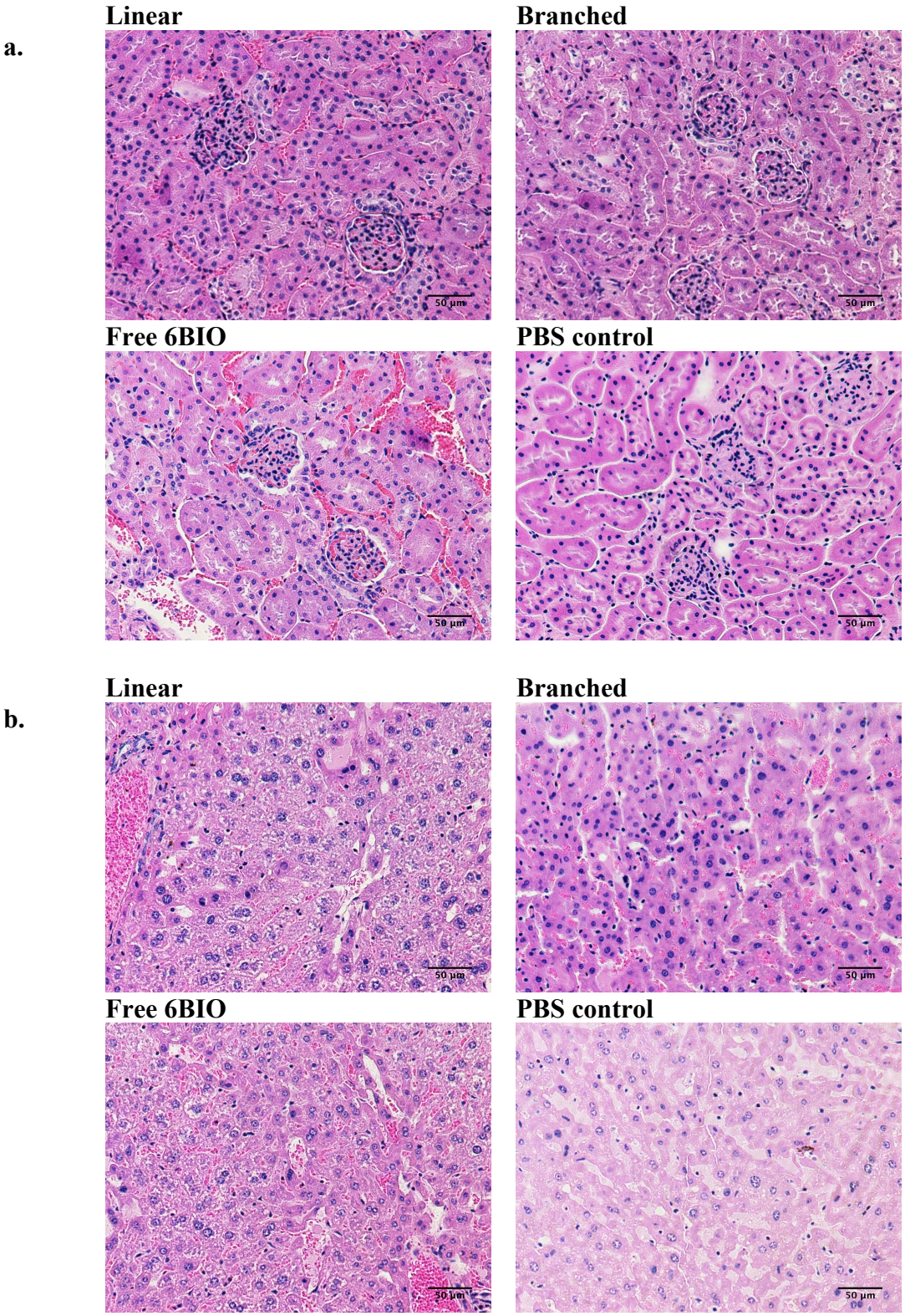

Figure 4.4. Histology sections of BIO-A2-D8, BIO-A2-K-D4, 6BIO, and PBS control of a) kidney H&E stain; b) Liver H&E stain.

CHAPTER 5

SUMMARY AND FUTURE PROSPECTS

5.1 Summary

Bone diseases are a major cause of decreased quality of life and increased morbidity among all age groups. In children and adolescents, these include bone cancers, such as osteosarcoma, and several genetic diseases [1–10]. In the elderly and immunocompromised, diseases of the bone include osteomyelitis, multiple myeloma, low bone density and osteoporosis, metastasis of other cancers to the bone, and nonunion and delayed union fractures. Though over a sixth of the U.S. population suffers from one or more of these diseases [11], research into possible treatments has been relatively undeveloped despite numerous possible treatment strategies [12–14].

A common thread among many of these diseases is that bone is either being degraded or grown. At these sites of bone turnover, increased therapeutic accumulation can be achieved by using targeting ligands such as aspartic acid octapeptide [15–29]. We designed a micelle using aspartic acid octapeptide targeting that can be coupled with the appropriate drug and adapted to treat several disease states.

The basic micelle construct focuses on the multifunctionality of each component to ensure simplicity of the final product. The targeting ligand, aspartic acid octapeptide, functions as both a targeting moiety as well as the corona of the micelle. In addition, the

drug payload is covalently bound to the micelle by a hydrolyzable linker and functions both as a therapeutic and stabilizing element to the micelle core. Joining the targeting ligand and drug is a flexible hydrophilic linker conjugated to a hydrocarbon tail for increased stability (Figure 5.1).

5.1.1 Micelles for treatment of osteosarcoma

Our initial studies of this micellar construct were on doxorubicin with the intention that the hydrophobic drug core could be changed, depending on the application. Loaded with doxorubicin, the stability was increased with the addition of more hydrophobic sections; however, increasing the hydrophobicity too much on the linear design began to cause nonmicellar aggregation. Branching the aspartic acid head group increased the conicity of the micelle, avoiding the previously observed undesired aggregation. Micelle size and shape of all constructs were confirmed using dynamic light scattering and cryogenic electron microscopy.

5.1.1.1 *In vitro* analysis of the micelle gave promising results for future *in vivo* work

All micelle structures bound quickly to hydroxyapatite as expected. Drug release occurred over several days and was positively correlated with the stability of each micelle. Critical to the micelle's success in this and other applications, drug-loaded micelles demonstrated toxicity to osteosarcoma cells, while the micelle structure without drug showed no toxicity at therapeutic doses.

5.1.2 Bone fracture targeted micelles

With a biocompatible micelle construct, we adapted the micelles to target anabolic agents to bone fractures. Two micelles were compared, varying only in that one was branched and the other linear. The modified micelles featured a GSK3β inhibitor linked to the micelle by a hydrolyzable oxime ester bond. The drug, 6-bromoindirubin-3'-oxime (or 6BIO) inhibits GSK3β and therefore increases Wnt signaling (Figure 5.2). With Wnt signaling, active progenitor cells differentiate into osteoblasts and are activated. The activated osteoblasts then increase bone growth dramatically, making this construct an ideal drug delivery system for repairing bone fractures [30,31].

Initial studies were used to determine *in vivo* targeting of the micelles. It was elucidated through a 24 h biodistribution study that the micelle accumulation was higher in fractures than in healthy bone. We found by doing time course SPECT/CT imaging that targeted drug accumulation in the fractures was far higher than previously thought and that the free drug clears through the liver-bowel route while the micelles preferentially are cleared through the kidneys and excreted in urine. The primary sites of off-target effects were the liver and kidneys, which were studied in greater detail in the treatment study. The critical information gathered from both biodistribution studies was that the branched micelle outperformed the linear micelle in both fracture to kidney uptake as well as fracture to healthy bone uptake.

Following the biodistribution studies, a drug efficacy study was performed. Fracture healing was measured in both the linear and branched micelle, free 6BIO, and PBS control groups. Both micelles demonstrated increased bone mineral density and fracture callus volume over the control groups. Histology of the liver showed no visible

toxicity, while the kidneys showed a small amount of glomerular constriction in both micelle groups.

By applying the micelles to both osteosarcoma and bone fractures, we demonstrated the versatility of the designed micelles. When comparing the micelles against each other, the branched structure appears to be superior. The branched unimer not only demonstrated improved targeting abilities, but it is more versatile in its ability to be stabilized with the addition of hydrophobic regions.

5.2 Future directions

The greatest potential for this drug delivery system lies with its ability to target fractures. With 300,000-620,000 delayed union and nonunion fractures a year in the U.S. alone, a fracture-targeted drug has a large market to drive development and is clinically relevant [33]. This fracture-targeted drug's clinical success depends on 1) refining the drug selection, 2) developing a proper drug-targeting moiety linker, 3) finding the optimal stability, and 4) completing preclinical testing.

5.2.1 Drug selection

6BIO is an effective bone anabolic agent. For clinical success, however, it is important to make sure other bone anabolics are not better. A great deal of research has gone into studying bone anabolic agents including GSK3β inhibitors,[30,31,34,35] prostaglandins [36–38], statins [39–45], bone morphogenic proteins [46,47], TGFβ [48,49], and parathyroid hormone [50–53]. The selection of an anabolic agent becomes complicated as many of the anabolic agents increase concentrations of other anabolic

agents. For example, the prostaglandin E series increases BMP2 production as well as bone turnover by upregulating RANKL [37,54,55], while statins increase BMP2 and prostaglandins [44,45]. Attempts have been made to compare the anabolic action of several drugs in several different scenarios [48,56–58], but an across-the-board comparison study of efficacy in treating bone fractures has yet to be done.

A series of studies determining several anabolic agents' fracture-healing capabilities would be an important development in the field. Initially, an *in vitro* study would be used to compare each anabolic agent and to determine an approximate baseline of mesenchymal stem cell activation and differentiation into osteoblast-like cells. Mesenchymal stem cells (MSCs) would be harvested from mice, plated, and grown until confluent in 6-well plates. Each bone anabolic agent would then be added at serial dilutions and incubated for 8 days. The media would be removed, and the cells would be incubated with osteogenic media for 15 days and stained with Alizarin red S for detecting calcium deposits [59].

Following the preliminary *in vitro* study, an *in vivo* study would serve to solidify the results. Each anabolic agent would be dissolved in a solvent such as N-methyl-2-pyrrolidone (NMP) and added to a poly(D,L-lactide-co-glycolide) (PLGA matrix (Atrigel). Commercially available 3-month-old mice would be used because they are fully-grown. Following fracture induction and stabilization using an intramedullary locking nail, the anabolic agent/matrix would be injected at the site of the fracture and released over time. The mice would be euthanized at 3 weeks, a time point at which we previously found demonstrable differences between treatment groups and controls. The femurs would then be excised and bone growth measured by microCT [60].

5.2.2 Linker selection

Proper linker selection is critical to clinical success. A proper linker can reduce the frequency of dose administration by extending drug release over several days. The rate is limited by the chance of the hydroxyapatite-adsorbed drug being encased by growing bone. An ideal release mechanism would include a fracture-specific release mechanism, releasing at a rate that is ideal for the drug delivered, and completely released before bone turnover encapsulates the drug in new bone.

Several degradable linkers, including enzymatic, pH-sensitive, and reduction-sensitive linkers should be considered. Enzyme-sensitive linkers are released by endopeptidases found in bone. Some target peptidases include cathepsin K [61,62], cathepsin B [63–65], and cathepsin L [66–68], where cathepsin K is the most specific to bone and has been studied in drug delivery to both bone cancers and osteoporosis [61,69]. Two problems with using an endopeptidase-specific degradable linker exist. First, if the drug reduces the number of osteoclasts in the area, then there will also be less cathepsin K to release the drug. Second, if the linker is attached to a drug on the inside of the micelle, significant steric hindrance may reduce drug cleavage significantly.

Several linkers rely on an acidic or basic environment to be released. Osteoclast lacunae have a pH around 4-4.5 [70,71]. At this pH, hydrazone and acetal linkers will release their conjugate drug. In addition, both linkers can be modified to release drug faster or slower by adding electron-withdrawing groups or electron-donating groups near the release site, respectively [72]. Again, if the drug reduces the osteoclast number in the area, the reduced pH of the lacunae will not be available and release may be hindered.

The majority of the fracture callus is at a neutral to basic pH (6.9-7.6) [73]. Oxime

esters, such as the one in our construct, release under neutral to basic conditions and, like the acid sensitive linkers, are tunable. Unfortunately, this pH range is also the normal physiological pH and gives no specificity to the fracture site. Thus, the specificity of release lies with the targeting ligand. For a base-sensitive linker to work, the cleavage rate must be slowed in order to release minimal drug in circulation prior to target accumulation.

Finally, glutathione is often released in the body in response to injury [74–76]. A reducible linker such as a tunable disulfide could be an effective way to deliver drug[72,77–79]. To the best of our knowledge, reducible bonds have yet to be examined in bone fractures.

Selecting a proper drug linker depends on the elucidation of several unknowns about the fracture microenvironment. A direct solution would be to study the rate of release in mouse femoral fractures. Near-infrared dyes are capable of being imaged through tissue. By targeting a near-infrared (NIR) dye to a bone fracture using aspartic acid octapeptide, a baseline accumulation and fluorescence could be established. By using the concepts of Förster resonance energy transfer (FRET), the fluorescence of the targeted NIR dye could be quenched by transferring its excitation energy to a neighboring Black Hole quencher dye. By targeting a NIR dye linked to a Black Hole quencher dye by one of the linkers listed above, the NIR dye would be quenched until it is gradually released by its respective stimuli (Figure 5.3) [80–82]. The release kinetics could be determined by measuring fluorescence at different time points and comparing the fluorescence to that of the control at the same time point. Once the quencher dye release began to plateau, if the predicted amount targeted is higher than the measured amount

released, then one might conclude that the rate was too slow and that the complex must have been encapsulated in bone prior to release.

5.2.3 Modification of micelle stability

Once the optimized drug and linker for clinical application have been confirmed, establishing the stability of the micelle in circulation is necessary. Previously we have demonstrated how to increase stability of micelles and that at injected concentrations the micelles are stable, but we have no *in vivo* data to determine whether the stability is sufficient to withstand the sheer forces and dilution experienced in the bloodstream, as well as the milieu of proteins and plasma. Micellar stability *in vivo* could be measured by encapsulating a NIR dye in the micelle. The micelle would be injected and intravital confocal microscopy would be used to measure fluorescence in the bloodstream over time[83–86]. The imaging can be performed noninvasively by focusing a Nikon A1R CLSM system on the blood vessels in the mouse ear lobe. The NIR dye-loaded micelle is then injected by tail vein injection. Images from three focal plains are collected every ten seconds for the first 5 minutes and then every 30 seconds for the remainder of the experiment. The imaging and experiment is stopped upon reaching background fluorescence, indicating that all of the intact micelles have exited the blood stream. If the micelle prematurely destabilized, a sharp peak of fluorescence would be detected due to a dramatic reduction in self-quenching, followed by a quick decrease in fluorescence [83,87]. Premature destabilization would indicate that the micelle's stability needs to be increased. Sufficiently stable micelles cause a certain degree of self-quenching of the dye, producing a moderate fluorescence up to several hours after injection, and would be

stabile enough to continue with further studies[83]. Alternatively, tritiated cholesterol can also be entrapped in the micelle and injected into mice. With a specific activity of 1.48-2.22TBq/mmol and a lower detection limit of beta counters being lower than 1Bq per liter [88], entrapment of minimal amounts of tritiated cholesterol may have smaller effect on composition and structure than entrapment of detectable levels of a NIR dye. With the tritiated cholesterol technique mice would then be euthanized at several time points and radioactivity of the fracture could then be measured. If the micelles prematurely destabilize, the tritiated cholesterol bone accumulation would be low.

If the micelle stability is insufficient, the branched construct can be stabilized by addition of more aminoundecanoic acids [89,90], equilibrating the micelle in solution longer prior to injection [89], or using one of the studied degradable linkers to cross-link the unimers within the micelle.

5.2.4 Preclinical evaluations

Critical to the micelle's success are preclinical evaluations, including a dose escalation study, a study identifying the types of fractures the micelle will repair, and studies demonstrating the drug's efficacy in other animals.

A dose escalation study will achieve several things for the development of the micelle. A dose escalation study will establish the optimal regimen for accelerated fracture healing and demonstrate a dose-dependent response to the drug and unveil any toxicity.

The proposed dose escalation study would be modeled after work performed in Chapters 3 & 4. Starting with 10 mice per group (6.9 nmol/kg/dose, 0.69 μmol/kg/dose,

69 μmol/kg/dose, 6.9 mmol/kg/dose and PBS), mice would be dosed intravenously by tail vein injection every 3 days, starting on the day of fracture induction. During the study, mice would be weighed and monitored to ensure the administered dose is not acutely toxic enough to cause weight loss. At three weeks, mice would be sacrificed and organs harvested. Due to results we obtained in the biodistribution studies (see chapter 4), the target organs and tissues that would be collected for analysis would be femurs, lungs, liver, kidneys, and blood. Bone densities of femurs would be measured using microCT. Bone fracture densities are expected to increase as higher dosages are administered until a maximum effective dose is reached and the increased bone density from drug administration plateaus. However, with some anabolic agents such as rostaglandins, overdosing may result in bone loss due to excess inflammation, and such a response would also be shown in a dose escalation study. Following microCT measurements, harvested femurs, lungs, liver, and kidneys would be sectioned and H&E-stained for general pathological analysis. Additional slides and stains could include tartrate-resistant acid phosphatase (TRAP) in order to identify suppression of osteoclasts, and dual calbindin D28k (CalD) and aquaporin-2 (AQP-2) staining of the kidneys to identify nephrotoxicity[91]. Finally, kidney toxicity could be measured using a urine ELISA of alpha glutathione S-transferase (alpha-GST), and liver toxicity could be measured using blood levels of transaminases (such as ALT and AST). Ideally, the maximum effective dose would be reached prior to any significant toxicity. If significant toxicity occurred at the maximum effective dose, then lower, less toxic doses would be used for additional studies.

In a clinical setting, large differences between groups of people and types of

fractures exist, making a dose expansion study important. A drug that accelerates healing in a juvenile mouse model and translates to accelerated healing in youth would represent a new standard of care for bone fractures; however, youth already have excellent bone repair mechanisms and success for this drug construct is more likely found in difficult-to-heal models. Nonunion fractures are a type of fracture that is often repaired with surgery, but a nonsurgical approach to assist with bone repair would substantially decrease morbidity. Mouse models representing delayed unions are well-established, and a bone anabolic may be able to accelerate healing in these as well [92–94]. However, a major issue that may affect targeting delayed-union fractures is low blood supply, so selection of this type of fracture should be carefully considered before investing too many resources to it. Fractures in mature and aging adults take longer to heal than in juveniles. It is thought that the cytokine response duration remains the same among age groups, but in the elderly either fewer osteoblasts are in place to repair the bone, or the osteoblasts present are in a more senescent state [95]. By increasing the time period that the cytokine response is active with an anabolic agent, accelerated healing may be possible. Aged models are established [48,96] and were used in our studies. Taking aged models a step further, osteoporosis induced by ovariectomy, low calcium, or hind limb immobilization would likely result in the most dramatic increases in bone healing over the controls [97,98]. Similarly, a clinically relevant model would be a mouse pretreated with bisphosphonates, impeding its ability to heal fractures.

Often, success in one animal does not translate to success in another animal. If success is observed in other animal models, such as rat, canine [99–101], porcine [102,103], or rabbit [104–106], the likelihood that human success will also be observed

greatly increases. Observing success in multiple animals is not only a requirement for the FDA, but it also increases industry interest. Porcine models are ideal because they are nonrodent and they are more commonly used for surgery than dogs [107].

5.3 Conclusions

The field of targeting anabolic agents to bone fractures is an exciting and largely untapped area. We have developed a bone-targeted micelle designed for treatment of various bone maladies, the most promising of which is likely fracture targeting. The development of this micelle system is still in its infancy; however, success in either osteosarcoma or bone fractures would improve the lives of many individuals.

5.4 References

[1] C.J.A. Bendel, H.J. Gelmers, Multiple enchondromatosis (Ollier's disease) complicated by malignant astrocytoma, Eur. J. Radiol. 12 (1991) 135–137.

[2] J.V. Bovée, J.F.G. van Roggen, A.M. Cleton-Jansen, A.H. Taminiau, H.-J. van der Woude, P.C. Hogendoorn, Malignant progression in multiple enchondromatosis (Ollier's disease): an autopsy-based molecular genetic study, Hum. Pathol. 31 (2000) 1299–1303.

[3] J.F. Cannon, Hereditary multiple exostoses, Am. J. Hum. Genet. 6 (1954) 419–425.

[4] K.L. Carroll, S.M. Yandow, K. Ward, J.C. Carey, Clinical correlation to genetic variations of hereditary multiple exostosis, J. Pediatr. Orthop. 19 (1999) 785–791.

[5] S. Fudge, R. Amirfeyz, D. Dimond, M. Gargan, Marble bone disease, Curr. Orthop. 21 (2007) 438–441.

[6] H. Hamersma, Osteopetrosis (marble bone disease) of the temporal bone, The Laryngoscope. 80 (1970) 1518–1539.

[7] C. Zawisch, Marble bone disease; a study of osteogenesis., Arch. Pathol. 43 (1947) 55–75.

[8] R.J. Lee, M.D. Paloski, P.D. Sponseller, A.I. Leet, Bent telescopic rods in patients with osteogenesis imperfecta, J. Pediatr. Orthop. (2015).

[9] G.A. Bellus, T.W. Hefferon, R.O. de Luna, J.T. Hecht, W.A. Horton, M. Machado, I. Kaitila, I. McIntosh, C.A. Francomano, Achondroplasia is defined by recurrent G380R mutations of FGFR3, Am. J. Hum. Genet. 56 (1995) 368–373.

[10] W.A. Horton, J.G. Hall, J.T. Hecht, Achondroplasia, The Lancet. 370 (2007) 162–172.

[11] R. Bartl, B. Frisch, C. Bartl, Osteoporosis: Diagnosis, prevention, therapy, Springer, 2009.

[12] U.N.I. of Health, others, Estimates of funding for various research, condition, and disease categories (RCDC), 2011.

[13] S.A. Low, J. Kopeček, Targeting polymer therapeutics to bone, Adv. Drug Deliv. Rev. 64 (2012) 1189–1204.

[14] D. Wang, S.C. Miller, P. Kopečková, J. Kopeček, Bone-targeting macromolecular therapeutics., Adv. Drug Deliv. Rev. 57 (2005) 1049–1076.

[15] H. Pan, M. Sima, P. Kopečková, K. Wu, S. Gao, J. Liu, D. Wang, S.C. Miller, J. Kopeček, Biodistribution and pharmacokinetic studies of bone-targeting N-(2-hydroxypropyl)methacrylamide copolymer-alendronate conjugates, Mol. Pharm. 5 (2008) 548–558.

[16] D. Wang, M. Sima, R.L. Mosley, J.P. Davda, N. Tietze, S.C. Miller, P.R. Gwilt, P. Kopečková, J. Kopeček, Pharmacokinetic and biodistribution studies of a bone-targeting drug delivery system based on N-(2-hydroxypropyl)methacrylamide copolymers, Mol. Pharm. 3 (2006) 717–725.

[17] B. Strömqvist, Femoral head vitality after intracapsular hip fracture: 490 cases studied by intravital tetracyche labeling and Tc-MDP radionuclide imaging., Acta Orthop. 54 (1983) 1–71.

[18] S. Holmberg, K.-G. Thorngren, Preoperative 99mTc-MDP scintimetry of femoral neck fractures, Acta Orthop. 55 (1984) 430–435.

[19] R. Lisbona, L. Rosenthall, Observations on the sequential use of 99mTc-phosphate complex and 67Ga imaging in osteomyelitis, cellulitis, and septic arthritis 1, Radiology. 123 (1977) 123–129.

[20] J.E. Seabold, F.W. Flickinger, S.C. Kao, T.J. Gleason, D. Kahn, J.V. Nepola, J.L. Marsh, Indium-111-leukocyte/technetium-99m-MDP bone and magnetic resonance imaging: Difficulty of diagnosing osteomyelitis in patients with neuropathic

osteoarthropathy, J. Nucl. Med. Off. Publ. Soc. Nucl. Med. 31 (1990) 549–556.

[21] W.T. Yuh, J.D. Corson, H.M. Baraniewski, K. Rezai, A.R. Shamma, M.H. Kathol, Y. Sato, G.Y. El-Khoury, D.R. Hawes, C.E. Platz, Osteomyelitis of the foot in diabetic patients: evaluation with plain film, 99mTc-MDP bone scintigraphy, and MR imaging, Am. J. Roentgenol. 152 (1989) 795–800.

[22] S. Basu, S.H. Moghe, T. Shet, Metastasis of humeral osteosarcoma to the contralateral breast detected by 99mTc-MDP skeletal scintigraphy, Jpn. J. Radiol. 27 (2009) 455–457.

[23] Ø.S. Bruland, A. Skretting, Ø.P. Solheim, M. Aas, Targeted radiotherapy of osteosarcoma using 153Sm-EDTMP: a new promising approach, Acta Oncol. 35 (1996) 381–384.

[24] C. Franzius, S. Bielack, S. Flege, J. Sciuk, H. Jürgens, O. Schober, Prognostic significance of 18F-FDG and 99mTc-methylene diphosphonate uptake in primary osteosarcoma, J. Nucl. Med. 43 (2002) 1012–1017.

[25] M. Alexandrakis, D. Kyriakou, F. Passam, S. Koukouraki, N. Karkavitsas, Value of Tc-99m sestamibi scintigraphy in the detection of bone lesions in multiple myeloma: comparison with Tc-99m methylene diphosphonate, Ann. Hematol. 80 (2001) 349–353.

[26] R. Lahtinen, M. Laakso, I. Palva, I. Elomaa, P. Virkkunen, Randomised, placebo-controlled multicentre trial of clodronate in multiple myeloma, The Lancet. 340 (1992) 1049–1052.

[27] K. Abe, M. Sasaki, Y. Kuwabara, H. Koga, S. Baba, K. Hayashi, N. Takahashi, H. Honda, Comparison of 18FDG-PET with 99mTc-HMDP scntigraphy for the detection of bone metastases in patients with breast cancer, Ann. Nucl. Med. 19 (2005) 573–579.

[28] G.J. Cook, S. Houston, R. Rubens, M.N. Maisey, I. Fogelman, Detection of bone metastases in breast cancer by 18FDG PET: differing metabolic activity in osteoblastic and osteolytic lesions., J. Clin. Oncol. 16 (1998) 3375–3379.

[29] N.A. Damle, C. Bal, G.P. Bandopadhyaya, L. Kumar, P. Kumar, A. Malhotra, S. Lata, The role of 18F-fluoride PET-CT in the detection of bone metastases in patients with breast, lung and prostate carcinoma: a comparison with FDG PET/CT and 99mTc-MDP bone scan, Jpn. J. Radiol. 31 (2013) 262–269.

[30] Y. Jiang, H.X. Liu, J.J. Guo, G.H. Tang, Y.F. Qian, Stimulation of bone formation in the expanding premaxillary suture with a GSK-3β inhibitor, Oral Dis. 19 (2013) 73–79.

[31] G. Sisask, R. Marsell, A. Sundgren-Andersson, S. Larsson, O. Nilsson, Ö. Ljunggren, K.B. Jonsson, Rats treated with AZD2858, a GSK3 inhibitor, heal fractures rapidly without endochondral bone formation, Bone. 54 (2013) 126–132.

[32] R. Baron, G. Rawadi, Targeting the Wnt/beta-catenin pathway to regulate bone formation in the adult skeleton, Endocrinology. 148 (2007) 2635–2643.

[33] E. Tsiridis, N. Upadhyay, P. Giannoudis, Molecular aspects of fracture healing:Which are the important molecules?, Injury. 38 (2007) S11–S25.

[34] N.H. Kulkarni, J.E. Onyia, Q. Zeng, X. Tian, M. Liu, D.L. Halladay, C.A. Frolik, T. Engler, T. Wei, A. Kriauciunas, T.J. Martin, M. Sato, H.U. Bryant, Y.L. Ma, Orally bioavailable GSK-3alpha/beta dual inhibitor increases markers of cellular differentiation in vitro and bone mass in vivo, J. Bone Miner. Res. Off. J. Am. Soc. Bone Miner. Res. 21 (2006) 910–920.

[35] R. Marsell, G. Sisask, Y. Nilsson, A.K. Sundgren-Andersson, U. Andersson, S. Larsson, O. Nilsson, Ö. Ljunggren, K.B. Jonsson, GSK-3 inhibition by an orally active small molecule increases bone mass in rats, Bone. 50 (2012) 619–627.

[36] D. Chikazu, Y. Fujikawa, H. Fujihara, H. Suenaga, H. Saijo, K. Ohkubo, T. Ogasawara, Y. Mori, M. Iino, T. Takato, Cyclooxygenase-2 activity is important in craniofacial fracture repair., Int. J. Oral Maxillofac. Surg. 40 (2011) 322–326.

[37] R. Tsutsumi, C. Xie, X. Wei, M. Zhang, X. Zhang, L.M. Flick, E.M. Schwarz, R.J. O'Keefe, PGE2 signaling through the EP4 receptor on fibroblasts upregulates RANKL and stimulates osteolysis, J. Bone Miner. Res. 24 (2009) 1753–1762.

[38] M. Weinreb, A. Grosskopf, N. Shir, The anabolic effect of PGE2 in rat bone marrow cultures is mediated via the EP4 receptor subtype, Am. J. Physiol. 276 (1999) E376–E383.

[39] J. Bradley, D. Cleverly, A. Burns, N. Helm, M. Schmid, D. Marx, D. Cullen, R. Reinhardt, Cyclooxygenase-2 inhibitor reduces simvastatin-induced bone morphogenetic protein-2 and bone formation in vivo, J. Periodontal Res. 42 (2007) 267–273.

[40] T. Maeda, A. Matsunuma, T. Kawane, N. Horiuchi, Simvastatin promotes osteoblast differentiation and mineralization in MC3T3-E1 cells, Biochem. Biophys. Res. Commun. 280 (2001) 874–877.

[41] B. Skoglund, P. Aspenberg, Locally applied Simvastatin improves fracture healing in mice, BMC Musculoskelet. Disord. 8 (2007) 98–103.

[42] Y. Ayukawa, E. Yasukawa, Y. Moriyama, Y. Ogino, H. Wada, I. Atsuta, K. Koyano, Local application of statin promotes bone repair through the suppression

of osteoclasts and the enhancement of osteoblasts at bone-healing sites in rats, Oral Surg. Oral Med. Oral Pathol. Oral Radiol. Endodontology. 107 (2009) 336–342.

[43] I.R. Garrett, G.E. Gutierrez, G. Rossini, J. Nyman, B. McCluskey, A. Flores, G.R. Mundy, Locally delivered lovastatin nanoparticles enhance fracture healing in rats, J. Orthop. Res. 25 (2007) 1351–1357.

[44] Y. Lee, X. Liu, A. Nawshad, D.B. Marx, D. Wang, R.A. Reinhardt, Role of prostaglandin pathway and alendronate-based carriers to enhance statin-induced bone, Mol. Pharm. 8 (2011) 1035–1042.

[45] M. Mori, T. Nishikawa, K. Masuno, T. Okamura, A. Tanaka, M. Shikimori, Statins: candidates for promoting bone formation via BMP-2, Oral Med. Pathol. 14 (2010) 81–87.

[46] G. Rawadi, B. Vayssière, F. Dunn, R. Baron, S. Roman-Roman, BMP-2 controls alkaline phosphatase expression and osteoblast mineralization by a Wnt autocrine loop, J. Bone Miner. Res. 18 (2003) 1842–1853.

[47] M. Murnaghan, L. McIlmurray, M.T. Mushipe, G. Li, Time for treating bone fracture using rhBMP-2: a randomised placebo controlled mouse fracture trial, J. Orthop. Res. 23 (2005) 625–631.

[48] I. Blumenfeld, S. Srouji, Y. Lanir, D. Laufer, E. Livne, Enhancement of bone defect healing in old rats by TGF-β and IGF-1, Exp. Gerontol. 37 (2002) 553–565.

[49] H.M. Nielsen, T.T. Andreassen, T. Ledet, H. Oxlund, Local injection of TGF-β increases the strength of tibial fractures in the rat, Acta Orthop. 65 (1994) 37–41.

[50] S. Choudhary, H. Huang, L. Raisz, C. Pilbeam, Anabolic effects of PTH in cyclooxygenase-2 knockout osteoblasts in vitro, Biochem. Biophys. Res. Commun. 372 (2008) 536–541.

[51] E.M. Greenfield, Anabolic effects of intermittent PTH on osteoblasts, Curr. Mol. Pharmacol. 5 (2012) 127–134.

[52] S. Kakar, T.A. Einhorn, S. Vora, L.J. Miara, G. Hon, N.A. Wigner, D. Toben, K.A. Jacobsen, M.O. Al-Sebaei, M. Song, P.C. Trackman, E.F. Morgan, L.C. Gerstenfeld, G.L. Barnes, Enhanced chondrogenesis and Wnt signaling in PTH-treated fractures, J. Bone Miner. Res. Off. J. Am. Soc. Bone Miner. Res. 22 (2007) 1903–1912.

[53] M. Tägil, M.M. McDonald, A. Morse, L. Peacock, K. Mikulec, N. Amanat, C. Godfrey, D.G. Little, Intermittent PTH(1–34) does not increase union rates in open rat femoral fractures and exhibits attenuated anabolic effects compared to closed fractures, Bone. 46 (2010) 852–859.

[54] M. Hirata, S. Harada, C. Matsumoto, M. Takita, C. Miyaura, M. Inada, Role of prostaglandin E in receptor activator of nuclear factor-κ ligand (RANKL) expression in osteoblasts induced by cell adhesion to bone marrow B-lymphocytes, J. Health Sci. 55 (2009) 832–837.

[55] S. Jurado, N. Garcia-Giralt, A. Díez-Pérez, P. Esbrit, G. Yoskovitz, L. Agueda, R. Urreizti, L. Pérez-Edo, G. Saló, L. Mellibovsky, others, Effect of IL-1β, PGE2, and TGF-β on the expression of OPG and RANKL in normal and osteoporotic primary human osteoblasts, J. Cell. Biochem. 110 (2010) 304–310.

[56] C. Begue-Kirn, A.J. Smith, M. Loriot, C. Kupferle, J.V. Ruch, H. Lesot, Comparative analysis of TGF beta s, BMPs, IGF1, msxs, fibronectin, osteonectin and bone sialoprotein gene expression during normal and in vitro-induced odontoblast differentiation, Int. J. Dev. Biol. 38 (1994) 405–420.

[57] F. Kandziora, R. Pflugmacher, M. Scholz, C. Knispel, T. Hiller, G. Schollmeier, H. Bail, G. Schmidmaier, G. Duda, M. Raschke, others, Comparison of BMP-2 and combined IGF-I/TGF-ss1 application in a sheep cervical spine fusion model, Eur. Spine J. 11 (2002) 482–493.

[58] M. Lind, Growth factor stimulation of bone healing. Effects on osteoblasts, osteomies, and implants fixation., Acta Orthop. Scand. Suppl. 283 (1998) 2–37.

[59] C.A. Gregory, W. Grady Gunn, A. Peister, D.J. Prockop, An Alizarin red-based assay of mineralization by adherent cells in culture: comparison with cetylpyridinium chloride extraction, Anal. Biochem. 329 (2004) 77–84.

[60] M. LI, H.Z. Ke, H. Qi, D.R. Healy, Y. LI, D.T. Crawford, V.M. Paralkar, T.A. Owen, K.O. Cameron, B.A. Lefker, others, A Novel, Non-Prostanoid EP2 Receptor-Selective Prostaglandin E2 Agonist Stimulates Local Bone Formation and Enhances Fracture Healing, J. Bone Miner. Res. 18 (2003) 2033–2042.

[61] H. Pan, P. Kopečková, D. Wang, J. Yang, S. Miller, J. Kopeček, Water-soluble HPMA copolymer—prostaglandin E 1 conjugates containing a cathepsin K sensitive spacer, J. Drug Target. 14 (2006) 425–435.

[62] S.K. Thompson, S.M. Halbert, M.J. Bossard, T.A. Tomaszek, M.A. Levy, B. Zhao, W.W. Smith, S.S. Abdel-Meguid, C.A. Janson, K.J. D'Alessio, M.S. McQueney, B.Y. Amegadzie, C.R. Hanning, R.L. DesJarlais, J. Briand, S.K. Sarkar, M.J. Huddleston, C.F. Ijames, S.A. Carr, K.T. Garnes, A. Shu, J.R. Heys, J. Bradbeer, D. Zembryki, L. Lee-Rykaczewski, I.E. James, M.W. Lark, F.H. Drake, M. Gowen, J.G. Gleason, D.F. Veber, Design of potent and selective human cathepsin K inhibitors that span the active site, Proc. Natl. Acad. Sci. 94 (1997) 14249 –14254.

[63] Y. Eeckhout, G. Vaes, Further studies on the activation of procollagenase, the

latent precursor of bone collagenase. Effects of lysosomal cathepsin B, plasmin and kallikrein, and spontaneous activation, Biochem J. 166 (1977) 21–31.

[64] J.S. Mort, D.J. Buttle, Cathepsin B, Int. J. Biochem. Cell Biol. 29 (1997) 715–720.

[65] P.L. Sannes, B.H. Schofield, D.F. McDonald, Histochemical localization of cathepsin B, dipeptidyl peptidase I, and dipeptidyl peptidase II in rat bone., J. Histochem. Cytochem. 34 (1986) 983–988.

[66] T. Goto, T. Tsukuba, T. Kiyoshima, Y. Nishimura, K. Kato, K. Yamamoto, T. Tanaka, Immunohistochemical localization of cathepsins B, D and L in the rat osteoclast, Histochemistry. 99 (1993) 411–414.

[67] J.M. Delaisse, P. Ledent, G. Vaes, Collagenolytic cysteine proteinases of bone tissue. Cathepsin B, (pro)cathepsin L and a cathepsin L-like 70 kDa proteinase, Biochem J. 279 (1991) 167–174.

[68] H. Kakegawa, T. Nikawa, K. Tagami, H. Kamioka, K. Sumitani, T. Kawata, M. Drobnič-Kosorok, B. Lenarčič, V. Turk, N. Katunuma, Participation of cathepsin L on bone resorption, FEBS Lett. 321 (1993) 247–250.

[69] E. Segal, H. Pan, P. Ofek, T. Udagawa, P. Kopečková, J. Kopeček, R. Satchi-Fainaro, Targeting angiogenesis-dependent calcified neoplasms using combined polymer therapeutics, PloS One. 4 (2009) e5233.

[70] S. Georges, C. Ruiz Velasco, V. Trichet, Y. Fortun, D. Heymann, M. Padrines, Proteases and bone remodelling, Cytokine Growth Factor Rev. 20 (2009) 29–41.

[71] O. Seksek, J. Biwersi, A.S. Verkman, Evidence against defective trans-Golgi acidification in cystic fibrosis, J. Biol. Chem. 271 (1996) 15542–15548.

[72] M. Srinivasarao, C.V. Galliford, P.S. Low, Principles in the design of ligand-targeted cancer therapeutics and imaging agents, Nat. Rev. Drug Discov. 14 (2015) 203–219.

[73] O. Swenson, Biochemical changes in the fracture hematoma, J. Bone Joint Surg. Am. 28 (1946) 288–293.

[74] P.J. Crack, J.M. Taylor, N.J. Flentjar, J. De Haan, P. Hertzog, R.C. Iannello, I. Kola, Increased infarct size and exacerbated apoptosis in the glutathione peroxidase-1 (Gpx-1) knockout mouse brain in response to ischemia/reperfusion injury, J. Neurochem. 78 (2001) 1389–1399.

[75] R.W. Hong, J.D. Rounds, W.S. Helton, M.K. Robinson, D.W. Wilmore, Glutamine preserves liver glutathione after lethal hepatic injury, Ann. Surg. 215 (1992) 114–119.

[76] M.E. Gerritsen, C.M. Bloor, Endothelial cell gene expression in response to injury., FASEB J. 7 (1993) 523–532.

[77] G.D.L. Phillips, G. Li, D.L. Dugger, L.M. Crocker, K.L. Parsons, E. Mai, W.A. Blättler, J.M. Lambert, R.V. Chari, R.J. Lutz, others, Targeting HER2-positive breast cancer with trastuzumab-DM1, an antibody–cytotoxic drug conjugate, Cancer Res. 68 (2008) 9280–9290.

[78] A.N. Koo, H.J. Lee, S.E. Kim, J.H. Chang, C. Park, C. Kim, J.H. Park, S.C. Lee, Disulfide-cross-linked PEG-poly (amino acid) s copolymer micelles for glutathione-mediated intracellular drug delivery, Chem. Commun. (2008) 6570–6572.

[79] P.D. Senter, Potent antibody drug conjugates for cancer therapy, Curr. Opin. Chem. Biol. 13 (2009) 235–244.

[80] M.C. Vicens, A. Sen, A. Vanderlaan, T.J. Drake, W. Tan, Investigation of Molecular Beacon Aptamer-Based Bioassay for Platelet-Derived Growth Factor Detection, ChemBioChem. 6 (2005) 900–907.

[81] J.H. Kim, S. Chaudhary, M. Ozkan, Multicolour hybrid nanoprobes of molecular beacon conjugated quantum dots: FRET and gel electrophoresis assisted target DNA detection, Nanotechnology. 18 (2007) 195105.

[82] S.A. Marras, F.R. Kramer, S. Tyagi, Efficiencies of fluorescence resonance energy transfer and contact-mediated quenching in oligonucleotide probes, Nucleic Acids Res. 30 (2002) e122–e122.

[83] Y. Oe, R.J. Christie, M. Naito, S.A. Low, S. Fukushima, K. Toh, Y. Miura, Y. Matsumoto, N. Nishiyama, K. Miyata, others, Actively-targeted polyion complex micelles stabilized by cholesterol and disulfide cross-linking for systemic delivery of siRNA to solid tumors, Biomaterials. 35 (2014) 7887–7895.

[84] Y. Matsumoto, T. Nomoto, H. Cabral, Y. Matsumoto, S. Watanabe, R.J. Christie, K. Miyata, M. Oba, T. Ogura, Y. Yamasaki, N. Nishiyama, T. Yamasoba, K. Kataoka, Direct and instantaneous observation of intravenously injected substances using intravital confocal micro-videography, Biomed. Opt. Express. 1 (2010) 1209.

[85] T. Nomoto, Y. Matsumoto, K. Miyata, M. Oba, S. Fukushima, N. Nishiyama, T. Yamasoba, K. Kataoka, In situ quantitative monitoring of polyplexes and polyplex micelles in the blood circulation using intravital real-time confocal laser scanning microscopy, J. Controlled Release. (2011).

[86] R.J. Christie, Y. Matsumoto, K. Miyata, T. Nomoto, S. Fukushima, K. Osada, J. Halnaut, F. Pittella, H.J. Kim, N. Nishiyama, others, Targeted Polymeric Micelles for siRNA Treatment of Experimental Cancer by Intravenous Injection, ACS

Nano. (2012).

[87] N.G. Zhegalova, S. He, H. Zhou, D.M. Kim, M.Y. Berezin, Minimization of self-quenching fluorescence on dyes conjugated to biomolecules with multiple labeling sites via asymmetrically charged NIR fluorophores, Contrast Media Mol. Imaging. 9 (2014) 355–362.

[88] Cholesterol, [1,2-3H(N)]-, 1mCi (37MBq) | PerkinElmer, PerkinElmer Inc. (n.d.). http://www.perkinelmer.com/catalog/product/id/net139001mc (accessed June 26, 2015).

[89] S.A. Low, J. Yang, J. Kopeček, Bone-targeted acid-sensitive doxorubicin conjugate micelles as potential osteosarcoma therapeutics, Bioconjug. Chem. 25 (2014) 2012–2020.

[90] J.N. Israelachvili, Intermolecular and surface forces, Academic press London, 1991.

[91] A.-L. Bauchet, R. Masson, M. Guffroy, M. Slaoui, Immunohistochemical Identification of Kidney Nephron Segments in the Dog, Rat, Mouse, and Cynomolgus Monkey, Toxicol. Pathol. 39 (2011) 1115–1128.

[92] I. Gröngröft, P. Heil, R. Matthys, P. Lezuo, A. Tami, S. Perren, P. Montavon, K. Ito, Fixation compliance in a mouse osteotomy model induces two different processes of bone healing but does not lead to delayed union, J. Biomech. 42 (2009) 2089–2096.

[93] S. Jingushi, K. Mizuno, T. Matsushita, M. Itoman, Low-intensity pulsed ultrasound treatment for postoperative delayed union or nonunion of long bone fractures, J. Orthop. Sci. 12 (2007) 35–41.

[94] M.E. Oetgen, G.A. Merrell, N.W. Troiano, M.C. Horowitz, M.A. Kacena, Development of a femoral non-union model in the mouse, Injury. 39 (2008) 1119–1126.

[95] R.A. Meyer, M.H. Meyer, M. Tenholder, S. Wondracek, R. Wasserman, P. Garges, Gene expression in older rats with delayed union of femoral fractures, J. Bone Joint Surg. Am. 85-A (2003) 1243–1254.

[96] T.T. Andreassen, C. Fledelius, C. Ejersted, H. Oxlund, Increases in callus formation and mechanical strength of healing fractures in old rats treated with parathyroid hormone, Acta Orthop. 72 (2001) 304–307.

[97] U.T. Iwaniec, K.A. Magee, N.G. Mitova-Caneva, T.J. Wronski, Bone anabolic effects of subcutaneous treatment with basic fibroblast growth factor alone and in combination with estrogen in osteopenic ovariectomized rats, Bone. 33 (2003)

380–386.

[98] Y.F. Li, E. Luo, G. Feng, S.S. Zhu, J.H. Li, J. Hu, Systemic treatment with strontium ranelate promotes tibial fracture healing in ovariectomized rats, Osteoporos. Int. 21 (2010) 1889–1897.

[99] S. Asamura, Y. Mochizuki, M. Yamamoto, Y. Tabata, N. Isogai, Bone regeneration using a bone morphogenetic protein-2 saturated slow-release gelatin hydrogel sheet: evaluation in a canine orbital floor fracture model, Ann. Plast. Surg. 64 (2010) 496–502.

[100] M.E. O'Sullivan, J.T. Bronk, E.Y. Chao, P.J. Kelly, Experimental study of the effect of weight bearing on fracture healing in the canine tibia., Clin. Orthop. 302 (1994) 273–283.

[101] E.H. Schemitsch, R. Jain, D.C. Turchin, J.B. Mullen, R.J. Byrick, G.I. Anderson, R.R. Richards, Pulmonary effects of fixation of a fracture with a plate compared with intramedullary nailing. A canine model of fat embolism and fracture fixation*, J. Bone Jt. Surg. 79 (1997) 984–96.

[102] D.G. Allan, G.G. Russell, M.J. Moreau, V.J. Raso, D. Budney, Vertebral end-plate failure in porcine-and bovine models of spinal fracture instrumentation, J. Orthop. Res. 8 (1990) 154–156.

[103] V.M. Chapman, M. Kalra, E. Halpern, B. Grottkau, M. Albright, D. Jaramillo, 16-MDCT of the posttraumatic pediatric elbow: optimum parameters and associated radiation dose, Am. J. Roentgenol. 185 (2005) 516–521.

[104] J.E. Carpenter, J.A. Hipp, T.N. Gerhart, C.G. Rudman, W.C. Hayes, S.B. Trippel, Failure of growth hormone to alter the biomechanics of fracture-healing in a rabbit model., J. Bone Jt. Surg. 74 (1992) 359–367.

[105] W.-J. Chen, S. Jingushi, I. Aoyama, J. Anzai, G. Hirata, M. Tamura, Y. Iwamoto, Effects of FGF-2 on metaphyseal fracture repair in rabbit tibiae, J. Bone Miner. Metab. 22 (2004) 303–309.

[106] A. Llinas, H.A. McKellop, G.J. Marshall, F. Sharpe, M. Kirchen, A. Sarmiento, Healing and remodeling of articular incongruities in a rabbit fracture model., J. Bone Jt. Surg. 75 (1993) 1508–1523.

[107] M.M. Swindle, A. Makin, A.J. Herron, F.J. Clubb, K.S. Frazier, Swine as Models in Biomedical Research and Toxicology Testing, Vet. Pathol. Online. 49 (2012) 344–356.

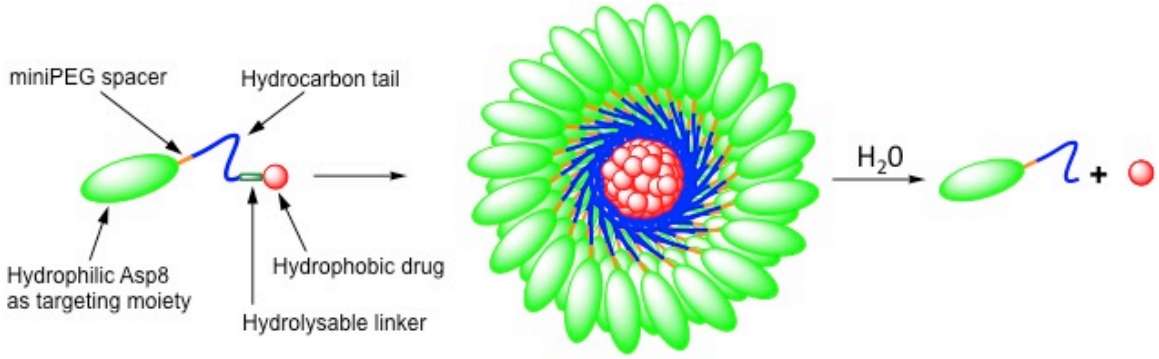

Figure 5.1: Basic construct, self-assembly, and release of the designed micelles.

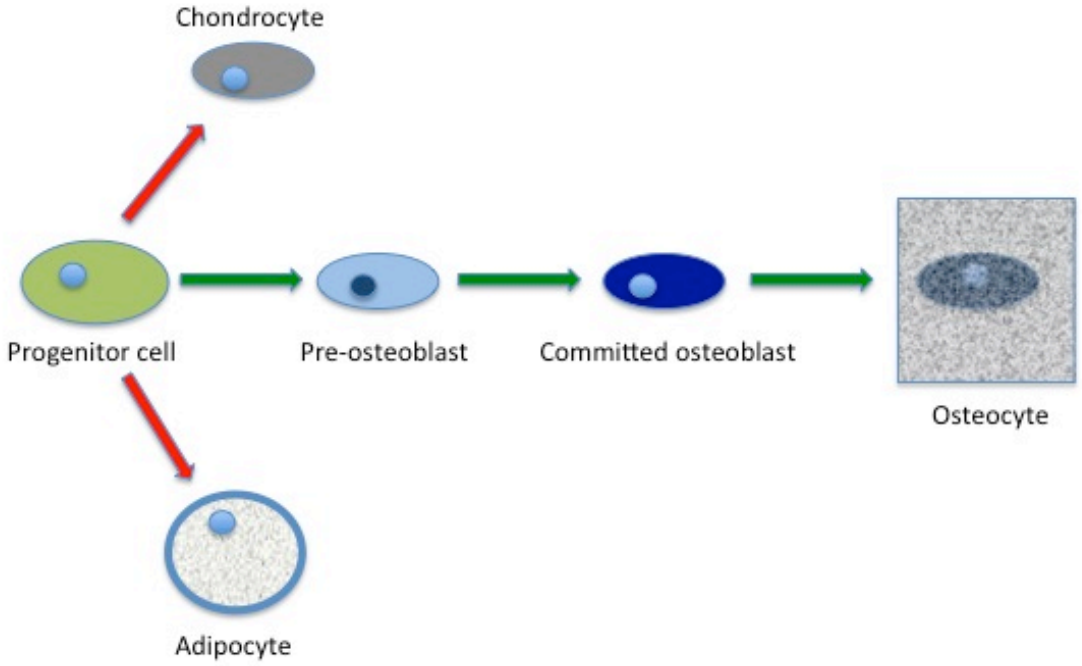

Figure 5.2: The differentiation and activation of osteoblasts through the Wnt/β-catenin signaling pathway. Green arrows indicate active Wnt signaling and red arrows indicate that GSK3β is active [32].

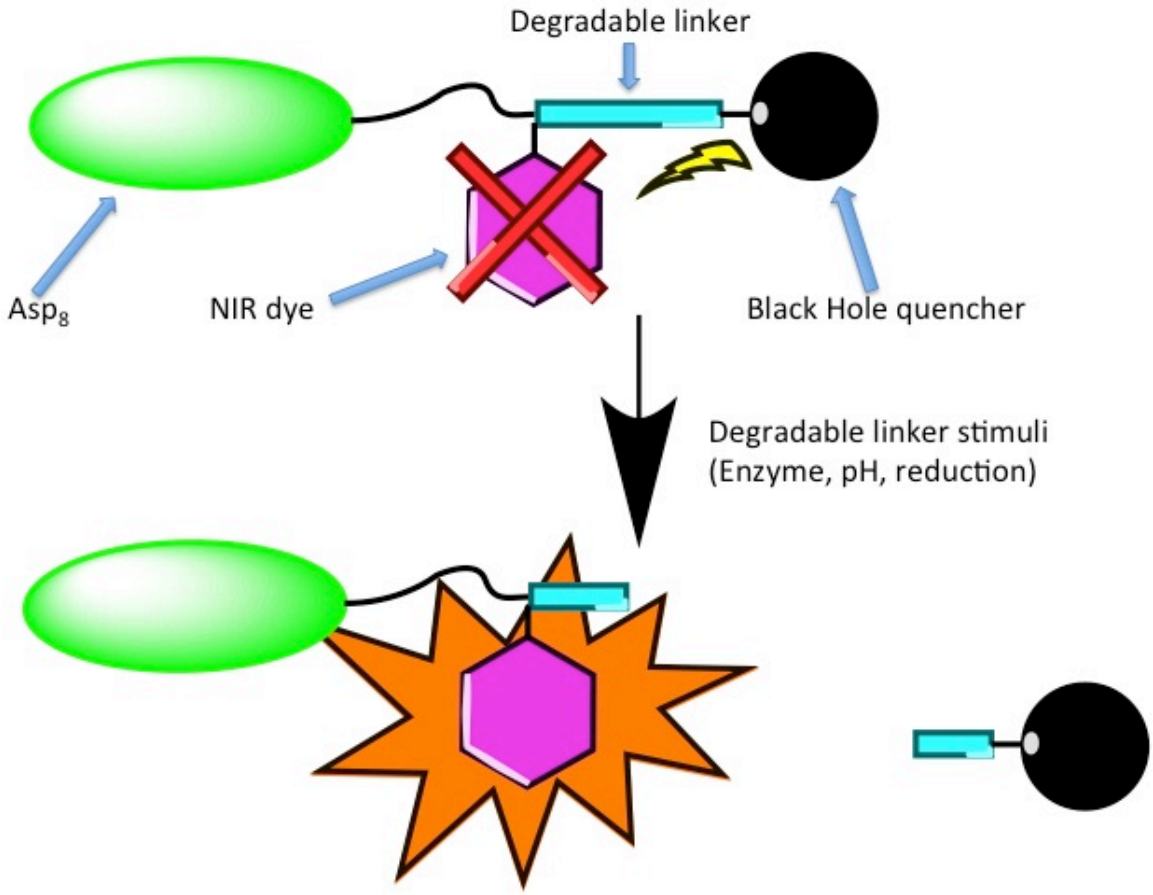

Figure 5.3: Black Hole quenching dyes are capable of reducing fluorescence of NIR dyes in close proximity. By targeting a NIR dye coupled by a degradable linker to a Black Hole quenching dye, one could measure the degradation of the linker at the fracture site. Upon degradation of the linker to a Black Hole quencher dye, the NIR dye fluoresces, and can be measured with a NIR imaging system.

APPENDIX A

CHAPTER 2 SUPPORTING INFORMATION

A.1 Fmoc-Hydrazine

The structure and purity of synthesized Fmoc-hydrazine were verified by 1H-NMR and analytical HPLC, as shown in Figures A.1 and A.2.

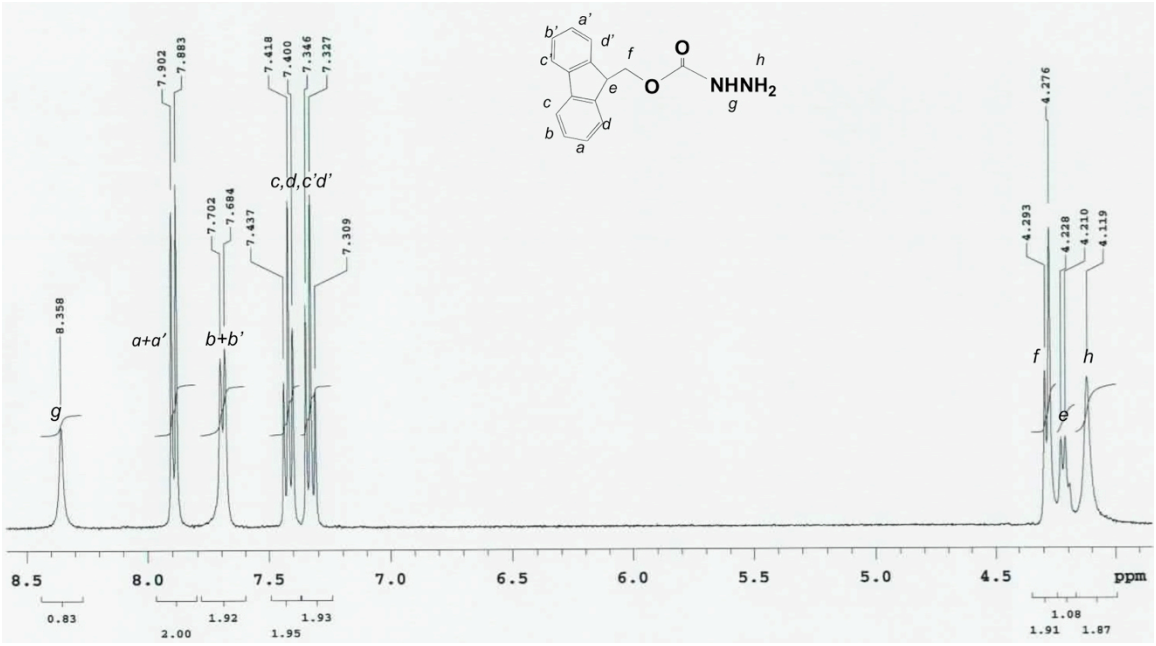

Figure A.1: ^{1}H-NMR spectrum of Fmoc-hydrazine (using DMSO-d6 as solvent on Mercury 400 spectrometer).

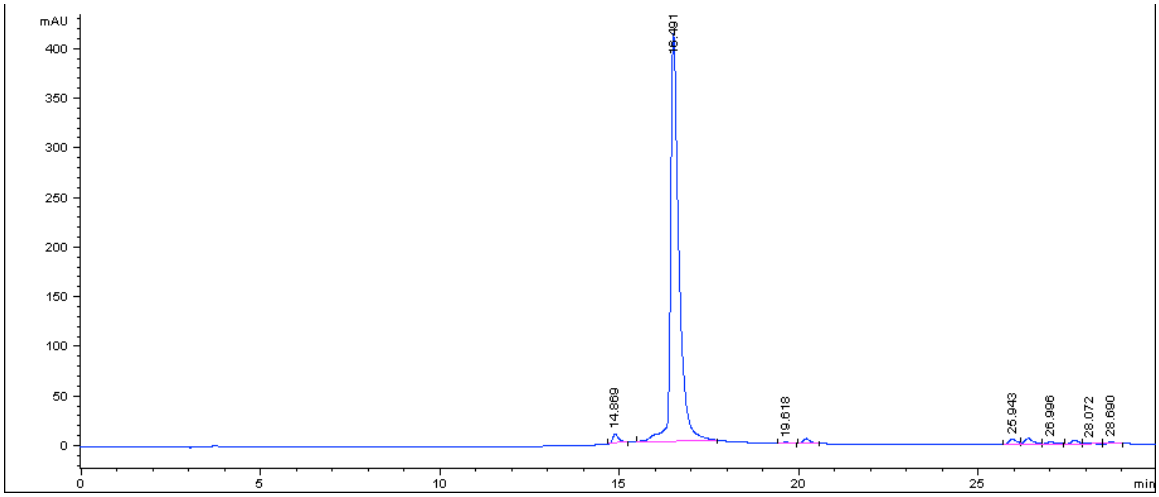

Figure A.2: HPLC elution profile of Fmoc-hydrazine using Agilent Technologies 1100 series (Zorbax C18 column 4.6×250 mm) with gradient method from 2 to 90% of Buffer B within 30 min and flow rate 1.0 mL/min (Buffer A: deionized water (DI H_2O) with 0.1% TFA, Buffer B: acetonitrile containing 0.1% TFA).

A2 Fmoc-aminoundecanoic acid

The synthesized Fmoc-aminoundecanoic acid was characterized with mass spectrum, ^{1}H-NMR and HPLC analytical profiles (A.3, A.4, and A.5, respectively):

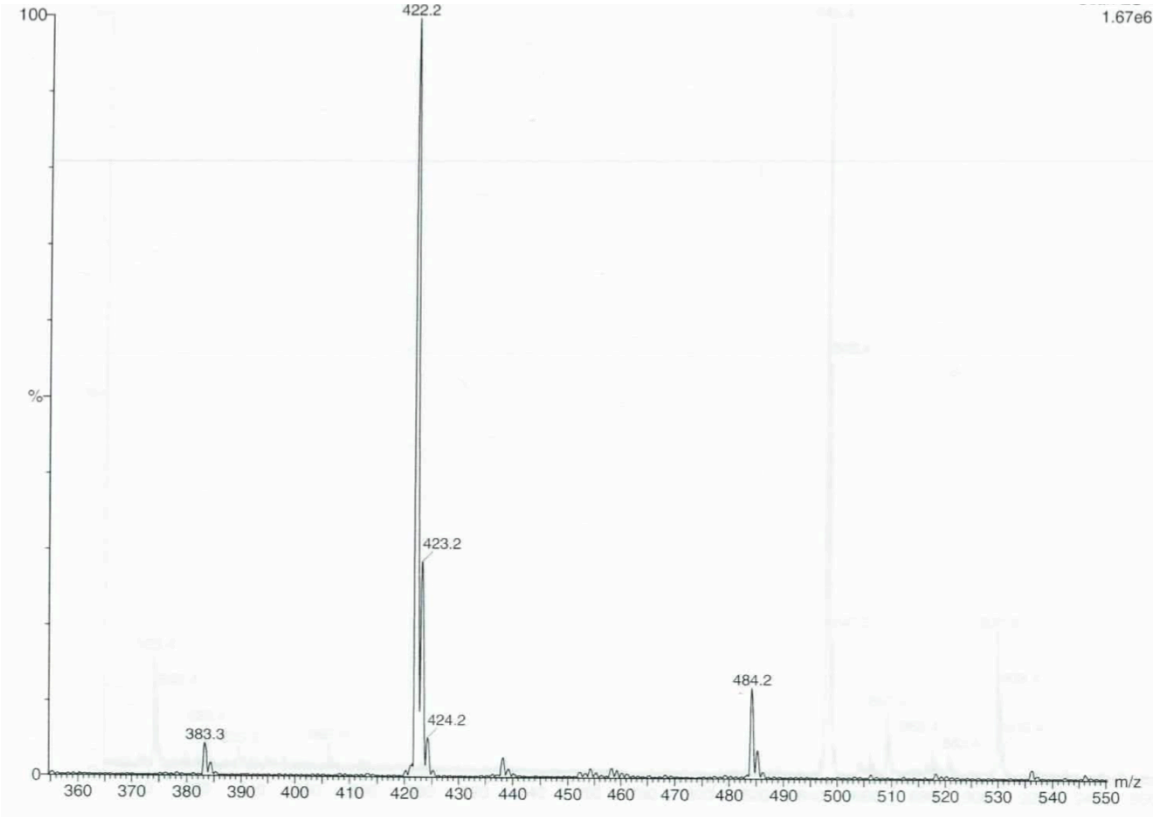

Figure A.3: MALDI-ToF mass spectrum of Fmoc-aminoundecanoic acid.

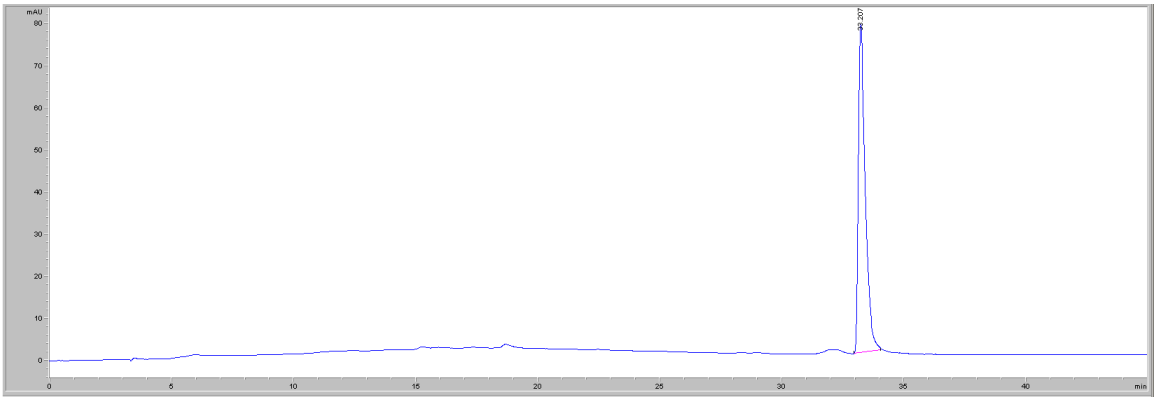

Figure A.4: HPLC profile of Fmoc-aminoundecanoic acid (Fmoc-AUA) using Agilent Technologies 1100 series (Zorbax C18 column 4.6×250 mm) with gradient method from 2 to 90% of Buffer B within 30 min and flow rate 1.0 mL/min (Buffer A: deionized water (DI H_2O) with 0.1% TFA, Buffer B: acetonitrile containing 0.1% TFA).

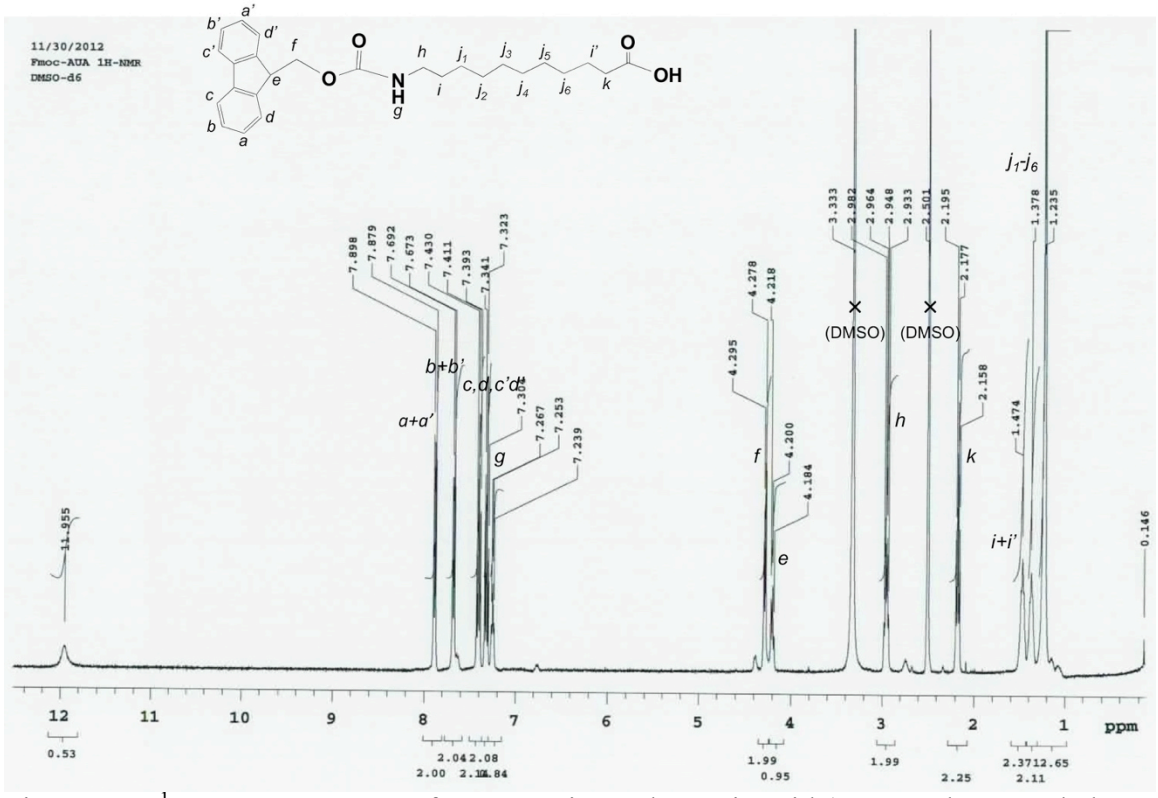

Figure A.5: ^{1}H-NMR spectrum of Fmoc-aminoundecanoic acid (DMSO-d6, recorded on Mercury 400 spectrometer).

A3 Characterization of unimers synthesized by solid phase peptide synthesis (SPPS)

Figures A.6-A.13 represent analytical HPLC and MALDI-ToF spectra of four unimers following solid phase peptide synthesis, cleavage, and preparative HPLC purification:

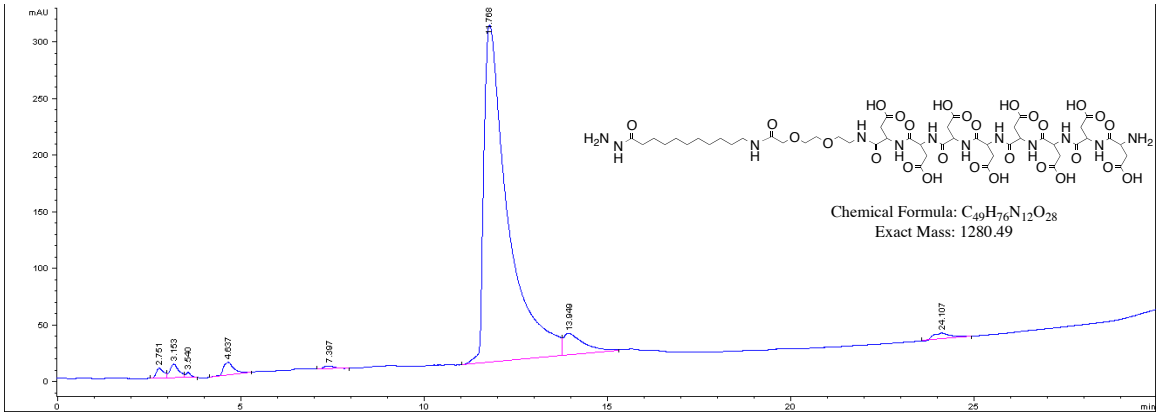

Figure A.6: Structure and HPLC profile of A1-D8.

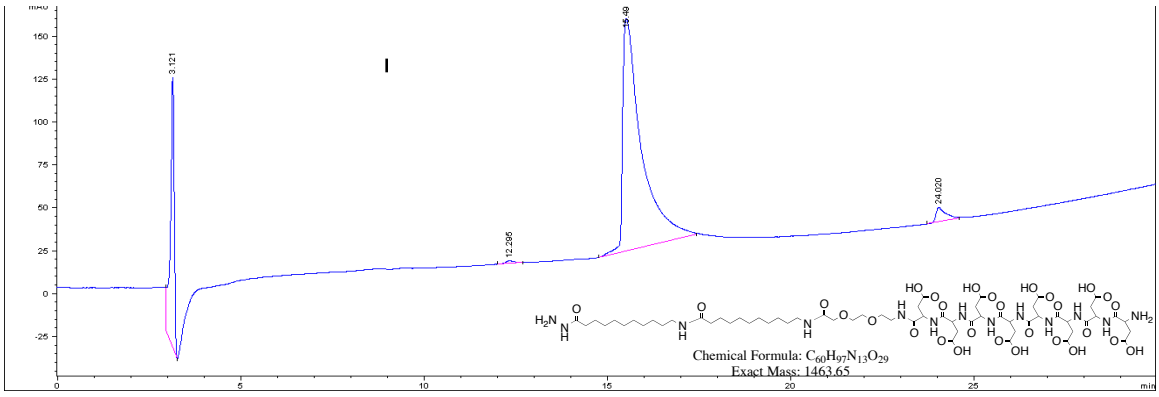

Figure A.7: Structure and HPLC profile of A2-D8.

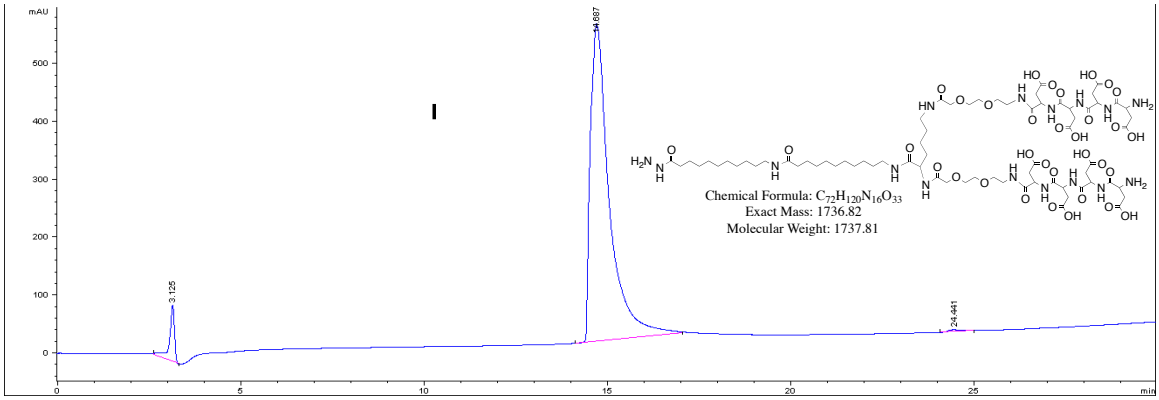

Figure A.8: Structure and HPLC profile of A2-K-D4.

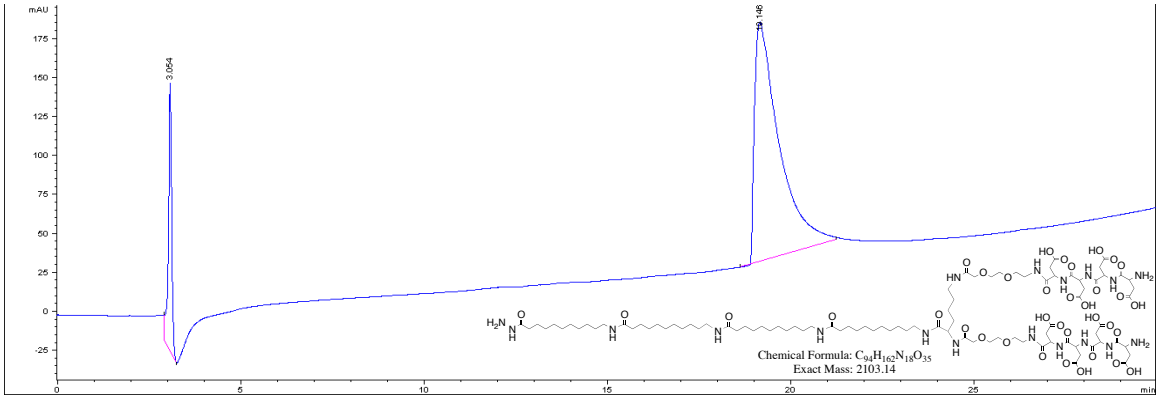

Figure A.9: Structure and HPLC profile of A4-K-D4.

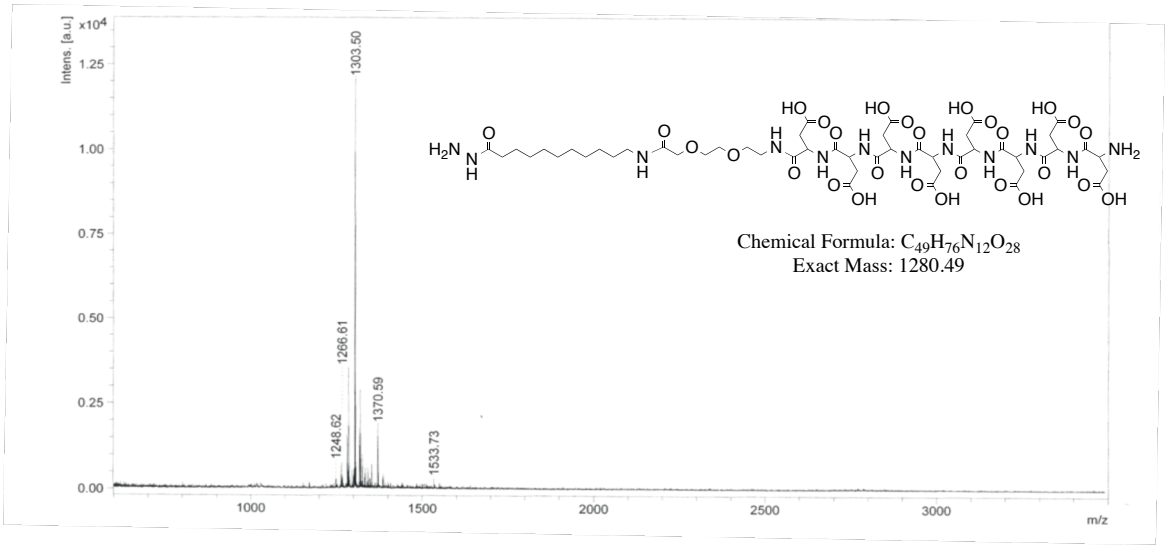

Figure A.10: Structure and MALDI-ToF spectrum of A1-D8.

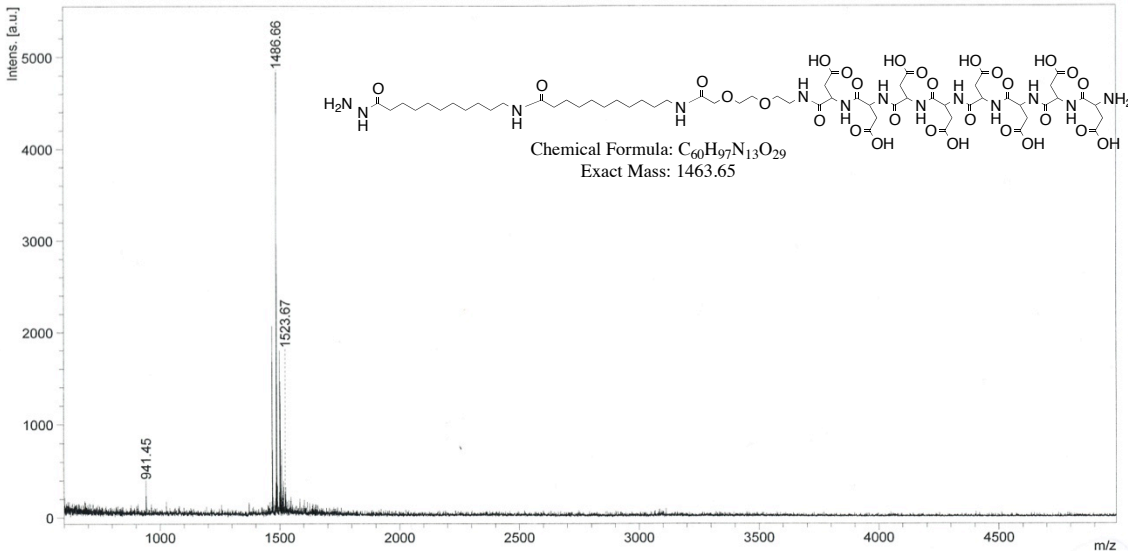

Figure A.11: Structure and MALDI-ToF spectrum of A2-D8.

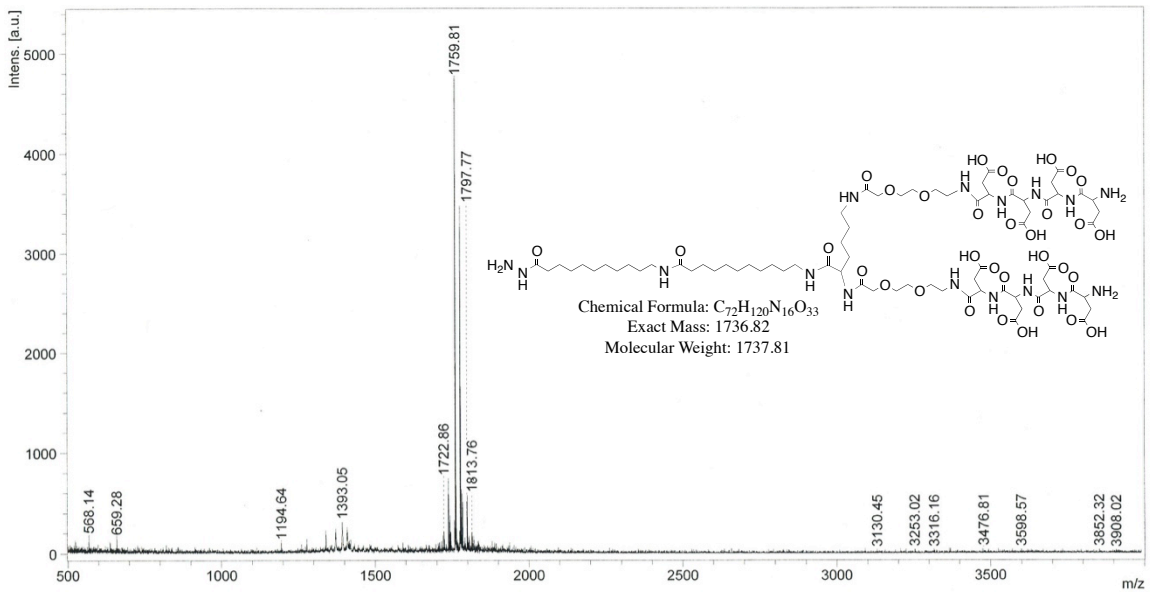

Figure A.12: Structure and MALDI-ToF spectrum of A2-K-D4.

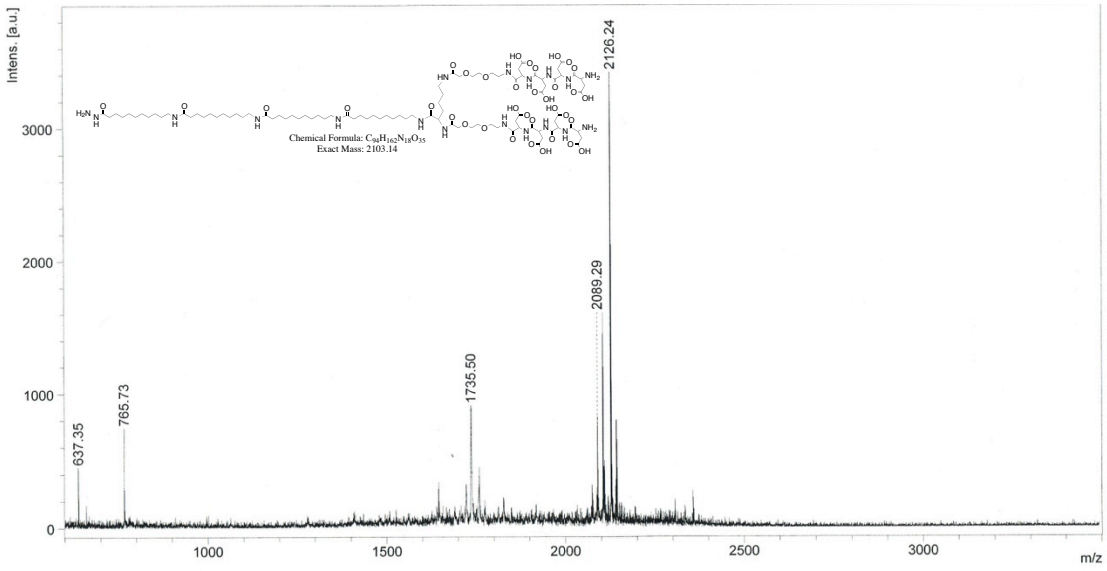

Figure A.13: Structure and MALDI-ToF spectrum of A4-K-D4.

A4 Characterization of DOX – unimer conjugates

Below are HPLC profiles (A.14-A.17) of the four unimers (described above) following conjugation to DOX via hydrazone bond and purification on a LH20 column:

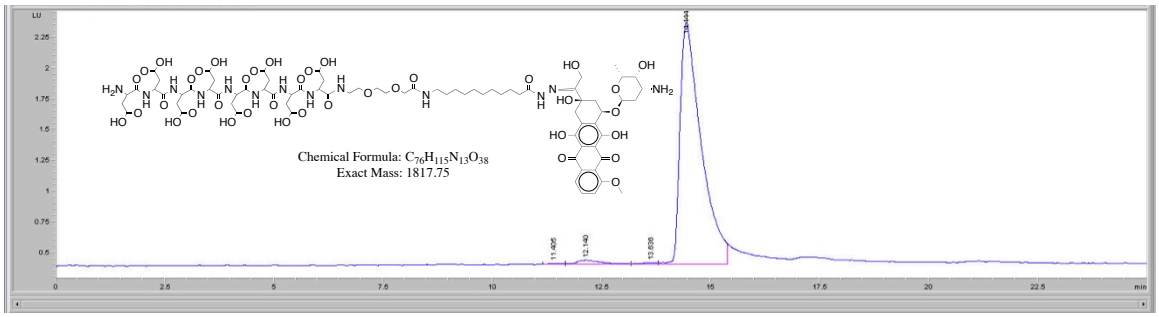

Figure A.14: Chemical structure and HPLC profile of DOX-A1-D8.

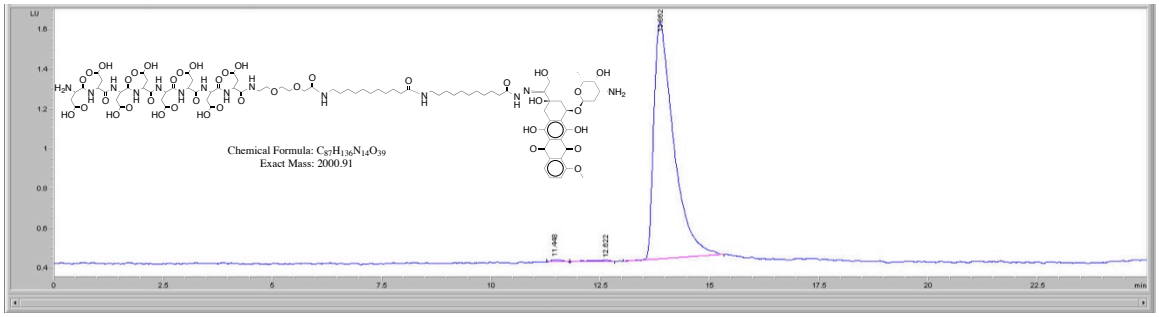

Figure A.15: Chemical structure and HPLC profile of DOX-A2-D8.

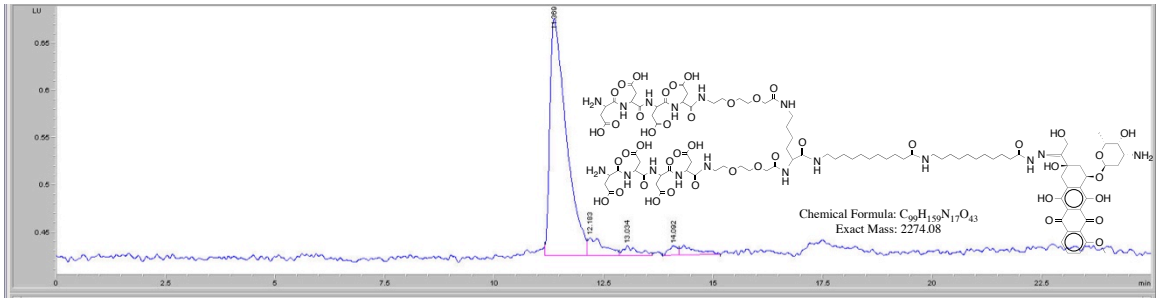

Figure A.16: Chemical structure and HPLC profile of DOX-A2-K-D4.

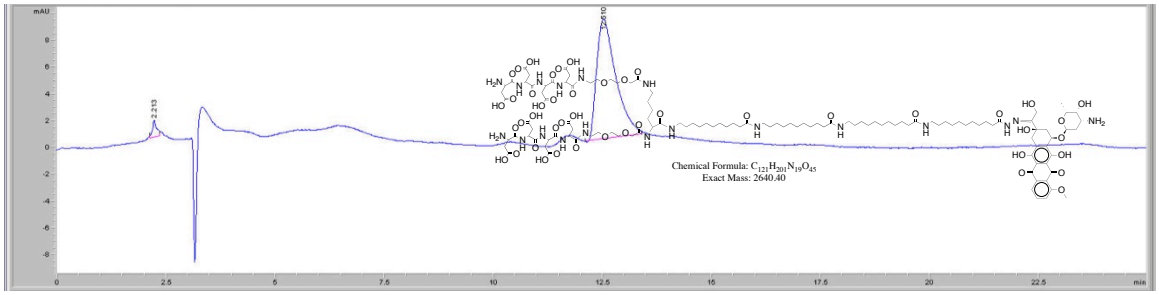

Figure A.17: Chemical structure and HPLC profile of DOX-A4-K-D4.

APPENDIX B

CHAPTER 3 SUPPORTING INFORMATION

B.1 Synthesis of 6′-bromoindirubin-3′-oxime (BIO)

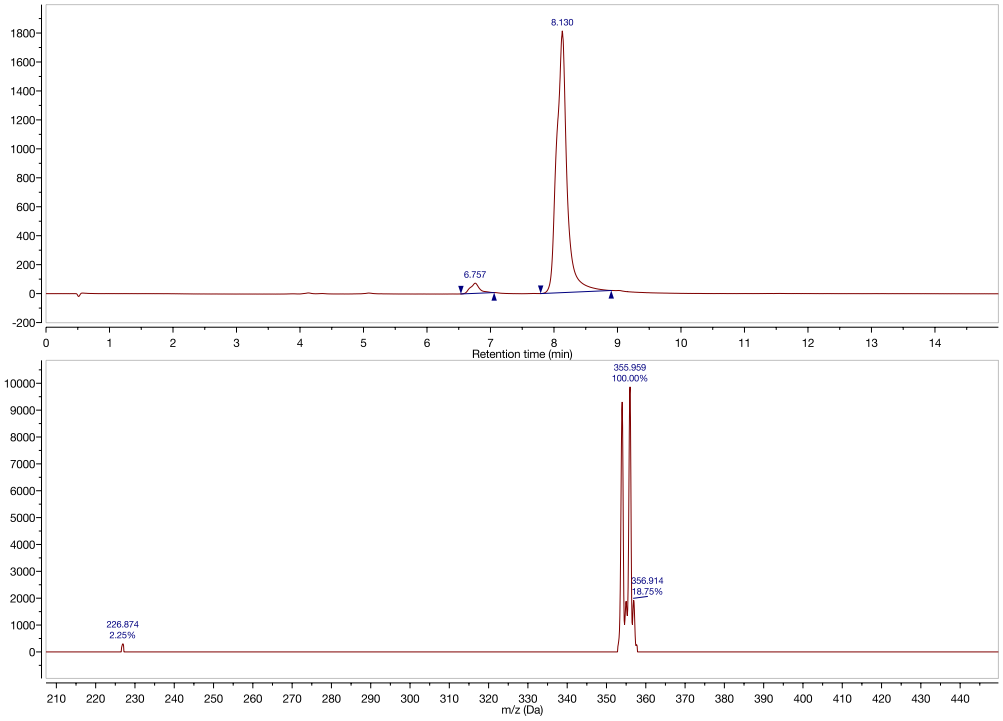

Figure B.1: HPLC and mass spectrometry of purified 6BIO. 6BIO contains a bromine, which is responsible for the two mass peaks.

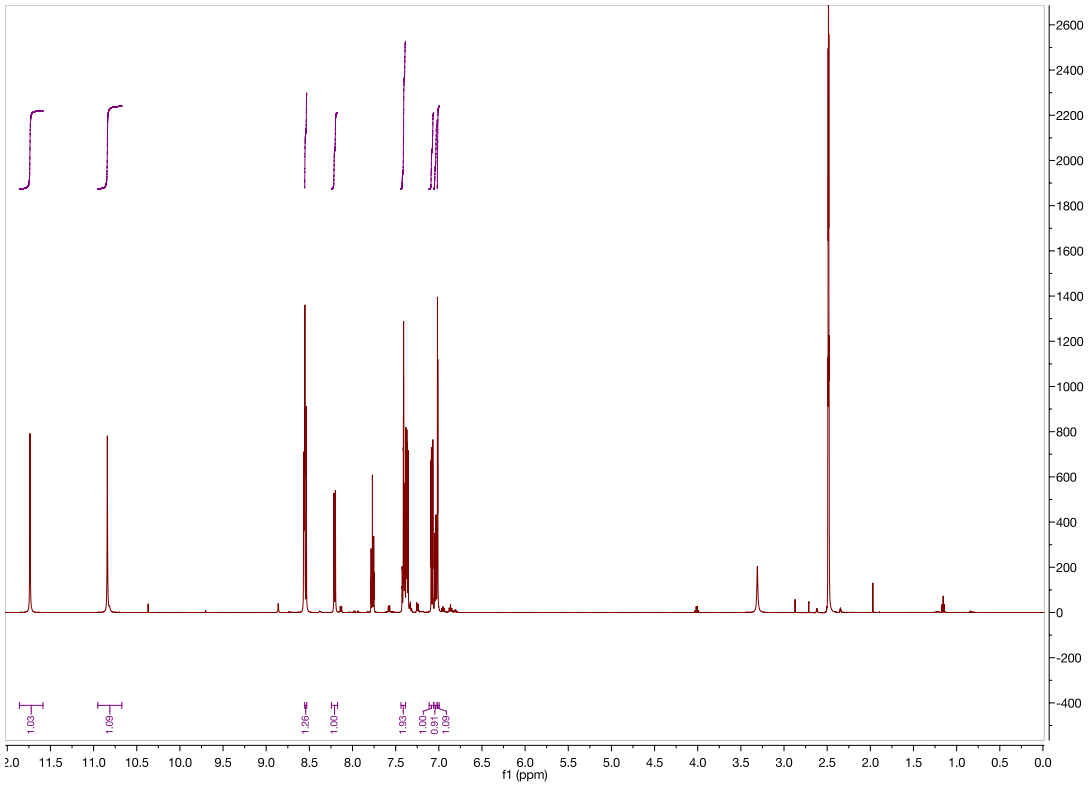

Figure B.2: NMR of 6BIO in DMSO. ^{1}H NMR (500 MHz, DMSO-d_6) δ 11.74 (s, 1H), 10.84 (s, 1H), 8.54 (d, J = 8.5 Hz, 1H), 8.21 (dd, J = 7.6, 1.0 Hz, 1H), 7.44 – 7.39 (m, 2H), 7.08 (dd, J = 8.4, 2.0 Hz, 1H), 7.06 – 7.02 (m, 1H), 7.01 (d, J = 2.0 Hz, 1H).

B.2 Conjugation of 6BIO to 2,2-Dimethyl-3-butynoic acid

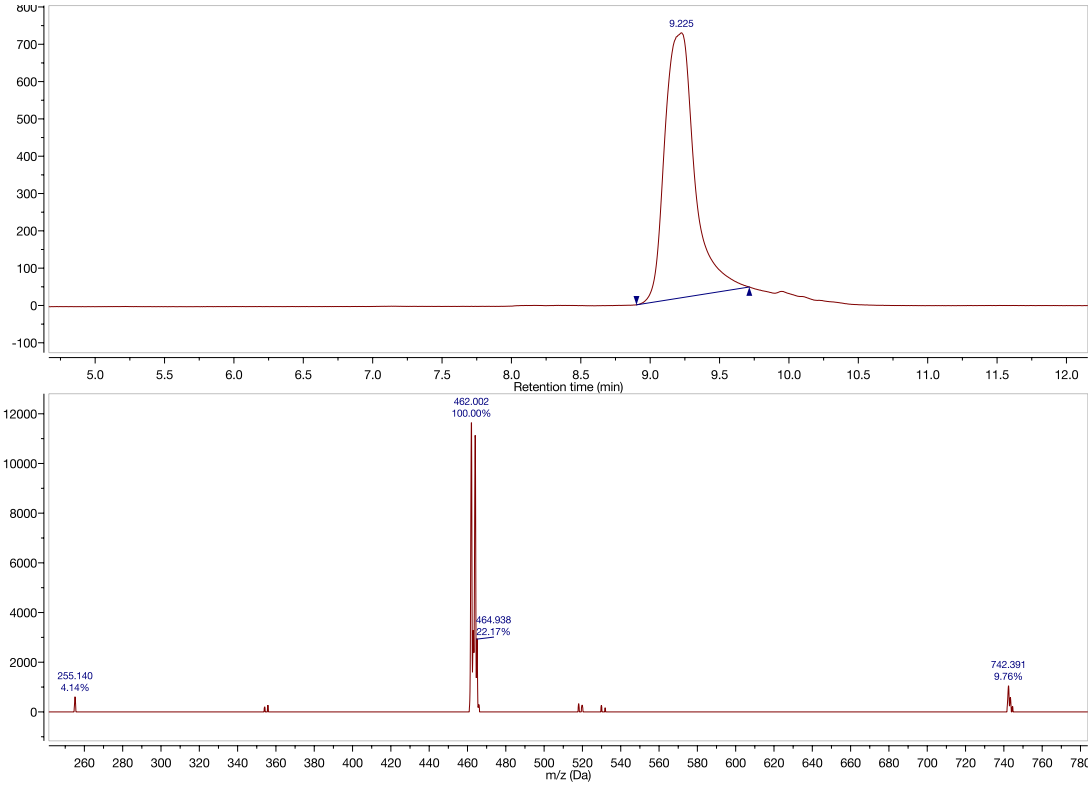

Figure B.3: HPLC and mass spectrometry of the purified product of 6BIO and 2,2-dimethyl-3-butynoic acid. 6BIO contains a bromine which is responsible for the two mass peaks.

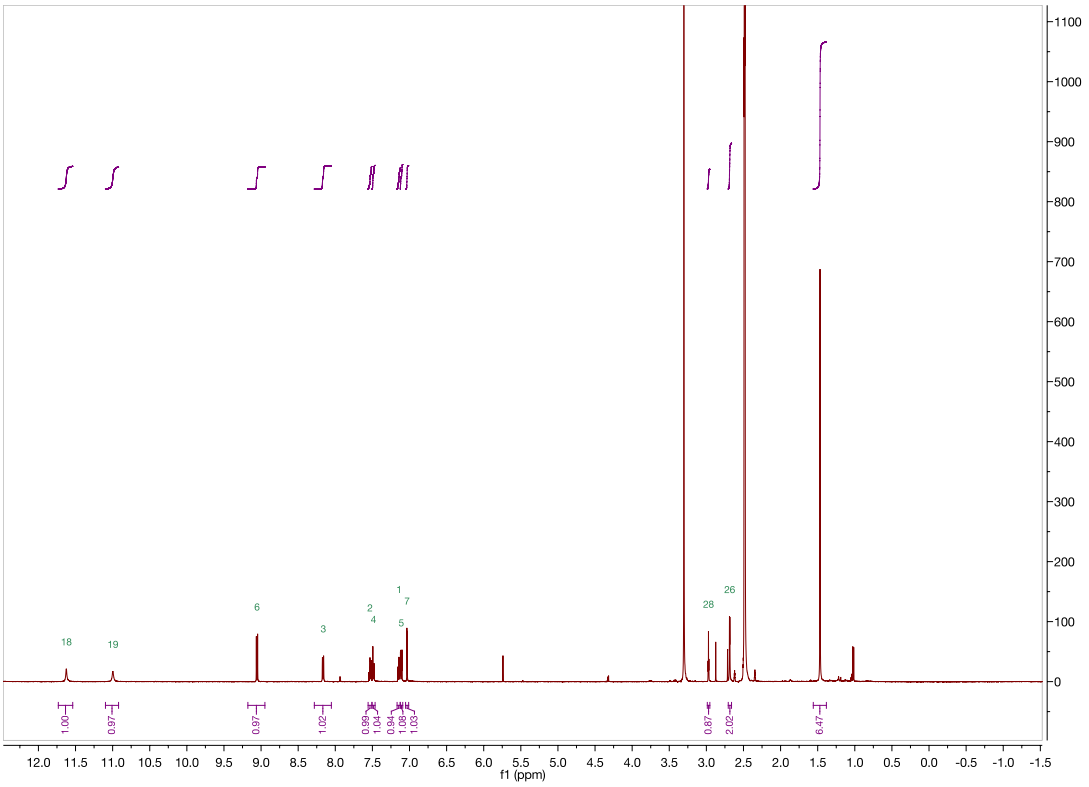

Figure B.4: NMR of the purified product of 6BIO and 2,2-dimethyl-3-butynoic acid in DMSO. ^{1}H NMR (500 MHz, DMSO-d_6) δ 11.62 (s, 1H), 11.00 (s, 1H), 9.06 (d, J = 8.5 Hz, 1H), 8.28 – 8.05 (m, 1H), 7.53 (ddd, J = 8.3, 7.2, 1.2 Hz, 1H), 7.49 (dt, J = 8.0, 1.0 Hz, 1H), 7.14 (td, J = 7.5, 1.2 Hz, 1H), 7.11 (dd, J = 8.5, 2.0 Hz, 1H), 7.03 (d, J = 1.9 Hz, 1H), 2.97 (t, J = 2.6 Hz, 1H), 2.69 (d, J = 2.7 Hz, 2H), 1.47 (s, 6H).

B.3 Synthesis of unimers

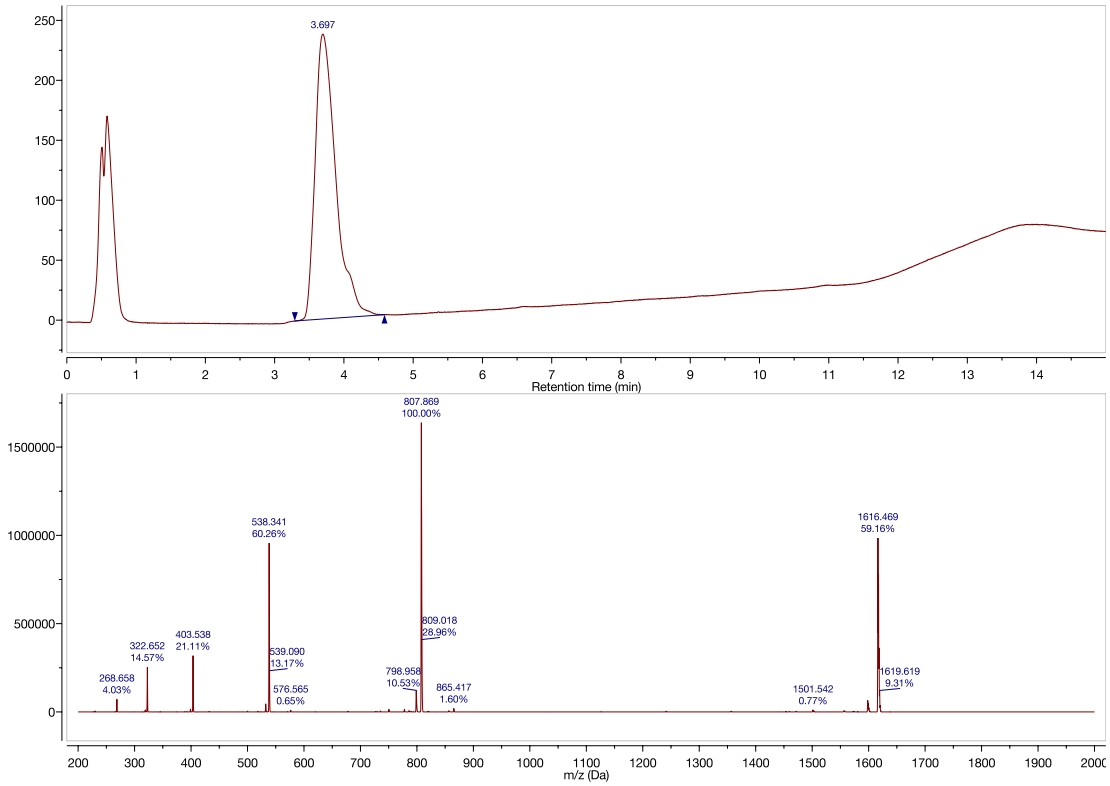

Figure B.5: HPLC and mass spectrometry of the unconjugated linear unimer A2-D8.

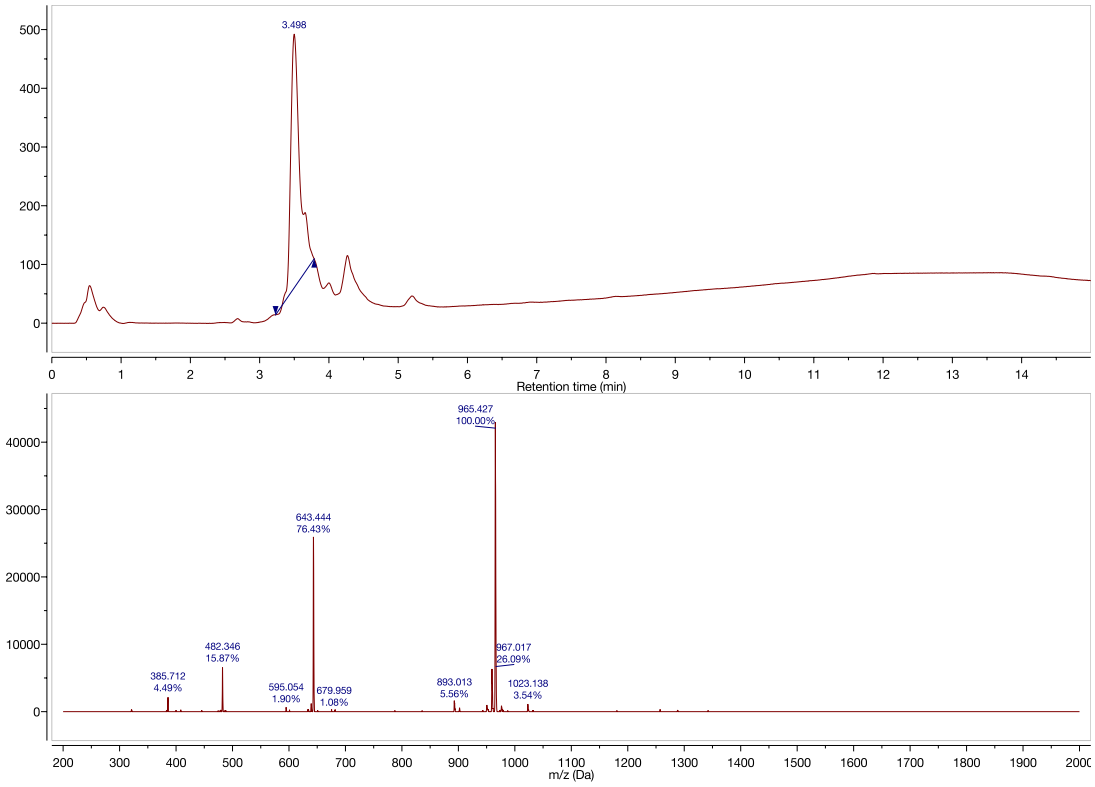

Figure B.6: HPLC and mass spectrometry of the branched unimer A2-K-D4.

B.4 Final ‘clicked’ unimers BIO-A2-D8 and BIO-A2-K-D4

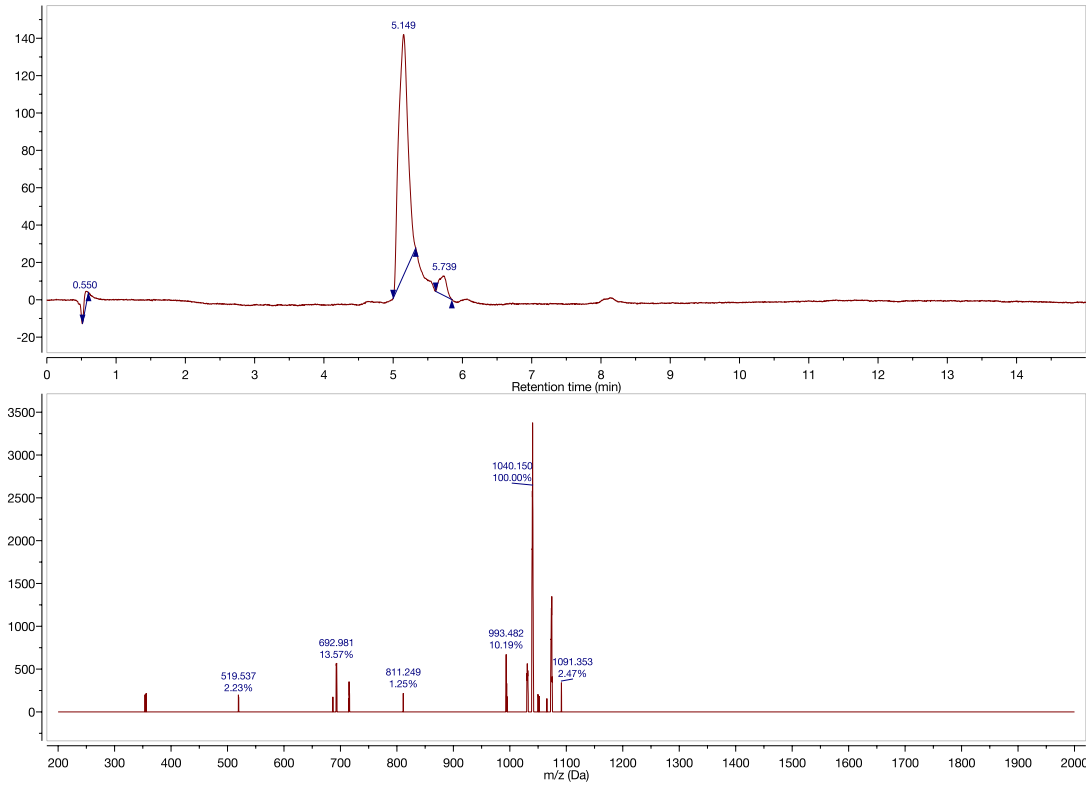

Figure B.7: HPLC and mass spectra of linear unimer BIO-A2-D8.

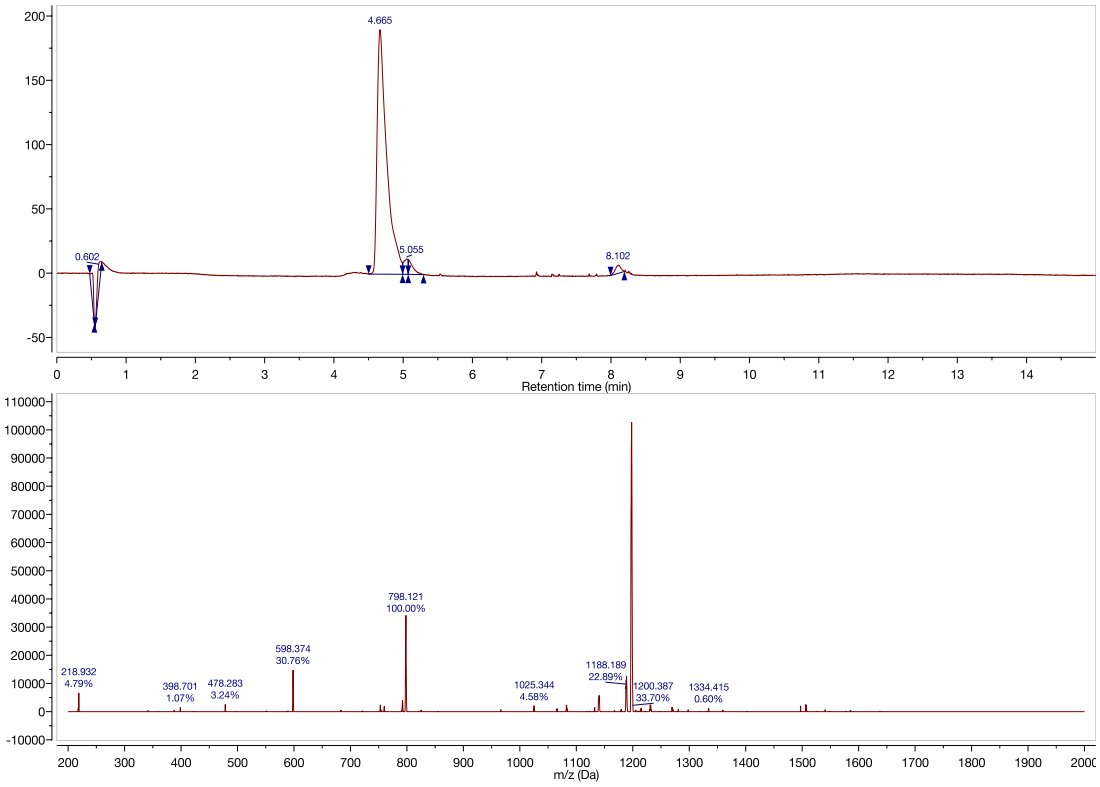

Figure B.8: HPLC and mass spectra of linear unimer BIO-A2-K-D4.

B.5 Release kinetics

BIO-A2-D8 0h

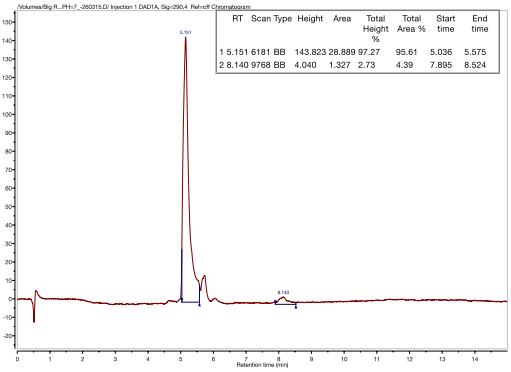

RT	Scan Type	Height	Area	Total Height %	Total Area %	Start time	End time
1 5.151	6181 BB	143.823	28.889	97.27	95.61	5.036	5.575
2 8.140	9768 BB	4.040	1.327	2.73	4.39	7.895	8.524

BIO-A2-D8 1h

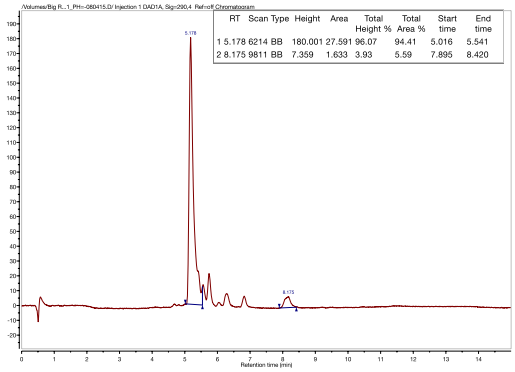

RT	Scan Type	Height	Area	Total Height %	Total Area %	Start time	End time
1 5.178	6214 BB	180.001	27.591	96.07	94.41	5.016	5.541
2 8.175	9811 BB	7.359	1.633	3.93	5.59	7.895	8.420

BIO-A2-D8 2h

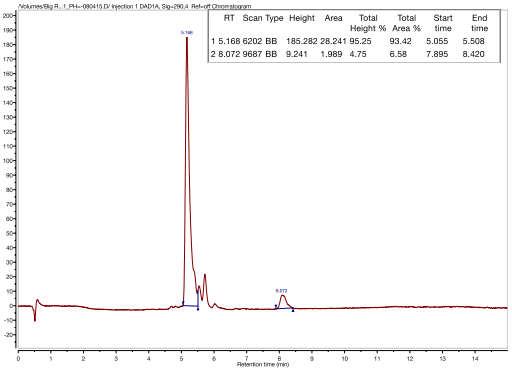

RT	Scan Type	Height	Area	Total Height %	Total Area %	Start time	End time
1 5.168	6202 BB	185.282	28.241	95.25	93.42	5.055	5.508
2 8.072	9687 BB	9.241	1.989	4.75	6.58	7.895	8.420

BIO-A2-D8 4h

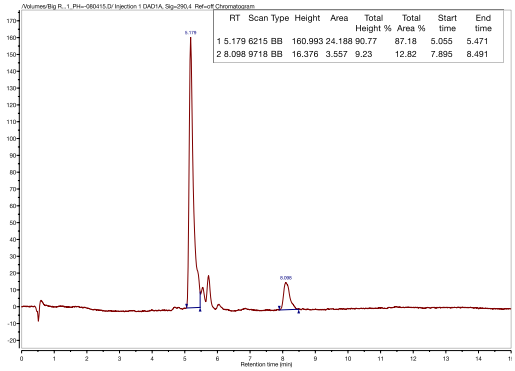

RT	Scan Type	Height	Area	Total Height %	Total Area %	Start time	End time
1 5.179	6215 BB	160.993	24.188	90.77	87.18	5.055	5.471
2 8.098	9718 BB	16.376	3.557	9.23	12.82	7.895	8.491

BIO-A2-D8 8h

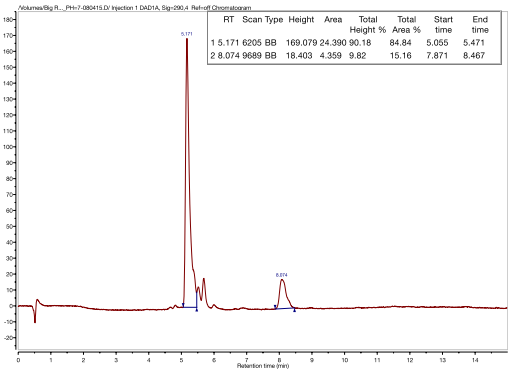

RT	Scan Type	Height	Area	Total Height %	Total Area %	Start time	End time
1 5.171	6205 BB	169.079	24.390	90.18	84.84	5.055	5.471
2 8.074	9689 BB	18.403	4.359	9.82	15.16	7.871	8.467

BIO-A2-D8 12h

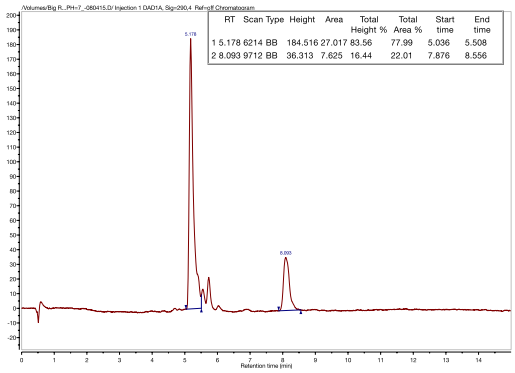

RT	Scan Type	Height	Area	Total Height %	Total Area %	Start time	End time
1 5.178	6214 BB	184.516	27.017	83.56	77.99	5.036	5.508
2 8.093	9712 BB	36.313	7.625	16.44	22.01	7.876	8.556

Figure B.9: HPLC graphs from the release kinetic study of BIO-A2-D8.

BIO-A2-D8 24h

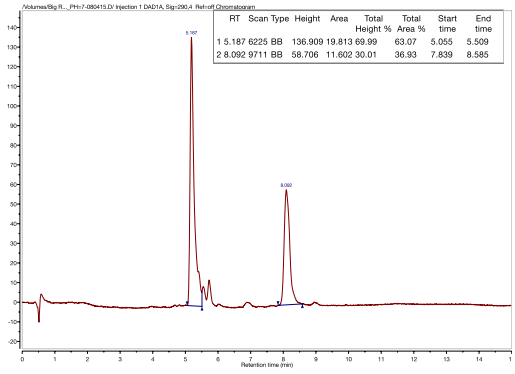

	RT	Scan Type	Height	Area	Total Height %	Total Area %	Start time	End time
1	5.187	6225 BB	136.909	19.813	69.99	63.07	5.055	5.509
2	8.092	9711 BB	58.706	11.602	30.01	36.93	7.839	8.585

BIO-A2-D8 48h

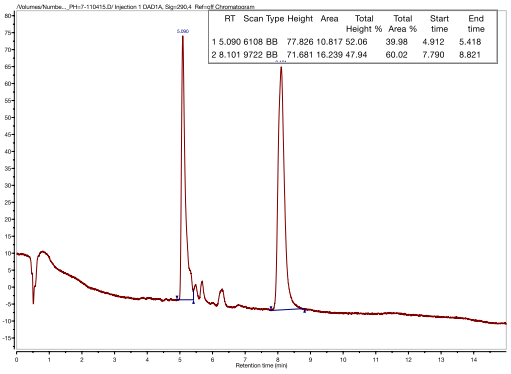

	RT	Scan Type	Height	Area	Total Height %	Total Area %	Start time	End time
1	5.090	6108 BB	77.826	10.817	52.06	39.98	4.912	5.418
2	8.101	9722 BB	71.681	16.239	47.94	60.02	7.790	8.821

BIO-A2-D8 72

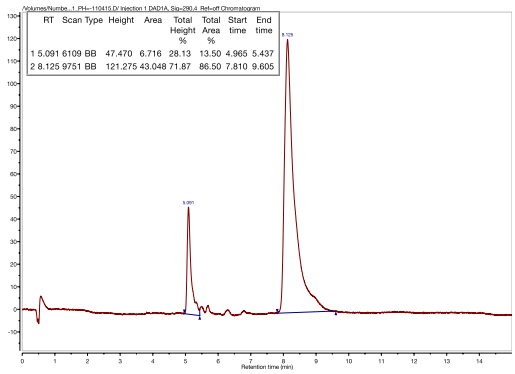

	RT	Scan Type	Height	Area	Total Height %	Total Area %	Start time	End time
1	5.091	6109 BB	47.470	6.716	28.13	13.50	4.965	5.437
2	8.125	9751 BB	121.275	43.048	71.87	86.50	7.810	9.605

Figure B.9: Continued.

BIO-A2-K-D4 0h

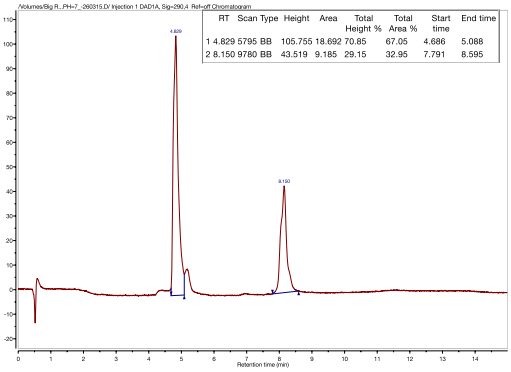

RT	Scan Type	Height	Area	Total Height %	Total Area %	Start time	End time
1 4.829	5795 BB	105.755	18.692	70.85	67.05	4.686	5.088
2 8.150	9780 BB	43.519	9.185	29.15	32.95	7.791	8.595

BIO-A2-K-D4 1h

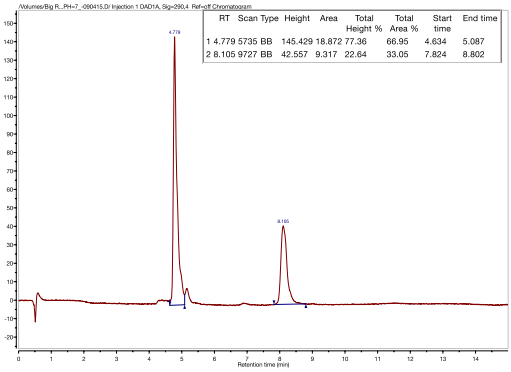

RT	Scan Type	Height	Area	Total Height %	Total Area %	Start time	End time
1 4.779	5735 BB	145.429	18.872	77.36	66.95	4.634	5.087
2 8.105	9727 BB	42.557	9.317	22.64	33.05	7.824	8.802

BIO-A2-K-D4 2h

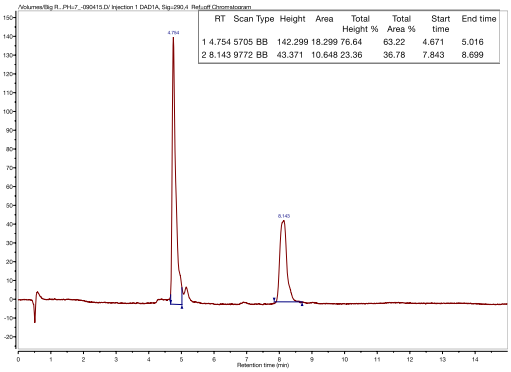

RT	Scan Type	Height	Area	Total Height %	Total Area %	Start time	End time
1 4.754	5705 BB	142.299	18.299	76.64	63.22	4.671	5.016
2 8.143	9772 BB	43.371	10.648	23.36	36.78	7.843	8.699

BIO-A2-K-D4 4h

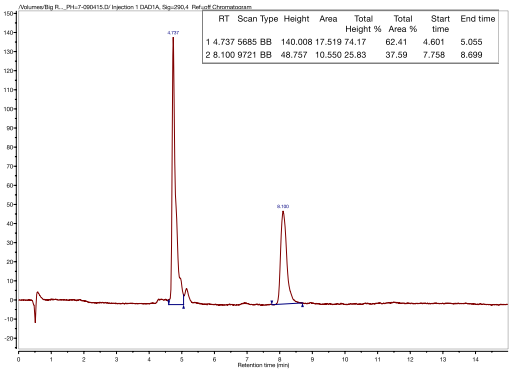

RT	Scan Type	Height	Area	Total Height %	Total Area %	Start time	End time
1 4.737	5685 BB	140.008	17.519	74.17	62.41	4.601	5.055
2 8.100	9721 BB	48.757	10.550	25.83	37.59	7.758	8.699

BIO-A2-K-D4 8h

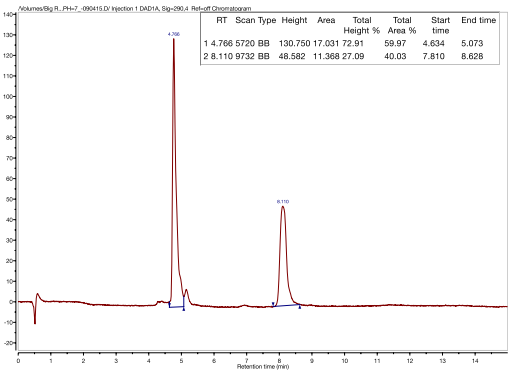

RT	Scan Type	Height	Area	Total Height %	Total Area %	Start time	End time
1 4.766	5720 BB	130.750	17.031	72.91	59.97	4.634	5.073
2 8.110	9732 BB	48.582	11.368	27.09	40.03	7.810	8.628

BIO-A2-K-D4 12h

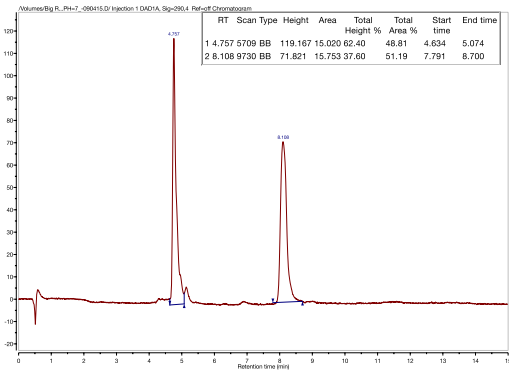

RT	Scan Type	Height	Area	Total Height %	Total Area %	Start time	End time
1 4.757	5709 BB	119.167	15.020	62.40	48.81	4.634	5.074
2 8.108	9730 BB	71.821	15.753	37.60	51.19	7.791	8.700

Figure B.10: HPLC spectra of release kinetics for BIO-A2-K-D4. A small amount of free 6BIO was present at time 0 and was used as a baseline for the other graphs.

BIO-A2-K-D4 24h	BIO-A2-K-D4 48h
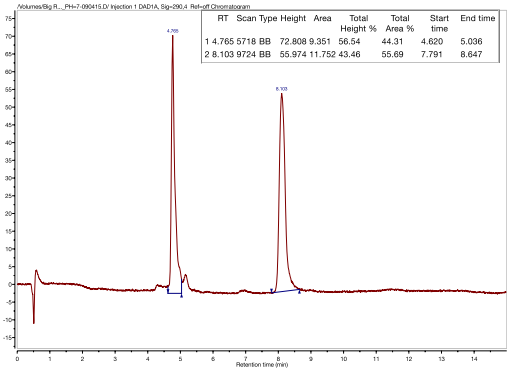	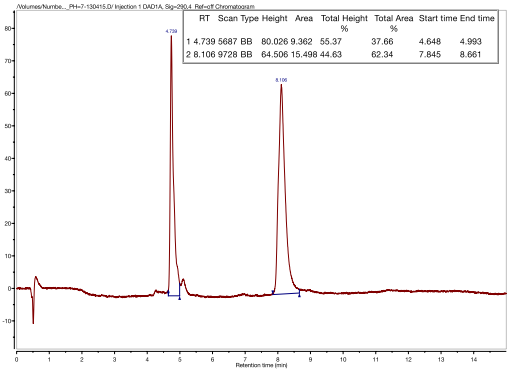
BIO-A2-K-D4 72h	
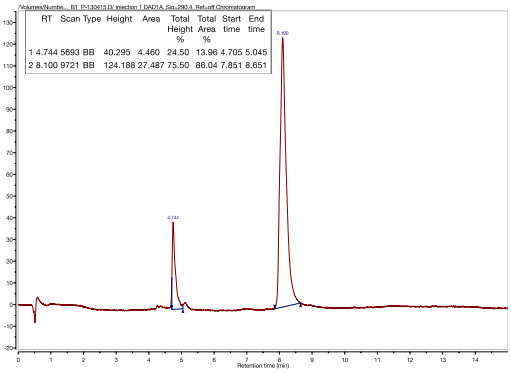	

Figure B.10: Continued.

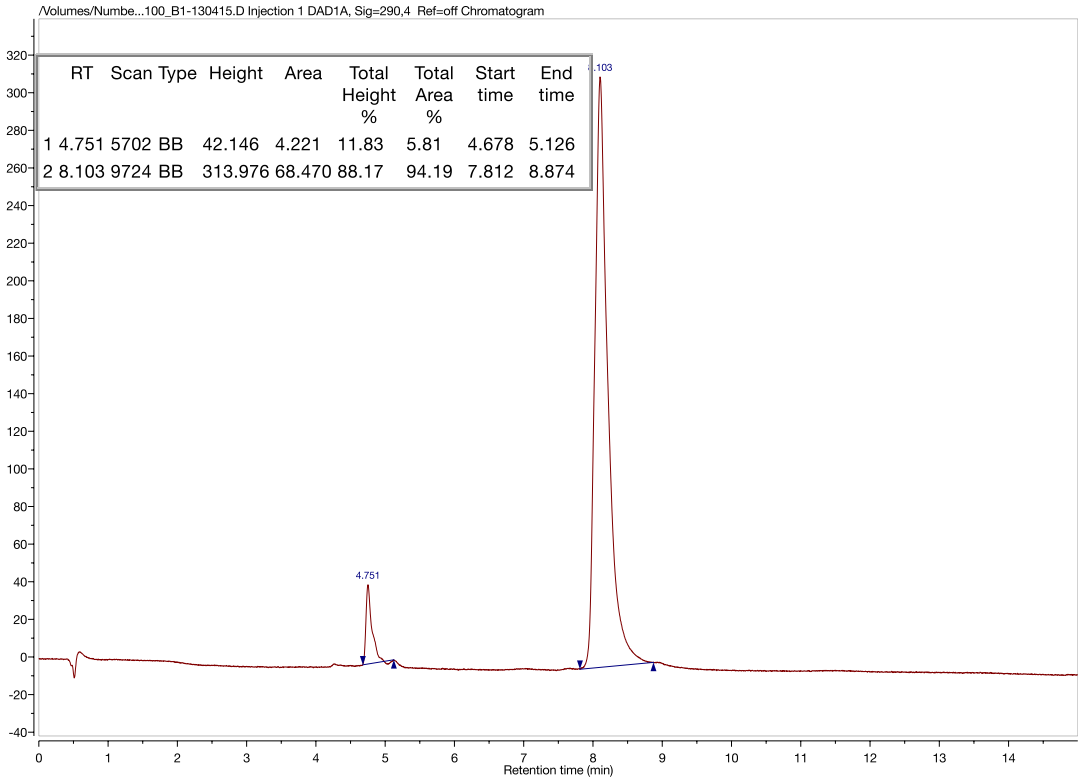

Figure B.11: Four hour release of BIO conjugated to 4-pentynoic acid at room temperature.

B.6 Iodination preparation

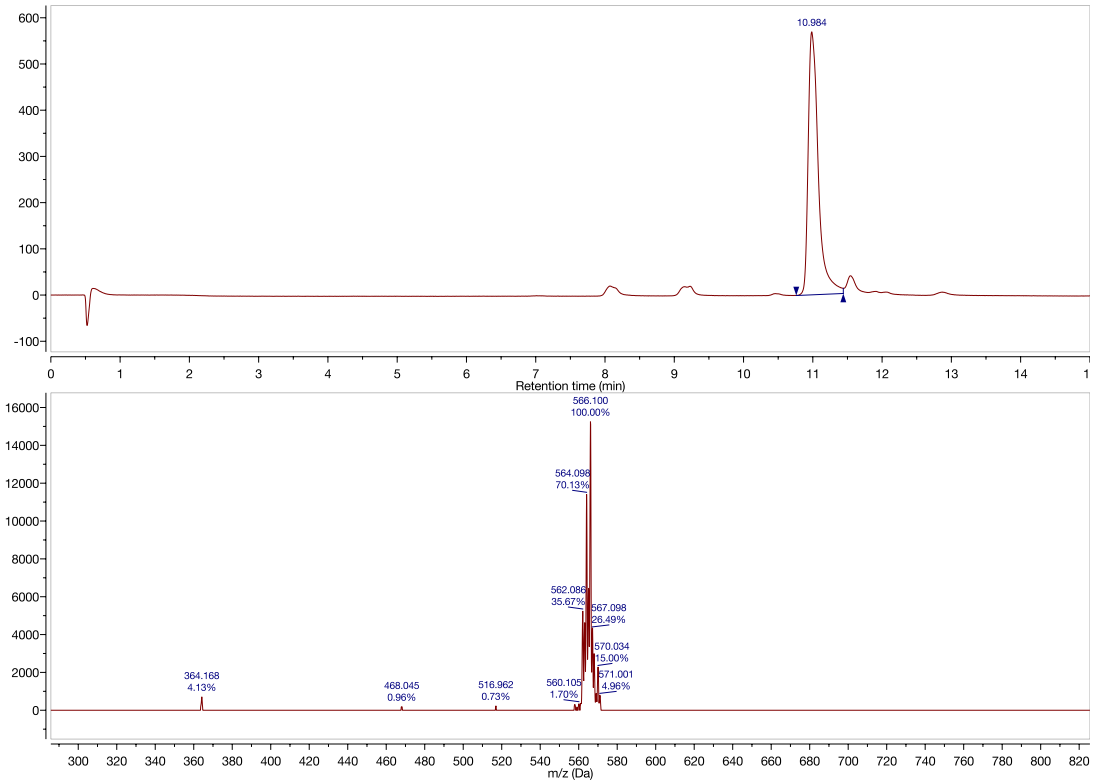

Figure B.12: HPLC and mass spectrum of stannylated 6BIO.

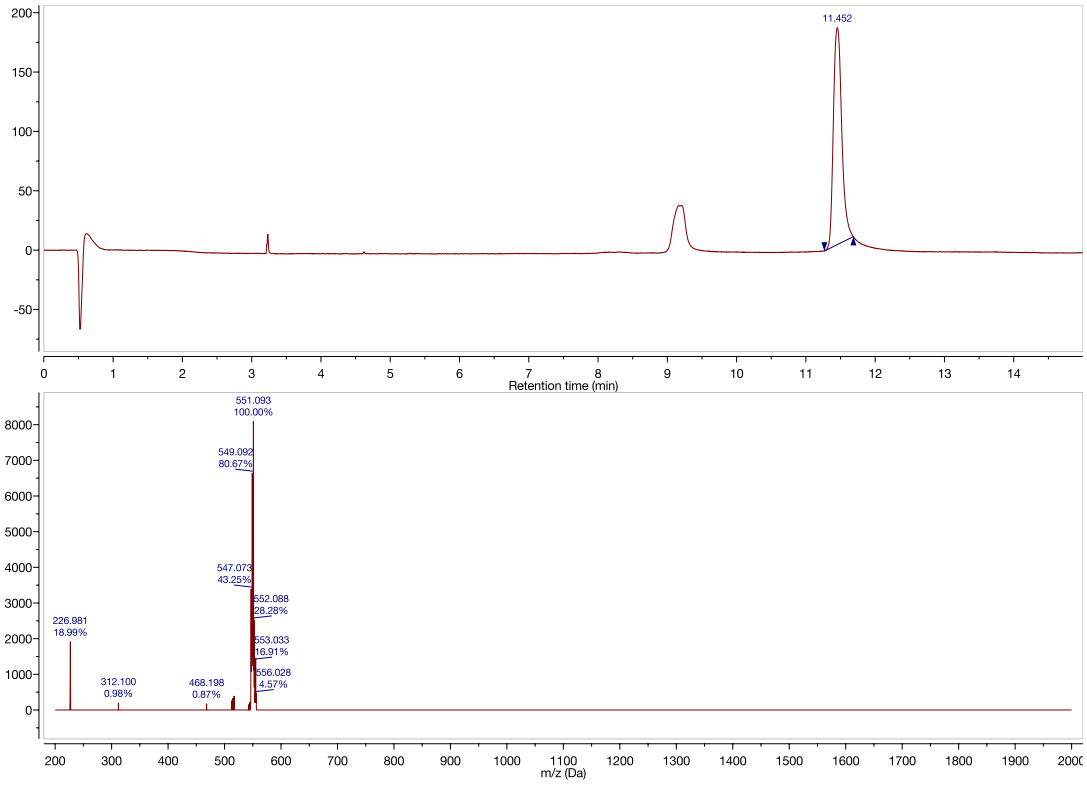

Figure B.13: Spectrum of o-alkylated stannylated 6BIO. As is frequent the case with tributyl-stannylated products, one butyl group is missing from the spectrum.

B7 Iodination

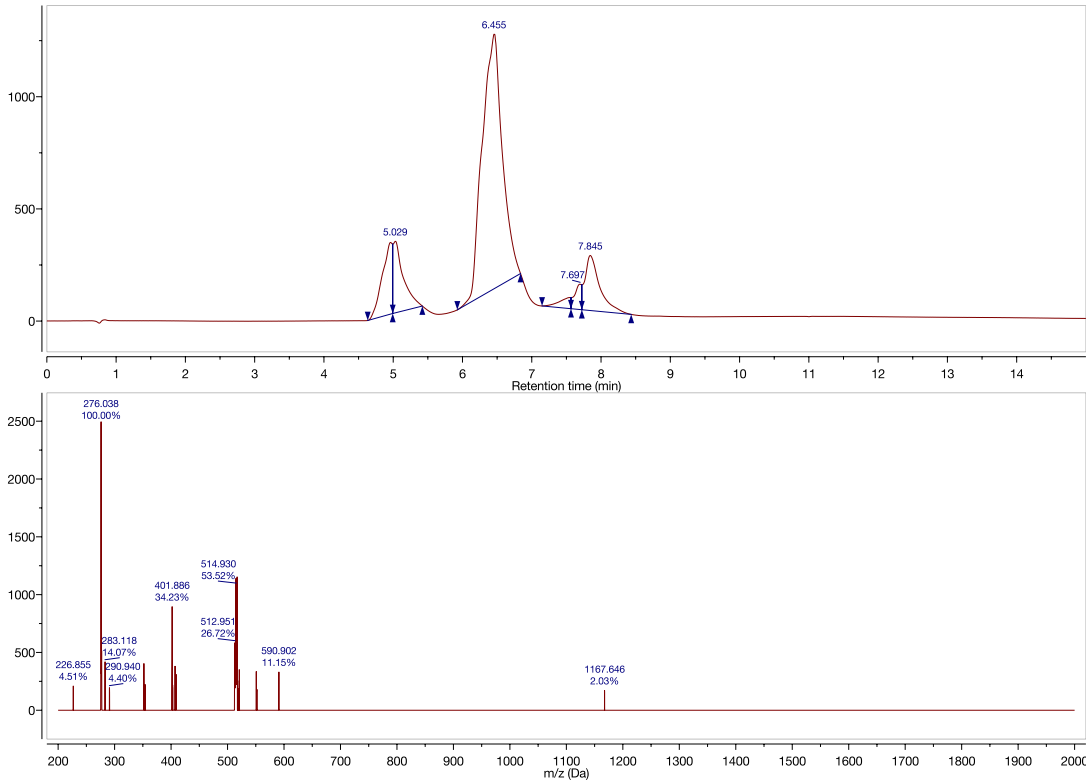

Figure B.14: Iodination of 6BIO. The iodinated peak is at 7.7 minutes. The primary peak is proteodestannylated 6BIO.

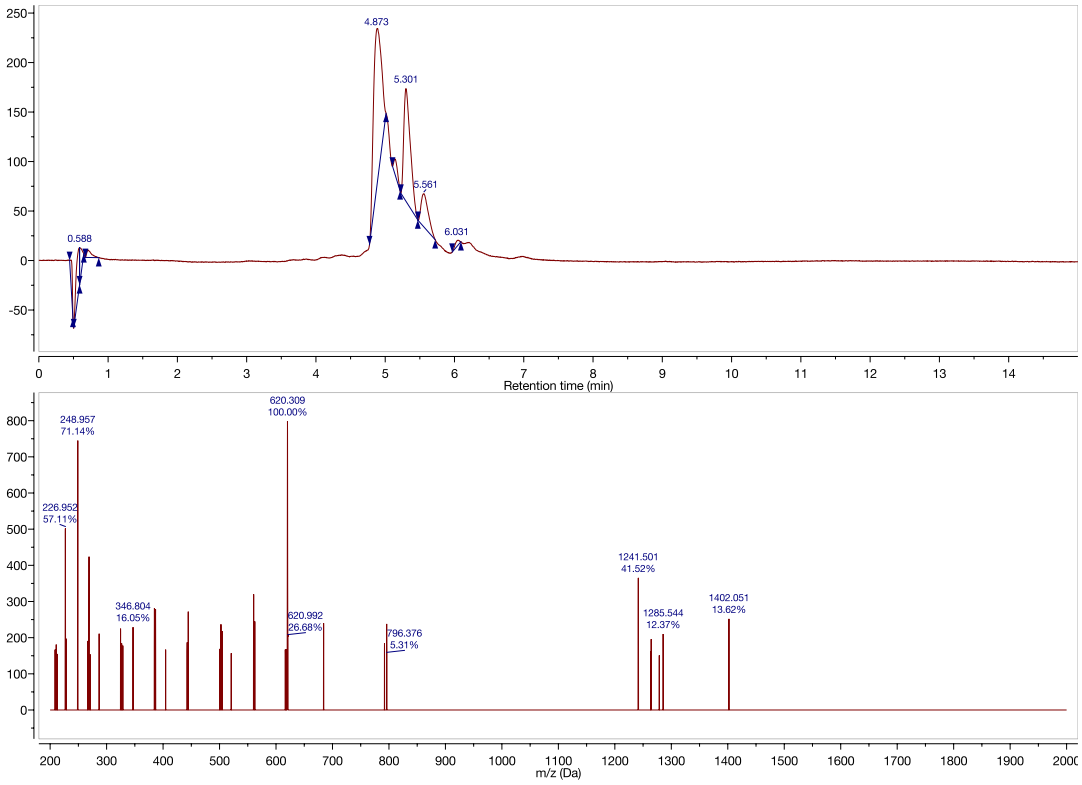

Figure B.15: Iodination of BIO-A2-D8. The iodinated peak is at 5.3 minutes. The primary peak is proteodestannylated BIO-A2-D8.

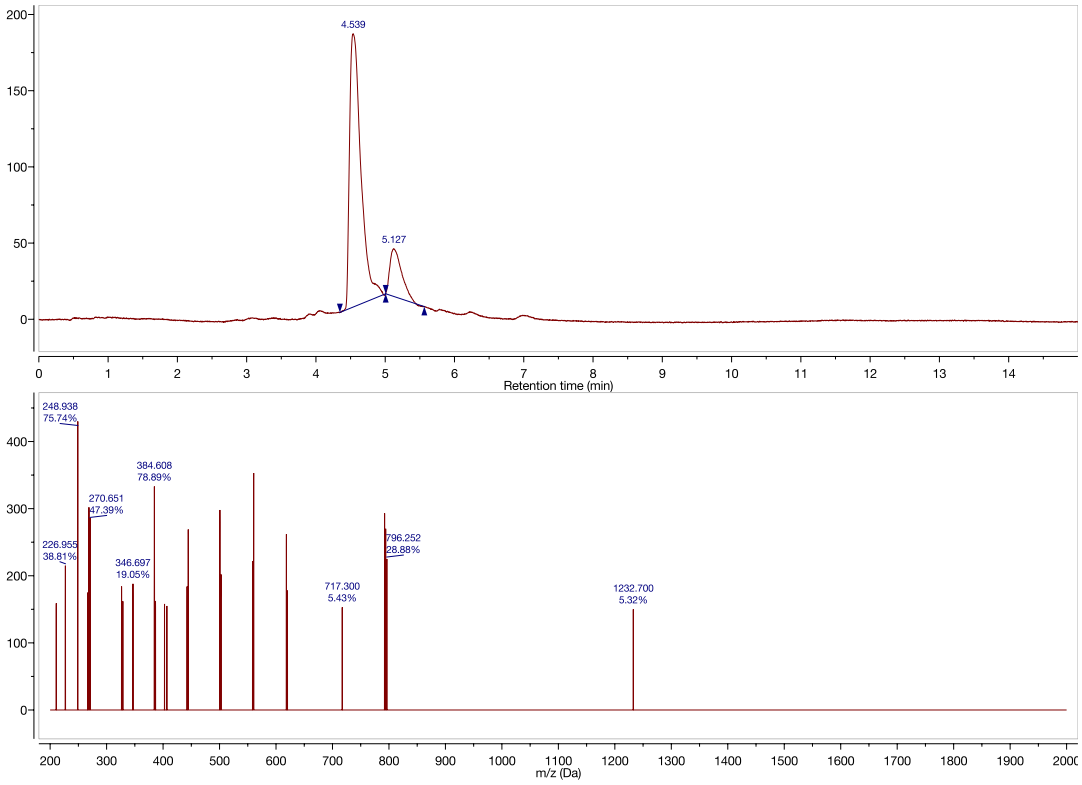

Figure B.16: Iodination of BIO-A2-K-D4. The iodinated peak is at 5.1 minutes. The primary peak is proteodestannylated BIO-A2-K-D4.

APPENDIX C

CHAPTER 4 SUPPORTING INFORMATION

C.1 Bone morphometric analysis

Table C.1: Bone morphometric analysis using the plate model (f indicates that the unimer is statistically different than the free drug and p indicates that the unimer is statistically different than the PBS control).

Plate Model	Linear	Branched	Free 6BIO	PBS
TV	60.5±3.4 [f,p]	66.7±6.8 [f,p]	48.1±5.8	43.9±8.8
BV/TV	0.411±0.019 [f,p]	0.411±0.011 [f,p]	0.341±0.015	0.333±0.022
Tb.N	5.24±0.12 [f,p]	5.66±0.11	5.73±0.20	5.78±0.18
Tb.Th	0.0789±0.0043 [f,p]	0.0728±0.0021 [f,p]	0.0596±0.0021	0.0581±0.0047
Tb.Sp	0.113±0.004	0.104±0.003 [p]	0.116±0.006	0.1157±0.0042
BS	633.6±35.4	752.7±71.3 [f,p]	541.9±57.0	503.7±97.6
BS/BV	25.9±1.5 [f,p]	27.6±0.8 [f,p]	33.8±1.2	35.3±2.7